Modelling of Dosator Filling and Discharge

by

Oscar Andres Angulo Pinzon

This thesis is submitted in partial fulfilment of the requirements for the award of the Degree of Doctor of Philosophy under the conditions of the award of higher degrees of the University of Greenwich

This research was carried out at The Wolfson Centre for Bulk Solids Handling Technology in collaboration with GlaxoSmithKline

University of Greenwich

August 2012

DECLARATION

I certify that this work has not been accepted in substance for any degree, and is not concurrently being submitted for any degree other than that of Doctor of Philosophy being studied at the University of Greenwich. It is also declare that this work is the result of my own investigations except where otherwise identified by references and that I have not plagiarised the work of others.

_____   _____

Oscar Andrés Angulo Pinzón, Candidate   Mike Bradley, Supervisor

ACKNOWLEDGEMENTS

Other industrial contributors that I thank include, John Swarbrick (Domo Friesland, UK) for his material donation; Seyfan Karlheniz (Harro Höfliger, Germany), Vittorio Calzonari and Leonardo Ercolani (MG2, Italy), and Pietro Pirera (IMA, Italy) for their industrial knowledge support.

Last by no means least, without the continuous encouragement and loving care of my partner Paula, my parents, sister and brother, it would have been much harder for me to finish this research project and I feel that the completion of this thesis has justified their support and sacrifices.

This research work is dedicated to the unfinished world of the science, that day on day evolves making our life easier. It is also dedicated to all the researchers in the powder handling and pharmaceutical areas that carry out investigations contributing to the welfare of people's life.

ABSTRACT

Dosators (and other machines operating on generally similar principles) are widely used in the pharmaceutical industry for dosing products that are delivered to the customer in powder form (i.e. capsules and dry inhaled powder applications). However a significant problem for this technology is the ability to predict how accurately and reliably, new formulations can be dosed from these machines prior to scale-up for manufacture.

Dosator filling machines have been on the market for over forty years, and their mechanisms have been refined over the time; in parallel with development work of formulation scientists. Despite the work that has progressed in both of these important fields, there has been only a limited improvement in the understanding of how the formulations behave when introduced into production line equipment. Typical problems include variation in potency and manufacturing dose weight – both being issues that can be difficult to predict and counter (especially where mainly the manufacturing process is undertaken on a batch basis).

Many manufacturing problems can be traced back to an inadequate understanding of the bulk properties of the powders at the formulation stage. Common issues encountered during full scale production include extended commissioning; high levels of out of specification materials (specifically through dose weight variation).

The project aims to provide a predictive tool to industry, the use of which can improve manufacturing efficiency, minimise costs and risk when launching new products.   The approach proposed focuses on the development of an analytical model for the pick up and discharge of powder into and out of dosators, based upon established particle/powder characterisation techniques combined with an improved understanding of dosator machine factors, constitutive models and geometry of the machine.

The model will be used to predict fill dose weights and filling/discharge behaviour of new products in dosator fillings systems; likewise, to investigate what changes in powder flow properties mean to dosator operation. Recommendations for the practical use of flow property measurement techniques in conjunction with the model are also outputs from this project.

To simulate the process and (very importantly) validate the model, a dosator single shot test-rig was engineered at The Wolfson Centre to measure forces acting on the dosator during the filling stage, the force required to eject the dose and the dose weight. In addition other important aids, such as a dosator demonstrator and an ultimate bearing application of soil mechanics, are key in the understanding of the process and estimate the stress distribution occurring in the stages of the operation.

In addition, the development of this research provides a better understanding of the compaction phenomena in dosator operation, and more importantly, critical flow properties and machine settings factors compromising the uniformity of the fill dose weight in production lines using dosator filling machines not mentioned in the literature yet. Although this project has focussed on dosators, the general concept could be applicable to other volumetric powder filling systems.

CONTENTS

FIGURES

CHAPTER 3. LITERATURE REVIEW

**CHAPTER 4. DETERMINING KEY PARAMETERS IN DOSATOR
OPERATION**

CHAPTER 5. MATERIALS AND POWDER FLOW CHARACTERISATION

CHAPTER 9.   3PI DOSATOR SINGLE SHOT TEST-RIG

CHAPTER 10.   CONCLUDING REMARKS AND RECOMMENDATIONS FOR FURTHER WORK

TABLES

NOMENCLATURE

API   Active pharmaceutical ingredient

C   Relative volume decreased

CC   Compaction curve

CI   Carr's compressibility index

C_r Compression ratio of the slug

D10   Media of the particle diameter where 10% of the population sample lies below this value

D50   Media of the particle diameter where 50% of the population sample lies below this value

D90   Media of the particle diameter where 90% of the population sample lies below this value

DFE   Domo Fonterra Excipients

DPI   Dry powder inhaler

FDA   Food and drug administration

Gap "h"   Clearance between the dosator undersize and the bottom of the trough

GSK   GlaxoSmithKline

HPLC   High performance liquid chromatography

K   Stress ratio or Heckel equation constant

LVDT   Linear voltage displacement transducer

NCE   New chemical entity

NIR   Near infrared spectroscopy

Pa   Pressure applied

PFT   Powder flow tester

PSD   Particles size distribution

q_u Ultimate bearing capacity

SEM   Scanning electron microscopy

μ Angle of internal friction

α Failure plane

α_m Angle of repose

ρ Bulk solid density

ρ_a Poured density

ρ_t Tapped density

σ_1 Major consolidation stress

σ_c Unconfined failure strength

σ_{h1} Horizontal stress inside the dosator

σ_{hb1} Horizontal stress in the powder bed

σ_N Normal/Vertical stress

σ_o Yield strength

σ_r Radial stress

σ_{VW} Vertical stress produced from the self-weight

σ_z Vertical stress

τ Shear stress

Φ_w Maximum wall friction angle

Chapter 1

Introduction

1.1.   Introduction

As its name describes, the dosator is a tool used to obtain a dose. Examples of equipment that operates along a similar principle are sampling tools used in geological engineering. I.e. core samplers (Hankinson) and thief probes. These are essentially slotted tubes that are pushed into the soil, rotated and retracted to obtain a core sample. In the context of this research programme, the dosator is one of the many filling systems used in the pharmaceutical industry to deliver powder solid doses of medicines into receptacles for different end applications (covered in more detail in chapter 2). Generally, a dosator takes the form of a tube with an internal piston/pin/plunger, which can be set to a given height to create a cavity proportioned to suit the metering application. The dosator is dipped into a powder bed to fill the cavity. The fill weight of the dose is a function of powder density, which, in turn, is a function of the powder flow properties, machine settings and other application specific variables. The dose is then ejected by the pin into a receptacle. The function of the dosator is to generate accurate and repeatable doses of powder to a controlled weight.

Dosator filling machines have been used in industry for over forty years, and refinements to their fundamental mechanisms have evolved over this time to suit the specific process requirements of end users. In parallel, formulators have tended to optimise powder blends (and therefore potency) with the objective of performance in medical applications. Unfortunately, these formulation developments rarely take into account the production processes necessary to produce the end product – with the result that many formulations tend to be sensitive to flow irregularities and bulk density variations. The problem is compounded further because pharmaceutical powders are complex blends manufactured in batches, yet these batches are notoriously inconsistent in their flow properties, due to inconsistencies in the raw input materials, blending and processing.

Manufacturability is often not given any importance at the formulation stage; thus, various problems, as production delays and wastage during commissioning, and more importantly, variations of the dose fill weight, come out during production due to the lack of process and

powder understanding. Variation of the dose weight in dosator filling applications (e.g. dry inhaled powders) could seriously impact upon the health of the patients.

The initiation of this research project was driven by GSKs' aim to improve manufacturing efficiency, minimise costs, save time launching new products to the market and concerns about production problems. GlaxoSmithKline had developed in collaboration with The Wolfson Centre for Bulk Solids Handling Technology at the University of Greenwich, this research project focussing on modelling the pressures acting in dosators in order to predict their performance and to control the dose weight. Although this project has focussed on dosators, the general principles are applicable to other powder filling operations, and the knowledge gained can be transferred to other capsule filling systems or tabletting processes. The Wolfson Centre has worked closely with the pharmaceutical industry to solve different solids handling problems. This project arose from discussions, previous projects and collaborations with GSK and the outputs are reflected in this thesis.

GlaxoSmithKline, as sponsor of the project, had provided support in the form of industrial supervision and material provision for the research. GSK Manufacturing uses dosator technology for capsule filling and inhaled products; around eleven new products are currently in development, due for launch between 2010 and 2014.

1.2.   Project objectives

The primary objective of the study outlined in this thesis, was to develop a model for the pickup and discharge of powder from dosator based filling machines, taking account of flow properties of the powder and the machine set up, based upon known powder mechanics characterisation techniques and constitutive models. Some factors affecting dosator operation have been published and discussed previously in literature, but some others, considered critical in this research, were observed following trials in The Wolfson Centre dosator single shot test rig.

A secondary objective of the project was to use a model (developed as part of the project) to investigate how changes in powder flow properties and machine set up impact upon dosator filling and discharge operation. The purpose of this aspect of the project was to provide GSK

with a predictive model/technique for assessing dose weight and flow behaviour at the formulation stage of product development.

An additional objective was to validate and calibrate the model by using a dosator single shot test-rig. Initially the intention was to use the 3PI single shot test rig owned by GSK, but the direction taken by the research dictated that it was more practical and efficient to construct a single shot test rig of Wolfson Centre design. However the 3PI test-rig was also used in the late stages of this project to observe the effect of the dosator speed on the operations. Having established the dominant factors involved in the dosator process, another requirement was to develop recommendations for the practical use of flow property measurement techniques in conjunction with the model, to predict the filling and discharge behaviour of new powders in dosators filling machines.

1.3.   Project preview

The structure of the thesis is as follows:

Chapter 2 presents, briefly, the main powder dosage systems used in the pharmaceutical industry. It focuses on dosator machines, describing the types of machines, their operation, key components and common dosator applications in industry. Likewise it lays out the dosator principle used in this research, because there are many variations in the dosator operating principles that are specific to the machines of different manufacturers. It also includes a brief description of pharmaceutical powders blend compositions commonly used in dosator systems and the typical ingredients used in blends. This chapter also covers a description of the most commonly employed methods of measuring powder flowability in industry and clarifies the principle followed in this research. Finally the application of soil mechanics to describe the stress distribution in the powder bed manifested in dosator operation is discussed.

Chapter 3 presents a broad survey of the literature published about dosator operation. It covers dosator systems, powder flow properties and the factors involved in the variation of the dose weight in dosator systems. It reviews a sample of the most relevant dosator models published and instrumentation of dosator filling machines. The last part of the chapter is

dedicated to key papers of ultimate bearing capacity application of soil mechanics - used to illustrate stress fields that could occur in dosator operation.

Chapter 4 describes the various stages of this research project determining the key parameters in dosator operation, in order to direct the development of the investigation. This chapter provides the reader with a better understanding of the factors initially considered affecting the dosator operation that led to the measurement of the particle/flow properties and the design of the experimental work described in the following chapters 5 and 6.

Chapter 5 describes the main four test powders used in this research and the critical particle/powder flow characterisation techniques relevant to dosator operation. The measurements of the flow properties and results are presented and discussed in this chapter.

Chapter 6 describes the design and methodology of the single shot test-rig engineered at The Wolfson Centre. This was the main test-rig used in this research to validate the model and conduct the research.

Chapter 7 presents the experimental results of the different tests undertaken in The Wolfson Centre single shot test-rig, with the four main test powders. Test conditions were based on dosator machine settings that were anticipated to have a significant effect on the dose fill weight.

Chapter 8 describes the model for the dosator filling and discharge operation developed in this research; it also presents The Wolfson Centre physical approach to explain the dosator operation and the tools used for it. It also presents the validation and discussion of the model by comparing the results obtained experimentally in the dosator test-rig, for the range of powders used, with the data generated from the dosator model.

Chapter 9 presents experimental work undertaken at GSK Harlow facilities using the 3PI dosator test-rig to study the effect of the dosator speed on the operation. It was suggested by the industrial supervisors to undertake some tests in their 3PI dosator single shot test-rig to compare the results with the experimental data obtained from The Wolfson Centre dosator test-rig. It is shown the comparison between the two test-rigs, observations and conclusions about the experimental session.

Chapter 10 presents the conclusions from this project and proposes further work to advance the outcomes produced from this investigation.

Chapter 2

Background

2.1.   Introduction

This chapter presents the background of dosator systems from the point of view of the process operation and the studies reported in this thesis. It describes the powder filling systems commonly used in the pharmaceutical industry and focuses on dosator machines in particular. A discussion is also presented regarding conventional methods for determining the flowability of powders used in the pharmaceutical industry.

The chapter is structured as follows. Section 2.2 describes, in general terms, the most common powder filling systems and classifies the machines by direct or indirect filling systems. Section 2.3 is focused on dosator machines and presents relevant topics to this research (concerning dosator operation). Section 2.4 briefly presents the typical composition of pharmaceutical blends, ingredients and the development stages of pharmaceutical formulations. In offering an overview of dosator operation and the pharmaceutical powder composition, section 2.5 illustrates the filling trend in dosators systems. These sections provide a broad overview of the process, but make no mention of the importance of the powder flow properties in dosator operation. Section 2.6 briefly explains the principles used in the pharmaceutical industry to measure the flowability of the powders and what principle is followed in this research work. The final section, 2.7, illustrates some applications of stress theory in powder and soil mechanics that complement dosator operation. A summary of the chapter linking the findings of the review to subsequent work is presented in section 2.8.

2.2.   Powder filling systems in the pharmaceutical industry

In the pharmaceutical industry a wide range of solid powder filling systems, which employ different technologies and principles, are used. Technologies such as vibration, compression, and vacuum, gravitational and pneumatic systems are frequently incorporated into equipment designs. It is difficult to find a general classification for these machines; nevertheless Podczeck & Jones (2004) classified them into direct and indirect filling methods. This

represents the most common classification found in literature (dosators belong to the indirect filling machines category). The appropriate selection of these systems dictated by the application, material(s) to use (for example powder, liquid, tablets or granules) and the dosage presentation required.

Filling systems are not only used in production lines, they are used in various stages of the product formulation. When pharmaceutical companies develop a new product, it passes through several stages before it is launched to the market. The drug discovery is the first stage, where the drug is discovered and designed; here New Chemical Entities (NCE's), or in some cases already existing drugs, are chosen due to the molecular and physiological potential to treat an illness. The next stage is the pre-clinical work, where experiments are carried out to understand more about the toxicity, pharmacokinetics and metabolism of the NCE. These can be performed in-vitro (in cells or micro organism) or in-vivo (in animals). Here the toxicity in major organs is assessed before proceeding with further development. The final stage is the clinical trial; this stage is divided by several phases described as follows. Phase 0 where micro-doses are tested in humans to correlate behaviour previously expected. Phase I employs a small group of people, who are under full time observation and the dose provided is increased. Phase II extends the trials in a larger group to determine the efficacy and dosing requirements. Phase III is performed in a yet larger group and evidences of the efficacy and safety of the drug are collected, while application for the drug approval is submitted to the regulatory agency, to make it available for urgent patients and revenues purposes. Phase IV carries out the drug's performance studies after its approval and commercialisation.

Each of the mentioned phases uses different filling system, early phases employ manual and bench filling systems and as the phases evolve the sample size increases and more efficient automated filling machines are used.

2.2.1. Direct filling systems

Direct filling systems are one of the oldest filling systems on the market; these systems transfer powder directly from storage vessel to the dosage receptacle. They are not very sophisticated pieces of equipment and no (or minimal) powder compression is involved in the process. Among this classification can be found two sub categories, described below.

2.2.1.1.   Auger-filling principle

This is the oldest semi-automatic technique of filling powders used in the pharmaceutical industries. Arthur Colton developed it in the first decade of the 20th century.
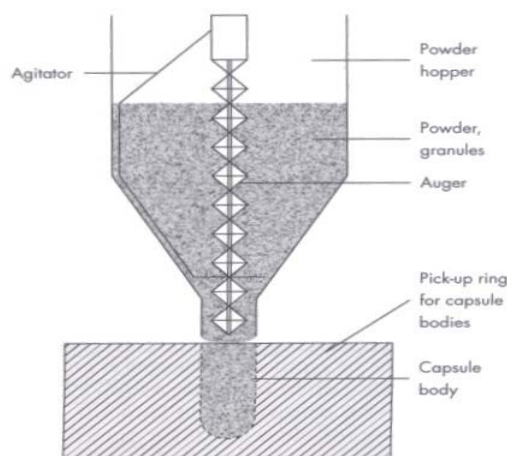
Figure 2.1. Capsule filling by auger method. For full explanation refer to the text. Reprinted from Podczeck & Jones (2004, p. 123).

Figure 2.1 shows the auger principle, where the powder in a hopper is dosed continuously and consistently by a central rotating auger, which typically operates in conjunction with a counter rotating stirrer/agitator. It is normally used for capsule filling applications, where capsule bodies are placed in bushings on a turntable underneath of the vessel. The dose weight is function of the auger speed, geometry (pitch and diameter) and the time the capsule spends underneath of the hopper outlet (Podczeck & Jones 2004, p. 123). These machines can fill from 40,000 to 80,000 capsules per hour.

According to Podczeck & Jones (2004, p.124) these machines can give poor repeatability issues due to powder randomly detaching from the last volumetric pocket of the auger when it stops. Additionally, the need for constant agitation within the buffer hopper combined with the preferential extraction of powder from the centre-line of the hopper combine to generate variable screw filling efficiency and hence variations in bulk density.

There are ranges of auger designs (developed through trial and error over many years) that can be utilised to suit different powder properties.

2.2.1.2. Vibration-assisted filling

There are a variety of machines using this principle in conjunction with different feeding systems and supporting technologies. This system is also used for capsule filling and Osaka Company (Japan) introduced this method to the market in 1960 (Podczeck & Jones 2004, p. 124). Shown in figure 2.2 is an overview of the four stages involved in vibration-assisted filling method of hard capsules of Shionogi Qualicaps.
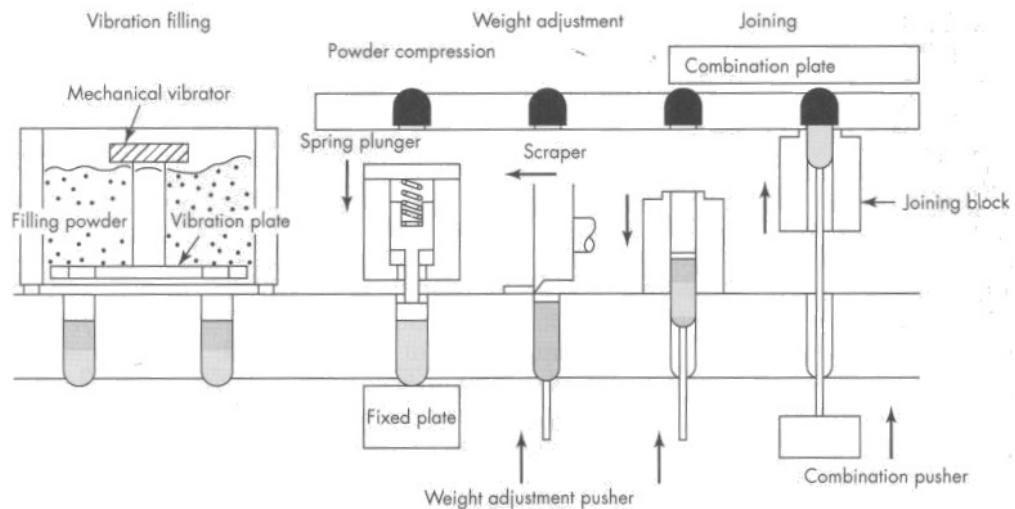
Figure 2.2. Vibration assisted filling. For full explanation refer to the text. Re-printed from Podczeck & Jones (2004, p. 124).

The capsule bodies are positioned, in the same way as auger machines, in a rotating turntable and pass underneath of the powder bowl. In the first stage the powder bowl has a mesh to which a mechanical vibrator is connected, this helps to the powder to de-agglomerate and flow to fill the capsules. The capsules are filled to the maximum capacity (which incorporates additional volume to allow for subsequent compaction). In the second stage the turntable rotates and the filled powder is compacted by a spring-loaded plunger but the dose is still longer than the size of the body itself. In the third stage the capsules are raised and excess material partially outside the turntable is removed by means of a scraper. In the final stage the capsule body is pushed upwards and the corresponding cap is joined and closed. The fill weight in this method is affected by rotation speed of the turntable, mesh size, and vibration level in the powder bowl, compression setting of the plunger and the lift height at which the dose is scraped.

Through the years this method has evolved and a range of size meshes are available on the market giving scope to fill different particle sizes into the capsules. Production machines using this system can produce up to 40,000 capsules per hour.

One of the current examples of vibration-assisted filling systems is the Xcelodose® micro-dosing system of Capsugel (Belgium) (Edwards 2010). This machine can produce from 600 to 1200 capsules per hour and is used ideally in Phase I and II of clinical trials, for doses from 0.1 mg up to several hundred milligrams.
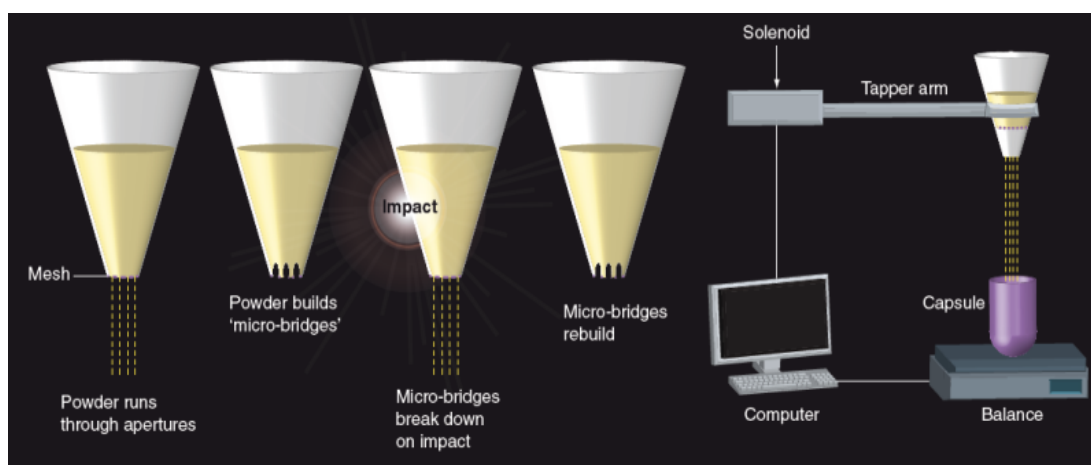
Figure 2.3. Xcelodose® powder micro-dosing filling system. For full explanation refer to the text.   Re-printed from Edwards 2010 with permission of the publisher and the author.

The Xcelodose system shown in fig 2.3 consists of a hopper with a screen across the outlet. The screen size is fine enough to ensure the powder will not flow under gravity alone (i.e. powder arches across the screen apertures). Controlled vibrations are then applied to the hopper/ mesh to reduce interparticle friction and cause discharge of the powder dose into the capsule body below. The dose weight uniformity of this principle is a function of the particle size, the powder flow properties (ability of the powders to bridge at the outlets), the dispenser head (size and number of holes) and the taps applied to the dispenser heads. There is no powder waste in this principle, all the powder is filled into the dosage forms, and this is the major advantage of this system.

2.2.2. Indirect filling systems

Indirect filling machines have become more sophisticated in recent years and offer significant increases in production capacity over direct filling systems; these machines combine some of the principles described above. The dose, in this type of filling system, is filled into a defined cavity; often using compression to define the shape and it is then transferred to the capsule. Manufacturers using these systems have produced modular machines that integrate the whole powder filling process, for a range of applications, into one machine in a reduced space. Modular machines allow the exchange of filling system and dosing packing presentation for various applications. Machines under this classification, which included dosators (the focus of this project), are described below.

2.2.2.1. Dosing wheel

This system is used in various industries (food, tobacco, etc) to meter powder or granules. Modifications to this principle of operation have been made for application to the dosing of cohesive powders for the pharmaceutical industry.

Figure 2.4 shows the dosing wheel principle (Coatsworth & Castle 1990, p. 2). The wheel (2) contains several cavities (6); these cavities are filled under gravity by the powder stored in the hopper (12), located on the upper part of the machine. The wheel rotates 180° and the powder is discharged under gravity to the dosage receptacle; there are various potential mechanisms used to feed the powder to the dosing wheel such as a plunger, hopper and vertical auger.
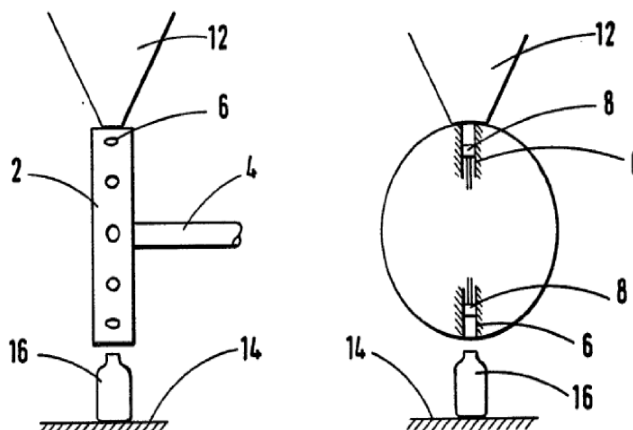
Figure 2.4. Dosing wheel principle. For full explanation refer to the text. Reprinted from Coatsworth & Castle (1990, p. 2).

One of the improvements to this system is the application of a vacuum to the cavities to encourage the flow into the wheel from the hopper and assure accuracy in the fill dose weight. Omnidose is one of the Harro Höfliger (Germany) products for dosing from 1 to 50 mg of powder and includes the vacuum system to a dosing wheel. Figure 2.5 shows its operation.

The key difference between this machine and a conventional dosing wheel is that it features a port at the base of the cavity that allows a vacuum pressure to be applied to hold the dose in place and assist the uniform powder flow from the powder bed into the cavity. This technique is used for filling micro-doses or powders with very cohesive properties. This machine is generally used in the formulation stage of development for new products or clinical testing phases.
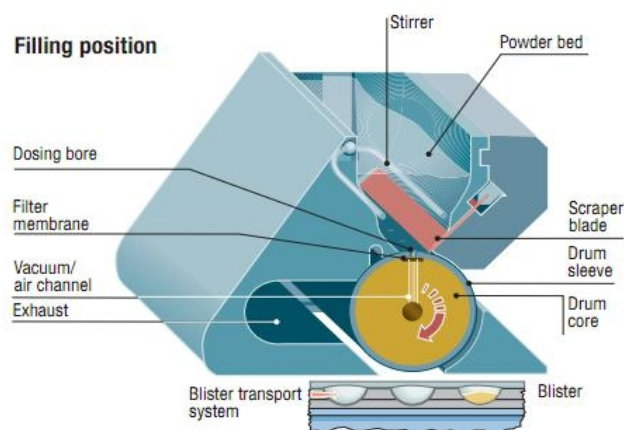
Figure 2.5. Omnidose by Harro Höfliger company, dosing wheel system with vacuum principle. For full explanation refer to the text. Re-printed from Omnidose Harro Höfliger customer leaflet.

2.2.2.2. Hot-melt extrusion principle

Extrusion technology has been widely used in the plastics industry for many years, but is a relatively recent application for the pharmaceutical industry. The objective, of the extrusion, is to convert a particulate material into an agglomerated product with uniform shape and density by forcing it to pass through a die under controlled conditions. It has been used in the pharmaceutical industry for the manufacture of dosage forms as tablets, pellets, granules and capsule filling.

Breitenbach (2002) describes this application in the pharmaceutical industry and figure 2.6 overviews the system. The principle consists of feeding a pharmaceutical blend (mix of polymer, drug and/or other excipients), into an extruder. Once the powder is fed into the system, it is forced through a barrel by one or two reducing capacity (tapered) screws which generate the high axial load required too extrude the blend through the end plate die, which determines the shape of the product. The extruded product is then cut to generate the individual doses. Successful extrusion requires, the correct level of moisture and heat are input into the material to melt the blend, in some cases electric or liquid heaters mounted on the barrel apply additional heat.
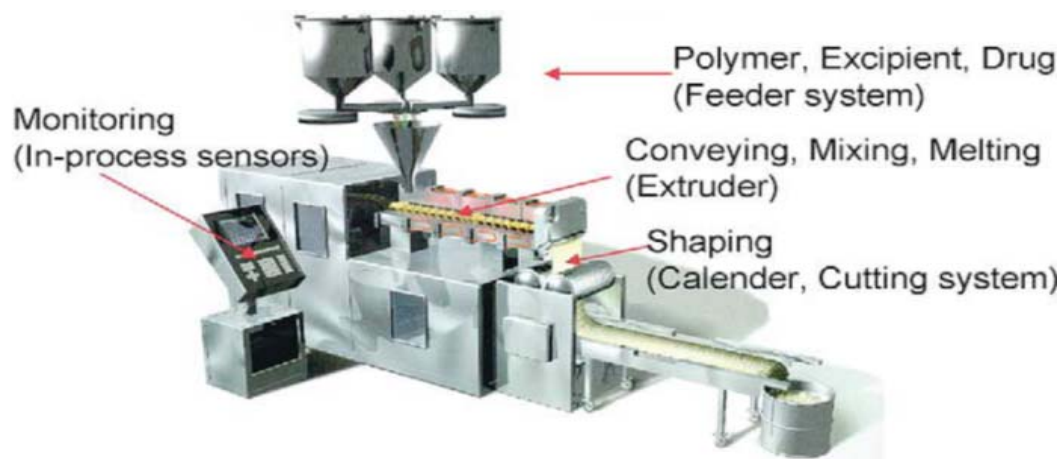
Figure 2.6. Hot melt extrusion principle. For full explanation refer to the text. Re-printed from Breitenbach (2002)

Different factors affect the final product as powder flow properties, shear force, residence time and pressure, screw design, cooling rate and shaping. This principle has advantages such as; the mixing and coating of the drug with other excipients, the uniformity of the density of the dosage form, the accuracy of the drug in the mix and good product dissolution properties.

2.2.2.3. Tamping filling systems

Tamping machines are also called dosing disc systems and use some of the features described in the previous sections. This is one of the major systems used for capsule filling. Podczeck & Jones (2004, p. 126) describes the operation of this system.

In these machines (see figure 2.7), the powder is contained in a cylindrical powder bowl that contains, at the bottom, a removal dosing disk with six dosing bores; a brass tamping ring in turn supports the dosing disk. The powder bowl rotates 360° degrees stopping at six stations with matching dosing bores. Normally the powder is fed from a hopper, to a dosing cone, which helps to distribute the powder horizontally into the powder bowl. As the dosing disk rotates, the first bore is partially filled through the gravity flow the powder in the bowl and then is tapped by a pin or "tamping finger". This process of partially filling and tamping is repeated in the following four stations until the required dose is obtained. The plug formed is transferred to the capsule body in the sixth station and rejoined to the capsule cap. The tamping force is generated by calibrated springs to avoid excessive pressure being applied to the powder at each tamping station, to maintain a relatively low plug bulk density as; excessive compaction hinders drug disintegration and dissolution in the patient's body.
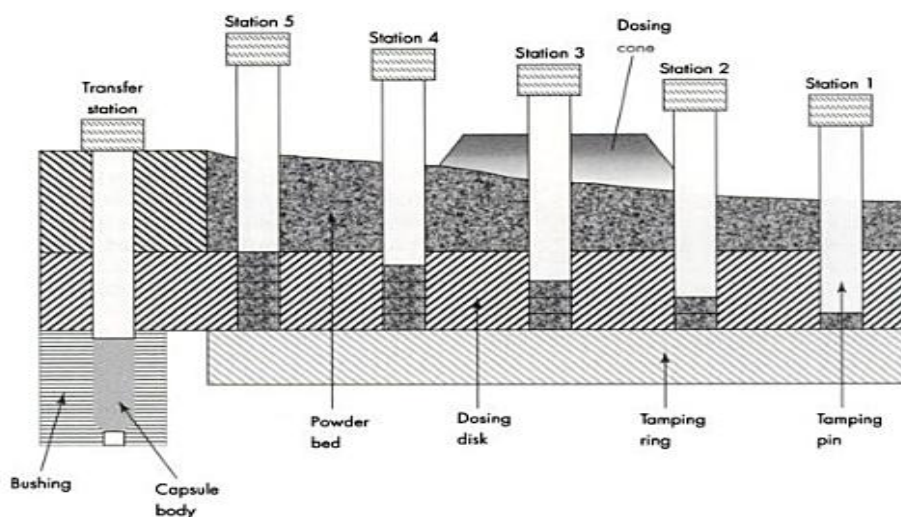
Figure 2.7. Tamping-filling mechanism. For full explanation refer to the text. Re-printed from Podczeck & Jones (2004, p. 127).

The fill weight on these machines depends on the pressure applied by the tamping pins, the powder bed height and dosing disk thickness; hence the latter two are controlled by the powder flow properties. Most of the powder actually enters to the dosing bores under gravity during the rotation rather than being pushed by the tamping pins (as is the common thought). Therefore this system relies on the powder flow properties (cohesion, friction). Taking account of the fact that powder behaviour tends to change from batch to batch this can cause production problems because machine settings may need to be adjusted following a batch change.

Tamping machines have up to 18 tamping pins per stage and can produce up to 150,000 capsules per hour. Tamping and dosator machines are the most representative capsules filling systems in the pharmaceutical industry. Both system compress the dose and use similar principles.

2.2.2.4.   Dosator nozzle machines

This type of filling system is the focus of the study in this thesis. The dosator comprises two parts, the body and the pin. The function of a dosator is to obtain small doses of powder all of the same target weight, from the bulk container of powder and transfer the dose to the packing receptacle.

a)   b)   c)
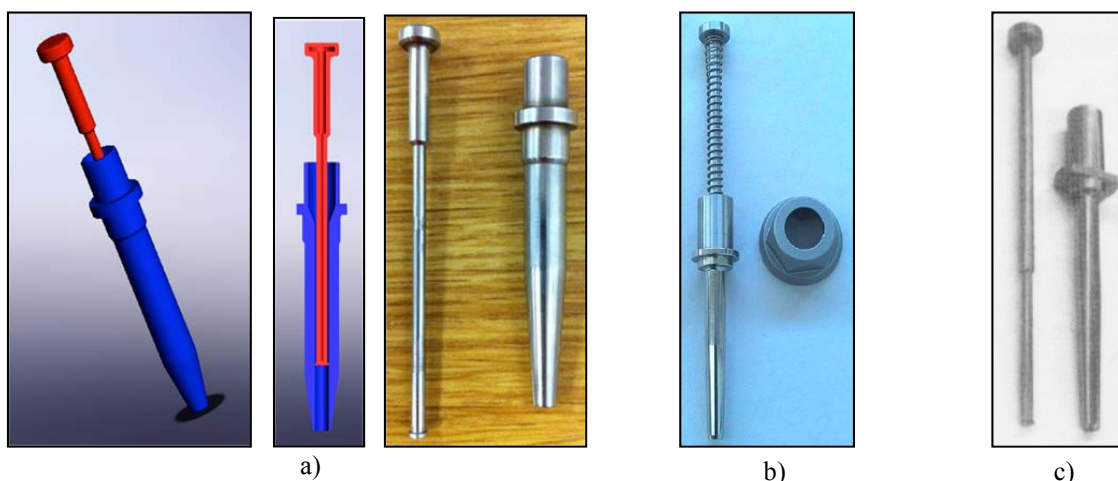
Figure 2.8. Dosator's pin and body designs: a) dosator used in this research provided by GSK; b) MG2 dosator (re-printed from customer leaflet); c) Harro Höfliger dosator (re-printed from Podczeck & Jones 2004, p. 130). For full explanation refer to the text.

Figure 2.8a shows the dosator used in this research (provided by GSK) and it is one of the various dosators used by GSK for the production of its products; the body, (blue), and the pin, (red), have a range of designs depending on the manufacturer and the application (see figures 2.8b and c). They are generally made from stainless steel. The dosator pin and dosator body internal diameter, shown in figure 2.8a, are Φ 3.375 mm and Φ 3.4 mm respectively (for more details of the dosator design used in this research refer to appendix 1).

As mentioned in chapter 1, the focus of this project is pharmaceutical filling systems. In order to develop the analytical dosator model, it was necessary to investigate the different

dosator machines operation applications and the factors affecting the fill dose weight; these are described in the following section.

Dosator systems could be a mix of the different filling systems mentioned earlier in this chapter. In this system generally the powder is fed from a hopper into a particulate bed of powder. The dose is obtained by compressing the dosator body into the powder bed and then transferring to the dosage form, where the pin is used to eject it.   More details of dosator principle and dosator filling machines are described in depth in the following section.

The relative standard deviation (RSD) of this dosing system is approximately 2% (Edwards 2010, p. 196) and the process is capable of producing approximately 3,000 to 250,000 capsules per hour (see table 2.3 showed later in this chapter), making this technology useful for the manufacture at both small-scale trials and full-scale manufacturing.

It is difficult to select the best or most universal filling system available in the market or to choose a dosator as the best filling system. There are several solid dosage filling systems existing and dosator is just one of them with pros and cons for different powders or range of packing presentations.

2.3.   Dosator filling machines

As mentioned previously, this section covers the most important aspects of dosator filling machines and its operation. It presents an overview of the principles, manufacturers, types, applications, trend and some features of this filling system. The content is focused on the powder filling operation and the main two dosator applications - capsule filling and dry inhaled powder filling products.

2.3.1. Dosator background

The original inventor of the dosator filling system cannot be traced in the literature, but it is likely that the idea came from Italy. Dosator filling machines appeared due to the increased drugs demand during the World War II and the first company, reported in the literature, to

commercialise dosator capsule machines was Zanazi (Italy) with the LZ-55 model in the mid 1950's (Jones 2006, p. 6).

It is believed that the dosator principle was derived from equipment for dosing cachets and Colton's automatic machine (Jones 2006, p. 5-6). Figure 2.9 shows the capsule body holder from Colton capsule filling machine in 1913, which was immersed into the powder bed as many times as required to achieve the fill dose weight desired. Figure 2.10 shows the device used to manually fill powder into cachets. The powder was compressed into the device in a separate receptacle (flat discs containing the same dimensions of the cachets) and ejected into the cachets obtaining the same fill weight in each cachet. The device was invented by Digne and was called "compresso-doseur"; these machines arrived in pharmacies in 1890's (Jones 2006, p. 5).
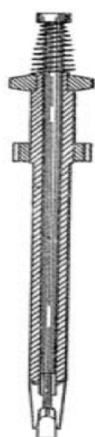
Figure 2.9. Colton's capsule body holder. Re-printed from Jones (2006, p. 3).

Figure 2.10. Manual device for filling cachets with powder. Re-printed from Jones (2006, p. 5).

From the early versions of dosator capsule filling machines, some features, like automatic separation of the capsule body and cap, were rapidly developed and the output was around 3,600 capsules per hour (Jones 2006, p. 6). Machines have evolved over time and they are now robust, modular, fully automated, with higher production capacity, efficiency, and control weight systems. Currently machines can produce up to 250,000 capsules/doses per hour (stated later in section 2.3) with range of dosator's geometry to produce different fill weights described later in this chapter.

2.3.2. Dosator principles

As mentioned before, a range of dosator operating principles can be found in the market and the differences between them vary principally on the manufacturers' experience in the field and the powder flow behaviour. One manufacturer might use different dosator operating principles according to the powder flow behaviour and the dosage application.

| 1. Incoming Stage | 2. Compaction Stage | 3. Retraction Stage | 4. Doctoring Stage | 5. Ejection Stage |
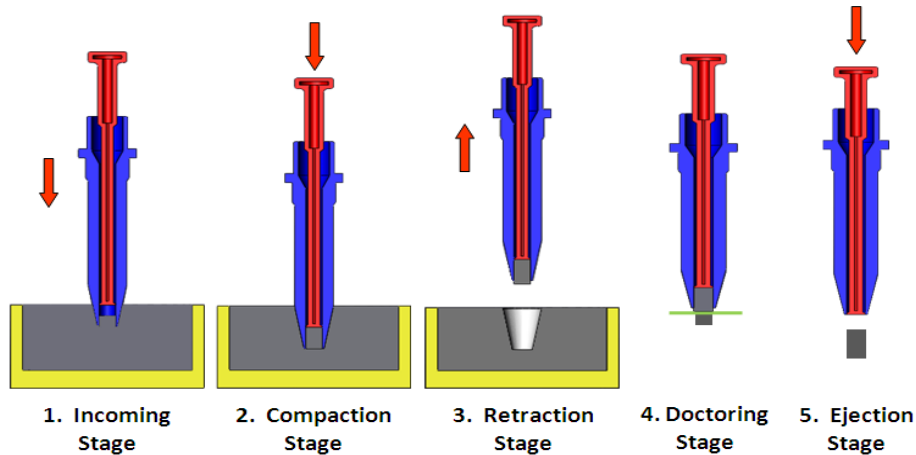
Figure 2.11. Dosator principle used in this research. For full explanation refer to text.

Figure 2.11 shows the dosator operating principle of interest in this research project (mainly used for dry inhaled powders). The powder is fed into a vessel, which is usually a rotating bowl and the system attempts to pick a powder dose with consistent, volume, bulk density and a smooth surface (without voids) and hence dose weight. The central plunger of the dosator (identified with red colour in figure 2.11) can be set a given height to form a cavity that will shape the dose. The filled weight is a function of powder density, which is related to the powders "state of compaction" and other variables. Variations to this principle are applied to obtain a "better" dosator performance in specific applications.

In stage 1 (of figure 2.11) the dosator is inserted into the powder bed to fill the defined volume (with a prefixed position of the plunger). Inserting the dosator deeper within the powder bed can create a volumetric element of powder compression or densification. In stage 2, the powder fills the cavity and the dosator reaches the end of the stroke. This action causes a small degree of compaction sufficient to lock the dose within the dosator. During the dosator insertion and once the dosator cavity is filled, the powder ahead of the dosator underside is either spread aside or compacted against the bottom of the bowl. In stage 3, the dosator body and pin are now retracted from the bed of powder. When the dosator assembly

is removed it should retain the plug of powder within the cavity. In stage 4, due to the cohesive nature of powders, often more powder than required is adhered to the underside of the dosator and is doctored/removed in a doctoring stage (note that this stage is not often applied in the industry), by means of a doctoring blade/tool. In stage 5 the dosator is moved over the required receptacle and moving the pin downward ejects the powder. The cycle is repeated, by either the powder bed and/or the set of dosators (as explained later in section 2.3.4.1) rotating ready for the next stroke.

Generally the machines incorporate a "re-conditioning" system to keep the powder bed level and state as homogeneous as possible. In essence the bed is ploughed over using a row of vertical pins submerged in the bed, then refilled using a hopper and finally re-levelled to a fixed height using a scraper. Section 2.3.6 of this chapter will discuss these systems in detail.

In contrast to the tamp-filling machines, in a dosator the plug is produced in a single compression step (giving more homogeneity of the bulk density). However, for effective dosing the powder must exhibit a critical degree of cohesive strength. If the dose is free flowing it can discharge prematurely under gravity between the retraction and ejection stages (e.g. stages 3 & 5 in figure 2.11). If the dose is too cohesive the powder will not fill consistently into the dosator during the incoming and compaction stages (e.g. stages 1 & 2 in figure 2.11). It was found in this research that the dose retention into the dosator is dictated by the ability of powder to retain lateral stresses and this topic is discussed in chapters 3, 4 and 5. The dose retention, powder flow properties requirements and factors affecting dosator operation are discussed in depth in chapters 5, 7 and 8.

The process typically delivers doses in the 20 to 800 mg range and the plugs are compacted with up to a 30 N force, as measured in this research work (see trials undertaken in dosator test-rig at The Wolfson Centre discussed in chapter 7). Other authors had published different magnitudes, for example Jones (2001) mentioned forces measured by other researchers from 25 N up to 130 N in filling capsules. The reasons of this discrepancy between the values could be the dosator principle applied and the powder flow properties. The powder particle sizes in this filling system normally vary between 40 and 500μm depending on the application.

The dosator operating principle can yield poor manufacturing performance, for very cohesive (fine) powders, and also as a result of unanticipated variations in the powder properties from batch to batch. Some of the problems involved in such a process concern the optimisation of the fill accuracy and reproducibility. Improvements to the dosating process have typically involved either compacting the powder contained in the cavity or the powder bed and impeding the induction of air into the cavity (for example by retracting the dosator piston as the apparatus moves through the powder bed). Appling a vacuum to the base of the powder bed and to the end of the piston can also generate benefits according to the available literature of dosator manufacturers.

The simplistic operating principle described above has been used in this research in order to identify the variables involved in the process, with the intention that this could be the starting point for an improved understanding of the dosator process. Thus, leading to the development of new operating principles and or better control of the key system variables in existing dosator systems.

2.3.2.1. Other dosator principles

Each manufacturer has their own system, design and operating principles, by which they provide a range of solutions and options to customers; they also provide the option for pharmaceutical manufacturers to customise the machines and engineer them according to their products and production needs.

As an example the operating principle of the MG2 machines (Gamberini 1985) is shown in figure 2.12. In stage 1 the central plunger strokes down until the dosator underside and powder bed are at the same level. In stage 2, the plunger is fixed and the dosator body is moved downward to create a dosing chamber, higher than the dose height desired; afterwards in stage 3, the dosator assembly descend and the cavity is filled until the end of the dosator stroke. Extra compression to the dose might be applied in stage 4, if required by the powder flow behaviour, by lowering the central plunger until the required dose height/density is achieved. Before the extraction of the dosator from the powder bed, in stage 5, the central plunger rises slightly leaving the dose slug free of contact. Finally the dosator retracts from the bed, in stages 6 & 7, to eject the dose in stages 8 & 9. Note that the dosator position changes between the stages 2 & 3 and stages 5 & 6 and it is due to the type of operation used

by these machines; it is described in section 2.3.4.1. The dosator in stage 10 moves up to be ready for the next stroke.
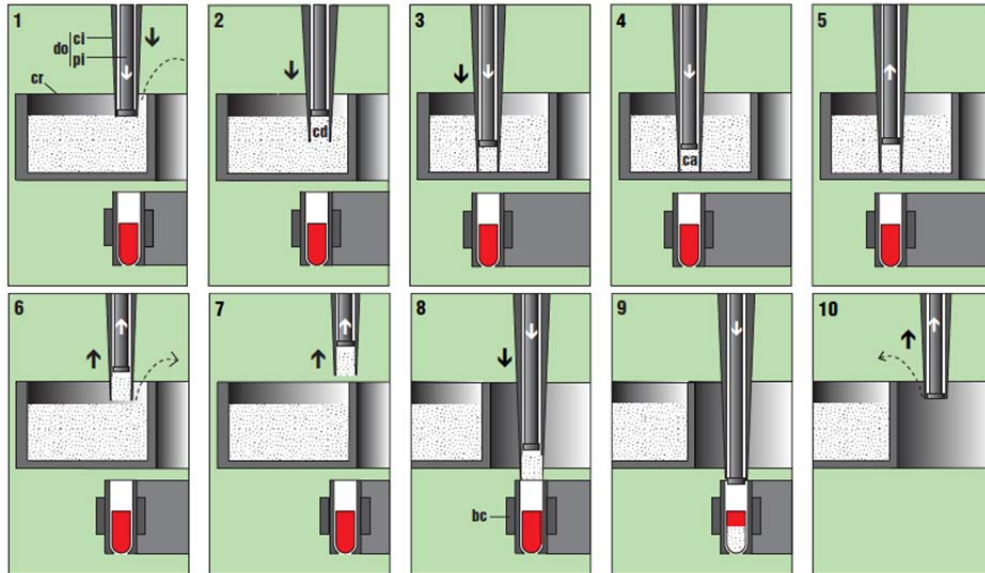
Figure 2.12. MG2 (Italy) dosator filling machine principle. For full explanation refer to text. Re-printed from MG2 customer leaflet.

Another example is the operating principle used by Zanazi series capsule filling from IMA (Italy), shown in figure 2.13.

| 1. | 2. | 3. | 4. | 5. |
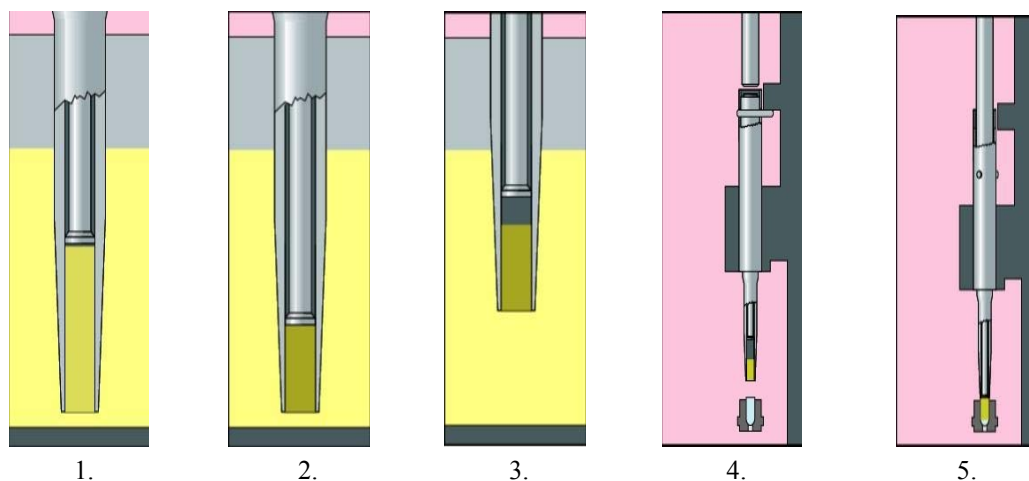
Figure 2.13. IMA (Italy) Zanasi dosator filling machine principle. For full explanation refer to the text. Re-printed from animation and customer power point presentation provided by IMA (Italy)[1].

In stage 1, the dosator assembly is inserted into the powder bed, and the central plunger is pre-fixed above of the required dose height. Once the dosator reaches the end of the stroke, in stage 2, the plunger is lowered to give extra-compression to the plug to the required dose

---

[1] Dosator animation provided by Pietro Pirera IMA's Product Manager for Encapsulation.

height/density. In stage 3 the dosator is retrieved and at the same time the central plunger is raised to leave the plug free of contact. In stages 4 and 5, the dose is transferred and ejected to the powder receptacle.

Figures 2.14a, b, c and d describe the three variations in the principle of operation of the dosator that are used and developed by GSK (Duffield 2005). For variation one, shown in figure 2.14a, the principle of operation is as follows. In the first stage, the pin's face and the dosator body underside are set at the same level, in the second stage they are lowered into the powder bed, compacting the powder ahead of the dosator. In the third stage the dosator pin is raised to the required dose length while the body is kept fixed. In the fourth stage the dosator moves downward forcing the slightly compacted material into the dosator assembly until the end of the stroke. In the fifth stage the dosator is retracted and the dose transferred to a blister pack and ejected in the sixth and seventh stages respectively.
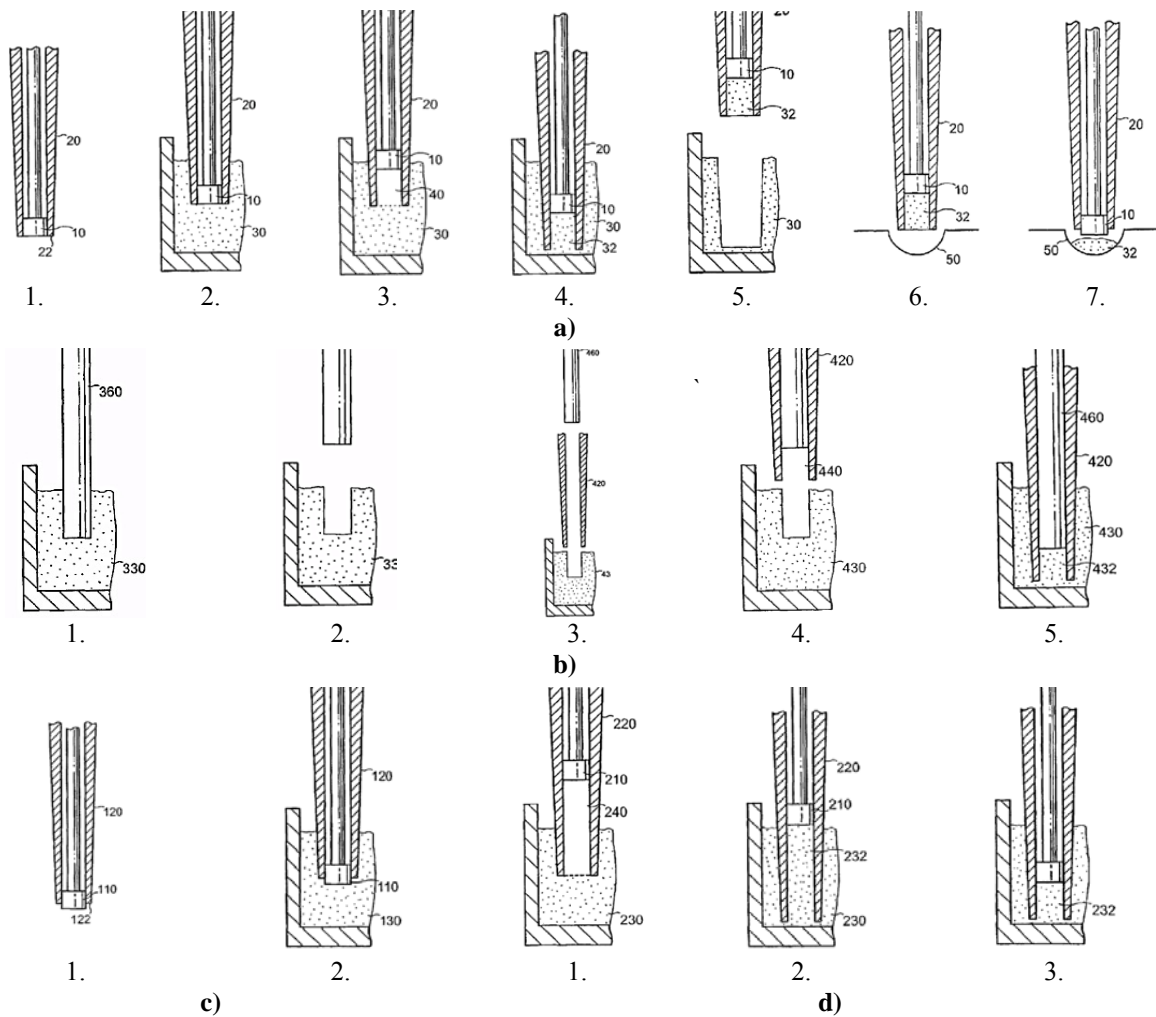
Figure 2.14. GSK dosator principles. For full explanation refer to the text. Re-printed from Duffield (2005).

The dosator operation principle, variants two, three and four use different methods to pre-compact the dose. The objective of this pre-compaction of the bed (stage 2 of variant 1 above), is to remove the air pockets and create and homogenous bed. This can also be achieved (variant 2) through the insertion of an external device as described in figure 2.14.b, where the powder bed is compacted by descending a rod with the same diameter as the dosator. Another approach (variant 3) shown in figure 2.14.c is as follows. In the first stage, the dosator pin protrudes below the dosator body, before pre-compacting the powder bed in the second stage. For the final variant (4) shown in figure 2.14d, the pre-compaction process is as follows. In the first stage the dosator pin is raised height equal to the stroke length. In the second stage the dosator body and pin are lowered into the powder bed and the cavity is partially filled. In the third stage extra compaction is applied to the dose, by adjusting the pin to the dose length required.

As can be seen in this section, there are ranges of different dosator operating principles that have been developed either by equipment or pharmaceutical manufacturers and all of them are similar. Nevertheless, the majority of principles modify first the powder bed conditions by pre-compacting the powder ahead of the dosator tip in one way or another. The aim is to have a uniform bed without voids, therefore the dose weight variation is minimised. On the other hand, Tan and Newton (1990b) found that the most uniform dose weights were achieved when no compressing force was applied during the filling process. They reported that increment of compression affected the repeatability of the fill weight, but did not explain why.

With so many different principles of operation available in the market, how does one decide which is the most appropriate for a given application. Is there a dosator operating principle that will work reliably for any powder? Is there a unique, efficient and reliable universal dosator filling machine? In practice it is likely that the differences in the flow properties of the materials being dosed e.g. level of cohesive strength, compressibility, wall friction may suit different operating principles. However the main problem to be addressed by this thesis is the lack of *understanding* of the dosator operation, and how the powder flow properties interact with the different dosator stages.

Once the dosator principle and the process are understood, then the factors affecting the system could be controlled and adjusted to obtain doses with the different characteristics required. By using the most simplistic of the dosator operating principle as described in figure 2.11, it is hoped that this research can deliver an understanding of the powder

behaviour and controlling machine factors (discussed in chapters 5, 7 and 8), in a process that has fewer steps than the ones offered by the machine manufacturers. This thesis proposes a phenomenological explanation of what happens during the dose procurement (described in chapter 8) and this could be a starting point for the development of other principles or the unification of the existing principles or the standardisation of new procedures.

2.3.3.   Dosator applications in the pharmaceutical industry

The main applications of dosator systems in the pharmaceutical industry are the filling of hard capsules and dry inhaled powders.   The differences between them are the packing presentation, the compression requirements of the dose and the fill dose weight.

Currently filling machines are modular and integrate the whole process in one single machine; dosator manufacturers build specific machines to a given pharmaceutical manufacturer's request.   Figure 2.15 shows an example of a capsule filling machine from IMA's (Italy) Zanasi series.   In the stations 1 and 2 the empty capsules are fed, opened and orientated.   Once the capsule body is ready, the dose is procured in the stations 3 and 4 from a dosing system, for example using a dosator or tamping principle.   Then, in stage 5 the machine removes any defective capsules and finally the capsules are closed, ejected and the bushings cleaned for the next cycle in the stages 6 to 8.   The machine modules are interchangeable, likewise the same powder can be filled in different capsule sizes, or other packing presentation, or the same capsule can be filled using different filling system.
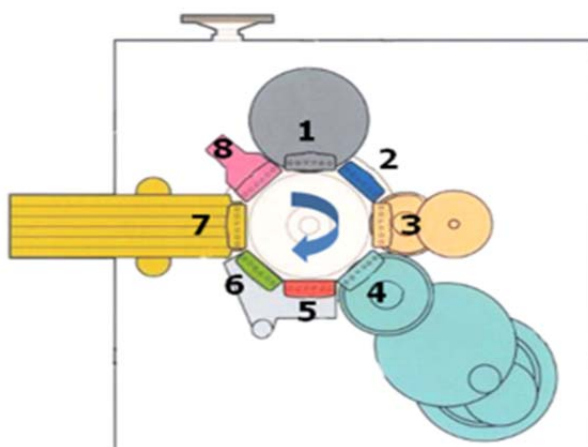
Figure 2.15. IMA's (Italy) Zanasi capsule filling machine stations. For full explanation refer to the text. Re-printed from IMA's customer leaflet.

Regarding to the capsule filling application, two kinds of capsules exist, namely hard and soft (Podczeck & Jones 2004). Hard capsules are used for powder dosage forms and are composed by two parts: the body and the cap. Soft capsules are a one-piece capsule usually used for liquids doses. Dosator systems have been the mainstay of capsule fillers for many decades and can fill capsules with a range of materials in powder, pellet, granule or liquid form. Most of what is known about the dosator operation, and its development, is due to the research in capsule filling from early 1970's to date (Jones 2006).

Capsule dimensions				
Capsule size	Cap diameter [mm]	Body diameter [mm]	Locked length [mm]	Capsule volume [mm^3]
000	9.91	9.55	26.10	1.37
00	8.53	8.18	23.30	0.91
0	7.64	7.34	21.70	0.68
1	6.91	6.63	19.40	0.50
2	6.35	6.07	18.00	0.37
3	5.82	5.57	15.90	0.30
984	5.32	5.05	14.30	0.21
5	4.91	4.68	11.10	0.13

Table 2.1. Example of hard gelatine capsule dimensions and filling capacities by Capsugel. Data obtained from www.sepha.com.

Dosators can fill most of the capsule sizes available on the market. Table 2.1 shows the general hard gelatine capsule sizes produced by Capsugel and a range of pharmaceutical companies uses these. Capsule size 5 is very small and difficult to handle in automatic machines, but is widely used in Phase I and clinical trials. The largest size 000 is used in veterinary applications.

Dosator Dimensions		
Dosator internal diameter [mm]	Capsule size	Dosing volume range [mm³]
3.4	5	30 – 120
4.2	4	58 – 183
4.8	3	87 – 257
5.3	2	120 – 340
5.8	1	160 – 450
6.5	0	225 – 615
7.3	00	305 – 875

Table 2.2. Harro Höfliger dosator dimensions for different capsule size. Data provided by the industrial sponsor.

Some dosator manufacturers had also standardised the dosator dimensions based on the capsule sizes available. Table 2.2 shows the range of Harro Höfliger dosator internal

diameter dimensions used by GSK in the manufacturing of their products. Sundry dosing volumes values can be achieved by adjusting the dose length (plunger/pin height) in the operation.

According to Augsburger (2002, p. 336), after tablets, capsules are the second most used dosage delivery form. Some of the benefits are as follows: tasteless, odourless, easy to swallow and attractive in visual presentation. Due to their simplicity, some Phase I development studies and initial clinical trials are undertaken using capsules. Capsules should be as small in size as possible to facilitate swallowing and for cost reduction purposes (packing and shipping costs); based on this, one disadvantage is the selection of the size as it is governed by the powder bulk density and some powders are difficult to fill into small sizes. There is also the problem of working in a non-controlled environment, as the moisture contents of the powder or storage environment can make the capsule soft, brittle or sticky.

More recently dosators have been used for filling respiratory powders. These applications place more demanding requirements on equipment. For deposition in the lung, doses are generally smaller, in the 10 and 20 mg range, with mean particles sizes of 5 μm or below (DEF Pharma website). The doses cannot be compacted to the same degree, as in capsule filling, and contain high proportions of fine particles. Any lumps or degree of compression, when patients inhale the powder from the delivery device, is likely to negatively impact to the dissolution and efficacy of the product.
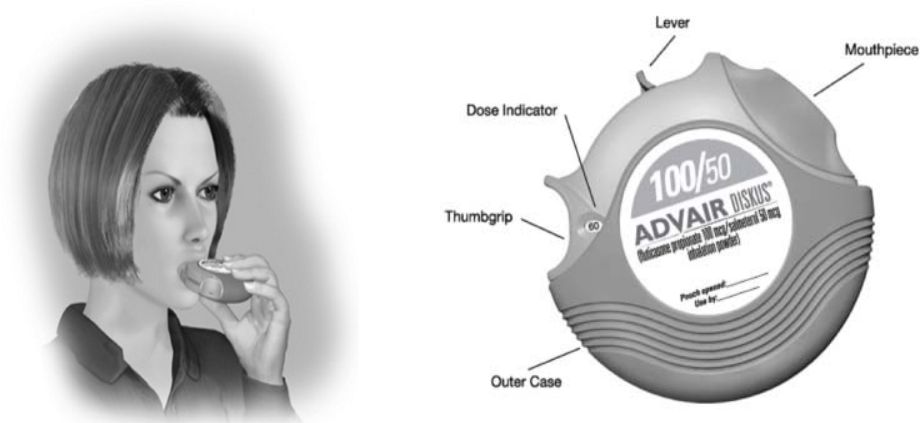
Figure 2.16. DISKUS respiratory delivery device, dry powder inhaler (DPI). Re-printed from GSK website.

Pulmonary administration is attractive to pharmaceutical companies for a variety of reasons, not only for local therapy in the lungs, but also for systemically acting drugs. Some of the

major advantages of this administration system are the rapid and predictable drug action, reduction of the dose weight and reduction of drug side effects.

a)   b)

Figure 2.17. DISKHALER, dry powder inhaler (DPI). a) delivery device, b) blister. Re-printed from GSK website.

Respiratory powders are filled into different powder receptacles the shape of which depends on the delivery device design. Dry inhaled powders are delivered to the patient using Dry Powder Inhalers (DPI's) (see figures 2.16 and 2.17) and blisters are normally used to load them with the product (see figure 2.17b).

In comparison with capsules, the doses in blisters are smaller and they can be from doses to long strips with different designs. Figures 2.16 and 2.17 show two examples of DPI's design used to deliver GSK products to patients. The blisters are placed into the DPI's where the plug is turned back into the "free powder form" (by means of the internal mechanism), and the patient finally inhales the dose.

The dosator principle plays an important role in filling dry inhaled powders, as the doses need a controlled degree of compaction, to ensure the DPI can reliably turn the plug back into a powder form for efficient delivery into the patient's body. Pulmonary powders normally need smaller quantity of the drug and variations of the dose weight in the production lines will affect the patient health.

2.3.4. Types of dosator filling systems

Irrespective of the dosator principle selected to obtain the dose, filling machines normally work on either continuous or intermittent basis (Podczeck & Jones 2004, p. 130). In the first case, the dosator obtains and ejects the dose in continuous motion, whereas in the second case, the dosator strokes vertically up and down in two separate movements and then either the dosator or the powder bed moves to eject the dose. The dosator pin is normally driven by hydraulic or pneumatic systems or spring return to retract the plunger. In the following sections the two systems are described.

2.3.4.1. Continuous dosator machines

Figure 2.18 presents the continuous dosator system used by MG2 (Italy) and shows the dosator position within the powder bed from the top and front view section of the machine; the stages in this figure are related with the stages presented previously in figure 2.12. This dosator system was first developed by MG2 in Italy (Ridgway 1987, p. 95).
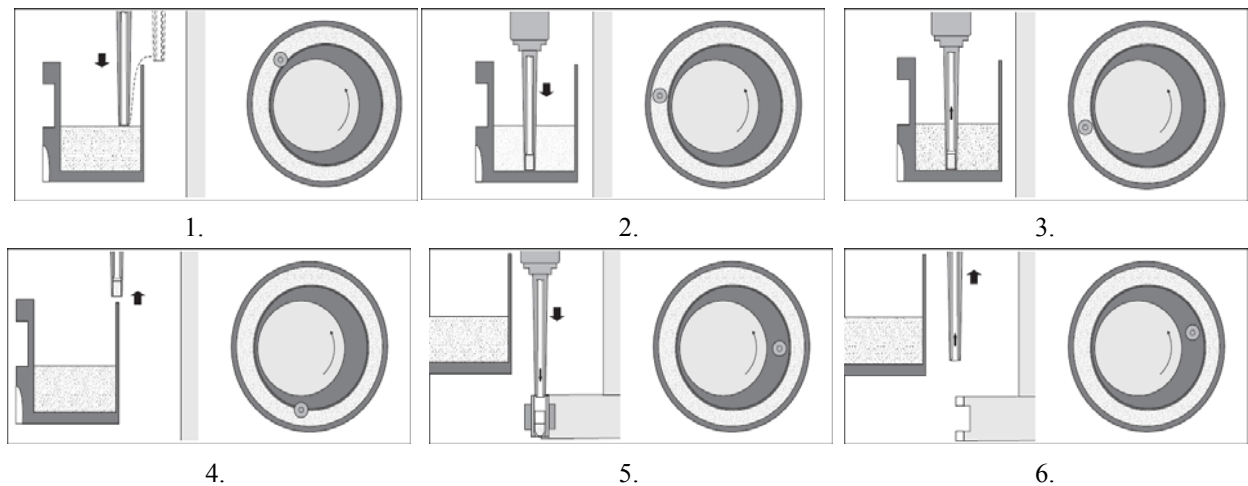
Figure 2.18. MG2 (Italy) continuous dosator machine. For full explanation refer to the text. Re-printed from MG2 customer leaflet.

In continuous machines, dosators are fixed to a turret, which it has smaller diameter than the off centre circular powder trough. Both the turret and the powder bowl rotate in the same direction at different speeds in a continuous movement. In the stage 1 and 2, the dosator descends diagonally leaving a furrow in the powder bed depth (see figure 2.19) and it travels from close to the inner wall to the middle of the trough due to the eccentricity between the

turret and bowl; once the dose is obtained, the dosator is diagonally lifted, in the stages 3 and 4; it continues travelling to eject the dose, outside of the trough, in the stage 5, and finally in the stage 6 the dosator is ready for the next cycle (Information provided MG2[2] and extracted from MG2 customer leaflet).

Figure 2.19. MG2 dosator filling machine. Pictures taken by The Wolfson Centre in a site visit to MG2 plant with MG2 approval.

MG2 is the leading manufacturer of this operating system; more information about their machine series and production capacity will be presented in section 2.3.5.

Some of the advantages of continuous motion machines are the large output range of doses and the reduced level of impact forces, in comparison with the pneumatic/hydraulic driven intermittent motion machines.

2.3.4.2.   Intermittent machines

Intermittent motion is probably the most common operation used in the industry. Figure 2.20 shows the Zanasi intermittent capsule filling machine from IMA (Italy), where from 6 to 64 dosators are grouped into two equal sets (of 3 to 32 dosators[2]). In operation (stage 1), the first set of dosators descend into a bed of powder and fill the cavity (stage 2), while at the same time the second set of dosators are positioned over the packing presentations where the doses are simultaneously ejected by the piston action. After the group of dosator have been lifted, they swap positions (stage 3) and the process is repeated.

---

[2] Information provided by Leonardo Ercolani, MG2 S.L.R.

<div align="center">1.   2.   3.</div>
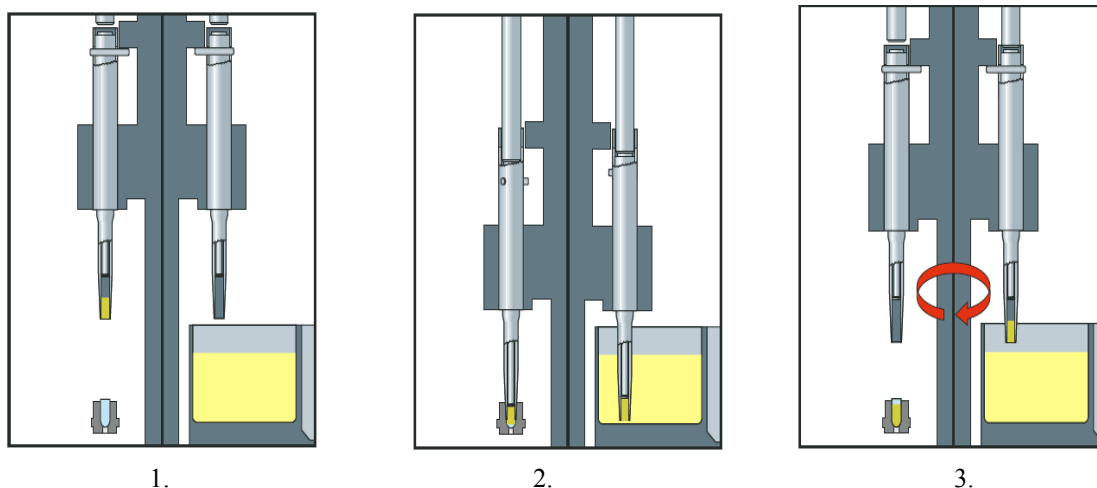
Figure 2.20. IMA's Zanasi intermittent capsule filling machine. For full explanation refer to the text. Reprinted from customer leaflet.

Harro Höfliger, IMA and Macofar are some of the representative manufacturers of this type of machine operation; dosator intermittent machine series of each manufacturer are mentioned in section 2.3.5.

The operation described above is the most common intermittent dosator system; nevertheless there are other intermittent systems. In some machines, dosators only move vertically up and down and the bed of powder swap positions with the empty capsule body turret. There is also the case where an arm supporting a group of dosators (see figure 2.21), obtains the dose from the powder bed and then transfers it, to the ejection station. The dosator pins in this figure are operated by hydraulic system from the top and retuned by springs.
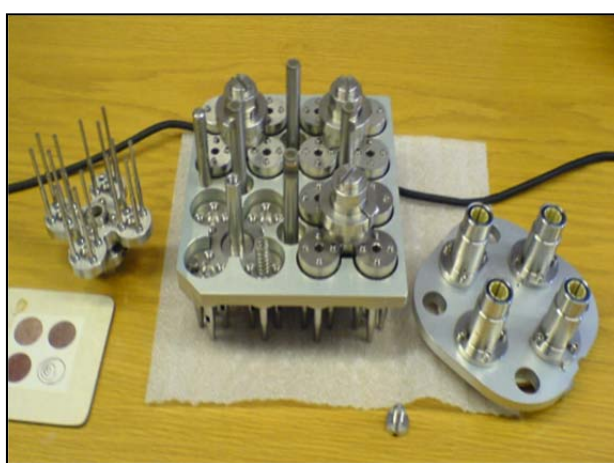
Figure 2.21. Marchesini Farcon filling head. For explanation refer to the text. Picture on the left provided by GSK industrial supervisors and the picture on the right taken by The Wolfson Centre in a progress meeting with GSK approval.

One of the advantages of the intermittent system is the reduced size of the trough with capacities as low as half a litre, despite of the large powder quantity of the continuous machines. The major disadvantage of these machines is due to the impact forces that are applied to the dose as it is transported between the filling and ejection stations.

2.3.4.3.   Enhancements of dosator filling machines

Apart of the conventional dosator machines seen in this chapter, recently other enhancements have been added to improve dosator performance in production lines. Manufacturers not only try to improve the operation by developing the dosator operating principles, they also try to improve the dosator performance with innovative features as outlined below.
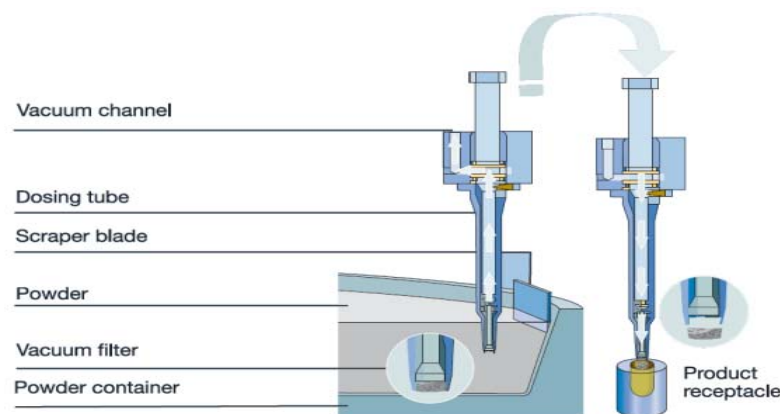
Figure 2.22. Harro Höfliger Modus C dosator vacuum system. For full explanation refer to the text. Re-printed from Harro Höfliger customer leaflet.

One of these improvements is to apply vacuum and/or air purge to the plunger (see figure 2.22) to secure the dose prior to discharge into a receptacle (Podczeck & Jones 2004, pp.131). The pin's face is replaced by a membrane, which is connected to a vacuum pressure line that assist the flow of powder into the dosator as it is dipped into the powder bed. When the dose is ready to be ejected, the negative pressure is reversed to give a mild air pulse. In this case the plug is not over-compacted and it is suitable for Phase I clinical trials through to full-scale manufacturing and dry inhaled powder applications where compaction of the dose is not required. Nevertheless, these systems are not suitable for blends with small particle sizes, as it is the case for dry inhaled powders with Particle Size Distribution (PSD) around 5 microns, that can pass through the membrane.

This method is interesting for pharmaceutical companies, as the adhesion of lubricants in the blend can be reduced or even excluded, and a range of freer flowing powders could be filled (Ridgeway 1987, p. 96). As the permeability of the material dictates the dose weight in this system and also assures the dose is locked into the cavity during transfer to the ejection stage, the air pressures can be adjusted to meet the powder flow requirements for manufacturing. A disadvantage is that the individual dosage tubes need to be independently calibrated, as central adjustment is not possible (Ridgeway 1987, p. 96). Vacuum dosators are mostly applied to continuous dosator machines and some of the manufacturers are Romaco (Italy), Harro Höfliger (Germany) and Perry Industries (USA).

Another feature incorporated into dosator machines is a system used to remove the excess powder which may protrude from cavity after the dosator is retrieved from the powder bed. As shown in figure 2.11, outlining the dosator operating principle used in this research, the extra material added at the bottom of the dose is removed in the doctoring stage. This stage was done manually in the experimental tests of this research (see figure 2.23), with a doctoring tool, designed for this purpose, where a fine wire removes the extra material at the bottom of the dosator.
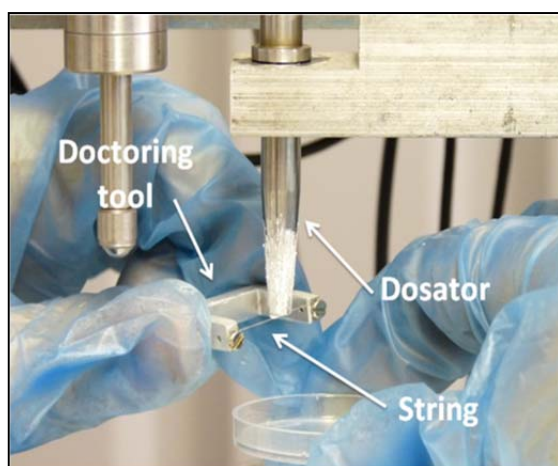
Figure 2.23. Doctoring tool used in this research to remove excess of powder at the bottom of the dose. Picture taken from The Wolfson Centre dosator single shot test-rig.
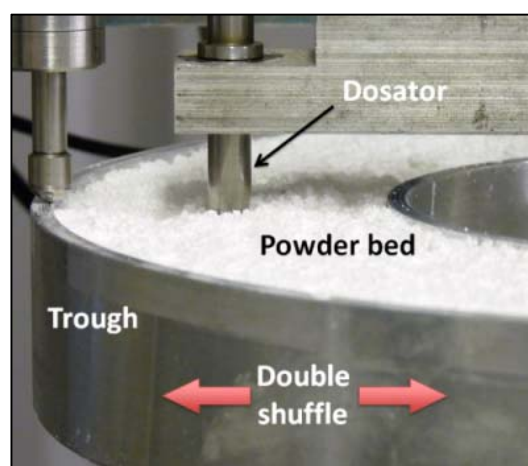
Figure 2.24. Double shuffle of the trough at the end of the stroke. For full explanation refer to the text. Picture taken from The Wolfson Centre dosator single shot test-rig.

Not many production machines use the doctoring system; however many intermittent machines series use a "double shuffle", a reversal of the direction of rotation of the powder trough at the end of the dosator stroke (see figure 2.24), to impart a shear stress across the tip to assist the remove the excess of material. Nonetheless, at the end of the stroke there is a gap

(named gap "h" in this thesis for simplicity purposes) between the dosator tip and the bottom of the trough and normally varies between 0.1 and 0.3 mm with tolerances from ±0.05 to ±0.4 mm[3]. This distance is not controlled in current industrial machines and this can have a dramatic effect on the consistency of the dose pre-compaction and fill weight. Chapters 7 and 8 present and discuss the problems associated with poor control of the gap at the end of the stroke (called gap "h" in this thesis), and as consequence of this the "double shuffle" might not achieve its purpose of removing excess of powder from the dose.

IMA (Italy), with the Zanasi series, offers another feature for dosator filling machines; the aspirating bowl solution to poorly compacting powders. The trough, containing the bed of powder, is equipped with a vacuum system that allows uniform and dense powder bed. The base of the powder bowl is fitted with a membrane connected to a vacuum system; once the bowl is filled, the negative pressure reduces the voids in the bed. IMA assures the constant dose density and lower variation of the dose weight using this vacuum system. Figure 2.25 shows the aspirating bowl manufactured by IMA.

Figure 2.25. IMA's Zanasi aspirating bowl. For explanation refer to the text. (Reprinted from Zanasi customer leaflet)

Another enhancement in dosator filling machines is the "clean-in-place" system (Podczeck & Jones 2004, p. 131). IMA with the Imatic series, which is equipped with this system, which performs a pre-washing, washing with detergent, rinsing and hot air drying.

Weight control is a very important feature in filling systems; current machines are equipped with advance systems. Some of them work with statistical weight control or weight control loop feedback (Podczeck & Jones 2004, p. 131). Meanwhile IMA uses laser light technology (Tarozzi 2006) to detect the height of the powder in the capsule and combine it with sensors

---

[3] Information provided by Pietro Pirera IMA (Product Manager for Encapsulation), Vittorio Calzonari MG2 (After Sales Manager) and Seyfang Karlheinz Harro Höfliger.

to infer the mass of product. Harro Höfliger on the other hand, with the Omni control Tablet and Capsule Nett Weighing machine, use microwave resonating technology to control the product weight[4]. The control weight of the filling machines is advanced and with this feature, faulty or partial filled capsules are removed instantaneously during the production. These reduce the occurrence of operational problems such as; failure of the dose during transfer and delivery, dose damaged during entry to the capsule body, doses with high/low density, empty capsules or blisters, capsules damaged during re-joining and some more described in chapters 7 and 9.

These enhancements are the most significant in the pharmaceutical industry for dosator filling machines and, as can be seen, there is a range of features and solutions for filling powders depending on the manufacturer, application and powder behaviour.

2.3.5. Dosator machines manufacturers

Many dosator manufacturers are located in Germany and Italy (Jones 2001), where early dosator machines were invented and first produced. Some of them are still family businesses and the most dominant dosator companies are: MG2, IMA and Romaco from Italy, and Harro Höfliger from Germany.

Dosator Manufacturers			
Manufacturer /Model	**Type of machine motion**	**Approx. Filling rate (Capsule per hour)**	**Machine options**
Harro Höfliger			
Modu – C Low speed (LS)	Intermittent	1,000 – 24,000	Vacuum dosator
Modu – C Mid Speed (MS)	Intermittent	100,000	
IMA			
Zanasi 6/12/25/40	Intermittent	6,000 – 40,000	Aspirating bowl and vacuum dosator
Zanasi Lab 8/16	Intermittent	8,000 – 16,000	
Zanasi Plus 48/70/85	Intermittent	48,000 – 85,000	
Imatic 100/150/200	Intermittent	100,000 – 200,000	
MG2			
Suprema	Continuous	48,000	
MG Compact	Continuous	6,000 – 48,000	
Planeta	Continuous	100,000	
G 70/100/140/250	Continuous	70,000 – 250,000	
Alterna A70	Continuous	70,000	
Labby R+D	Continuous	3,500	
Romaco – Macofar			
CD 40/60	Intermittent	40,000 – 60,000	Vacuum dosator

Table 2.3.   Actual main capsule filling dosator manufacturers.   Information collected it from manufacturer's website and customer leaflets.

---

[4] According to dosator Harro Höfliger's customer leaflet.

Table 2.3 list the main dosator manufacturers, their machine series, production capacity and type of dosator machines (for hard capsule filling applications). Manufacturers can also adapt these machines for respiratory applications, or design machines to meet customer requirements.

Figure 2.26 shows some of the dosator capsule filling machines listed in table 2.3, and shows the modular construction and integration of the whole process in one single machine.

Figure 2.26. Dosator filling machines: a) MG2 Suprema, b) MG2 G140, c) MG2 Compact, d) IMA Imatic 150, e) Harro Höfliger Modu-C, f) Romaco CD40. Re-printed from manufacturer's website and customer leaflets.

The Wolfson Centre visited MG2 and Harro Höfliger plants to see the capsule filling process, machine manufacturing and exchange knowledge about dosator filling systems. The outcome of these visits is presented in chapter 10.   The Wolfson Centre also visited Bosch, one of the principal manufacturers of tamping filling machines, as they expressed interest to work with dosators in the future.

2.3.6. Powder bed re-conditioning system in dosator machines

It was mentioned previously in this thesis that dosator principles and enhancements vary from one manufacturer to another and there is not a universal method, principle or device. In the same way dosator filling machines are equipped with various powder bed re-conditioning systems. The most common system is showed in figure 2.27a & b, which respectively shows the MG2 continuous motion capsule filler and the laboratory dosator test-rig (3PI intermittent motion dosator test-rig at GSK Harlow), which use the same basic system.

a)   b)
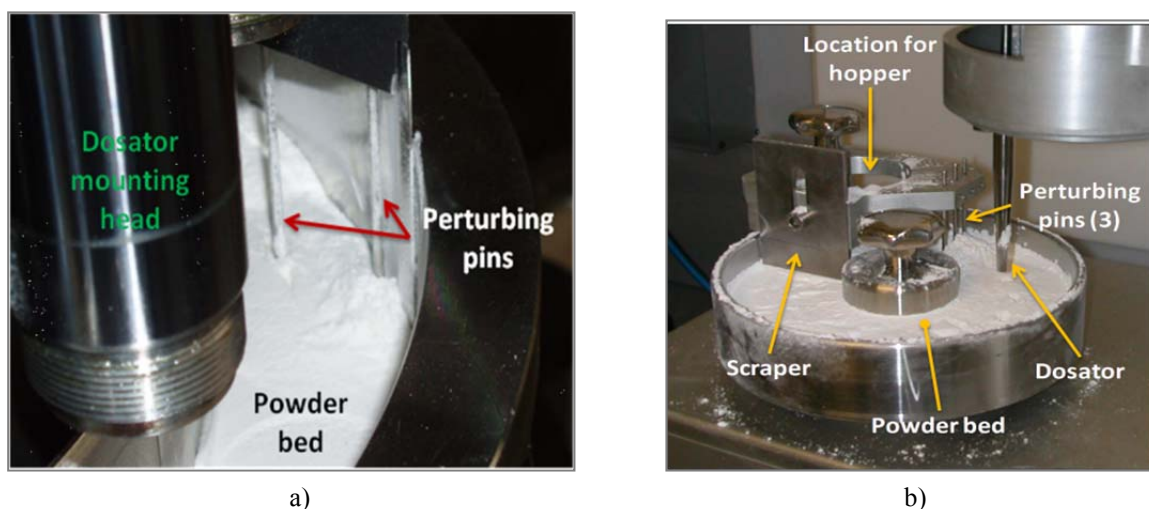
Figure 2.27. Powder bed re-conditioning system: a) MG2 continuous capsule filling machine, b) 3PI intermittent motion dosator test-rig property of GSK. Pictures taken by The Wolfson Centre at MG2 plant and GSK Harlow with the companies' approval.

After the dose procurement, the powder bed in the trough is perturbed by means of a number of vertical pins (normally three) that plough up the compacted zones in the powder bed left by the dosator strokes. Afterwards the trough is refilled with powder (fed from a hopper), and the bed levelled with a scraper ready for dose acquisition. Experimental tests undertaken in this research using the 3PI single shot test rig (described and discussed in chapter 9) indicated that this system does not provide a uniform and homogeneous powder bed.

2.3.7. Advantages and disadvantage of dosator systems

Dosator operation has numerous advantages and disadvantages in comparison with other filling operations and some of them are presented in this section.

Some of the advantages are as follows. Compared with tamping filling operation and tableting process, the dose is obtained and compacted in a single step, being more homogeneous in density. The stresses applied to the powder can be modified for specific applications, as dry inhaled powders demand low compression. A range of materials can be filled (not only powders) in different forms and quantities (most of the capsule sizes can be filled) by doing minor adjustments in the system. Capsules and respiratory blister packs are the major dosator filling applications, because the rapid local drug action and convenience of swallowing. The modular construction of the dosator machines allows the pharmaceutical manufacturers to modify the process, for example by changing easily the dosage packing presentation or the capsule sizes or the material to be fed, etc. Dosator manufacturers offer range of solutions and options to meet pharmaceutical manufacturer's needs as described in 2.3.4.3.

This filling system also has a few down sides, as follows. One of them is the waste of material from the bowl container; there is a greater volume of material than is actually used during the operation. For example GSK 3PI dosator test-rig has 26 mm powder bed width, 20 mm depth where approximately dosators with up to 6 mm diameter are used stroking in the middle of the bed; the rest of the powder in the bed is not used. With the current understanding of the process, it is not suitable for the dosage of small quantities (below 10 mg) and cohesive materials. The lack of operational understanding of the level of compaction of the dose due to machine setting factors that are not controlled, contribute to the variation of the dose weight and therefore potentially compromise the efficiency of the drug in patients (in applications like dry inhaled powders). For machines running intermittently, the material flow property requirements are even more demanding to ensure the dose is retained in the cavity prior to the ejection stage, while subjected to acceleration forces as the machine transfers dose from the pickup to ejection station. There is not a universal dosator operation principle, method, procedure or design. These machines do not include an environment control system to avoid variations in moisture content during the process (this issue increases the installation costs to the end user).

The advantages and disadvantages presented here are from the point of view of the dose procurement developed in this thesis.

2.4.   Pharmaceutical powders used in dosator systems

In order to understand the powder flow behaviour in dosator applications, it is important to understand what the pharmaceutical powders are composed of (what ingredients and excipients are used), their quantities and particle sizes; these broaden the understanding of the flowability of the powders during the operation. This section shows an overview of the blend ingredients normally used in dosator systems and their application like dry inhaled powders.

Pharmaceutical powders are normally blends composed of two or more ingredients. Normally, a fine Active Pharmaceutical Ingredient (API), which is the drug itself, and coarse inactive ingredients (excipient) compose the blend. The excipient could be dominant in one blend, depending on the product and application. Notwithstanding in dry inhaled powders it is often only one excipient (generally called a carrier); which in this type of blend is typically α Lactose Monohydrate, to which the API particles tend to adhere onto the surface.   In respiratory products, the powders are designed for the API (small and light) to attach to the carrier at the dose manufacturing stage and detach during the patient inhalation - following the air stream into the lungs. As the carrier is denser it won't be so readily entrained and it will end up in the digestive system.

The API is a raw material with typically very poor flow properties (rendering it difficult to handle), whereas excipients can be engineered for specific purposes. Excipients are numerous and they can be classified according to usage, for example: to reduce adhesion between powder and surfaces (anti-adherents), to give mechanical strength (binders), for coating, to help separation inside patients body (disintegrates), to increase/decrease bulk volume (fillers and diluents), to mask unpleasant API tasting (flavours), to improve appearance (colours), to prevent ingredients from clumping together or prevent sticking to a surface or reduce friction (lubricants), to reduce interparticle friction and cohesion and promote powder flow (glidants), moisture proofing (sorbets), to make ingredients more palatable (sweeteners), preserve the life (preservatives) and many more. The quantity of the excipient in the blend affects the product characteristics, properties, performance and behaviour (Podczeck & Jones 2004).

The excipient most widely used by the industrial collaborator (also used in dry inhaled powders application and in the experimental work of this thesis) is α Lactose monohydrate. Lactose, like other excipients, is a food substance obtained from milk; it is a carbohydrate also known as milk sugar (DFE website). Lactose is produced in range of shapes (crystalline and

amorphous) and different particle sizes, giving different properties and behaviours to the blends. To manufacture the lactose, milk is separated into curds and whey. The whey is composed of a solution of water, protein and lactose. Once the protein solution is separated from the whey, the remaining solution is called wet edible lactose crystals.

Different processes are applied to these lactose crystals and the results are the following types of lactose (see figure 2.28): α Lactose Monohydrate (crystallised at temperatures below 93.5^{o}C and it can be obtained from fluidized bed dried and micronized or milled or sieved process), β Lactose (crystallised at temperatures above 93.5^{o}C and it can be obtained from roller dried and milled or sieved process) and amorphous Lactose (it can be obtained by rapidly spray drying).

<center>a)   b)   c)</center>
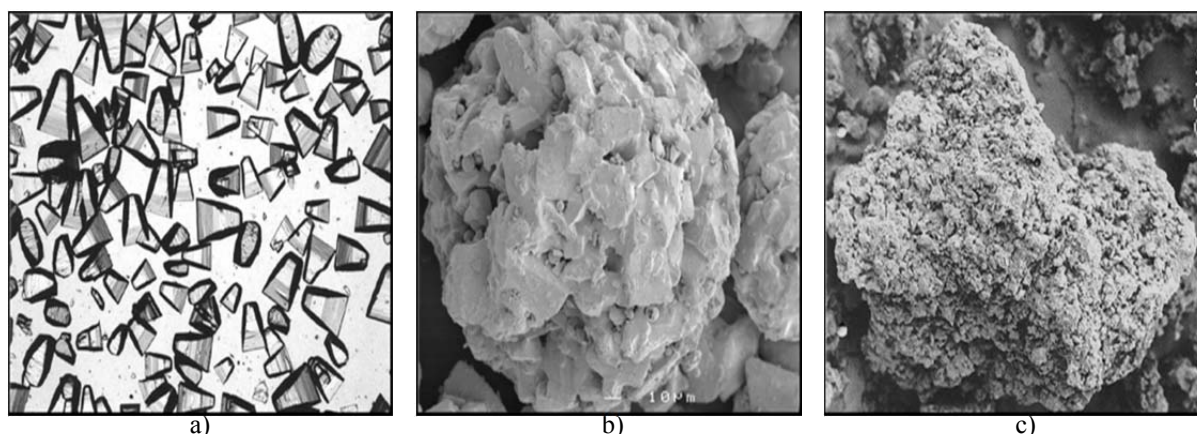
Figure 2.28. Types of lactose in the pharmaceutical industry: a) α Lactose Monohydrate crystals, b) β Lactose roller dried crystals, c) Amorphous spray dried Lactose crystals. Pictures re-printed from DFE Pharma website.

This range of Lactose products have been designed with different particle sizes and shapes and properties that affect the bulk powder behaviour to suit different industrial processes. Figure 2.28 shows the different particle shapes of the mentioned Lactose types. The α Lactose Monohydrate particles are crystalline particles with predominant pyramidal shape, they are widely used for dry inhaled applications for their poor binding properties, good flowability and low moisture content (out of 5% normal water content only 0.2% is free moisture[5]). The particles are hard and brittle.

New drug development takes typically 10 years and it is a costly activity. Formulation is undertaken in the early stages of the drug development and it is at this stage where powder flow properties are inherited. Certainly, potency of the drug is the aim of developing a NCE; for this reason the chemical properties are primordial during the powder formulation. Due to

---

[5] From DFE Pharma website.

the extremely limited quantities of powder available at this stage only basic standard powder flow techniques that require small quantities of material are undertaken, such as the angle of repose and tapped density (to obtain Carr's index or Hausner ratio, described in section 2.6), are applied to the blends to define the flowability. It is believed in the pharmaceutical industry that these methods are reliable and suitable to understand the flow behaviour of the powders; notwithstanding, these tests do not provide a quantitative statement concerning flowability and time consolidation of the powders (Schulze 2008, p. 173 & 177).

Product manufacturing starts with bench-scale production in the phase III of the powder development (in most cases the filling system and machinery used in this stage are not the same used to commercialise the product); nonetheless manufacturing and powder flow problems usually do not come to light until the drug is approved and the full-scale manufacturing is entered into. Problems at the manufacturing stage delay production and generate extra costs not included in the budget; this represents a significant loss to the pharmaceutical companies. These problems could be prevented at the formulation stage if formulators and manufacturing engineers could work together and apply other recognised powder flow measurements techniques (discussed in chapter 5) in parallel to the drug development. Powder behaviour could be predicted beforehand and enhancements can be made before scale-up.

2.5.   Filling trends in dosator systems

The trend in the pharmaceutical industry is to eliminate the carrier in the blends and manufacture small doses of only API to be supplied by respiratory tracts; cohesiveness and poor flow are normally properties of these kinds of powders with normally particle size of 5 μm or below. GSK have a number of NCEs, which would ideally be dosed using dosator technology; some of them are respiratory applications and the powder compact must be friable following the dosing. The need for improved understanding of dosator operation and measurement of powder flow techniques is necessary to deal with new compounds that have greater levels of fines and hence poor flow behaviour.

2.6.   Measuring the powder flowability in the pharmaceutical industry

The term "powder flowability" can be defined as the ability of the powder to flow (Prescott & Barnum 2000); in manufacturing processes, it is related to the behaviour of the powder when it is handled. During the development of new pharmaceutical products, the flowability of the material is normally measured at the formulation stage. This is generally measured using two methods[6]: the angle of repose and the tapped density (to be used for the Carr index and/or Hausner ratio). These tests are used because they are quick, easy to understand and require relatively small volumes of material. However neither test actually measures powder flowability and reviews by a number of researchers have found that they cannot reliably discriminate powder flow behaviour in industrial processes. According to Schulze (2008, p. 172,176) the aforementioned methods depend upon the testing equipment, test procedure, do not measure the strength of the powder at different levels of stress, have low repeatability and do not take account of the time consolidation in storage or during the process.

The alternative approach to powder flow property measurements, which is the established method favoured by powder specialists in industry and academia, is to measure the flow function (described later in section 2.6.3). This approach generates more repeatable results and accurate information about the flowability of the materials at different consolidation stresses and over time periods of static storage.

The mentioned tests are explained in detail below.

2.6.1.   Angle of repose

According to Schulze (2008, p. 172), generally the angle of repose, α_m, is the slope of a conical pile of loose material. The material is normally poured through a funnel (see figure 2.29.a), which is located above a bottom plate. The material forms a heap and by measuring its slope the flowability of the material is determined.

There are other ways to measure the angle of repose such as the drained and dynamic angle of repose. The drained angle of repose is represented in figure 2.29b, where the material is discharged into a container with flat bottom and central outlet, and the angle of repose is the

---

[6] Based on the literature review and observations in conferences attended by the author.

slope of the remaining material left aside of the container. Whereas the dynamic angle of repose is measured in a rotating cylinder showed in figure 2.29.c. There are more methods to measure the angle of repose; however the mentioned ones are the most representative of those used in industry.
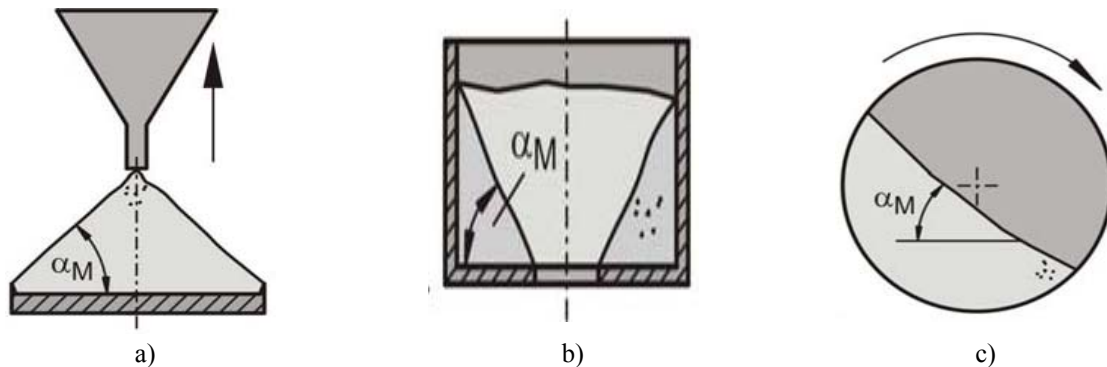
Figure 2.29. Angle of repose tests: a) poured angle of repose; b) drained angle of repose; c) dynamic angle of repose. For full explanation refer to the text. Re-printed from Schulze (2008, p. 172).

According to Schulze (2008, p. 172) and Podczeck & Jones (2004, p. 105), this method has poor reproducibility and in some cases, such as dealing with cohesive powders, the slope is not constant making it difficult to quantify. The test depends on the outlet diameter, angle and material of the funnel. Dynamic effects could take place as the powder is falling from above and sliding down the surface. The powder is loose and is not pre-compacted to measure the effects of the flowability at different levels of compaction (for the case of the silo design and storage, or for pre-compacted powder beds in filling systems, or time consolidation effect in storage and packing of powders). The shape and capacity of the funnel or container will affect the measurements, as the powder is consolidated by stresses acting on the mould after filling and flows depending on the angle of discharge. In the dynamic angle of repose, the test depends on the rotating speed, the dilation of the powder (due to the quantity of air entered during the movement of the material) and the relation between the cylinder diameter and particle size. Other situations such as segregation or agglomeration can be presented while measuring the angle of repose Schulze (2008, p. 172).

Also, Gold et al (1966) demonstrated that the angle of repose is an unreliable indicator of the flow properties; this paper is mentioned in chapter 3.

2.6.2. Tapped density

In this test, the powder is poured into a volumetric glass test pipe that is secured at its base, as illustrated in figure 2.30. The powder initially occupies certain volume (illustrated with the blue dotted line in figure 2.30). The weight and the poured volume of the sample are recorded. This gives the poured bulk density. Afterwards, the pipe is repeatedly tapped by mechanical action and the particles are re-arranged reducing the sample volume and increasing the bulk density (illustrated with the red dotted line in figure 2.30). This is the tapped bulk density.

The poured density (or true density) and the tapped density are used to calculate the flowability of the powders using the Carr index (Carr cited by Podczeck 2004, p. 111) or the Hausner ratio (Hausner cited by Podczeck 2004, p. 111).
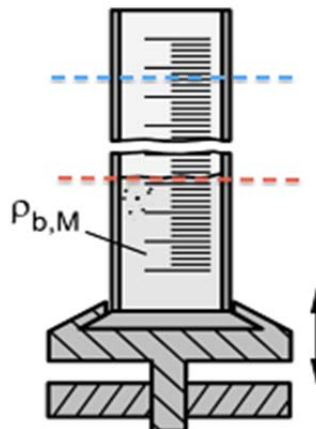
Figure 2.30. Tapped density test for Carr's index and Hausner's ratio. Re-printed from Schulze (2008, p. 176).

The Carr index is expressed in percentage by the equation [2.1] (Podczeck 2004, p. 111), where ρ_A and ρ_T are the poured and tapped density respectively.

$$CI = 100 * \left(\frac{\rho_T - \rho_A}{\rho_T} \right) \qquad [2.1]$$

The Hausner ratio is expressed by the equation [2.2] (Podczeck 2004, p. 111), where CI is the Carr index.

$$H = \frac{100}{100 - CI} = \frac{\rho_T}{\rho_A} \qquad [2.2]$$

Small CI values indicate good flowability (normally for incompressible powders with similar ρ_T and ρ_A values). Tables 2.4 and 2.5 show the flowability guidelines for the use of Carr's compressibility index and Hausner's Ratio published in Podczeck & Jones (2004, p. 111) and recommended by Copley manufacturer.   The Hausner ratio is less widespread and is considered that a value of <1.25 is free flowing and above that is poor flowing for Podczeck & Jones (2004, p. 111). It can be seen from both tables that there is not a unique flowability standard; in fact table 2.5 does not distinguish properly the flow type, it was found difficult to interpret a "passable flow" or "very very poor flow" instead of "very poor flow".

CI [%]	Flow type
< 15	Free flowing
15 - 25	Good
25 - 35	Acceptable/poor
> 35	Extremely poor/no flow

Table 2.4. Carr's compressibility index (CI) flowability guidelines for tamping and dosator filling machines. Information obtained from Podczeck & Jones (2004, p. 111)

CI [%]	Flow type	H
<10	Excellent	1.00 – 1.11
11 – 15	Good	1.12 – 1.18
16 – 20	Fair	1.19 – 1.25
21 – 25	Passable	1.26 – 1.34
26 – 31	Poor	1.35 – 1.45
32 – 37	Very poor	1.46 – 1.59
> 38	Very, very poor	>1.60

Table 2.5.   Carr's compressibility index (CI) and Hausner's ratio (H) flowability guidelines of Copley manufacturer. Information obtained from customer leaflet.

The tapped density is considered to represent the tightest packing state of the material (Podczeck & Jones 2004, p. 111).   To reach this particle packing state, there are several considerations about the number of taps to measure the tapped density; normally this value is recorded after the 10, 500 and 1250 taps. Some researchers use only in between 100 – 150 taps as it has been seen that the density does not change for several powders after this number of taps[7].

According to Schulze (2008, p. 76), the tapped density test is device-dependent due to factors like test pipe diameter, wall friction and the magnitude of the taps. The magnitude of the taps depends on the machine manufacturer and the taps can lead to inertia forces acting on the powder; depending of the stiffness of both, the apparatus and the bulk solid, these inertial

---

[7] Recommendation from the PhD students of the Science School at the University of Greenwich

forces vary. This test does not quantify flowability or time consolidation of the powder.

2.6.3. Flow function

The most significant advancement in the understanding of powder mechanics was due to the work of Andrew Jenike (Jenike et al. 1961 & 1964) who adapted soil mechanics techniques to develop what is still the standard design method for silos to ensure reliable gravity flow. The method relies on measured powder flow properties, of which the principal measurement is the flow function. This method was used in this thesis to measure the flowability of the materials, as it is a technically more sound approach for quantifying the powder behaviour in a manufacturing process (Jenike et al. 1961 & 1964 and Schulze 2008).

The concept of the flow function is best illustrated by the unconfined failure test/uniaxial test, which is illustrated in figure 2.31. In the unconfined failure test, the specimen is pre-compacted under the major principal consolidation stress, σ_1, in a cylindrical mould (see figure 2.31.a). The mould is removed, so the sample is unconfined (horizontal stress is zero) and a vertical failure stress is then applied to the specimen and increased (see figure 2.31.b) until the stress becomes critical and the specimen fails (see figure 2.31c). The peak stress at failure is the unconfined failure strength ($\sigma_1 = \sigma_C$).

| a) | b) | c) |
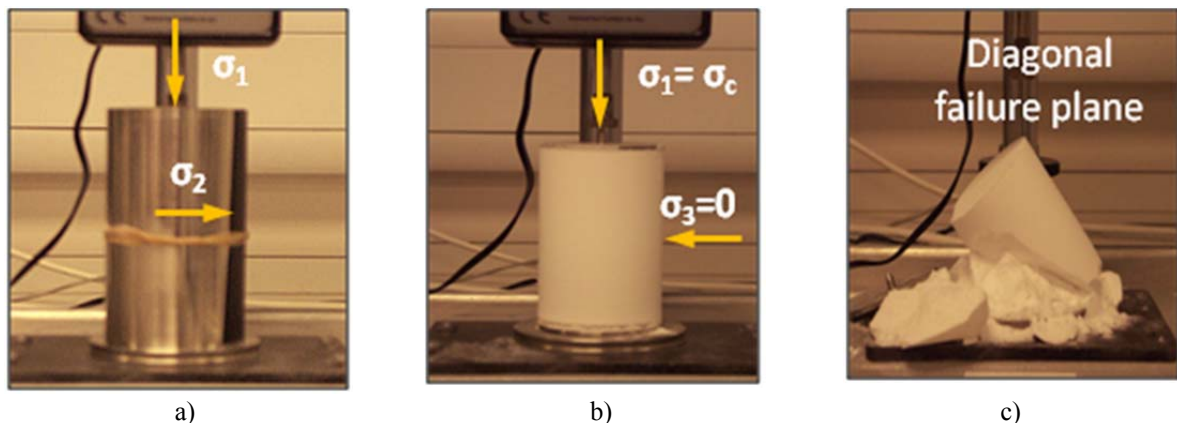
Figure 2.31. Unconfined failure test: a) pre-compaction, σ_1, of the specimen in a constrained space; b) vertical stress applied until failure of the specimen when $\sigma_1 = \sigma_C$; c) failure of the specimen. For full explanation refer to the text. Pictures taken by The Wolfson Centre.

While the above unconfined failure test clearly illustrates a measurement of powder flowability, this test is not very reproducible. Therefore the preferred method for measuring the flow function is to use a shear tester. Shear testers measuring the flow function follow the

ASTM 6128 test procedure developed for the Jenike shear cell. The test process is as follows; the sample is sheared to critical consolidation under the first normal stress, σ_1, replicating the consolidation process in the uniaxial test, (see figure 2.31.a). Because the unconfined failure strength, σ_c (see figures 2.31.b and c), cannot be measured directly, the normal stress is then reduced to a lower value so the specimen is put it in an over-consolidated condition. The powder sample is then sheared to measure the over-consolidated failure strength. This process is repeated over a range of reducing stresses and the measurement extrapolated back to zero to determine the unconfined failure strength, and the first point on the flow function. This whole process is then repeated using a range of increasing consolidation stresses to create the entire flow function.

As mentioned before, the flow function (see curve A in figure 2.32) is the result of series of tests of unconfined failure strength, σ_c, as a function of major principal stress, σ_1. From the magnitude of these stresses it is possible to calculate the flow factor, ff_c, by dividing σ_1 over σ_c; this factor determines the flowability of the material as non flowing, very cohesive, cohesive, easy-flowing and free flowing, as shown in figure 2.32. Depending on the major principal consolidation stress level, the powder will behave differently and could cross different zones of the graph in figure 2.32.
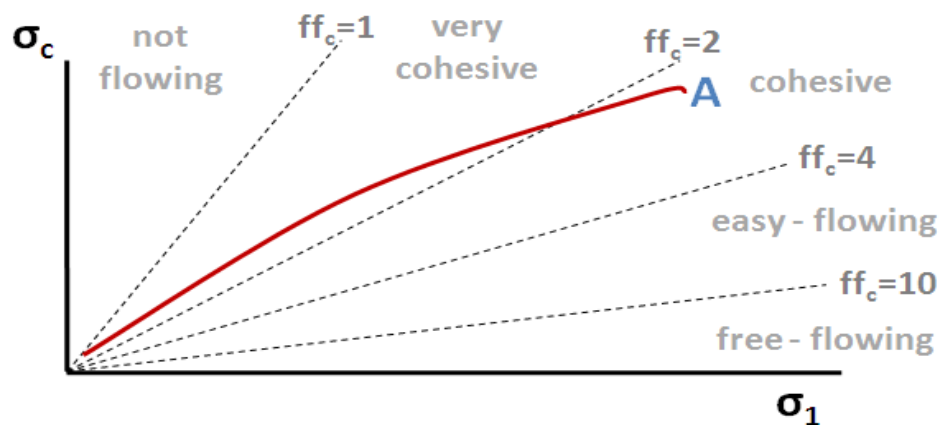
Figure 2.32. Flow function example. Re-printed from Schulze (2008, p. 42).

The flow function is the main flow property and there are several machines that can measure it, some of the most representative in the market are the Brookfield PFT, Schulze RST-XS and Freeman FT4 with shear cell attachment.

This property gives an indication of how easy or difficult it could be to handle the powder and fill the dosator; therefore it also provides information about the powder bed behaviour during the process.
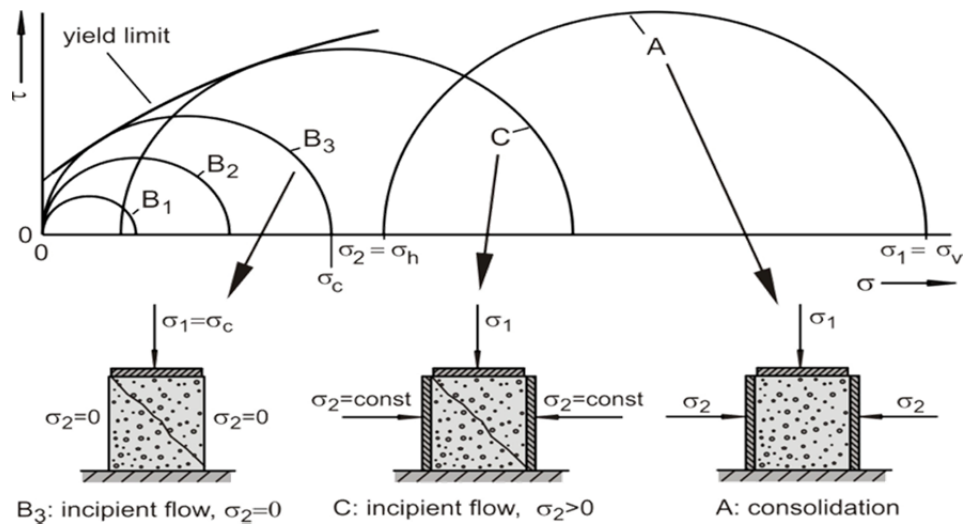
Figure 2.33. Comparison between stress in the Mohr's stress circle (top) and the uniaxial compression test (bottom) to determine the flow function. Re-printed from Schulze (2008, p. 40).

Figure 2.33 shows the representation of the unconfined failure strength and major consolidation stress Mohr's circle (top) and the analogy with the uniaxial compression test (bottom) undertaken by Schulze (2008, p. 40). From the right to left in figure 2.33, the first circle (A) represents the consolidation stage in both tests. The circle is formed by the values of σ_1 and σ_2 along the "x" axis. In the second part of uniaxial test the cylinder is removed and the material is loaded until failure occurs; the circle B3 represents the stresses in this failure stage where the major consolidation stress, σ_1, becomes the unconfined failure strength, σ_C along the "x" axis. It can be seen that the circle, B3, starts at the origin of the graph because there is no resistance in the horizontal direction; circles B1 and B2 are also vertical stresses applied to the specimen prior to failure. Tangential to these circles, is traced the yield limit that represents the limit of the powder to flow at that specific consolidation stress.

As stated before, the powder is subjected to different consolidation stresses, which imply numerous yield limits to construct the flow function. Figure 2.34 shows the Mohr's stress circle in the Brookfield PFT software. Five yield limits can be distinguished (straight coloured lines), each tangential to a pair of Mohr circles. The powder flow testers normally measure these yield limits by applying simultaneously horizontal and sharing stresses until the material flows. From each yield locus (limit) the software calculates the Mohr stress circles

for the consolidation σ_1 and unconfined failure conditions σ_C using the Mohr stress circle and therefore the σ_1 and σ_C values are determine locus in the flow function curve; which is then determined by plotting the σ_1 and σ_C values obtained at each consolidation level.
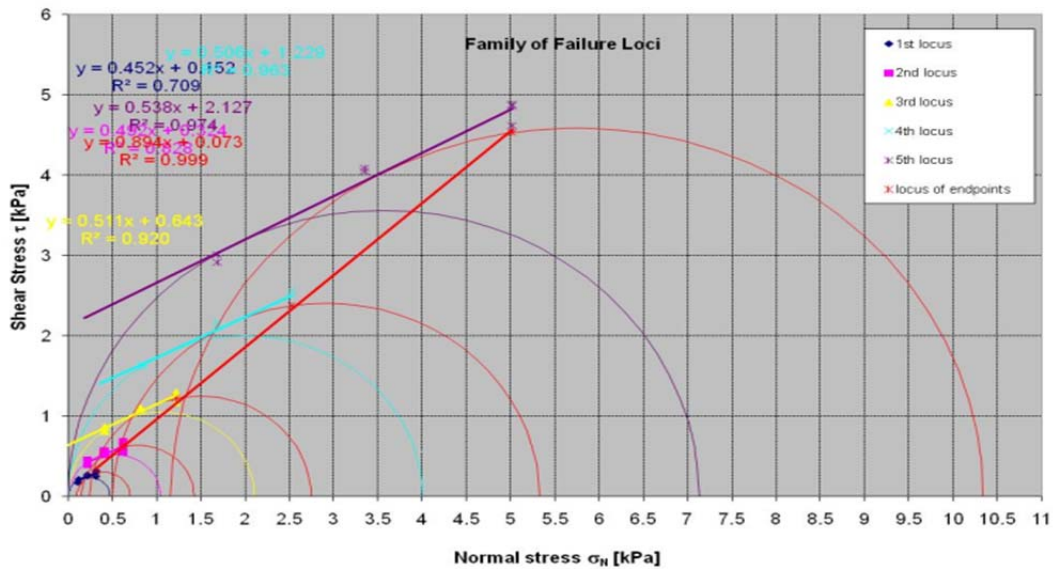
Figure 2.34. Example of the Mohr stress circle when measuring a flow function in the Brookfield PFT. Reprinted from Brookfield PFT software.

Based on The Wolfson Centre experience, it is more reliable to measure the flowability of the material using the concept of flow function rather than other "traditional" methods; this is also seen with the flow tester comparison undertaken by Schulze 2008. The flow function method has the advantage of consolidating the powder, until the steady flow state is reached, prior to measuring its strength at failure. It is possible also to apply controlled stresses in the measuring plane and also obtain uniform stress distribution. With the commercial shear tester, during a flow function test other flow properties such as the effective angle of internal friction, cohesion and bulk density (compaction curve),are also recorded during the test. By implementing small changes in the test procedure and shear cell components, it is possible to measure also the effective angle of wall friction. All these properties are derived from the concept of flow function and reveal information about the flowability of the material. These flow properties relate to the flow or no flow discharge behaviour from storage vessels and feeders but there are other failure properties that need to be considered to describe the behaviour in a dosator. Chapters 5 and 7 present the most relevant powder flow properties for the dosator filling systems considered in this research and also present some new techniques that were developed for this project.

2.7. Possible stress distribution in dosator operation

This section presents powder and soil mechanics applications found describing the stress distributions relevant to different stages in a dosators operation. The stress distribution of a Janssen effect application describes the stress distribution in the dosator and ultimate bearing capacity applications describes the possible powder bed pre-compaction ahead of the dosator at the end of the stroke.

2.7.1. Janssen effect application pushing a column of material upwards in a vessel

Janssen developed a one dimensional differential element slice method to describe the distribution of internal stresses in the vertical section of a silo. The Janssen effect principle is illustrated in figure 2.35a.
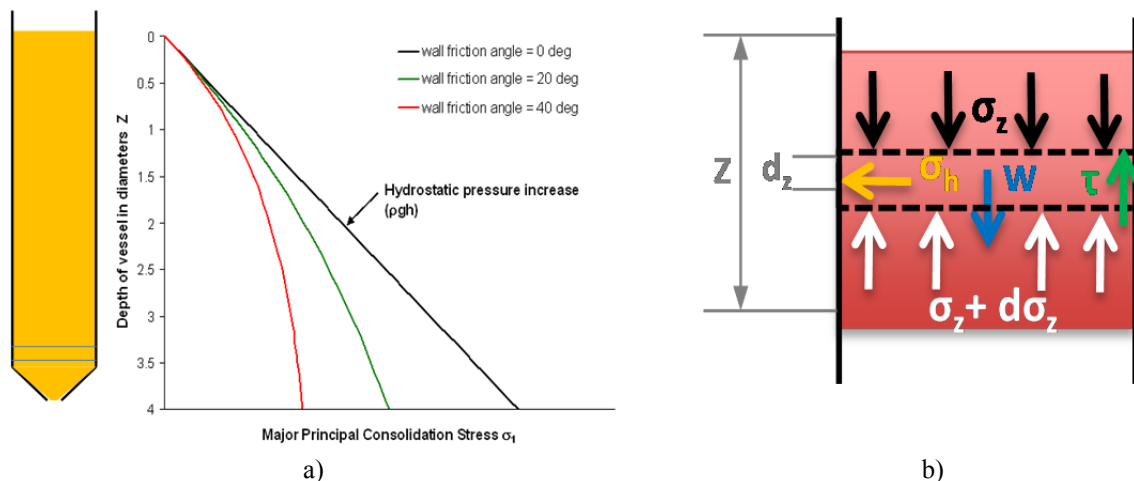
Figure 2.35. Janssen effect stress distribution in silos: a) stress distribution example in silos for different wall friction (re-printed from The Wolfson Centre short course presentation); b) stress diagram of a differential slice inside the silo. For full explanation refer to the text.

If the silo is filled with a powder that exhibited no friction against the walls (series in black colour), the stress distribution is governed by $\rho.g.h$ and will increase linearly with the depth in the silo; the powder in this case would behave as a liquid. If the presence of wall friction is taken into account, then the linear increase in stresses will decay exponentially to a constant value at great depth in the silo. The decay in the stress curve is due to the friction between the solid and the silo walls (series in green and red colour). In comparison to the hydrostatic (frictionless) stress distribution, the wall friction gives a negative feedback effect which reduces the increase in the wall friction to an asymptote; where the self weight and the stress

transferred are balanced by the wall friction around the boundary of the slice. As the magnitude of the wall friction increases the asymptotic stress that the distribution is tending to at a great depth, reduces (series in red colour).

Figure 2.35b shows the stress diagram in a horizontal differential slice of powder across the silo. It can be seen that the vertical normal forces acting on the slice are the self weight, the weight of the material above and reaction stresses from the material below. In the horizontal direction the stress ratio of the powder determines the magnitude of the horizontal stress or wall normal stress. Under the action of the wall normal stress, the presence of wall friction generates a limiting vertical shear stress (due to slip at the wall) that is proportional to the horizontal stress. While the shear stress cannot exceed the limit dictated by the wall friction angle, the actual shear stress could be significantly below this limit depending on boundary conditions.

In the case of dosator we are interested in the reverse application of the Janssen effect where the powder is being pushed up into an infinitely long tube. Arnold, McLean & Roberts (1982, p. 1.7) and Schulze (2008, p. 263) studied the case where a plug of material is forced up a tube, as illustrated in figure 2.36a. In this situation the wall friction resists the movement of the powder. As the length of the powder plug increases, the force required to push it into the tube increases exponentially. This implies that there is a critical dose length at which force becomes infinite. This is an application that is of interest in this project for the dosator filling process where the material is being pushed upwards into the dose cavity, resisted by the cavity wall friction around the circumference of the dose.

a)   b)
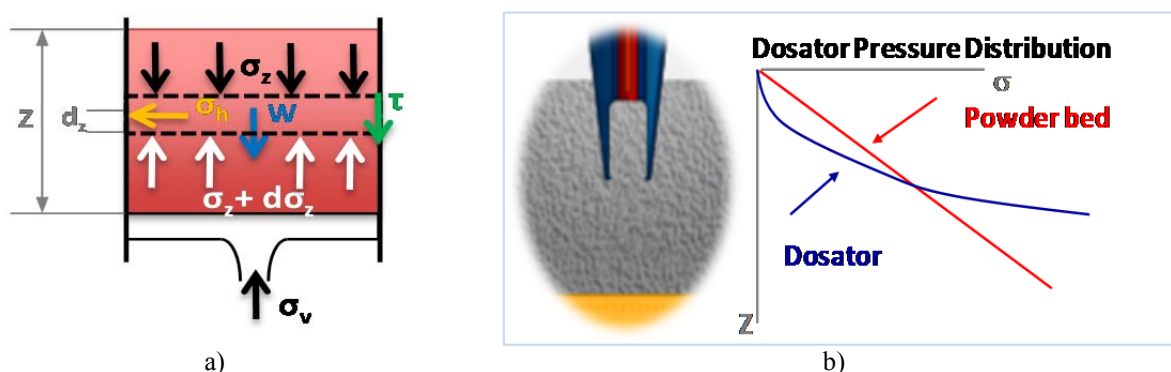
Figure 2.36. Janssen effect application. a) Stress diagram in a powder slice of the Janssen effect application forcing a column of bulk material up; b) lateral pressure distribution in dosator operation. For full explanation refer to the text.

A summary of the model assumed for the dosator filling is presented below. The pressure in the powder bed (assumed to be in the middle of infinite expanse of material), increases linearly being affected only for the self-weight as wall friction effects are ignored and it is shown in figure 2.36b. However for the dosator, as it strokes down into the powder bed material is forced up into the tube but the force increases exponentially with the depth due to the wall friction effect. The implication of the two different distributions is that the point where the curves of the lateral stresses distribution of the dosator and powder bed cross (see figure 2.36b) represents the maximum amount of material that can be entered into the cavity and it depends on the dosator geometry and powder flow properties.

The force equilibrium balance on the horizontal slice element shown in figure 2.36a, gives the following equation [2.3] (see appendix 2 for more information of the equation development), described by Arnold, McLean & Roberts (1982, p. 1.7) and Schulze (2008, p. 263):

$$\frac{d\sigma_v}{dz} - \sigma_v . K \frac{U}{A} . \tan(\phi_x) = g . \rho_b \qquad [2.3]$$

Where "K" is the stress ratio (described later in sections 4.3.1, chapter 4 and 5.4.5, in chapter 5) between the vertical "σ_h" and horizontal "σ_h" stresses (see equation [2.4]), "U/A" is a geometric factor for the vessel shape, "$\tan(\varphi_x)$" is the co-efficient of wall friction (see equation [2.5]), "g" the gravitational force, "ρ_b" the bulk density, "Z" the length of the bulk solid column and "σ_v" the required vertical stress to push the bulk material upward the tube.

The stress ratio values are << 1 and it is expressed as (Schulze 2008, p. 12):

$$K = \frac{\sigma_h}{\sigma_v} \qquad\qquad \text{when } \sigma_v >> \sigma_h \qquad [2.4]$$

The wall friction co-efficient is expressed as (Schulze 2008, p. 71):

$$\tan(\varphi_w) = \tau / \sigma_h \qquad [2.5]$$

The solution of the differential equation [2.3] for the vertical stress is presented in the equation [2.6] as follows (Schulze 2008, p. 263):

$$\sigma_v = -\frac{g . \rho_b . A}{K . \tan(\phi_x) . U} + \left[\sigma_{vo} + \frac{g . \rho_b . A}{K . t \, an(\phi_x) . U} \right] e^{\frac{K . \tan(\phi_x) . U . z}{A}} \qquad [2.6]$$

Without surcharge stress (σ_{vo}=0) it follows the equation [2.7] (Schulze 2008, p. 263):

$$\sigma_v = \frac{g \cdot \rho_b \cdot A}{K \cdot \tan(\phi_x) \cdot U} \left[e^{\frac{K \cdot \tan(\phi_x) \cdot U \cdot z}{A}} - 1 \right] \qquad [2.7]$$

Where in all the cases A/U=D/4 for cylindrical vessel shape.

The Janssen effect application suited well the dosator operation and the exponential theoretical stress distribution increases with the depth, as it is shown in figure 2.36b. This exponential increment of the forces was also observed in the experimental work of this thesis (described in chapter 7).

In figure 2.36b, the maximum point where the both stress distributions cross is an ideal situation where there is not dose length restriction (i.e. a column of infinite length) and that point represents the maximum amount of powder that can be pushed into the dose chamber. I.e. the frictional forces around the dose cavity wall exceed the vertical stress ahead of the dosator, so material spreads around the dosator rather than flowing into it. This situation was observed in the experimental work when lowering the dosator without pin in the dosator test-rig tests. However as the dosator strokes down the stress in the bed increases very slightly due to the self-weight of the material in the trough, therefore the stress at the bottom of the dosator increases and more material is forced; this is explained in detail in chapter 8.

2.7.2.   Relation between stress distribution in ultimate bearing capacity application of soil mechanics and dosator's powder bed stress distribution.

A review of the powder mechanics literature was undertaken to try and find examples of stress conditions replicating the powder pre-compaction occurring in a dosator. This search found no relevant papers so a wider search of soil mechanics theory was undertaken. Numerous papers were found concerning the bearing capacity of soils, in particular the case of the bearing capacity of a shallow bed of soil above a hard rock base. This closely matches the conditions of powder pre-compaction as the dosator approaches the base of the trough at the end of the stroke.

It should be pointed that soil mechanics is focused on the study of the forces applied to the soils under stable conditions before the failure; in this manner, it is safe to build structures and

buildings. In powder mechanics, what is important is the failure condition to make the material flow.

The capacity of the ground to support forces is called *bearing capacity* in soil mechanics. Likewise, the *ultimate bearing capacity* is the maximum stress required to produce a failure in the soil; the main factors affecting it are the physical properties of the footing (shape, size, depth and roughness), penetration of the footing within the soil, and the mechanical properties of the soil (Terzaghi 1943 and Meyerhof 1951).

The compression and ultimate bearing capacity of shallow foundations of cohesive soils between rough plates/hard rock base is a topic that have been studied by numerous researchers described in this section. Their approaches considered different factors in the quantification of the ultimate bearing capacity at the mentioned situation; topics such as soil flow properties (as angle of internal friction), plasticity yield criterion and experimental factors that vary with the physical properties of the footing.

Figure 2.37 shows the ultimate bearing capacity "q_u", the failure surface underneath of the foundation and the boundaries of the zones of plastic equilibrium for a distributed load. According to Pfeifle & Das (1979), there is an active zone formed by a wedge of soil that pushes the soil outwards passing through a transition zone (with a form of log spiral fans) to a passive zone.

a)   b)
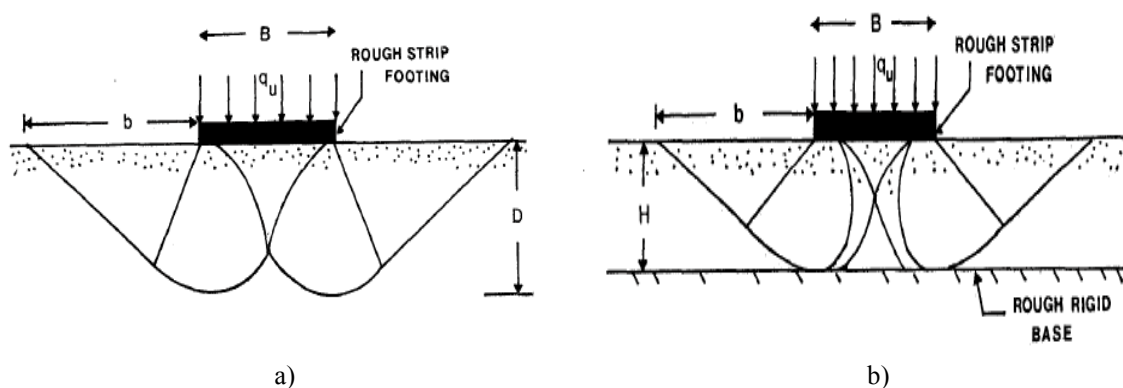
Figure 2.37. Failure surface under rigid rough continuous foundation: a) rigid base at great depth; b) rigid base at shallow depth. For full explanation refer to the text. Re-printed from Pfeifle & Das (1979, p. 2).

Some authors use an angle of 45^0 for the triangle formed in the active zone and some other $45^0 - \phi/2$, where ϕ is the angle of internal friction. There are two cases illustrated in figure 2.37 where the rigid rough base is located at great and shallow depth. In the case of shallow

depth (figure 2.37b) the stress distribution is affected by the height "H" and consequently the stresses bounce against the rigid base and the zones are squeezed in comparison to figure 2.37a.

Previously, Prandtl (1923) studied the compression of cohesive soils between two plates based on Henckyschen plastic balance (see figure 2.38); it proposed a geometrical solution to the stress distribution in cohesive soils between the plates for point and distributed loads.
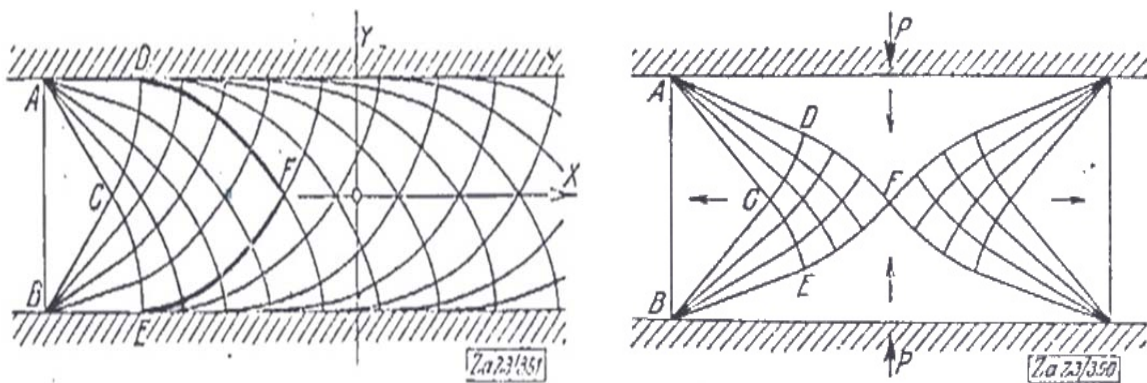
Figure 2.38. Prandtl's solution to the stress distribution when compressing cohesive soils between two plates. For full explanation refer to the text. Re-printed from Prandtl (1923, p. 405).

His geometrical solution was based in the analysis of the stress distribution and shear failure of a block compressed between two rough plates; he described also the different stress zones developed in the material.

Moreover, Meyerhof (1951) studied the plastic zones near to the foundation for a shallow and deep foundation with rough base in cohesive soil. Figure 2.39 illustrates the study and it can be seen how the stress dissipates within the soil depending the boundary conditions.   Figure 2.39a specifically shows the stress distribution in a shallow foundation where the stresses disperse to the ground surface. For deep foundation (figure 2.39b) the roughness of shaft has impact in the stress distribution; the left side of the graph is for smooth shaft (pronounce stress distribution) and the opposite for rough shaft. It can also be appreciated that the increment in the stress distribution in the footing changes towards the centre.

Theory contains factors in terms of mechanical properties of the soil and physical properties of the foundation. The bearing capacity was found to increase with the foundation depth and therefore surface friction was significant comparing it with the base resistance in cohesive soils than in cohesionless soils. The agreement between the theoretical and practical results varied with the cohesion of the material and an empirical compressibility factor was

introduced; for deep foundations the resistance was less than the estimated. The analysis was done for circular and strip foundations. It was found that in general bearing capacity increases with physical and roughness properties of the foundation and depends on the shape of the foundation.
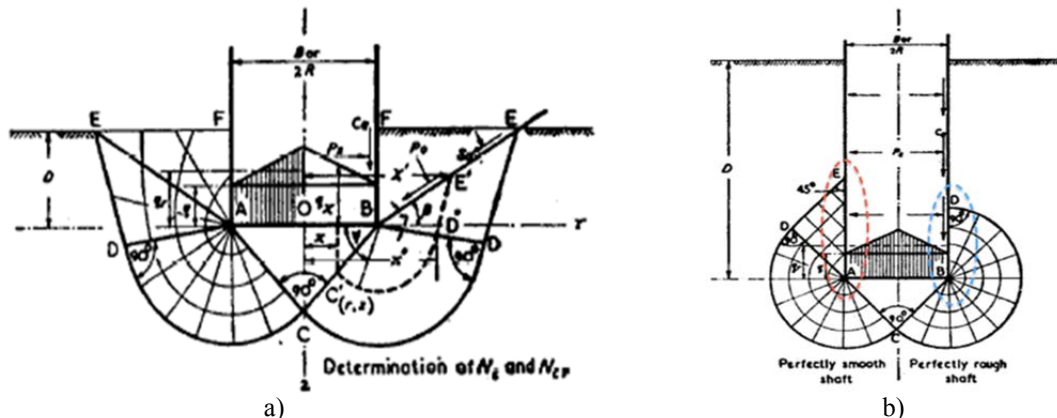
Figure 2.39.   Plastic zones around the foundation in cohesive material: a) shallow foundation; b) deep foundation. For full explanation refer to the text. Re-printed from Meyerhof (1951, p. 312)

Meyerhof & Chaplin (1952) studied the stress distribution for footings on a cohesive soil with shallow rough base (see figure 2.40); the outcome of their study was a fusion of the previously mentioned approaches. It can be seen in figure 2.40 for cases of both wide and narrow footings with the resulting stress distributions in the soil. For the case of the wide footing (half of the footing, figure 2.40a), the stresses in the footing increase to the centre and the stresses in the cohesive medium are squeezed and shifted aside. For narrow footings (figure 2.40b), the stresses in the footing remain constant and the previous approach of failure (Meyerhof 1951 and Prandtl 1923) is followed. This approach is also discussed in chapter 8.

They found that when cohesive soils were under compression between rough plates, the yield pressure of the soil increased with roughness of the plates and decreased with the separation between them. Experimental work was in good agreement with the theoretical assumption of the incremental increases of the bearing capacity with the adhesion of the material to the base and the decreasing thickness of the layer of soil. The experiments suggest that the vertical stress-strain relation of the soil in the tests is the same in the standard compression test of the material. This paper well illustrates the stress behaviour observed in dosator operation.
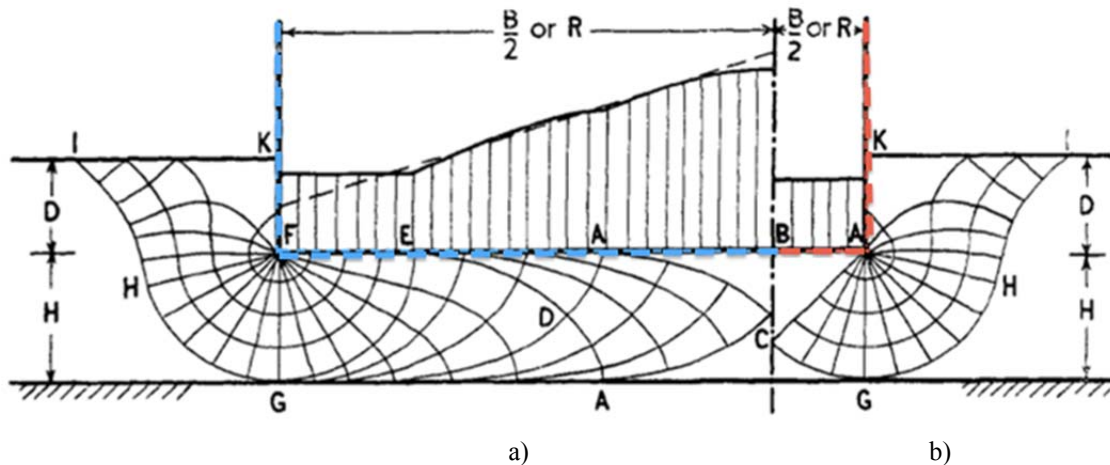
a)   b)
Figure 2.40.   Plastic and contact pressure for footing on cohesive soil with rough base: a) wide footing; b) narrow footing. For full explanation refer to the text. Re-printed from Meyerhof & Chaplin (1952, p. 24).

Based on the equilibrium of stresses and plasticity yield criterion, it was proposed that there is a radial and vertical stress distribution governed by the following equations:

$$\sigma_r = \frac{2mc(R-1)}{H} - 2c\sqrt{\left(1 - \left(\frac{2mz}{H}\right)^2\right)} + A \qquad [2.8]$$

$$\sigma_z = \frac{2mc(R-r)}{H} + A \qquad [2.9]$$

Where σ_r and σ_z are the radial and vertical stresses in the system (see figure 2.40). Also, m = tan(φ), "φ" is the angle of internal friction, "c" is the cohesion of the material, "R" is the radius/width of the footing, "H" the gap between the footing base and the rough base, "z" a radial position within the radius/width of the footing and "A" as follows:

$$A = \left[\frac{sin^{-1}m}{m} + \sqrt{(1 - m^2)}\right]c \qquad [2.10]$$

Due to the high magnitude of the forces in soil mechanics, by comparison with powder mechanics, the value of cohesion is a single value in the equations 2.8, 2.9 and 2.10 and is not dependant on the stress. The value of the "φ" is the measurement of the angle of the internal friction, probably because it was assumed rough plates and there is a layer of material formed at the wall/soil interface resulting in the internal friction causing flow. In powder mechanics, cohesion depends on the stresses, also the dosator and trough surfaces are smooth, material failure therefore occurs predominantly at the walls. This paper is a significant contribution to this thesis as a cross reference to what was thought to be happening inside a dosator.

Marshall (1966) worked on the compression of a slab of cohesive and cohesionless soil between plates. He presented expressions for the stress and velocity fields for the load carrying the capacity of the soil in the case when the weight of the soil is negligible.

Mandel & Salecon (1972) calculated the bearing capacity of a soft ground layer on a rigid base using the theory of limit equilibrium obeying Coulomb's yield criterion. The expressions to calculate the capacity implicated non dimensional correction factors that depend on the angle of internal friction (varying between 0^0 and 40^0). Other authors like Prandtl, Reissner, and Lundgren & Mortensen proposed the correction factors. It was found that the capacity, as function of the ratio B/H (where B is the diameter/width of the footing and H the thickness of the soil layer), depends on the friction condition between the soil and the base.

Meyerhof (1973) studied the bearing capacity of sand layers overlaying clay. The influence of the thickness of the sand in theoretical and experimental investigation was seen to depend on the bearing capacity, friction angle, the shape and depth of the foundation.
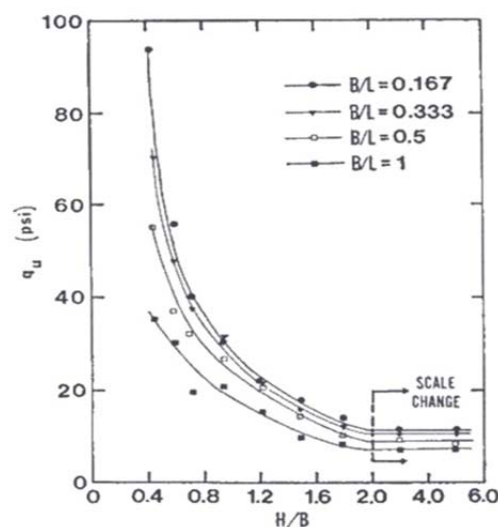
Figure 2.41. Variation of the ultimate load as function of the H/B (H = height of the cohesive material layer, B and L width and length of the footing respectively). For full explanation refer to the text. Re-printed from Pfeifle & Das (1979, p. 5)

Pfeifle & Das (1979) worked on the bearing capacity of surface footings of sand layers resting on a shallow rigid rough base. The experimental values of the correction factors, mentioned in Mandel & Salecon (1972) and Meyerhof (1974), compared well with the theoretical values proposed. It is mentioned that at very small depth, H/B less than about 0.6 (where H is the

56

thickness of the soil layer and B diameter/width of the footing, see figure 2.41), grain crushing took place.

The above mentioned authors concur with the increment of the bearing capacity with the proximity to the base and the effect of the relation between this proximity and foundations width. This application of soil mechanics is in good agreement with the powder and stress behaviour ahead of the dosator assumed and observed in this research; trials in the dosator single shot test-rig and dosator demonstrator confirmed this behaviour (described later in chapters 7 and 8). Figures 2.39 and 2.40 could be good approaches of what physically happens in dosator filling system and could explain the powder compression behaviour ahead of underside of the dosator. Similar behaviour of figure 2.41 was also observed and measured in the experimental work of this thesis (described in chapters 7 and 8); the variation was found to be more significant in dosator operation as the gap with the bottom of the trough at the end of the stroke is very small in current machines.

2.8.   Summary

The chapter has reviewed the different dosator operating principles used in the pharmaceutical industry. A simplified operating principle as described in section 2.3.2 will be the focus of the experimental and theoretical study in this thesis as presented in chapters 8.

The review has highlighted a number of flow property characterisation techniques, including the shear testing approach, which is the accepted standard technique will be used to characterise the materials in this work. These tests and other novel tests are presented in chapter 5.

Ultimate bearing capacity applications in soil mechanics replicated some of the possible stress distribution experimented in dosator operation. Further analysis of these applications and the adaptability to powder mechanics could provide valuable information to dosator and other filling systems. Soil bearing capacity models for a situation that closely resembles pre-compaction process in the dosator. These models are used in the phenomenological approach proposed by this thesis to explain the dose obtaining in this filling system (later described in chapter 8).

Chapter 3

Literature Review

3.1.   Introduction

This chapter presents the published literature relevant to this project. As the main dosator application is capsule filling, there are wide range of investigations published on this topic and most of what is known about dosators is thanks to them. Capsule filling has been studied by numerous researchers; publications can be found from the late 1960's onwards containing several subjects related to dosator filling systems. Thanks to these researchers, dosator operation is still progressing and being investigating.

The majority of publications are related to the variability of the fill dose weight as a function of the powders chemical properties and the level of adhesion of excipients to the formulation. Therefore these factors are normally linked to manufacturing parameters like machine speed, capsule sizes, dosator dimensions, dosator wall surface finish, particle size and powder flowability; these matters have been well covered by researchers over the years. There however very limited number of studies about the factors affecting the fill dose weight from the manufacturing point of view, and thus the need for a close study of the compaction mechanism during the dosator operation remains.

Jones (2001) presented a complete scope of the investigations of filling powders in capsules. It was a useful paper for the literature review of this research; it collects several researches in dosator systems.

The term flowability, in the literature studied, is often attributed to either the adhesion of lubricants to the host particles in the formulation or to tests such as the angle of repose and Carr's index. These "so called" flowability tests were not followed in this research for the reasons explained in chapter 2, section 2.6.

In this chapter, the dosator process investigations were grouped into research related to the effect of powder compression and flow properties in product formulation shown in section 3.2 and research correlating flow properties and dosator machine settings in section 3.3.

Investigation of the powder bed conditions are presented in section 3.4 and current publications of dosator models predicting the fill dose weight are presented in 3.5. Finally, section 3.6 presents soils mechanics applications that maybe useful for illustrating the behaviour and possible stress distributions in the powder during the dosator operation.

3.2.   Powder flow properties and powder formulation

Since the 1920's the compaction of powders has been studied with a view to predicting the bulk solids density in industrial processes. Walker cited by Denny (2002) proposed the first compaction equation for predicting volumes as a function of the axial pressure applied. Denny (2002, p. 163) mentioned that surveys show that there are over 200 publications per year about compaction in the literature. Each industry tends to use different equations for reasons linked to the research priorities or the kind of powder used to develop the equation. The pharmaceutical industry normally uses the Kawakita [3.1] and Heckel [3.3] compaction equations (Denny 2002).

The Kawakita equation (Kawakita cited by Denny 2002) is expressed as:

$$\frac{P_a}{C} = \frac{1}{a.b} + \frac{P_a}{a} \qquad [3.1]$$

Where the term "P_a" is the pressure applied and the parameters "a" and "b" are constants, which are obtained from the slope and intercept of the P_a/C as function of P_a. The parameter "a" is equivalent to the value of the initial porosity and "b" has dimensions of the reciprocal of stress. The relative volume "C" [3.2] is expressed as follows:

$$C = \left(\frac{V_o - V}{V_o}\right) \qquad [3.2]$$

Where V_0 is the initial volume of the powder bed and V is the volume under applied stress.

The Heckel equation (Heckel cited by Denny 2002) is expressed as:

$$K = \frac{1}{3.\sigma_o} \qquad [3.3]$$

Where "K" is a constant related to the ability of the material to deform and "σ_o" the yield strength of the material studied.

These two compaction equations have been studied for years as they have claimed able to relate physical properties with compaction of materials. Denny (2002) studied them in detail and concluded that they do not relate densification behaviour to the physical and mechanical properties of the material being compacted and proposed a modification of these equations to express the compaction of the materials. Also it was stated that the Kawakita equation works for limited range of materials.

Gold et al. (1966) compared results from the angle of repose test and powder flowmeter (variable rotating cylinder designed by Gold), for range of powders previously classified empirically as glidants. It was found that some glidants did not necessarily increase flow rate and many of them that lowered the angle of repose but did not necessarily improved flow behaviour. It was also stated that from the comparison between the two methods used, the angle of repose was not a reliable method for evaluating flow behaviour.

Takagi, Sugihara & Kimura (cited in Jones 2001) were the first researchers to publish a paper using dosator dosing system; a Pedini XXXI machine was used. They related uniformity of the capsule fill weight to compression ratio of the slug, C_r, by calculating the difference between bed height before and after the compression by the piston divided by the original height. It was characterised common used diluents by their particle size, absolute density and angle of repose. Furthermore it was showed the effect of adding lubricants to these diluents.

Irwin et al. (1970) investigated the relationship between flow rate of different blends of Clomacran Phosphate and fill weight uniformity. Different blends were prepared by mixing API with different lubricants at different grades. Data suggested that differences in particle size were responsible in part for the observed weight variation; large particle sizes showed less variation and small particle sizes presented greater variation. Apart from the particle size, other factors were found to affect the dose fill weight such as batch-to-batch variability and concentration of the API.

Regarding to the dose strength, Gold et al. (1971) studied the strength of granules and found a correlation between the strength and both the particle size and formulation concentration.

Miyake et al. (cited in Jones 2001) showed that plug formation was a compaction phenomenon related to the compression ratio "C_r" expressed by Takagi et al. (cited by Jones 2001). Capsules were filled using three different common diluents and a range of machine settings, bed heights and positions of the piston inside the dosator body. The most uniform

fill weight was obtained when the dosator piston was set at half the depth of the powder bed. The diluents were characterised by measuring their particle size, the angle of repose and the bulk densities (true, tapped and apparent). The machine used it was a Zanasi Z-25R dosator.

Chowhan & Chow (1980) and Chowhan & Yang (cited in Jones 2001) investigated the problem from another point of view. They considered the theoretical approach of consolidation of loosely packed powders in cylindrical containers, finding a linear relationship between filling weight uniformity and powder consolidation ratio. A range of powder blends were placed in series of cylinders of increasing diameter and a load was applied to the surface measuring changes in the volume, using the Zanazi dosator. This showed that powder compactibility increased as bulk density decreased and at low values of bulk density they were linearly related. Weight variation was found to be directly related to the powder consolidation ratio.

Mehta & Augsburger (1981) studied the effect of different glidants fractions in slug hardness, drug dissolution and fill weight dose variability. The study used an instrumented Zanazi automatic dosator filling machine. The hardness of the doses was measured in a bench-type hardness tester. It was found that the level of the compaction of the dose compromises the dissolution effects in the patient's body.

Newton & Bader (1981) predicted the maximum tapped bulk density of blends from measurements of individual components. The study also predicted the bulk density of the blends in capsule filling using a method that packed the powder at maximum tapped bulk density. This method was less satisfactory for the prediction of bulk density of conventional filling systems that involve compression of the powder within the capsule shell.

Podczeck & Miah (1996) studied the influence of particle size and shape on the angle of internal friction and the flow factor of 8 different blends in an annular shear cell. Tests were undertaken for powders with different particle sizes and shapes and blends with a range of lubricants concentrations. For unlubricated powders, it was found that the flow function depended on the particle shape whereas the angle of internal friction depended on the shape and particle size. When the lubricant was added to the blends, the lubricant content, flow function and angle of internal friction were dependent only on the particle shape.

Newton & Bader (cited in Jones 2001), studied the usefulness of internal angle of friction Φ for assessing capsule filling. Capsules were filled by compression and tamping, and a relationship was found between the lower values of Φ the higher the fill weights.

Podczeck (1997) studied the adhesion of powder to stainless steel tamping pin faces. It was found that the powder adhesion to tamping pin's face reduced with surface coating and the best results were obtained using a surface finished coated with chromium nitride.

Heda, Muteba & Augsburger (2002), studied the formulation requirements of dosator and dosing disc automatic capsule filling machines. In this research Hofliger-Karg GKF-400 dosing disk machine and Zanasi LZ-64 dosator machine were used. For the three formulations chosen, the Carr's compressibility index, the ejection force, plug braking force at a specified compression force during the operation and the drug dissolution rate were measured. These parameters were used to evaluate the fluidity, lubricity, compactibility and dissolution of the powders. The results suggested that there is an optimal degree of fluidity of the formulation for a successful encapsulation. It was found that the formulation should meet different flow criteria for the two filling process with a lower lubricant needed for dosing disc machines and higher degree of compactibility needed for the dosator machines.

3.3.   Powder flow properties and dosator machine settings

Jolliffe & Newton (1978, 1980, 1982, 1983a, b, c) investigated the powder behaviour during dose formation and mechanics in the dosator machine. They considered that the filling capsule process depends on the formation and retention of the powder plug that requires the formation of a stable arch at the nozzle outlet. This assumption was derived from arching condition theory in mass flow hoppers and involved study of powder flow properties namely the flow function, bulk density, angle of wall and internal friction (from Jenike wall friction measurements) for range of size fraction of Lactose between 15.6 and 155.2 μm. Wall friction angle θ, was determined on ground and turned stainless steel surface. The critical outlet diameter to retain the dose within the dosator cavity and minimum stress to maintain arch formation was determined. Values of θ were applied to theoretical equations derived from previous investigations of the authors and showed that the strength required to ensure arching increased with particle size up to 40 μm, above that value it became constant. Simple

dose retention experiments were done by filling the dosator and move it up and down at different machine speeds. Good retention performance around a particle size of 40 μm was observed; above this value dose retention was difficult or impossible. The freer flowing the powder the greater the compressive stress required, thus angle of wall friction needed to be lower to permit the stress to be transmitted through the plug. Likewise this was supported by tests run with polished wall surfaces inside the dosator (to reduce wall friction), which improved filling and uniformity. It was proposed a nozzle with two different wall surfaces that could be used with high wall friction area close to the outlet to assist in arch formation, and low wall friction elsewhere to assist filling. Uniform fill weights were noted with fine particles sizes over a wide range of compression ratios. The filling ability was linked to powder compaction and best results were obtained with fine cohesive powders because their greater volume reduction by comparison with coarse free flowing powders.

Based on the dosator process understanding developed through the research reflected in this thesis, the author has reservations about the factors affecting the dose retention (wall friction and the development of and arch) in dosators operation exposed by Jolliffe & Newton (1978, 1980, 1982, 1983a, b, c). Dose retention point of view in this thesis is discussed later in chapter 5, section 5.4.5.3.

Jolliffe & Newton (1980) also attributed uniformity of fill weight to changes in the wall friction by powder coating the dosator inner wall surface over time. The trends of fill weight, compression and ejection stresses (of three fractions of Lactose) were constant after around 15-20 capsules were filled. The fill weight dropped in the first 15-20 capsules filled and which the authors suggested was caused by a reduction of the dose volume due to the coating of the powder in the dosator inner-wall. A wall friction angle increase was measured (using Jenike shear cell) as the wall became coated. In this thesis, it was observed that for some materials, an incremental increase in the wall friction angle occurred with increased shear displacement during long travel wall friction tests, but it was not possible to observe the trend described in this paper. Nonetheless, it is known from the Wolfson Centre experience in this field, that in pharmaceutical production lines the first and last 15% of the production is often wasted as the products do not meet the required specification; in dosator machines this can be translated to the time needed for the factors in the system to stabilise, one of them could be the powder coating on the dosator inner-walls described in this paper.

Woodhead & Newton (1981) studied the influence of the dosator pin and body inner wall clearance to fill weight and showed significant effect. It was stated that if the clearance was too small the air could not escape and if too big powder was left behind on the piston's face. The influence of the powder permeability and dosator design was not studied in this thesis; nevertheless, it was observed in the experimental work of this thesis, that the mentioned clearance could play an important role in dosator operation as material can built up in between this clearance making the pin jam during the dose procurement.

Tan & Newton (1990a, b, c, d, e, f) published a series of papers studying powder properties and machine performance. Five commonly used excipients were sized and graded into fractions less than 45 μm. The powders were characterised by angle of repose (α), Carr's compressibility index, Carr (cited in Jones 2001) Hausner's ratio, Hausner (cited in Jones 2001) Kawakita's constants, Kawakita & Ludde (cited in Jones 2001) angle of internal flow (θ), Varthalis & Pilpel (cited by Jones 2001) Jenike's flow factor (FF), Jenike (cited in Jones 2001) and angle of effective friction (δ), Carr & Walker (cited in Jones 2001). The powders were filled into the MG2 simulator reported previously by Jolliffe et al. (cited in Jones 2001) with modifications to the computer use to collect the data. The filling was carried out over range of compression ratios, C_r Takagi et al. (cited in Jones 2001). Sample of capsules were taken, weighed and mean and coefficients of variation calculated. The coefficient of variation was related to powder bed density and the variation in compaction stress. There was no correlation between weight variation and flow function (cohesion) and effective angle of internal friction. The surface texture, Ra, of two different dosator nozzles (smooth and rough) was measured by profilometry, and scanning electron micrographs, while the powder-wall friction was measured using an annular shear test. The filling tests were carried out on a clean and coated nozzle and did not show significant difference in fill weight uniformity between two powders (microcrystalline cellulose and pre-gelatinised starch) irrespective of the particle size or whether dosator walls were clean or powder coated. Nevertheless microcrystalline cellulose presented dose retention problems for the coarse particle size fraction and it was showed that wall texture is a factor of minor influence on powders with a low particle interlocking. Further, research was then aimed at the influence of compaction ratio on capsule fill weight. Clean and coated nozzles were used in an MG2 simulator. For all powders there was a decrease in the fill weight with an increase in compression ratio, which was attributed to coated nozzle wall and loss of powder behind the piston underside. Powders with small particle size fraction required some compression to be retained in the nozzle. High

compression ratio in powders with wide particle size distributions caused the piston to jam in the nozzle. The level of material adhered to the dosator walls decreased with particle size and increased with compression ratio. In the last work published from this series, the measured bulk densities of the plugs were compared, with those calculated/predicted from powder bed density and the known piston displacement during filling. Capsules were filled at a range of compression ratios and samples were weighed. Correlation between values was poor because of the weight variation, which it was more notable in fine powders with higher compression settings.

Britten, Barnet & Armstrong (1996) found that plug formation was highly affected by speed of compression rather than the speed of pin/dose ejection. Higher speeds led to a less consolidated dose and lower dose weights. However, higher pressures reduced plug weight variations.

Tattawasart & Armstrong (cited in Jones 2001) studied lubricant concentration, dosator pressure and piston height and setting on the properties of lactose doses. Their analysis showed that plug porosity was dependent upon piston pressure, while plug weight and length were dependent upon piston height. Ejection pressure was dependent upon both piston pressure and height. Lubricant at a concentration of 0.5% by weight provided adequate lubrication for lactose in this research.

Podczeck et al (1999) compared the filling of granules into hard gelatine capsules using a dosator (Zanazi) and tamping (Bosch) filling machine. These were used with four different size fractions of Sorbitol instant. It was found that the filling performance was independent of the machine type used. For coarse particle sizes the tamping machines were slightly better. With the dosator filling machine the doses were denser than the tamping filling machines. For low plug density, tamping filling machines were found to be more suitable and for greater compression dosators were found to be better.

3.3.1. Dosator machine instrumentation

Instrumentation of dosator machines is important for scientist and drug developers because it is not possible to precisely measure of drug dissolution without being able to precisely control the compression on the filling machines (Augsburger cited by Jones 2001).

Due to the geometry, design and operation of the dosator filling machines, it has been difficult to measure the forces acting within the instrument during the compression cycle. A few researchers have published their work and they have mainly used Zanazi LZ-64, Zanazi AZ-20 and MG2 simulator machines. In the majority of the work the dosator pin has been instrumented with range of force sensors and linear voltage displacement transducer's (LVDT's).

Significant differences in the range of forces acting in the dosator have been published in these works and the variation in magnitude could be attributed to differences in the powder used, the dosator operating principle and the machine set ups at the time of the trials.

Cole & May (1975) instrumented the first dosator filling machine (Zanazi LZ64) by attaching a pair of strain gauges to the shank of the piston using a planetary gear system to overcome geometry and machine operation problems. Different formulations with different quantities of lubricants were used for the study; mostly microcrystalline cellulose and modified corn starch fractions. Forces along the Y axis of the dosator pin where measured; filling and ejection pin forces were registered from 25N up to 130N. Ranges of blends were filled into capsules. They noted a residual force recorded between the compression and ejection stages, which it was ascribed as expansion of the powder plug. The capsule fill weight and force variations were attributed to the quantity of lubricants in the blends. In these trials the amount of compaction of the dose was dictated by the powder bed depth and the pre-fixed dosator pin height were fixed, so any differences in the magnitude of the measured forces could be attributed to the properties of the powder.

Small & Augsburger (1977) introduced some modifications to the Zanasi machine by using mercury contact swivel to pick up the signals from the strain gauges, enabling the application of compressive forces to the piston during the plug formation. They observed the same compression, retention, ejection and drag forces observed by Cole & May (1975), but the traces were different.

Small & Augsburger (cited by Jones 2001) ran tests with microcrystalline cellulose, lactose and starch to examine the effects of the powder bed height, piston height, lubricant type, lubricant concentration and compression force with the ejection force. The ejection force increased with compression force and was proportional to powder bed and piston height.

Mehtha & Augsburger (1980) instrumented a dosator capsule filling machine Zanazi LZ 65 and added a LVDT. This was used to obtain compaction profiles and force-displacement curves to evaluated compression in the blends and facilitate lubricant evaluations. By adding the LVDT, they detected that the maximum compressive force was reached slightly before the maximum piston displacement; this was attributed to of the overload spring. The machine was used for further studies between plug dissolution and plug strength.

Veski & Marvola (1991) reported tests undertaken using an MG2 dosing tube and piston. The dosing tube was attached to a plastic plate which was joined to a balance; enabling the measurement of forces during the compression. The piston was fixed to a lever and spring system that moves up and down. The powder was poured into the tube and then compressed by means of the piston. The equipment was used to measure and compare compression forces with dissolution of the powders.

Mony, Sambeat & Cousin (1977), Mehtha & Augsburger (1981), Botzolakis & Augsburger (1984), Maury et al (1986), Hauer, Remele & Sucker (1993a, b) El-Shaboury et al (1993), Guo & Augsburger all cited by Jones (2001) and Rowley et al (1983) used other methods to measure the forces during the dosator operation (ex. quartz load washers) and mainly investigate the effect in strength, ejection force and dissolution properties of the doses by adding lubricants in different concentrations to the formulation.

3.3.2. Dosator machine simulators

Due to the complex geometry and operation of the dosator production machines, there were developments of dosator simulators to facilitate measurement of dosator forces, especially during plug ejection.

Jolliffe & Newton (1980) reported the first simulator of a dosator type machine. They used a non-rotating capsule filling rig with a MG2 dosator nozzle with strain gauges. The dosator was attached to a crosshead assembly which enabled it to be inserted into the powder bed to a precise depth. It applied compression to the doses through the dosator pin, driven by a pneumatic system. The paper does not mention precisely the dosator principle used, whether this is due to a fixed volume cavity descending into the bed, or whether in addition the pin is lowered to compact the dose. The dosator was equipped with an LVDT sensor to measure

position and strain gauges to measure ejection stresses, during the trials. The objective of the investigations was to study powder coating of the dosator walls. For this reason the simulator was used to determine when the filling and ejection forces were stable in order to know the dosator weight difference for this condition, by comparison with the initial start-up values.

As rotary machines appeared, Jolliffe & Newton (1982) fixed the position of a turret, from a dosator MG2 G36 machine, and built a simulator where the powder bed rotated around the fixed dosator in exactly the same manner as the production machines. They instrumented the dosator pin with a strain gauge and LVDT and the dosator body with a LVDT too. The simulator was used to correlate improved dosing as a function of increased particle size, over a 20 to 100 μm range. The increase in the particle size reduced the compressibility and the wall friction angle of the powder. Jolliffe & Newton (1983) used an MG2 G36 machine to confirm the results of the MG2 simulator.

Britten, Barnett & Armstrong (1995) developed a dosator simulator that measured radial and axial stresses and used an LVDT to monitor the movement of the powder bed and dosator plunger, simulating the action of Macofar 13-2 dosating capsule-filling machine. Britten, Barnett & Armstrong (1996) used this simulator to study the effect of lubricants on axial and radial pressures. It was found that plug properties, strength, density and length were affected more by the speed of compression rather than the speed of the dose ejection.

3.4.   Powder bed conditions

Irwin et al. (1970) mentioned in their research that the powder bed condition affected the fill weight uniformity.

Woodhead et al. (1982) developed a gamma-ray attenuation technique to study the porosity of powder beds. The powder used in this research was lactose monohydrate with three different particle size distributions. The studied showed wide local porosity variation in the three particle size fractions studied. They expected the coarser free flowing size fractions to pack more uniformly; such a simple trend was not observed. It was stated that the lack of uniformity in the feed tray could lead to an unacceptable variation in fill weight.

Demetry et al (1998) developed a system to measure uniformity in powder beds after die filling. It used a tactile sensor at the bottom of the moulding dies, in between rubber mats, for

assessing the bulk density uniformity of powders. Non-uniform mass distribution after the filling process was detected.

3.5.   Models of dosator filling systems

Reier et al. (1968) presented one of the first approaches correlating powder properties and semiautomatic capsule filling machine settings. A mathematical model to predict fill weights in formulations was developed relating weight variation to: machine speed (turntable speed), capsule size, powder specific volume, flowability and presence of lubricants. After computer analysis, the mentioned properties were the variables of three polynomial equations, and surface contours charts were generated from them. The results from these charts showed that for a given capsule size and machine speed, specific volume almost determine the mean capsule weight. Specific volume was obtained using tapping density method divided by weight of powder. Flowability was measured using the angle of repose method; it was stated that the authors realized that what is measured in this procedure (area occupied by the powder passing through a glass funnel) was maybe interparticle and powder-surface friction rather than flowability. Particle size was measured by sieved analysis and it was found internal correlations between particle size responses and specific volume and/or flowability, but this factor was eliminated as correlation coefficients did not significantly vary without them. This research used a Lilly model 8 capsule filling machine. The model reveals that the fill weight was dependent on specific volume, flowability, machine speed and capsule size. The weight variability was a function of machine speed, specific volume, powder flowability and the presence of lubricants, but independent of the capsule size. The equations proposed [3.4] [3.5] [3.6] are as follows:

$$Y_1 = 630.71 - 34.37(X_1) + 1.92(X_1)^2 + 1185.99(X_2) + 561.99(X_2)^2 - 421.46(X_3) + 110.34(X_3)^2 - 11.20(X_4) - 24.31(X_1.X_2) + 8.27(X_1.X_3) - 433.57(X_2.X_3) \quad \textbf{[3.4]}$$

$$Y_2 = 25.73 + 0.27(X_1)^2 + 40.15(X_2) - 10.01(X_3) + 1.83(X_3)^2 - 14.84(X_4) + 3.23(X_4)^2 - 0.60(X_5) - 4.22(X_1.X_2) - 0.54(X_1.X_4)$$
$$\textbf{[3.5]}$$

$$Y_3 = 4.28 + 0.04(X_1)^2 + 0.23(X_3)^2 - 1.86(X_4) + 0.45(X_4)^2 - 0.13(X_5) - 0.15(X_1.X_3) - 0.11(X_1.X_4) \qquad \textbf{[3.6]}$$

Where:

Y_1= mean gross capsule weight, (mg),

Y_2= capsule weight standard deviation, (mg),

Y_3= capsule weight coefficient of variation, (%),

X_1= machine speed, (r.p.m.),

X_2= capsule size, (ml),

X_3= specific volume, (ml/Gm),

X_4= flowability, (sq. in. Area of the funnel outlet to flow),

X_5= presence of talc (+1) or absence of talc (-1), (ml).

This work is a good approach and presents an interesting model to overcome production problems. From the point of view of this thesis, the model is limited as it does not include powder behaviour, compression and other factors involved in the operation that compromise the dose procurement.

Recently Khawam (2011) and Khawam & Schultz (2011) proposed a mathematical model for powder encapsulation in dosator machines. The model covers several of the different dosator operating principles mentioned in chapter 2, where in some cases the filling experiments include pre-compaction of the powder. The plunger has different positions, before or after the dosator insertion into the powder bed, with the aim of achieving dose densification. The model consists of the integration of different factors like spring tension (that actuates the piston), pre-compression and compression densification factors (f_1 and f_2 respectively, relate the different piston positions during the operation) and the weight of the dose (that integrates volume of the dose chamber, powder density and pre-compression densification factor). The pre-compression densification factor "f_1" includes a flow factor "F" that is not well explained in the papers. Ideally "F" varies between 0 and 1 and it is determined experimentally, but there is not enough information published about how was calculated. The parameters of the model are as following:

- Powder bulk density in the dosator [3.7]:

$$\rho_{dosator} = \rho_{bulk} * f_1(p) * f_2(p) \qquad [3.7]$$

Where ρ_{bulk} is the bulk density, f_1(p) [3.8] is the pre-compression densification factor (relates the pre-compaction of the powder during the insertion of the dosator into the powder bed) and

$f_2(p)$ [3.9] the compression densification factor (relates the compression of the powder from the piston).

$$f_1(p) = \big((1 - F) * \ln(f_1(p)_{set})\big) + 1 \qquad\qquad [3.8]$$

Where F is the powder flow factor, $f_1(p)_{set}$ is the set pre-compression densification factor (relation of the powder bed depth "H_{powder}" divided by the initial height of the piston "H_{piston}").

$$f_2 = \frac{H_{dosator}}{H_{plug}} \qquad\qquad [3.9]$$

Where $H_{dosator}$ is the minimum value between powder bed depth and the initial piston height, and H_{plug} is the dose length.

- Compression factor X that is the relation of the displacement of the achieved displacement of the piston ΔH divided by the set piston displacement H_{com}.

- Flow factor F. It is not related with Carr's index, flow function or Heckel compressibility parameters. It is calculated experimentally.

- Spring factor k [3.10]:

$$H_{piston} = H_{\substack{max \\ piston}} - \left(k\left(H_{\substack{max \\ piston}} - H_{\substack{set \\ piston}}\right)\right) \qquad\qquad [3.10]$$

Where H_{piston} is the initial piston height, $H_{max/piston}$ is the maximum piston height and $H_{set/piston}$ is the piston the set piston height.

- Various heights like the mentioned maximum piston height $H_{max/piston}$, powder bed depth H_{powder}, set piston height and displacement $H_{set/piston}$ and H_{com} and piston diameter D_{piston}.

The model proposes an equation for the maximum dose fill weight "W" [3.11]:

$$W_{max} = \left(\left(\frac{D_{piston}}{2}\right)^2 * \pi * H_{dsoator}\right) * \big(\rho_{bulk} * f_1(p)\big) \qquad\qquad [3.11]$$

The paper suggests simplified equations for the early drug development to estimate the maximum fill weight that can be encapsulated and the minimum powder bulk density

required.   The authors proposed an interesting approach of the dosator operation and integrated different dosator principles used in the production line machines.   From the point of view of this thesis, the model does not discriminate between two powders and does not take account of the bulk density changes during the operation.   Also it does not take into account the powder flow properties and wall friction effect resisting the entrance of the powder into the dose chamber.   In the paper it is assumed efficient lubrications of the material overcomes friction issues.   It is a simplistic approach and does not analyse in depth the dosator operation principal.

3.6.   Summary of the literature review and route forward

It can be seen in this chapter that much research has been published relating to capsule filling and dosator operations since the 1960's.   It is a very broad research area and there is still a wide range of topics to be cover by future generations.

What was not found in these publications was research relating to the factors, considered critical in this project, that are directly involved in the densification of the dose.   In the same way, factors encountered in the literature were not linked to the powder flow properties and machine set up.   An explanation of this discrepancy could be due to the nature of the industry, because healing an illness is what the products are created for and therefore dissolution and potency are the primordial areas of study.   It has been noticed that explanations and solutions to the production problems are sought in the adhesion of lubricants to the formulation rather than the identification and control of parameters or the predicted flow behaviour from early stage of the drug development.   These problems could be overcome with the measurement of the powder flow properties in the formulation stage and adjustment of the machine settings in the production process.

In the pharmaceutical industry, powder characterisation has focused on the chemical and dissolution properties, with flow properties only considered when production problems arise or when new products are ready to be launched to the market.

From the published literature reviewed, it can be seen that there is a lack of understanding of the dose manufacturing process and dosator operation in this industry, from both pharmaceutical and machine manufacturers.   It is the opinion of the author that it is

imperative that prior to the manufacturing stage the base line flow properties of a new product should be known. These properties could then be used in conjunction with the models developed in this project to determine base line settings for the dosator. If this indicates that the flow properties are troublesome then re-formulation using different additives or additive levels can be used to improve the uniformity of the fill dose weight, as a last resort.

Compression of solids in industrial operations is a complex subject that has been studied in depth and there are significant things to understand.

Researchers have indirectly noticed some of the factors considered critical in this research and comments had been made about them on their publications, such as the condition of the powder bed.

The models published are simplistic, considering only the change in volume of the dose and do not relate factors encountered in this thesis, that compromise the fill dose weight such as the compactibility of the material, other flow properties and critical machine factors.

Chapters 1, 2 and 3 provided a complete panorama of the dosator operation and the researchers in this topic. The following chapter shows various stages of this research project determining the key parameters affecting the fill weight in dosator operation. Naming these factors, exposes the reasons for the flow property measurements presented in chapter 5, the test plan followed with the dosator test-rig described in chapters 6 and 7, and the proposed model presented in chapter 8.

Chapter 4

Determining Key Parameters in Dosator Operation

4.1. Introduction

This chapter describes the different stages that this research project went through in chronological order, leading ultimately to the identification of the key factors affecting the variations of the fill dose weight in current dosator filling machines.

The research was initially conducted based on the published information (presented in chapter 3), GSK's in-house understanding of dosators systems, collaboration with dosator manufacturers and, The Wolfson Centre's experience from previous investigations and consultancy work in this field. It was necessary to request details about the dosator operation from the manufacturers; MG2, Harro Höfliger and IMA who kindly responded with required information. GSK are constantly researching the subjects that affect their products and have worked closely with dosator manufacturers through different projects that have contributed to the dosator process understanding. Other tools, like the dosator demonstrator and early trials in the dosator single shot test-rig engineered at the Wolfson Centre (discussed in detail in chapters 6, 7 and 8), were also used for this evaluation.

All the external contributions received were valued for the development of the research; likewise the mentioned sources were key in the identification of the critical factors in dose control and the understanding of this filling system.

4.2. Summary of in house knowledge and findings of literature

The review of the literature showed that few authors (Gold et al. 1971, Jolliffe & Newton 1978, 1980, 1982, 1983a, b & c, Chowhan & Chow 1980, Newton & Bader 1981, Mehta & Augsburger 1981, Tan & Newton 1990a, b, c, d, e & f, Takagi, Sugihara & Kimura cited in Jones 2001, Miyake et al. cited in Jones 2001, Chowhan & Yang cited in Jones 2001, Walker cited by Denny 2002, Khawam 2011 and Khawam & Schultz 2011) had looked at links

between dosator behaviour and powder properties.   These studies have found that the principal cause of:

- dose weight variations is a result of changes in the bulk density as a function of addition level of the API/carrier, lubricants or free flow ingredients to the blend as well as the particle size of the excipient. Generally as the additive level increases, and or particle size reduces the bulk density reduces, and the dose weight variation increases.

- poor dose retention is due to a low cohesive strength of the material. Generally as the material becomes more cohesive it can form an arch across the dosator preventing unintended discharge.

The work of Joliffe & Newton (1978, 1980, 1982, 1983a, b & c) also found a link between dose weight variation and the angle of wall friction, the higher the wall friction the more inconsistent the dose.

Regarding the dosator machine settings, the only significant assessment undertaken was by Woodhead & Newton (1981) who studied the clearance between the dosator pin and body and Reier et al. (1968) and Britten, Barnet & Armstrong (1996) who looked at dosator speed. The reported effect of low clearance was reduced filling efficiency of the cavity. The dose weight was found to be inversely proportional to dosator speed.

Much of the above was supported by the in house consultancy experience of The Wolfson Centre, much of which coming from the Mk IV filling project for Relenza to troubleshoot existing dosator equipment on different production lines, measuring differences between powders that were relatively easy or difficult to process. In summary this found that different powder blends behave in different ways and that dose weight control was far more difficult for some powders than for others. The materials that were more compressible gave troublesome processing behaviour, as well as those with high wall friction and high stress ratio.

However where this thesis disagrees with the finds of the literature are over the importance of the cohesive strength for dose retention, which be discussed in section 4.3 and the importance the cohesion/adhesion of the powder to the wall i.e. the coating of the powder onto the dosator surfaces.

The mentioned projects carried out by The Wolfson Centre, led to the trialling of the wall adhesion test, i.e. using a Jenike flow function test procedure with a wall cell to measure the effect of wall adhesion for "sticky" powders. These were undertaken at The Wolfson Centre using many differing surface materials and finishes, and they showed that the choice of material and method of finishing has a very strong effect on this wall adhesion characteristic.

4.3. Preliminary modelling

It was anticipated that the processes of filling and discharging a dosator tube with a cohesive powder could be modelled analytically using existing powder and soil mechanics theory, based initially on a one-dimensional approach which is well proven for the case of powder flow in cylindrical silos (Arnold, McLean & Roberts 1982 and Schulze 2008). The model requires inputs based on the measured bulk flow properties using techniques established and recommended by Jenike et al. (1961& 1964), Arnold, McLean & Roberts (1982) and Schulze (2008), for measuring the bulk density, wall friction and the stress ratio.
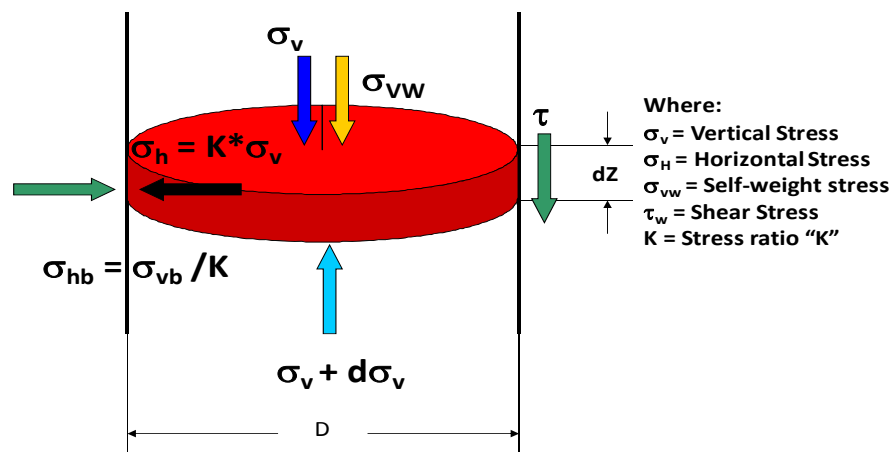
Figure 4.1. Representation of the stresses acting in a differential powder element slice assumed for dosator operation; based in Janssen effect application moving a column of powder upward in a vessel (Arnold, McLean & Roberts 1982 and Schulze 2008. For full explanation refer to the text.

Figure 4.1 shows the forces acting in a differential powder slice inside the dosator; this force balance is described in figure 2.36a, section 2.7.1 illustrating a specific case of the Janssen effect of a column of powder being pushed upwards in a vessel. In the vertical axis, there is a vertical stress either transmitted from the previous slice or from the pin's face, σ_V, a vertical contribution from the self-weight, σ_{VW}, a vertical contribution of the friction (opposite

direction to the powder motion), τ, and a resultant transmitted to the next slide or to the powder bed, $\sigma_V + d\sigma_V$. As the system is constrained there is a horizontal stress inside the dosator, σ_h, and another lateral stress in the bed, σ_{hb}.

4.3.1. Stress ratio

A 1-dimensional model for the dosator described in chapter 8 was developed based on the Janssen method described in chapter 2, section 2.7.1, figure 2.36 and figure 4.1. As the dosator is a volumetric system, the powder in the dose chamber tries to expand laterally as result of the compression during the insertion and ejection stages. It was anticipated that this lateral stress in the dosator would have a significant effect on the wall friction and dose retention.
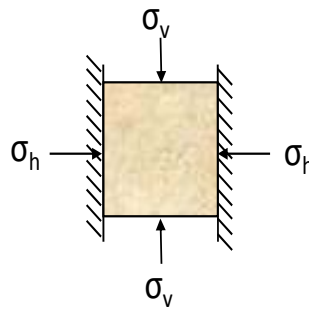
Figure 4.2. Bulk solid element under vertical compression, constrained by two vertical walls. For full explanation refer to the text. Re-printed from Schulze (2008, p. 12).

The lateral stress effect was studied through the stress ratio K. In powder/soil mechanics, the stress ratio is defined as the relation between the vertical stress "σ_V", applied to a specimen in a constrained space, and the horizontal stress resulting from the vertical compression assuming frictionless internal walls (Schulze 2008, p. 12) (see figure 4.2).

The stress ratio K of a powder typically varies between 0.3 and 0.6 (Kwade, Schulze & Schwedes cited in Schulze 2008, p. 12), whereas for the case of liquid it would be 1.0.

4.3.2. Rankine stress state

At this point it is necessary to describe the concept of the Rankine stress states. That is that the stress conditions cannot be defined uniquely but only within a specified range. If we consider the stress in a powder bed, in the vertical direction this increases linearly with depth. However, the stresses in the horizontal direction cannot be resolved without reference to the boundary conditions. From consideration of the Mohr-coulomb failure criterion for a powder as shown in figure 4.3, for a given vertical stress σ_y, there are two possible limits for horizontal stress σ_x during flow, depending on whether this greater than or less than σ_y.
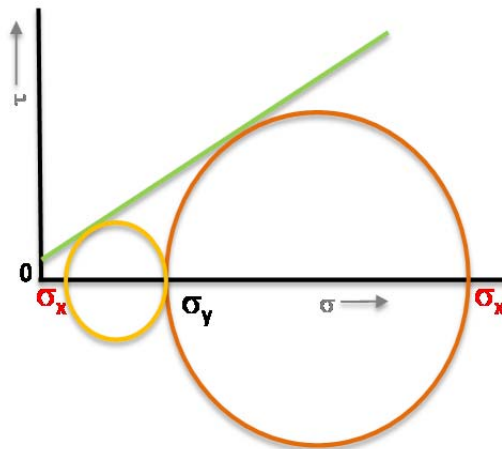
Figure 4.3. Rankine stress and Mohr coulomb failure criteria. Re-printed from Nedderman (1992, p. 31). For full explanation refer to the text

The lower limit for the horizontal stress σ_x is obtained if the walls the container are slowly moved apart to cause flow (see figure 4.4a), known as the active state of stress. This is assumed to be occurring in the powder bowl of the dosator. The upper limit for the horizontal stress σ_x is obtained when the walls of the container are slowly moved together to cause failure (see fig 4.4b), known as the passive state of stress. This is assumed to be occurring in the dosator cavity.

a)   b)
Figure 4.4. Rankine stress state: a) active; b) passive. Re-printed from Nedderman (1992, p. 32). For full explanation refer to the text.

Thus considering the dosator operation, as the body strokes down into the powder bed, material flows into the cavity until the horizontal stress in the dosator equals the horizontal stress in the bed. At which point material cannot longer flow into the cavity and powder spreads ahead of the dosator tip. This situation is shown schematically in figures 4.5a & b on stress versus bed depth space and on a Mohr-Coulomb diagram.   Hence in the powder bed $\sigma_h = \sigma_v/k$, but in the dosator $\sigma_h = \sigma_v * k$.
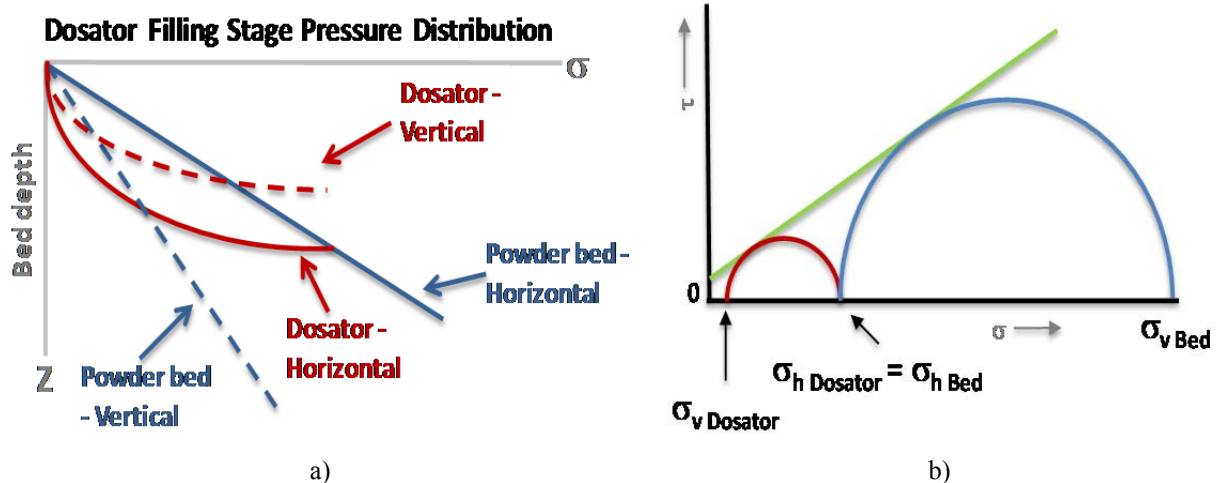
Figure 4.5. Dosator model with assumed: a) stress distribution in the dosator and powder bed; b) Mohr-Coulomb diagram for the stress in the dosator and powder bowl. For full explanation refer to the text

4.4. Experimental dosator test-rig and evolution of the project

Initially the intention was to use the 3PI single shot test rig owned by GSK for the experimental work of this thesis; this test-rig was designed to replicate the production operation of dosator filling machines (described in chapter 9). The main features of this test-rig are the weight control of the doses and measurements of the ejection force; it can achieve approximately 377 strokes per hour.

However, for this research it was considered important to understand the compression behaviour of the dose during the filling stage as well as the ejection behaviour. A low dosator stroke and ejection speed was selected in order to accurately measure the forces in the filling and ejection stages. To achieve these experimental objectives with the 3PI test-rig, would have required significant modification, including a sensor to monitor pin position and dosator's body force and position. Economically this instrumentation was not feasible and the

outputs did not guarantee meeting The Wolfson Centre requirements (details are presented in chapter 9).

It was decided to engineer a cost effective dosator single shot test-rig at The Wolfson Centre (details are presented and described in chapters 6 & 7) for the experimental work of this research. The test-rig was instrumented with dosator pin and body position/force transducers and low dosator stroke speed. The speed of the dosator could provide accurate measurements of the forces but there was a query about the issue of the speed scale up to the production operation.

Powder bed condition in production filling machines (Irwin et al. 1970, Woodhead et al. 1982 and Demetry et al 1998) was another concern for The Wolfson Centre. For this reason The Wolfson Centre test-rig was not equipped with a bed re-conditioning system, in order that this could be prepared homogeneously, so as not to affect the force measurements in the dosator (described in chapters 6 & 7).

The use of the single-shot dosator test rig could enable verification of the model, and showed what effects can be modelled effectively and where limitations lie in dosator operation. This lead to a rational definition of what tests should or could be done during the development stages of a project, to optimise the accuracy of predictions about powder performance in the dosator system through which it is filled.

Early observations in trials undertaken in The Wolfson Centre dosator single shot test-rig and the development of the initially proposed model enriched the research and dictated a change in the direction of investigation. These interpretations led to the identification of the most critical machine setting factors in the dose procurement of this filling system, namely the clearance gap between the tip of the dosator and the base of the trough at the end of the stroke which has not been published in the literature and this lead to a re-structuring of the dosator model proposed in this thesis.

It therefore seems reasonable to suppose that further development should enable this model to give a degree of prediction of how easy or difficult a given powder is likely to be to fill in a dosator-type system, based on measurements of the powder flow properties and wall friction which can be done on a small scale in the laboratory.

3PI test-rig was not discarded from the project. It was used in the last stages of the project to corroborate the scale up of the dosator speed and its effect in the dose procurement. The Wolfson Centre carried out tests at GSK Harlow facilities to accomplish this topic.

It is worth mentioning that permeability of the powder was another factor depicted from the literature reviewed (Woodhead & Newton 1981) affecting the dosator operation. It is frequently associated with the dosator speed, as the air might not permeate efficiently through the particles arrangement and to the clearance between the dosator pin and dosator body inner-wall (Woodhead & Newton 1981).

During the powder compression, air entrained within the powder possibly can create issues such as storing energy within the dose, released later, in turn creating further variability in dose weight. In this thesis, permeability was not considered to be an important issue because the low operating speed of the dosator test-rig sufficient time was given to the powder to displace gas (generated from reducing particle voidage) permeating through the clearance between the dosator pin and body or the interface dose/powder bed. However, comparing the particle properties, size and density presented in chapter 5 with Geldarts classification (Schulze 2008, p. 222), suggest that the Lactohale 300 is in the non-fluidising Group C, while the other three are on the boundary between non fluidising (Group C) and fluidising (Group A). This was in contradiction with the permeability tests undertaken where all materials exhibited non-fluidising behaviour.   Unfortunately these tests were less than satisfactory (refer to appendix 3 for more details). The main problems encountered measuring the permeability of the powders were the dimensions ratio between the cylindrical sample, the gas flow and the powder resistance of the powder to the gas flow.

Notwithstanding, permeability is linked to the packing behaviour of the particles and this thesis measured the particle density of the powders used in this research. Some appreciations regarding to this matter are discussed in chapters 5 and 7.

4.5. Summary

This chapter provided an overview of the different stages of the project determining the factors affecting the dosator operation. It was briefly presented the initial particle/powder flow properties and machines factors anticipated by The Wolfson Centre and encountered in

the literature review affecting the dose obtaining.   These findings oriented the development of the test-rig and the course of the research.

The following chapters, 5, 6 and 7, show the particle/powder flow properties and machine setting factors selected by this thesis as the critical ones affecting the fill dose weight.

In chapter 9 can be found the outputs and results in the 3PI test-rig studying the dosator speed issues.

Chapter 5

Materials and Powder Flow Characterisation

5.1. Introduction

This chapter presents the test powders used in this research work and their characterisation in terms of the particle and bulk flow properties. The powders considered were *Relenza* (an inhaled product) and a range of inhalation grade lactose fillers, namely: Inhalac230, Sorbolac400, Lactohale100, *Lactohale200* and *Lactohale300*. It was decided, with the consent and advice of the industrial sponsor, to work with four main powders as detailed in section 5.2. The measurements of the particle properties, size, shape and distribution are presented in section 5.3. The bulk powder flow properties measurements, the flow function, wall friction, cohesion, bulk density, stress ratio and void fraction are presented in section 5.4. A summary of chapter is given in section 5.5. The majority of test procedures of the particle and flow properties are standard; however, the test equipment to measure the stress ratio property was designed for this research and it is presented a detailed description in section 5.4.5.1.

5.2. Materials

The four main powders selected for testing in The Wolfson Centre dosator single shot test-rig were namely: *Lactohale200*, *Lactohale300*, *Relenza* and a *bimodal blend* between the *Lactohale200* and *300*.

5.2.1. Lactohale

Lactohale is a lactose α monohydrate brand of DFE Pharma, the number after the brand describes the grade of the lactose. Lactohale is commonly used as carrier for inhalation purposes, mainly because its non-toxicological behaviour and the acceptance by registration authorities. Carrier size fractions are selected for flow properties in order to obtain good dose

measuring reproducibility, but also on their interaction properties with the drug particles; their production can be designed o specific filling process and API[8].

Lactohale200 is milled controlled lactose (it can be adjusted to different D50 required by the customer) that has a degree of cohesion. The particles normally have an irregular shape with various amounts of fine particles that can be removed by air classifying. D50 for this powder is in the range of 50 to 100 μm[8].

Lactohale300 is micronised lactose with D50 below 5 microns. It is generally used for agglomerates of drugs and microfine lactose particles; it is a highly cohesive powder with size comparable to an API[8].

5.2.2. Relenza

Relenza is a respiratory product of GSK. According to the information provided by the industrial sponsor, it is a blend comprised by weight of 20% API and 80% Lactose α monohydrate. The API of *Relenza* is Zanamivir and as typical inhalation active, the D50 is around 3 μm with extremely poor flow properties.

5.2.3. Bimodal blend

The fourth powder used, at the suggestion of GSK, was a *bimodal blend* of the *Lactohale 200* and *300*. The aim of this blend was to match *Relenza* particle size distribution as the two grades of the selected lactose presented similar particle size distributions (PSD) to the *Relenza* blend ingredients. I.e. the *Lactohale300* has a PSD consistent with the Zanamivir API and the *Lactohale 200* has a consistent PSD to the lactose carrier as described in section 5.3.1.

To produce the blend the Lactohale samples were mixed to the same proportions used for the carrier and API in *Relenza* using a domestic blender. 1 kg of the *bimodal blend* was prepared. The blender had a relative movement between the blades and the bowl and both of them were operated at the low speed settings (blades 505 rpm and bowl 21 rpm) to prevent the formation of dust and fine particles loss. The industrial sponsor could not provide the mixing time used

---

[8] DFE Pharma website

for Relenza in industrial operation. Thereby, the total mixing time was assumed 6 min; particle size distribution (PSD) tests were applied to the blend showing good results matching satisfactorily Relenza PSD.   The ingredients were mixed in the same way as it is normally done for *Relenza* preparation[9]; 50% of the coarser powder (*Lactohale200*) was blended alone for 1 min, then the fine powder (*Lactohale300*) was added and blended for 2 min and finally the rest of the carrier was added and mixed for a further 3 min.

5.3.   Particle characterisation

The particle properties, the size and distribution of the powders used in this research were measured using spectrometry (dry laser diffraction) and imaging analysis (SEM) techniques. The particle densities were measured using a pycnometer. Details of particle size distribution technics are described in the appendix 4.

5.3.1. Equipment, instrumentation and methodology

The laser diffraction equipment used was a Malvern Instruments, Mastersizer S version 2.19 that it has 300 mm range lens. The pressure and analysis model for the tests were set at 1,5 bar and polydisperse respectively.

The School of Science at the University of Greenwich, using a Cambridge Instruments Stereoscan S360, carried out the SEM imaging.

The particle density was measured using a Quantachrome multipycnometer UPY-30 that employs the Archimedes fluid displacement principle. The gas used in the pycnometer was nitrogen.

Representative sub-samples for particle analysis were taken by scooping the powder in different areas of the bag and then it was stirred with a fine stick to get homogeneity in the sample. The sample was taken using a ¼ cup measuring spoon.

---

[9] Information provided by the industrial sponsor

5.3.2. Results and discussions

The mean results of the particle size distribution tests, undertaken in the Mastersizer, are presented in both figure 5.1 and table 5.1. Figure shows the volume percentage sample as function of the PSD, whereas shows the D10, D50 and D90 mean of each powder. Each PSD test was measured 3 times and the coefficient of variation is showed also in table 5.1.
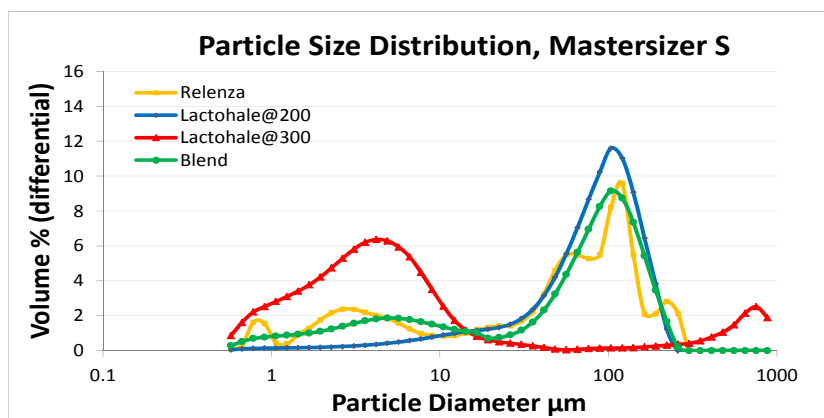
Figure 5.1. PSD of the powders used in this research. For full explanation refer to the text.

It can be seen clearly in figure 5.1 the *Lactohale200* PSD, the powder is composed by a large particle size (in between 100 and 200 µm) with few portion of fines. For *Lactohale300* can be confirmed that is composed by small particle size in the order of 4 – 8 µm. It can be seen that there is a second peak in *Lactohale300* size distribution, just below 1000µm, this was attributed to the particle agglomeration during the sweeps in the test due to the highly cohesive nature of the powder; it is also reflected in the D90 in table 5.1.

Particle Size Distribution Test – Particle Size [µm]											
Powder	Lactohale200			Lactohale300			Relenza			Bimodal blend		
PSD	Mean	SD	CV%	Mean	SD	CV%	Mean	SD	CV%	Mean	SD	CV%
D10	17.10	0.04	0.25	1.60	0.06	5.74	2.15	0.05	2.13	2.75	0.12	4.45
D50	80.51	0.14	0.18	3.92	0.20	5.13	54.29	1.27	2.34	67.36	1.62	2.40
D90	144.94	0.49	0.33	360.70	315.52	87.47	145.28	4.44	0.03	143.24	2.59	1.81

Table 5.1. Mean PSD of the powders used in this research; results from the Mastersizer S. SD = Standard Deviation, CV% = Coefficient of variation (percentage). For full explanation refer to the text.

The *Relenza* curve showed irregular size distribution with multiple peaks. This could be also attributed to the agglomeration of the particles during the test, due to the strong adhesive forces between particles that makes difficult the identification of single particles. Nevertheless, two main heaps can be seen in the curve around 3µm and 150 µm that could describe the particles sizes of the API and carrier respectively. The Lactose *bimodal blend*

showed smooth curve and can be clearly identified the two particle sizes corresponding to *Lactohale200* and *300*. The *bimodal blend* satisfactory matched the *Relenza* PSD, confirming a good blend process and good selection of the ingredients.
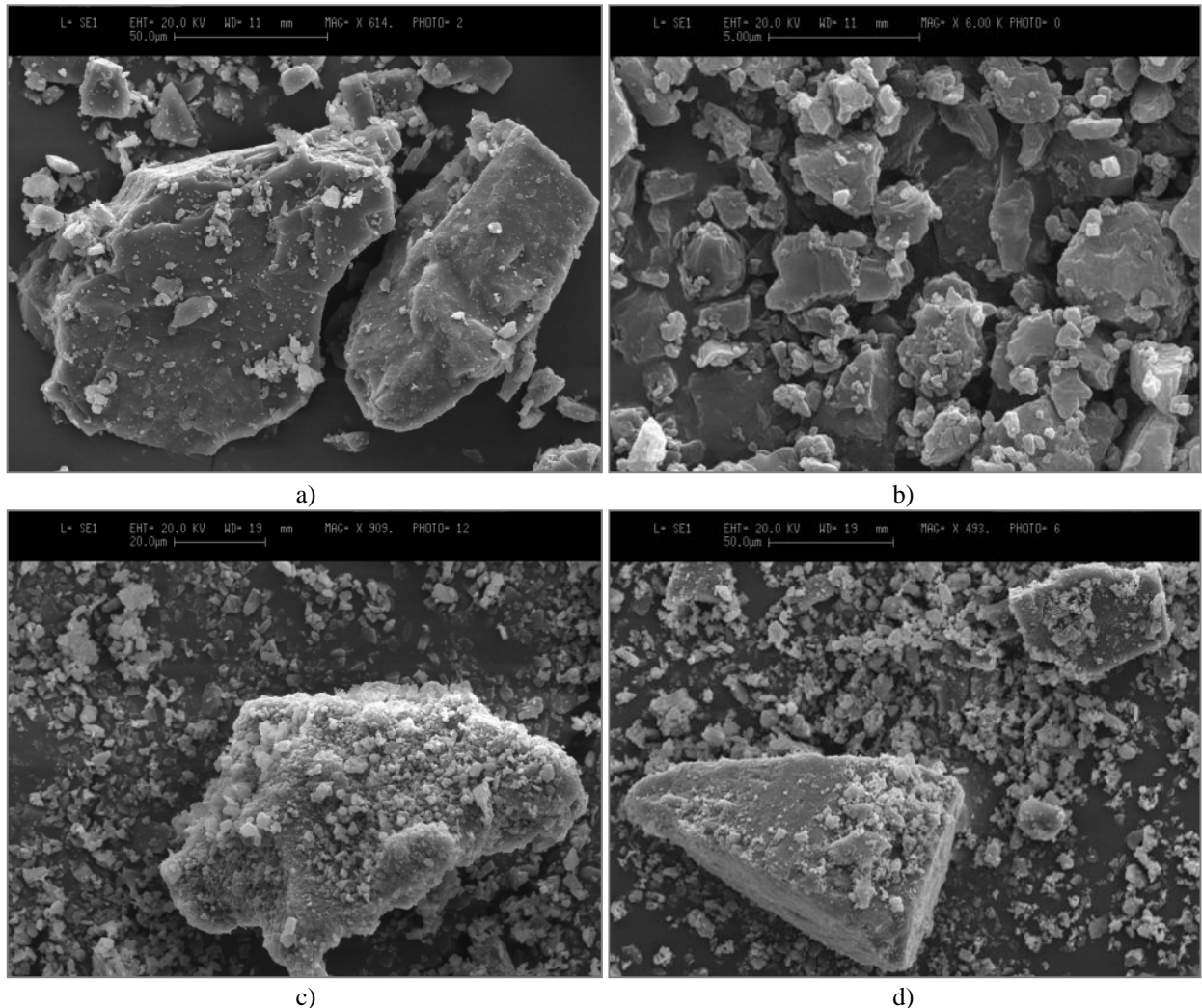
Figure 5.2. Particle size of the powders used in this research using SEM: a) *Lactohale200*; b) *Lactohale300*; c) *Relenza*; d) lactose *bimodal blend*. For full explanation refer to the text.

Overall particle size distribution results showed good repeatability. However, *Lactohale300* with the smallest particle size and highest cohesion, showed major variations in the tests; the same was thought to likely happen with the lactose *bimodal blend* and the results confirmed the expectations (see D10, D50 of *Lactohale300* and D10 of lactose *bimodal blend* in table 5.1).

The SEM test results are shown in figure 5.2a, b, c & d for *Lactohale200, Lactohale300, Relenza and the Bimodal Blend*. The images were taken at different magnifications due to differences in powders particle size range. Inspection of figure 5.2 shows that all powders are

in good agreement with the mean particle size obtained from the laser diffraction test and the manufacturer's technical sheet. Also the SEM images of the two lactoses suggest low particle packing (few contact points between particles) and adhesion forces in *Lactohale200* (see figure 5.2a), whereas large cohesion and tight packing (several particle contact points) in *Lactohale300* (see figure 5.2b). Figures 5.2 c&d show the attachment between the powders that constitute the blends used in this research. For *Relenza*, the SEM image suggests better particle attachment between the fine and coarse particles than in the lactose *bimodal blend*. The observation of significant fines detachment in the blend might suggest that this will be freer flowing than the *Relenza*.

 Table 5.2 shows the particle densities that were measured for the four test powders using the pycnometer. All materials had very similar values. The two lactose excipients had the extreme densities and the blends similar values were in between.

Particle Density			
Powder	Average particle density kg/m^3	SD	CV%
Lactohale200	1577.0	0.004	0.24
Relenza	1555.9	0.008	0.52
Bimodal blend	1554.2	0.009	0.58
Lactohale300	1549.4	0.011	0.67

Table 5.2. Particle density of the powders used in this research. SD = Standard deviation, CV%= Coefficient of variation (percentage). For full explanation refer to the text.

The particle size has a significant impact on dosator operation as it affects the flow and compaction properties of the powders. It also affects the dissolution of the drugs and aerosolised particle properties in dry inhaled powder applications. Pharmaceutical powders are challenging to manufacture; from the production process point of view, the particle size should be larger for best handling and flowability results (Podczeck & Jones 2004).

Nevertheless, pharmaceutical blends must contain API's that are normally small particle sizes, in the case of dry inhaled powder applications no larger than 10 µm particle size to be able to reach the lungs after the patients inhalation. Small particles can follow the airstream, but heavy and dense particles cannot; they are deposited on the mucosa or trachea walls or go directly to the stomach. Children or elderly patients cannot easily induce a strong airstream therefore heavy particles are not suitable. Smaller particles also dissolve quicker and

aerosolise better[10]. Particle sizes below 3 μm are considered unsuitable for deposition
(Podczeck & Jones 2004).

Particle size influences the packing behaviour of the pharmaceuticals blends. As the particle
reduce in size, surface forces (friction, van der Waals') dominate over gravity forces and the
packing structure becomes more open; therefore powder flow properties are affected.

5.4. Bulk flow property measurements

Presented below are the bulk flow property measurements undertaken with the four test
powders. In technically tests a sub-sample of the order of 1 kg to 50 g was taken for testing,
as dictated by the cell volume of the tester to be used and spread out on a tray to break up
agglomerates. All tests were undertaken at ambient conditions of temperature and humidity.

5.4.1. Flow function property measurement

The primary powder flow property is the flow function (described in chapter 2, section 2.6.3)
is used to measure the flowability of the powders.

a)   b)   c)
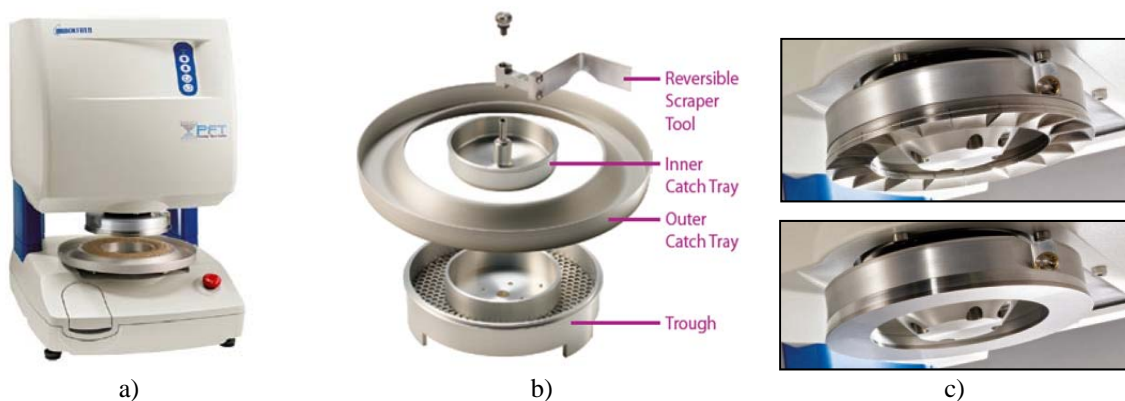
Figure 5.3. Brookfield powder flow tester (PFT) and components: a) PFT tester; b) trough and powder bed
accessories; c) types of lids, vain lid (top) and flat wall friction lid (bottom). Re-printed from manufacturers
customer leaflet. For full explanation refer to the text.

The equipment used to measure the flow function was the Brookfield Powder Flow Tester
(PFT) shown in figure 5.3a. It follows the test procedure ASTM 6128 to analyse and

---

[10] Proceedings from the APS Inhalation 2009 at The University of Nottingham conference attended by the author

characterise powder flow behaviour in industrial processing equipment. To measure this flow property, the tester is set using a vain lid (see top figure 5.3c). The tester is automated and measures the flow properties using the annular and Jenike shear tests techniques.

5.4.1.1.   Test conditions

The flow function tests were undertaken using the standard volume 263 cc shear cell, running the standard flow function test. This measures the flow properties over a range of five consolidation stresses in a geometric progression that generates values of approximately, 0.6, 1.2, 2.5, 5 & 10 kPa.

5.4.1.2.   Results and discussion

Figure 5.4 shows the flow function results obtained for the four main powders used in this research. The materials are ranked as follows in order of reducing flowability: *Lactohale300*, *bimodal blend*, *Relenza* and *Lactohale200*. As was expected from the PSD tests and the powder manufacturer technical sheet, the flow function of the *Lactohale300* and *Lactohale200* confirmed the corresponding cohesive and easy flowing behaviour. However depending on the stresses in the system the relative behaviour of the powder can change as seen in the flow function results; this information cannot be derived from the PSD tests.

From the flow function and PSD test, can be seen the cohesive nature of the *Lactohale300* and it might present high friction forces against surfaces and possible sticky behaviour as it is the general conduct of cohesive powders[11]. The opposite case can be thought for *Lactohale200* as the particle size was higher and presented a lower resistance to flow. Nonetheless, cannot be anticipated the behaviour of other flow properties based on this information, as it is unknown how the particles could interact with one another.

In figure 5.4 can be seen the flowability variance between the two blends used in this thesis; although they have similar PSD, the flow behaviour differs. Probably the poor adherence of the fine particles to the coarse in the *bimodal blend*, observed in the SEM tests in figure 5.2, explains its cohesive behaviour governed by the fine particles. Moreover the good attachment

---

[11] Based on The Wolfson Centre experience in the field.

of the API to the lactose in *Relenza* blend maybe beneficial to the flowability with the
behaviour of the mix governed by the coarse lactose particles. The results suggested that
other flow properties, of the *Relenza* and *bimodal blend* used in this research, will be
different.
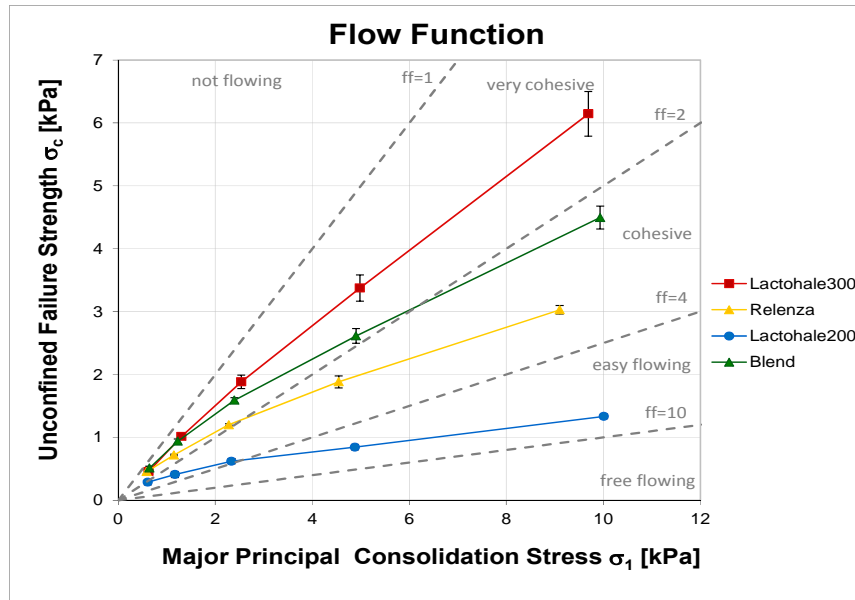
Figure 5.4. Flow function test of the powders used in this research in the Brookfield PFT. For full explanation
refer to the text.

One of the potential issues with the flow property measurements is the low consolidation
stress range of the testers, compared to those experienced in dosator operation. The flow
function was measured up to 10 kPa whereas the stresses in the dosator test-rig (described in
chapter 7) were around 2.5 MPa. The relative flow functions of the powders might change at
this high stress; however based on the experience of The Wolfson Centre, this property tends
not to have big variations at high stresses. None of current powder flow testers can operate at
the stresses level attained in dosator tests.

Various factors can affect the flowability of the powders. One of them is the sensitivity to
moisture in the working environment. Moisture contain test were undertaken to the powders
used in this thesis and showed low sensitivity to pick up moisture (see appendix 5). Probably
the reason is that all the powders used in this research are/contained Lactose powder
(described in section 5.2) and the particles have an internal water molecule able to detach at
extreme environmental conditions. Nevertheless, handling them at different environmental
conditions affect their flow behaviour. Another factor is the proportion of the ingredient in
the blends. Normally the mass containing proportion of the API in a blend does not exceed

20%; greater than that can lead to poor flow properties (Podczeck & Jones 2004, p. 101).

The flow function provides key information about the handling of the powder during the dosator operation as a function of the compression stresses; in other words, it indicates the difficulty to fill the dose chamber depending of the level of the stresses in the system. Most of the powder flow property relies on the powder behaviour measured in this property

5.4.2.   Tapped density flowability test and results

Tapped density tests were carried out on the four powders used in this research. The equipment used was the Copley JV1000 tapped density tester, at the School of Science at the University of Greenwich, and 200 taps were applied to the samples[12]. The preparation of this test is mentioned in section 2.6, chapter 2. The powders were tested three times; the mean Carr's index, Hausner's ratio results and the coefficient of variation of the tests are showed in table 5.3. Based on the results obtained and the flow manufacturer guidelines (shown in table 2.5, in chapter 2), the *Lacothale300*, *Relenza* and *bimodal blend* have similar flowability.

	Tapped Density Test											
Powder	Lactohale200			Lactohales300			Relenza			Bimodal blend		
	Value	Flow	CV%	Value	Flow	CV%	Value	Flow	CV%	Value	Flow	CV%
CI %	18.64	Fair	0	23.69	Passable	7.68	24.12	Passable	8.73	22.41	Passable	20.28
HR	1.23	Fair	0	1.31	Passable	2.39	1.32	Passable	2.81	1.29	Passable	5.77

Table 5.3. Carr's compressibility index (CI) and Hausner's ratio (HR) flowability tests of the powders used in this research. Tests carried out in Copley JV1000 tapped density tester. CV% = coefficient of variation (percentage). Flow patterns from manufacturer guidelines showed in table 2.5 in chapter 2. For full explanation refer to the text.

The powders with a degree of cohesion presented higher coefficient of variation, especially the *bimodal blend*. Probably is due to the test procedure filling the test pipes and the visual reading of the poured density. The powders are manually dispensed into the test pipes where they can be aerosolised, when falling into the pipe, provoking an inaccurate measurement of the poured density. This confirms that the tapped density test is a device-dependant and is not suitable to describe the flowability of the powders as discussed before in section 2.6, chapter 2.

---

[12] Suggestion from the PhD students at the School of Sciences at The University of Greenwich.

5.4.2.1. Comparison between the results of the flow function and tapped bulk flowability test

The powder behaviour obtained from the tapped density tests does not correlate with the flow function test results. Besides, the flow patterns from the tapped density test, showed in table 5.3, do not match with the physical behaviour observed handling the powder during the experimental work of this thesis. The tapped density is limited and provides general information of the flowability of the powders, but does not give an indication of manufacturing behaviour.

5.4.3. Wall friction failure property measurement

To evaluate the wall friction properties, four series of wall friction tests were undertaken with the four materials. It was also used the Brookfield PFT to measure this property by changing the test set up to standard wall friction and using the flat lid showed at the bottom of figure 5.3c (refer to section 5.4.1 for more information of the normal internal flow properties set up).

The first set of tests was done to quantify the resistance exerted by the dosator inner-wall to the powder intake into the dose chamber. This test was undertaken following the standard testing procedure of a Jenike type wall friction test in an automated powder flow tester. It used a stainless steel 304 2B wall sample to measure the resistance of the powders to be sheared under stress controlled tests. The finishing of the dosator inner-wall surface and the wall sample used in the tester did not differ greatly. According to the information provided by the industrial sponsor showed in the appendix 1, the surface finish of the dosator used in this thesis was Ra 0.1 and the stainless steel wall sample surface finish in the test was cold rolled 2B, being both comparable[13].

As expressed in chapters 2, 3 and 4, this thesis is concerned about the wall friction at the base of the trough, which affects the lateral spreading of the powder ahead of the dose at the end of stroke (when gap "h" is approached).   With the intention of observing this effect and the possible repercussions in the powder bed stress distribution and the variation of the dose weight, some of The Wolfson Centre dosator test-rig tests were done by changing the surface finishing of the trough with a fablon plastic film (commonly used to protect workbenches).

---

[13] According to British Stainless Steel Association website

Thereby the second series of tests was used a standard wall friction test by covering the wall surface sample with the fablon film.

The third series of tests were undertaken following a long shear displacement wall friction test setting in the PFT. The aim was to investigate the wall friction variation with shear displacement over large distances commensurate with the friction in the dosator over large number of strokes on a manufacturing line. According to observations in The Wolfson Centre dosator test-rig trials and manufacturing experience of the industrial sponsor, the friction behaviour changes with the time.

The four series of tests were undertaken by running a flow function test on the Brookfield PFT with a wall friction lid, in order to measure the adhesion/wall cohesion between the powder and wall at zero normal stress.

5.4.3.1.   Results and discussion of wall friction tests on stainless steel

The standard mean wall friction test results are shown in figures 5.5a & b; presented as wall friction loci (shear stress) and friction function (angle of wall friction) respectively. The angle of wall friction was calculated from the tangent of the shear and normal stresses of the results. The powders are ranked as follows in order of reducing wall friction: *Lactohale300*, *Relenza*, *bimodal blend* and *Lactohale200*. The results in figure 5.5a were fitted in a linear trend line.

As expected from the above properties measured, the *Lactohale300* has greater resistance to shear against the stainless steel wall sample than the *Lactohale200*; this could be attributed to the cohesive nature of the powder and particles size having major contact points against the surface. Wall friction angles above 30° are typically considered high according to the Wolfson Centre consultancy experience. This is the lower limit for the internal friction of free flowing materials (Jenike et al. 1961, 1964). It appeared that the *Lactohale200* governed the behaviour in the *bimodal blend* showing low wall friction effects; based on the poor attachment between fine and coarse particles (seen in the SEM tests in figure 5.2d) and the flow function results (see figure 5.4), it was expected a steeper wall friction trend line.

Wall friction is one of the most important properties in the characterisation of powders and in bulks solids handling affects equipment design for reliable flow and structural stability

(Bradley & Berry (2009); dosators cannot be the exception within the powder handling applications in the industry where the wall friction is involved.
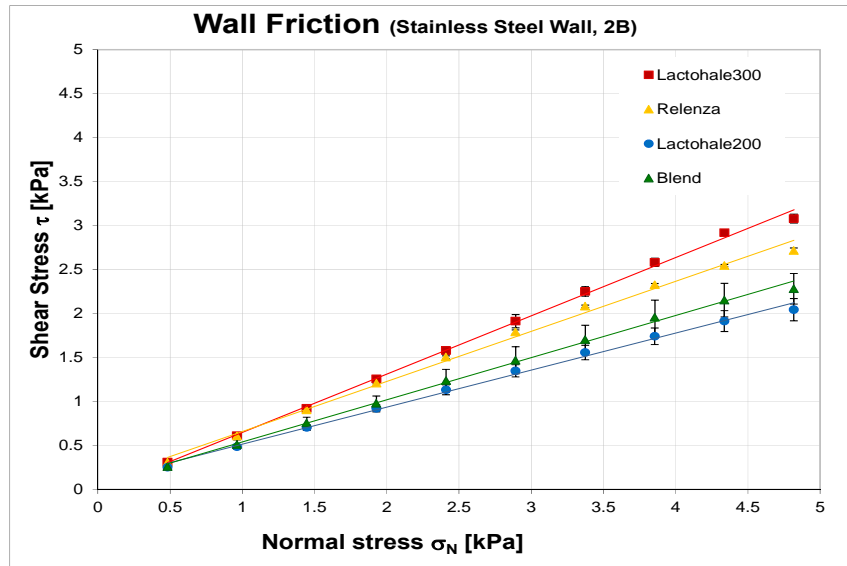
a)
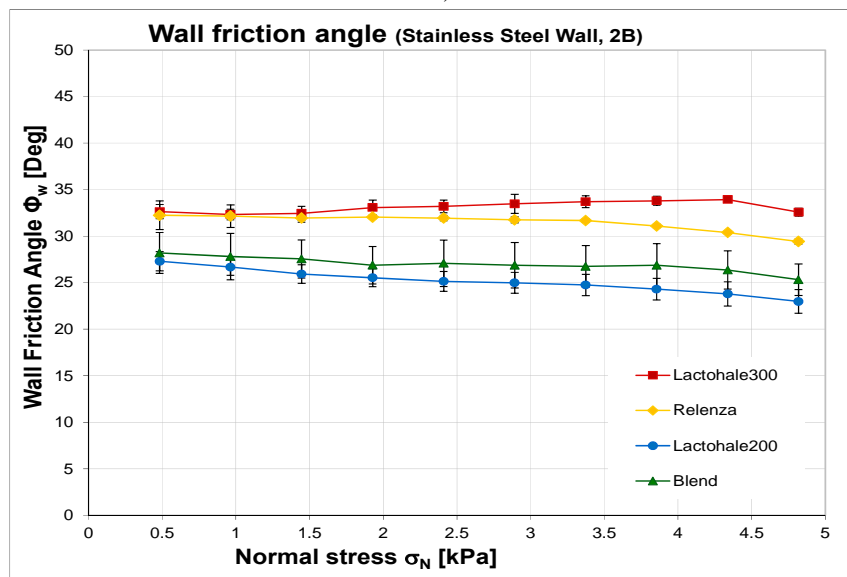
b)

Figure 5.5. Stainless steel wall friction test results of the powders used in this research: a) shear stress τ as function of the normal stress σ_N; b) angle of wall friction Φ_w as function of the normal stress σ_N. Data obtained from the Brookfield PFT. For full explanation refer to the text.

Wall friction is critical in the dosator system at the filling and ejection stages, when the powder enters into the dosator (described in section 2.7.1 in chapter 2) or when the plug is pushed out of the cavity to the packing receptacle. Wall friction in not constant inside the dosator, it varies with the length, as it was described in the Janssen effect application (see section 2.7.1 in chapter 2). This behaviour was demonstrated in longer doses obtained in the dosator test-rig (showed in chapter 7, section 7.7).

In this thesis, wall friction is also believed to be present at the bottom of the trough when dosator finishes its stroke; in current machines is likely to happen as the gap "h" is minimal. This topic is also discussed in the later section 7.6.5 in chapter 7 and chapter 8.

5.4.3.2.   Results and discussion of wall friction tests on fablon film

Figure 5.6a & b shows the results of the second set of tests using the standard wall friction test with the fablon film surface finish.
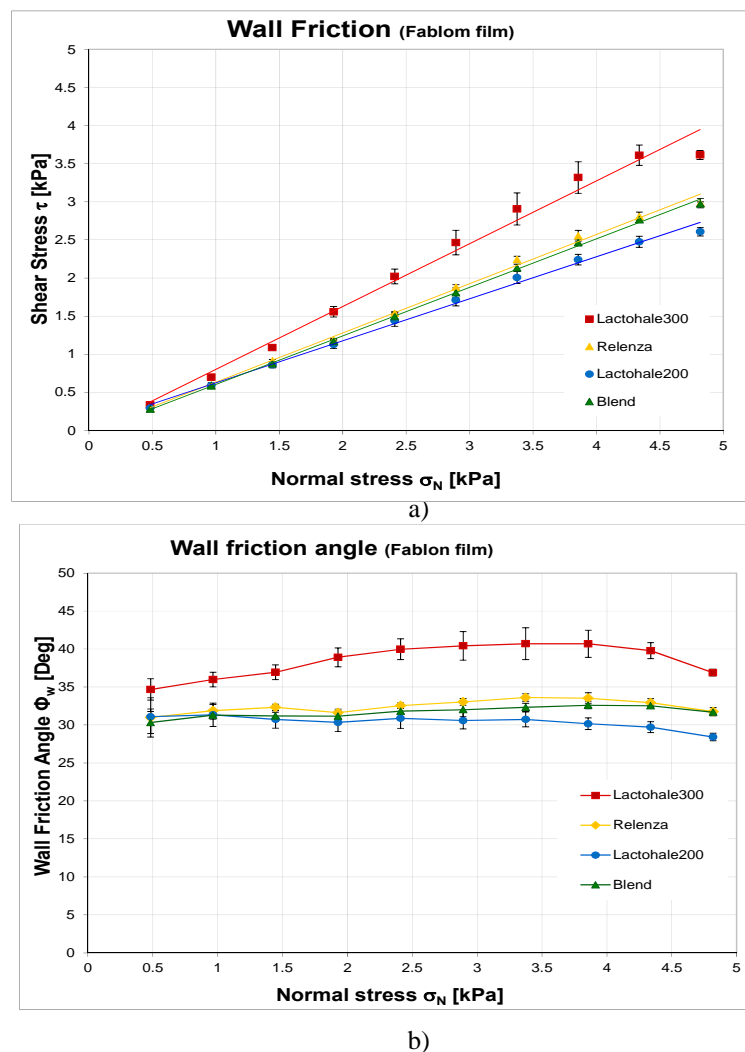
Figure 5.6. Fablon film wall friction test results of the powders used in this research: a) shear stress τ as function of the normal stress σ_N; b) angle of wall friction Φ_w as function of the normal stress σ_N. Data obtained from the Brookfield PFT. For full explanation refer to the text.

Similar to the first set of tests, the data is presented on shear stress, τ, and angle of wall friction, Φ_w, axes respectively, as function of the normal stress, σ_N.

The results in figure 5.6a were fitted with a linear trend line. The wall friction increased significantly for all four powders with the change of the wall sample surface; however *Relenza* showed the smallest increase and Lactoahle300 the highest. Relenza and bimodal blend presented similar values. The powders are still ranked in the same order as for the stainless steel with *Relenza* and the *bimodal blend* having very similar values.

5.4.3.3. Results and discussion of long shear displacement wall friction tests on stainless steel

In the long wall friction tests, *Relenza* and *Lactohale300* showed higher powder adhesion to the wall surface than the rest of powders. Figure 5.7 shows the state of the lid before and after the *Relenza* long wall friction test; notorious powder build up can be seen in figure 5.7b. This problem probably can be overcome by changing the dosator inner-wall surface, as mentioned by Joliffe & Newton (1980).

a)   b)

Figure 5.7. *Relenza* lid build up in the long wall friction test: a) clean lid before the test; b) dirty lid after the test. Test undertaken in the Brookfield PFT. For full explanation refer to the text.

Figure 5.8 shows the same behaviour for *Lactohale300* less even than the presented in *Relenza*. For this cohesive powder concentrated build up can be seen in different areas of the lid. This could be attributed to the powder behaviour or to the lid surface state or to the uneven application of the load.
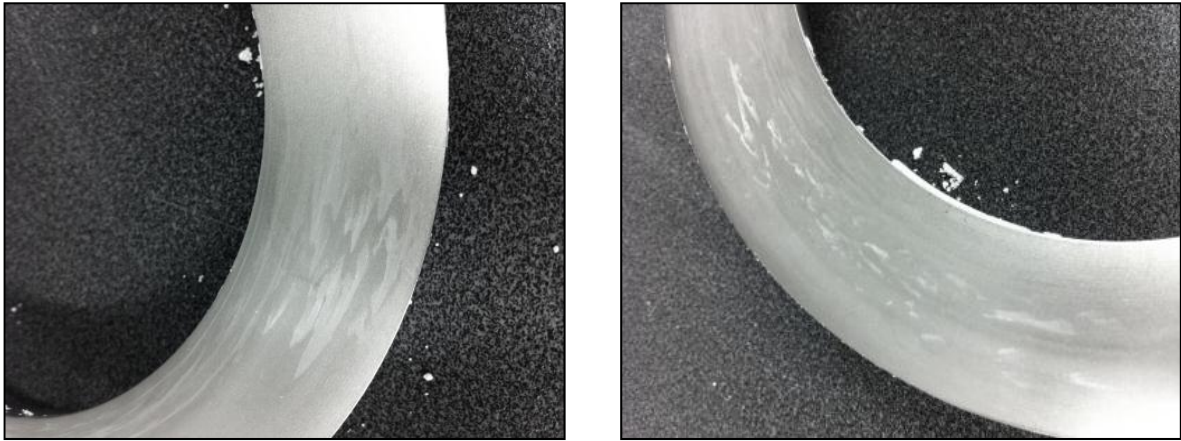
Figure 5.8. *Lactohale300* lid build up in the long wall friction test. Test undertaken in the Brookfield PFT. For full explanation refer to the text.

The long wall friction test could be useful to observe the powder build up to the dosator surface with time. *Relenza* did not show significant increments of the wall friction between the normal and long tests, but showed considerable powder adhesion to the stainless steel lid surface. The build up of the powder to the wall surfaces in dosator production lines could be an advantage for stability of the system as long as the adhesion of powder does not increase too much. For some powders the wall friction is reduced with time creating a layer of powder that may be beneficial for the entrance and ejection of powder in the dose chamber; but for other powders the wall friction tends to increase according to Bradley & Berry (2009) and the results shown in figure 5.9.
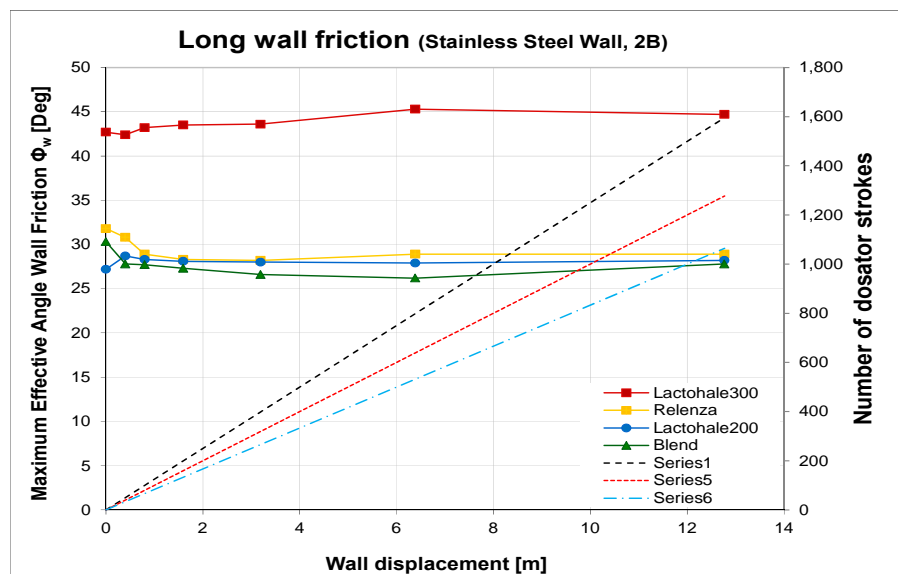
Figure 5.9. Long shear displacement wall friction test on stainless steel sample and equivalence to the number of dosator strokes for different dose lengths. Test undertaken in the Brookfield PFT. For full explanation refer to the text.

It can be seen in figure 5.9 the evolution of the wall friction for the four powders with shear displacement. The "x" axis represents the equivalent accumulative wall displacement developed with time in the tests. The two lactose grades, showed an incremental increase of wall friction angle over the shear displacement, this was more significant for the cohesive *Lactohale300*. The two blends showed decrease in the wall friction in comparison to the initial state, probably due to surface segregation effects, with the coarse particle rising to the surface resulting in a reduction in the number of particle contacts and therefore the friction.

Moreover, this test could be even more useful to dosator operations to estimate the number of strokes needed to reach a wall friction condition or the wall friction displacements for different dose lengths of the products. The secondary vertical axis in figure 5.9 is the calculated dosator strokes equivalent of the wall displacement in the long wall friction test. The dotted lines correspond to the doses with lengths of 4, 5 and 6 mm and diameter of 3.4 mm. It was taken into the account that the displacement in the dosator inner-wall would correspond to double of the dose length per stroke, because the dosator inner-wall is sheared twice in one stroke, when the powder enters into the dose chamber and again during the ejection of the dose.

Expected Production Time [min] To Reach Wall Friction Displacement						
Wall friction displacement [m]	0.4	0.8	1.6	3.2	6.4	12.8
Dose 4	3	6	12	12	48	96
length 5	2	5	10	10	38	77
[mm] 6	2	4	8	8	32	64

Table 5.4. Expected production time [min] to reach wall friction displacements of figure 5.9 for dose lengths of 4, 5 and 6 mm; based on the assumption of 1000 dosator strokes per hour. For full explanation refer to the text.

Furthermore, if dose length and the dosator stroking rate are known, it could be calculated when a specific or critical wall friction value would take place during the dose manufacturing. Table 5.4 shows the expected dosator manufacturing time to reach certain wall friction angle or wall displacements from figure 5.9, assuming dosator stroking of 1000 cycles per hour.

The above appreciation is a valuable output of this research that not only complements the powder flow behaviour information but also can help to predict and avoid typical production line problems; such as dosator pin jamming that commonly delays the dose manufacture.

Figure 5.10 shows the results of the ejection forces as function of the dosator cycles/strokes of five powders (property of GSK); the tests were undertaken by GSK in the 3PI dosator single

shot test-rig. In the graph, can be distinguished the special behaviour of the yellow and blue powders; there is an increase of the ejection force (that probably is governed by the wall friction) as the number of strokes increases until the dosator pin jammed in the experiment. These trials were carried out by GSK to see when the dosator would jam for different powders. If the results showed in figure 5.10 are correlated with the long wall friction tests of the powders, the evolution of the wall friction could be studied and the critical dosator jam stroke predicted. Furthermore, from this assumption it can be derived a novel characterisation technique for dosators and other filling systems to avoid pin/dose jam in production lines.
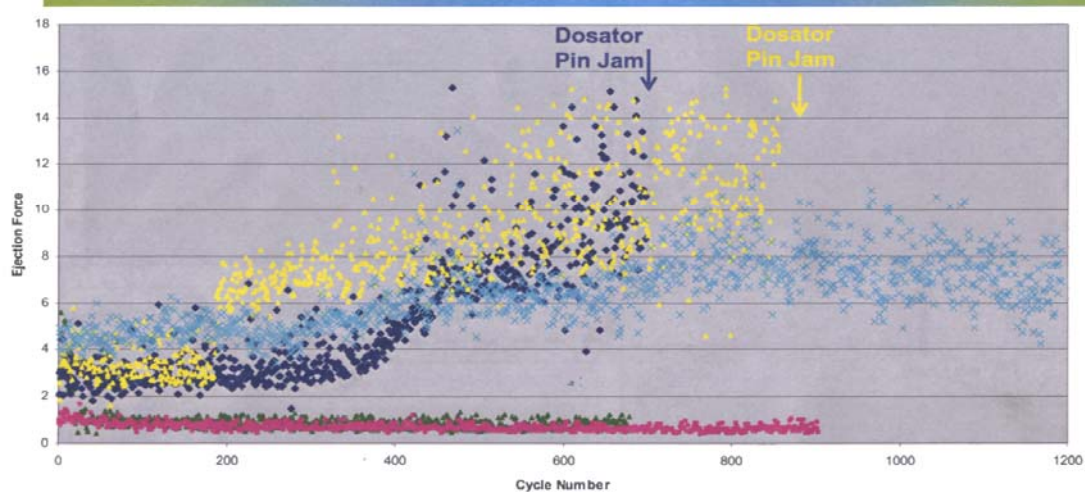
Figure 5.10. Ejection force as function of the dosator cycles/strokes of 5 powders (GSK powders) in the 3PI dosator single shot test-rig property of GSK. Graph provided by the industrial sponsor. For full explanation refer to the text.

Bradley and Berry (2009) showed that for some powders the evolution of wall friction with time could be critical and considerably affect the industrial process. Probably for some powders the powder build up to the surfaces increases the wall friction with the shear distance before reaching a stable value.

The set of tests discussed in this section, showed the powder behaviour of a range of diverse wall friction situations; in the same way it could be possible to predict the powder behaviour if the dosator/trough lining material is changed or how would the wall friction during the production of products. These tests also could contribute to study the wall friction develop effect that takes place at the bottom of the trough and it is unknown how is the migration of the powder aside or the changes in the stress distribution in the powder bed.

100

Current wall friction tests provide good information about the powder behaviour of this property; however there are still to be developed testers that can measure the property in the range of dosator application to verify if this behaviour is similar as expected from present testers.

5.4.3.4.   Powder wall cohesion and adhesion properties measurement

The term adhesion here is used to refer to the coating of the powder to the dosator wall when shearing it; whereas the term cohesion is referred to the linkage between particles or the resistance between particles to prevent separation. In this thesis, the adhesion is also named as wall cohesion. For some researchers, the adhesion of the powder to surfaces is associated to the tensile strength between the powder and the wall, but this is not the case in this research.

The adhesion of the powder to the wall surface can be measured from the wall friction test. The shear stress value at the point where the *wall yield locus* intersects with the "y" axis (shear stress "τ" axis at the normal stress $\sigma=0$), is called adhesion, τ_{ad} (Schulze 2008, p. 72). Values $\tau_{ad}>0$ are found for powders that can adhere to the pin face due to large adhesive forces. In the same way, when measuring the flow function, the shear stress value at the point where the *yield locus* intersects with the "τ" axis (at the normal stress $\sigma=0$) is called cohesion, τ_c, (Schulze 2008, p. 62).

The adhesion property was not measured from the definition expressed by Schulze (2008, p. 89) because the data was difficult to extract from the wall friction measurements in the PFT; it was selected the "wall flow function" technique as it has been found to give better results in the experience of The Wolfson Centre in the field. The technique uses the standard flow function test procedure to measure a family of failure loci over a range of increasing stresses to produce a wall flow function. This represents the potential process occurring at the tip of the dosator pin and at a base of the powder trough for low values of gap "h", i.e. applications where the powder is compacted against a wall surface under a large stress and then relaxed, before measuring the tensile force between the powder and wall surface.

The adhesion property was measured using the "wall flow function" technique suggested by Bradley et al. (2009). Here the standard flow function was undertaken using the flat lid

showed in figure 5.3c and preparing a level surface of powder in the bed. The results of the standard flow function conventionally expressed as the "unconfined failure strength σ_c" as function of the "major consolidation stress σ_1"; for the "wall flow function" these results are interpreted like the "wall cohesion c_w" as function of the of the "wall normal stress σ_w". It was argued by Bradley et al. (2009, p. 1) that at low stresses there is not significant wall cohesion, but above a threshold value, the wall cohesion suddenly increases and therefore the values are proportional to stress; hence potential for the powder to adhere to the wall. The adhesion of the four powders was also measured by covering the wall sample with fablon film.

5.4.3.4.1.   Results and discussion

Figure 5.11 presents the results of the adhesion test for the powders used in this research with two wall sample surfaces namely: stainless steel 2B and fablon film. The results were fitted in a linear trend lines. The wall cohesion values (vertical axis) are the stresses against the wall but do not measure the adhesion of the powder to the walls.

Generally the tests using the stainless steel wall (see figure 5.11a) presented similar wall cohesions for all four materials. However the *bimodal blend* showed lowest wall cohesion and *Lactohale200* the highest wall cohesion; which are contrary to the behaviour observed in the experimental work in the dosator test-rig. Figure 5.11b shows the results of the fablon surface and the powders behaviour changed apart from the *Lactohale200* with respect to the stainless steel test. The *Lactohale300* presented steeper trend line and greater values of the wall cohesion than the rest of the powders; this could be attributed to the cohesive nature and high share forces of the powder against rubber/plastic surfaces. The powders in this test can be ranked same as the flow function rank previously presented.

Bradley et al. (2009) proposed a model to calculate the critical thickness of powder build up "t" based on the measured wall cohesion from the "wall flow function". The expression is as follows:

$$t = \frac{c_w}{\rho_b \cdot g} \qquad [5.1]$$

Where "c_w" is the wall cohesion, "g" acceleration due to gravity, "t" the critical thickness of the powder build up required for the self weight of the layer to overcome the wall cohesive strength and "ρ_b" the bulk density.
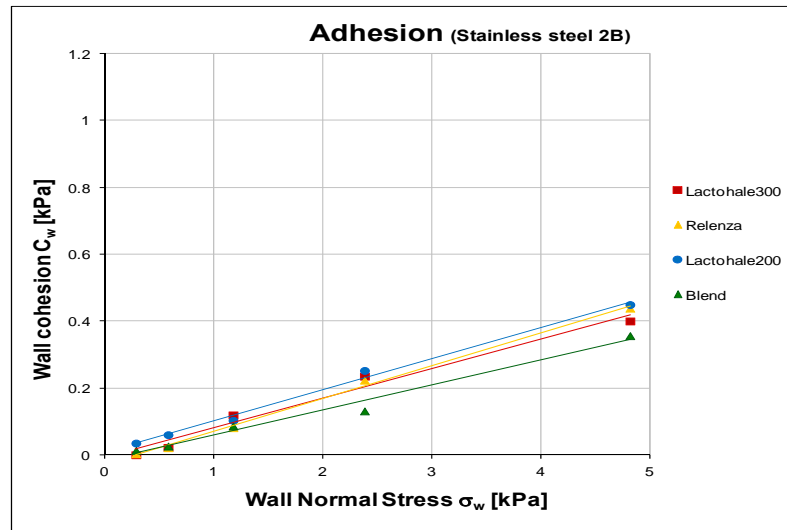
a)
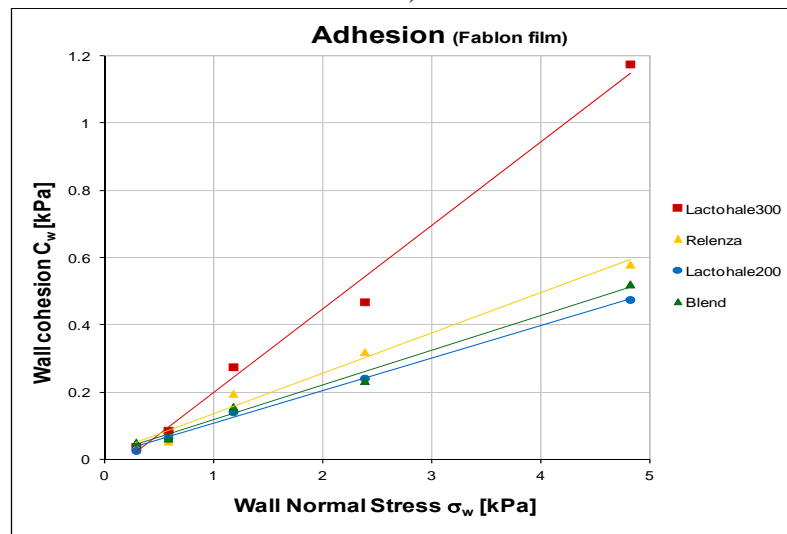
b)

Figure 5.11. Wall cohesion of the powders used in this research. Using the "wall flow function" technique proposed by Bradley et al. (2009) in the Brookfield PFT with two wall surfaces: a) stainless steel; b) fablon film. For full explanation refer to the text.

Figure 5.12 shows the equivalent thickness of powder layer build up on the surface (to overcome the wall cohesion), "t", as function of the wall normal stress. The density was calculated as function of the normal stress using the compaction curve described in section 5.4.4. The results were fitted in a linear trend line and the powders were ranked in order of reducing powder build up on surface as follows: *Lactohale300*, *Relenza*, *Lactohale200* and *bimodal blend*.

The results suggest that using the fablon film as surface finishing, the *Lactohale300* would stick more than against stainless steel surfaces. *Lacothale200* did not present changes in the adhesion behaviour when changing the finishing surface.
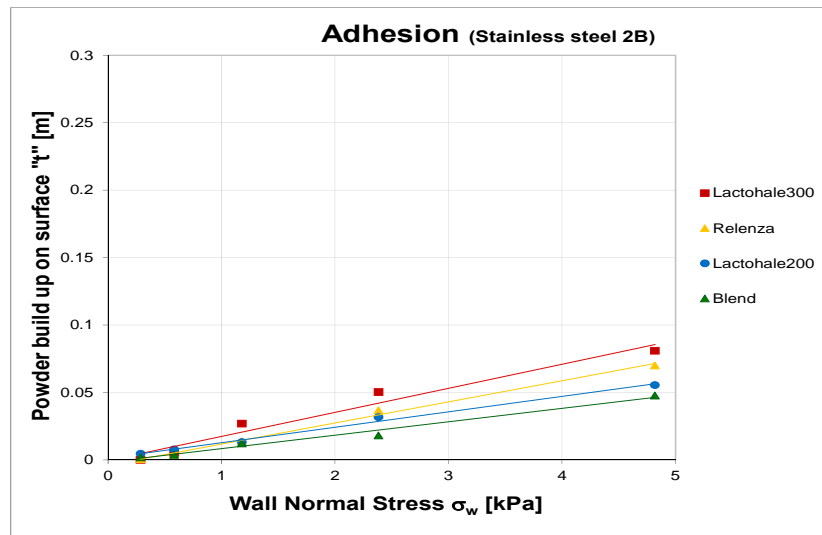
a)
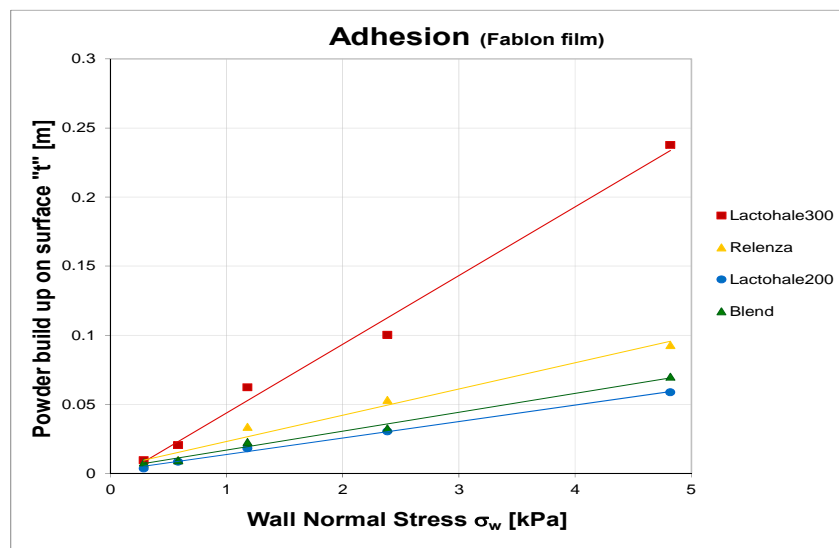
b)

Figure 5.12. Powder build up on surface as function of the wall normal stress for different wall surfaces: a) stainless steel; b) fablon film. For full explanation refer to the text.

Measuring of these properties complements the understanding of the powder behaviour. From the cohesion property, it can be seen how strong the adhesion forces between the particles are; from the "wall flow function" technique, it can be seen the tendency of the powder to adhere to surfaces. The last one does not predict the powder built up in dosator, as there are other phenomena in the dosator operation when approaching to the end of the stroke, but give an idea of the tendency of the powders to build up.

One of the limitations to measuring this property was the PFT stress range that is considerably lower compared to the stress range in dosator operation.

There are three main situations in dosator operation where the adhesion of the powder to surfaces takes place and can consequently trigger problems in the dose procurement. These problems are discussed in detail in chapter 7, section 7.4.6 and they are namely: powder covering coating of the dosator inner-wall with time, powder adhesion to the trough and adherence of doses to the pin's face.

5.4.4. Bulk density property measurement

In this thesis the compaction curve (CC) was used to study the changes of the bulk density as a function of the normal stress for the powders tested in this work. There were challenges measuring this property because the high stresses occurring in dosator operation (of the order of 2.5 MPa measured in the dosator test-rig, described in chapter 7) cannot be achieved in standard commercial equipment for quantifying powder flow properties with a representative powder sample. These challenges were:

- equipment with large force range,

- representative samples,

- and developing a technique compressing powder from 0 to 10 MPa

To measure this property, two machines were trialled, the Brookfield QTS texture analyser and a Civil Engineering uniaxial compression tester used to compress concrete samples (see figure 5.13).

All the testers work under the same principle explained below. The QTS operates by lowering a beam load cell to compress a sample contained in a cylindrical cell; the software digitally displays the force and displacements measurements as a function of time. Conversely, in the Civil Engineering tester the sample is pushed against the beam connected to a proving ring, the deflection of which is used to gauging the compression force; the data is collected manually reading the dial gauges connected to the beam's displacement and the beam's compression ring.

a)   b)
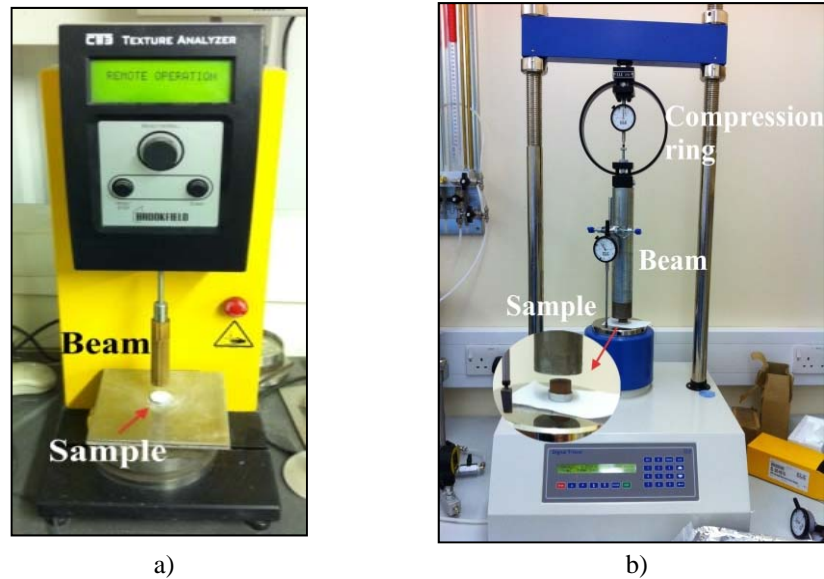
Figure 5.13. Testers used to measure the compaction curve: a) Brookfield QTS Texture Analyser; b) Civil Engineering uniaxial compression tester. For full explanation refer to the text.

The QTS has a force sensor with a range up to 100N while Civil Engineering tester has compression rings with a range from 2 to 28 kN. Due to the superior load range, the Civil Engineering compression tester was considered for measuring the compaction curve in the 70 MPa range. However this possibility was abandoned because the diameter of the plunger (50 mm) was greater than the dimensions of the cell sample (25 mm) and it was necessary to place a spacer to vertically stress the sample; this spacer compacted the sample before the test start altering the sample state (see figure 5.13b). Details of these tests are shown in the appendix 6.

The Brookfield QTS Texture Analyser was the selected instead to quantify the compaction curve. It showed better results and accuracy than the other testers considered in this thesis to measure this property in the range of dosator operation stresses. The reasons and results are show in the appendix 6.

5.4.4.1. Methodology

The initial tools used to measure the compaction curve in this research were the QTS uniaxial press and a Jenike shear cell with a cell diameter of 95 mm and height of 16 mm. This gave a maximum consolidation stress of 14 kPa using the standard 10kg load cell.

106

In order to be able to reach high stresses occurring during dosator operation, the sample rings dimensions were reduced. A range of cell rings were used with diameters and heights of 95x16, 54x14, 22x4, 22x15, 10x10 and 7.5x7.5 mm showed in the appendix 6. It was necessary to gradually reduce the dimensions of the cell to make sure that the compaction curve was accurate and followed the same trend. These cell areas generated compaction stresses of; 0.01, 0.04, 0.3, 0.3, 1.2 & 2.2 MPa when used in conjunction with the standard 10kg load cell of the QTS.

The sample was carefully prepared by breaking the lumps and trying to avert voids in the sample. Then, the maximum load of the tester was applied by the beam/plunger at speed of 0.5 mm/s; the later can be adjusted, but it was decided to set it low for better test resolution and increase the measured points at high stresses.

According to the manufacturer's technical sheet the accuracy of the load is ± 1 g and the displacement ± 0.1 mm. The variance of the load would not significantly affect the test measurements, except at very low stresses, but the displacement tolerance could affect the results depending on the cell height. The other potential error is inconsistent filling of the powder in the smaller diameter cells, due to the agglomeration of the more cohesive power leaving inconsistent voids in the sample.

5.4.4.2. Results, compaction curve model and discussion

Bulk density curves measured for Relenza with the QTS using the range of cells are presented in figure 5.14[14]. Can be seen good agreement of the trend using different cells, especially in figure 5.14b where the small difference are appreciated. Ultimately, the cell with diameter and height 7.5x7.5 mm was chosen to measure the compaction curve for the rest of powders.

The small size of the cell could present issues when filling it, especially for cohesive powders. For this reason, three tests were undertaken for each powder to verify the repeatability of the test; figures 5.15 and 5.16 show these results for all the powders used in this research using different "X" axis scale to appreciate the differences.

---

[14] Normal stress "X" axis (fig 5.14a) expressed in "Pa" as used in the dosator model described in chapter 8
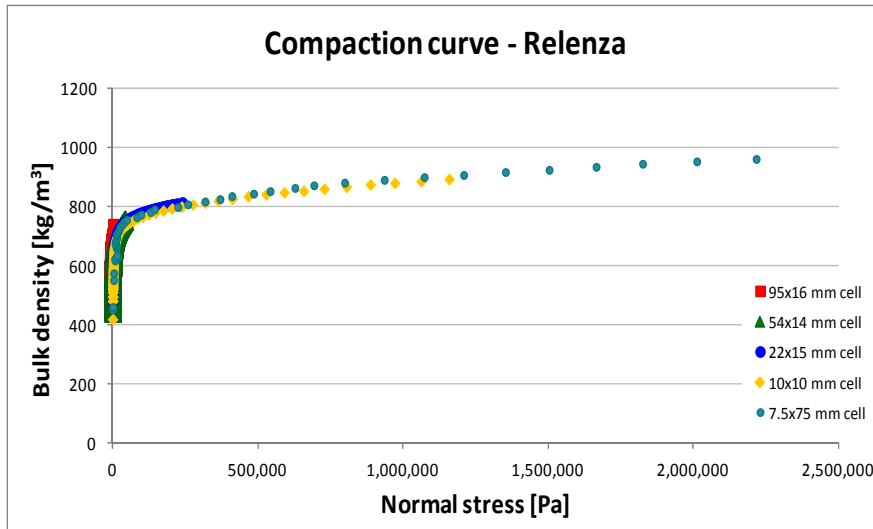
a)
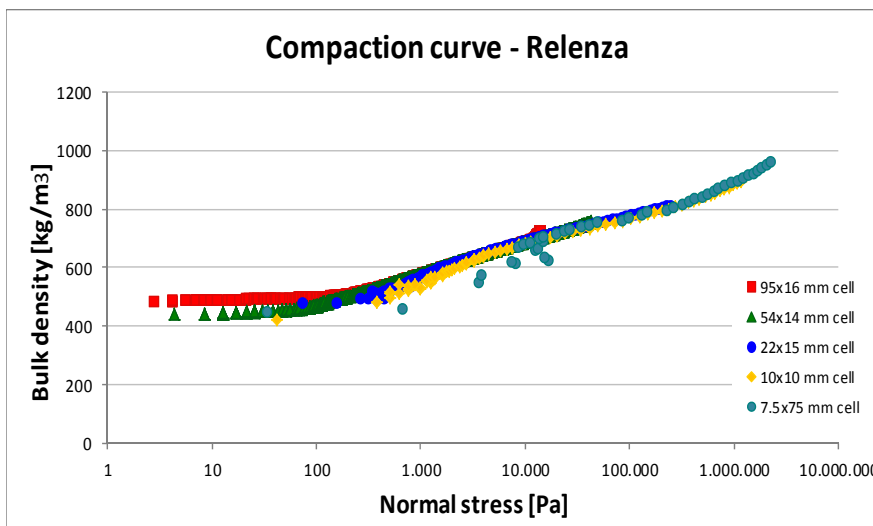
b)

Figure 5.14. *Relenza* compaction curves with different sample cell dimensions used in the Brookfield QTS
Texture Analyser: a) linear "X" axis; b) logarithmic "X" axis. For full explanation refer to the text.

The outcome of the set of tests for all powders was satisfactory to this thesis; the tests showed
acceptable repeatability in all the cases. *Lacothale200* and the *bimodal blend* presented better
repeatability of the CC at high stresses than *Lactohale300* and *bimodal blend*. Relenza and
Lactohale200 (less compressible powders) presented noise in the measurements, probably due
to difficult of the particles to rearrange at the beginning of the test. The curve shape of the
cohesive powders (*Lactohale300* and *bimodal blend*) in figure 5.15 presented different shapes
than the other two powders at low stresses.
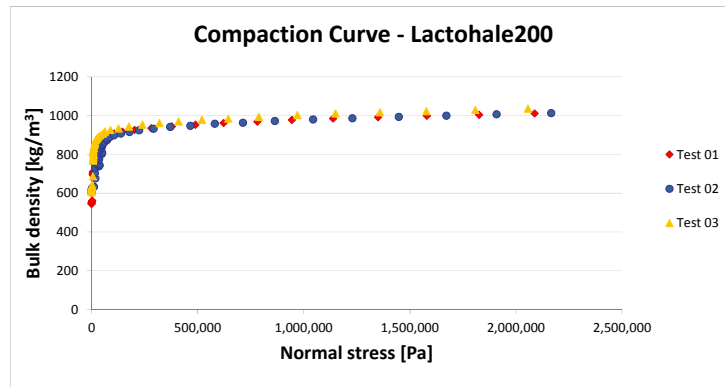
a)
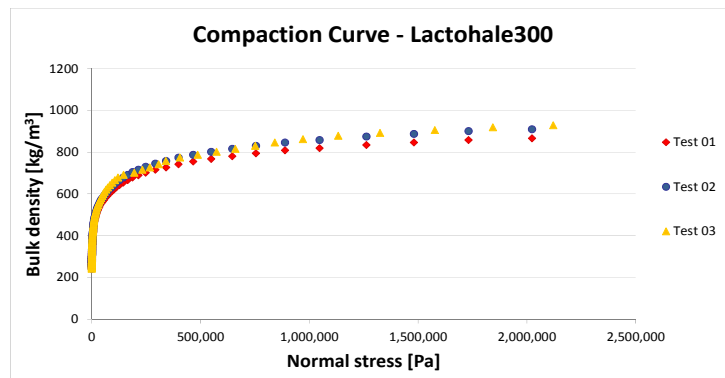
b)
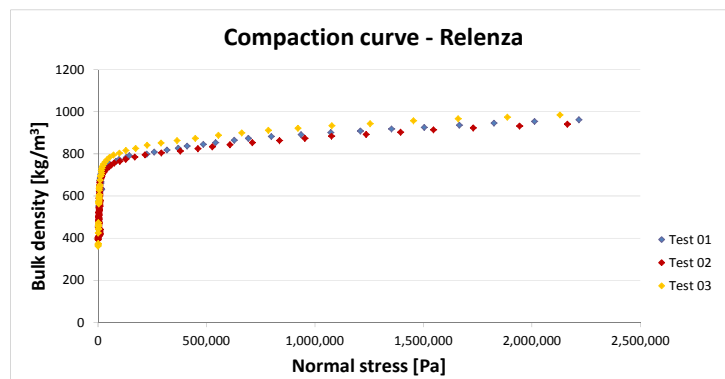
c)
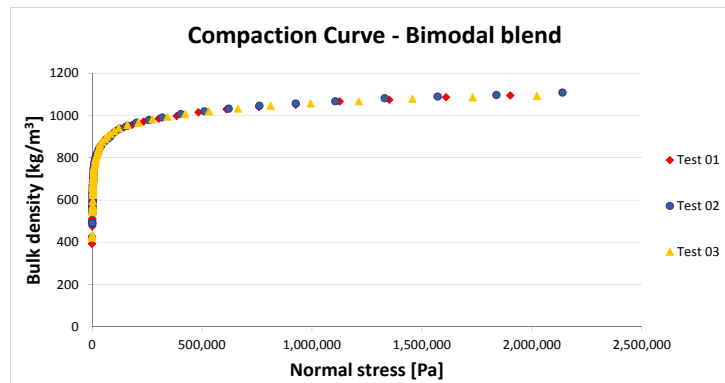
d)

Figure 5.15. Repeatability of the compaction curve results in the Brookfield QTS texture analyser, using linear
"X" axis: a) *Lactohale200*; b) *Lactohale300*; c) *Relenza*; d) Lactose *bimodal blend*. For full explanation refer to
the text.
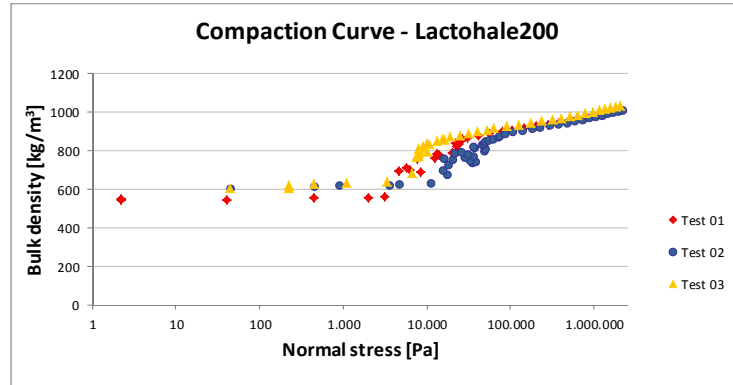
a)
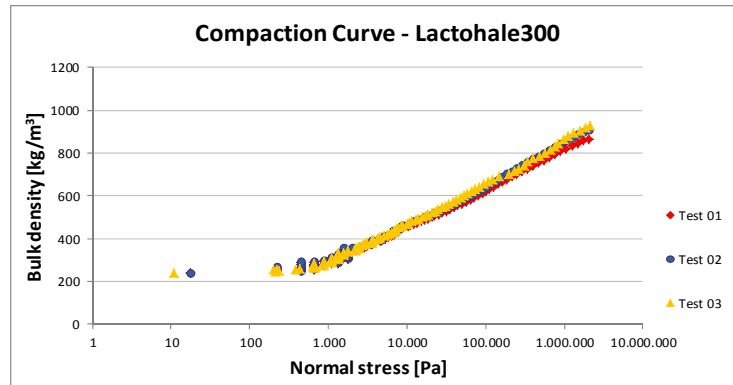
b)
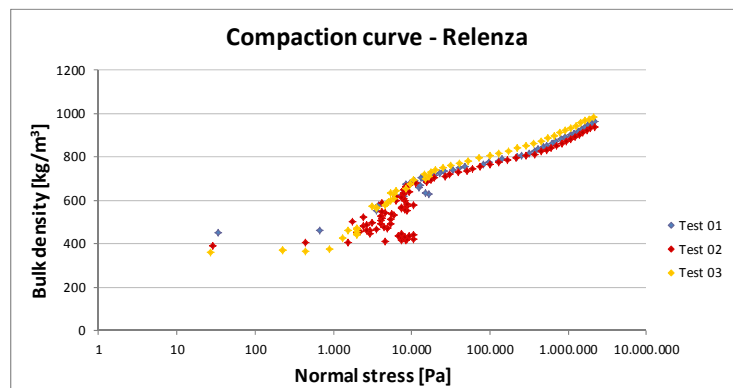
c)
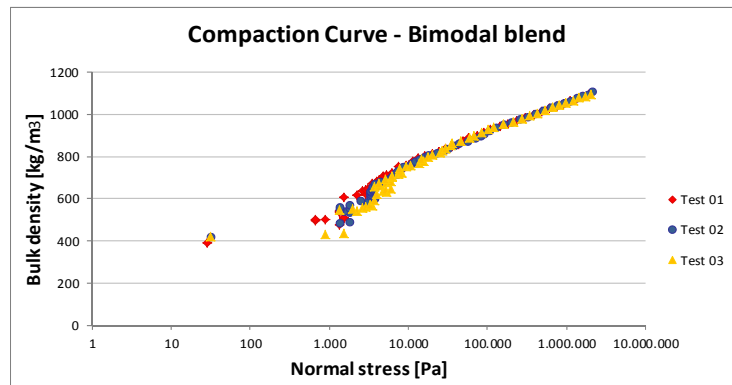
d)

Figure 5.16. Repeatability of the compaction curve results in the Brookfield QTS texture analyser, using logarithmic "X" axis: a) *Lactohale200*; b) *Lactohale300*; c) *Relenza*; d) Lactose *bimodal blend*. For full explanation refer to the text.

Figure 5.17 shows the effect of this error in the QTS measurements. It altered the beam displacement data by $\pm$ 0.1 mm.

The effect of this error is not drastically significant, but for predictions of larger stresses the trend could be in disagreement. Based in these results, it is advisable to perform at least three tests per powder.

a)

b)
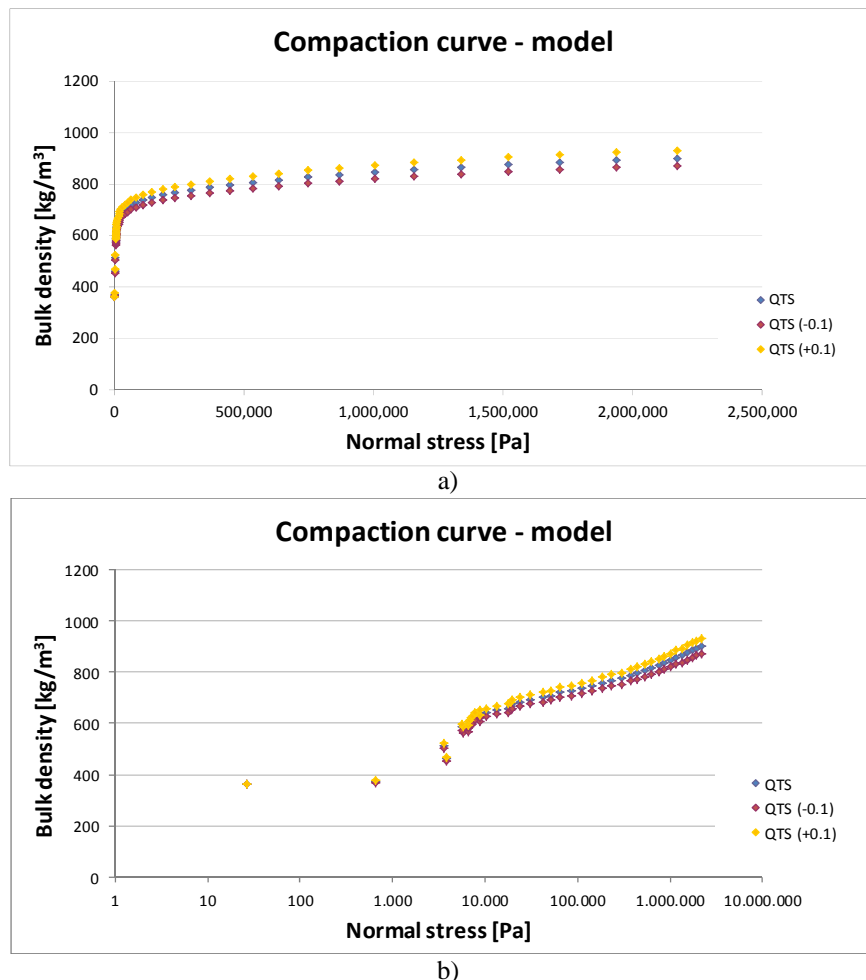
Figure 5.17. An effect of the 0.1 mm QTS beams displacement error in the compaction curve results; using the cell with diameter and height of 7.5x7.5 mm: a) linear "X" axis scale; b) logarithmic "X" axis scale. For full explanation refer to the text.

The data from the QTS tests presented significant scatter, which is function of the wide range of data, test speed and signal noise, wherefore precluded the normalisation of data to quantify deviations. This scatter and the large quantity of data obtained at the lower stresses lead to great density variation at the beginning of the test and to miscalculations using the trend fitting data tool in Excel to obtain a relation of the density as function of the stresses.   In addition, logarithmic and power curve fitting in Excel fitted data from the origin and the compaction curve starts at the poured density value (see appendix 6 for more details).

This is the most important powder flow property because the filling operation is volumetric but the dose is specified by weight. As a result changes in bulk density causes weight variations and therefore process problems. Bulk density changes can occur either from the intrinsic particle properties (particles size, shape, surface properties, which will define gravity packing behaviour) or machine setting (blending time, applied stress and process type; e.g. granulation, milling, sieving, etc.) during processing.

The bulk density can change during the insertion and compaction stages of the dosator operation (stages described in section 2.3.2 in chapter 2). As mentioned in chapters 3 and 4, it was anticipated that the homogeneity of the density of the powder in the bed could affect the fill dose weight.

As describe in the Janssen effect application (in section 2.7.1 in chapter 2) and the measurement of the wall friction property (described in section 5.4.3), the bulk density is affected in the filling stage by the wall friction and vertical forces exerted in the process (described in section 2.7.1 in chapter 2 and discussed in chapter 8).

Consequently, dose density affects the dose strength; the degree of the compaction in the dose can compromise the delivery device performance, the powder dissolution and potency in dosator's dry inhaled powder application.

Considering that the compaction curve is one of the most important flow properties affecting dosator operation, this thesis proposes a straightforward curve fit model. The model consists of either of the traditional logarithmic or power equations with the addition of the "Y" axis intercept c using either the forms $y = (a.ln(x)+b)+c$ or $y = (a.x^b)+c$. However, a power curve fitting model was chosen because it showed better data fit for the powders tested (see appendix 6). The factors a, b and c proposed in the compaction curve model were acquired by adjusting first c to the poured bulk density value and the other two factors reducing the addition of the errors between the density values in the experimental data and the model until the curve fitted.

The overall compaction curve results for all the materials used in this research are showed in figure 5.18 with their respective model values. It can be seen that the bulk density changes as a function of the compression stresses and the compressibility behaviour of the powders.
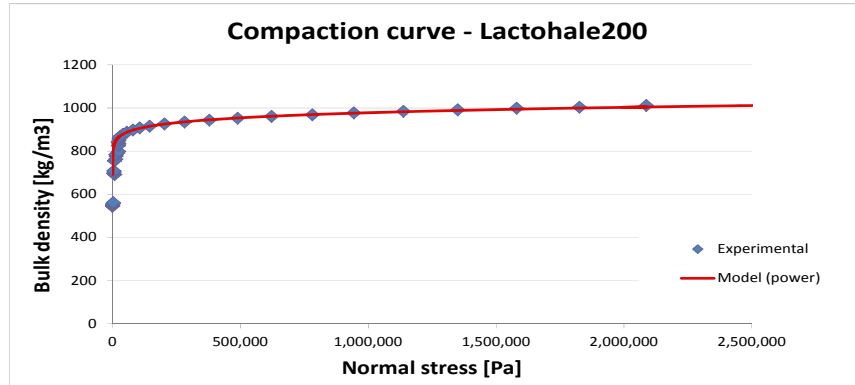
a)
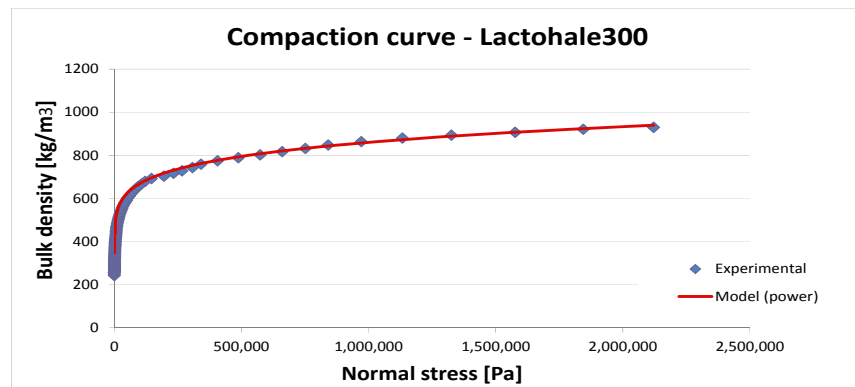
b)
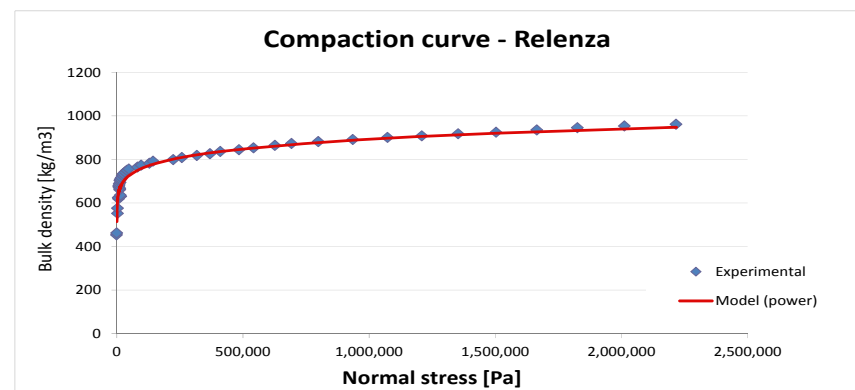
c)
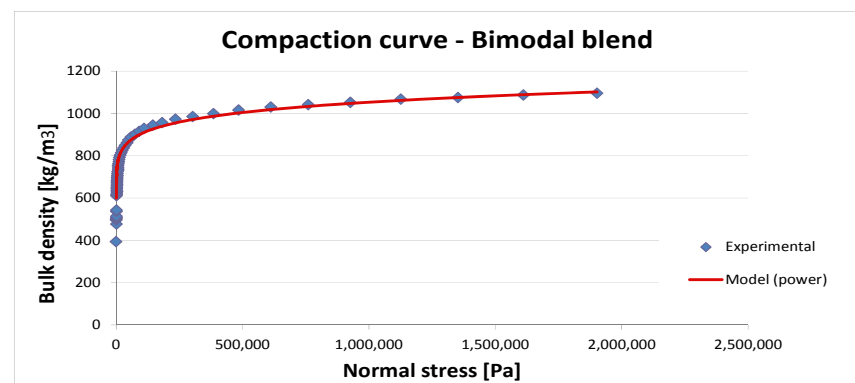
d)

Figure 5.18. Compaction curve model of the powders used in this research: a) *Lactohale200*, $y = 145.x^{0.08}+540$; b) *Lactohale300*, $y = 68.x^{0.16}+240$; c) *Relenza*, $y = 100.x^{0.12}+360$; d) *Bimodal blend*, $y = 145.x^{0.11}+390$. Data obtained from the Brookfield QTS texture analyser. For full explanation refer to the text.

113

Lactohale200 and *Relenza* showed similar curve shapes, steeper at lower stresses. *Lactohale200* presented the most incompressible behaviour from all the powders used and also was the easiest flowing based on the flow function measurement. *Lactohale300* and the *bimodal blend* were very compressible; both powders presented similar compression behaviour judging by the difference in between the poured density and the density at higher stress and by the shape of the compression curve. *Lactohale300* showed to be more compressible than *bimodal blend*. Meanwhile Relenza and the lactose *bimodal blend* with similar PSD (refer to results in section 5.3.2 anf figure 5.2) had similar poured density but different compression behaviour; this can be explain by the attachment level of the fine and coarse particles from the SEM results and showed in figure 5.2 .

Density prediction and Compressibility of the Powders					
Powder	CC Density [kg/m^3]			Compressibility %	
	Poured	$\cong$0.1 MPa	2.5 MPa	$\cong$0.1 MPa	2.5 MPa
Lactohale300	240	665.75	958.09	64	75
Bimodal blend	390	928.24	1123.06	58	65
Relenza	360	815.69	945.80	56	62
Lactohale200	540	907.43	1011.20	40	47

Table 5.5. Compressibility of the powders used in this research in comparison to the poured density. Densities obtained from the compaction curve (CC) measured in the QTS. For full explanation refer to the text.

The compressibility behaviour and ranking of the powders used above was confirmed calculating the density at three different stress conditions using the compaction curve model. The conditions chosen were as follow: the poured density (0 MPa), 2.5 MPa and a value close to 0.1 MPa (approximately stress within the curvature of the CC). Table 5.5 shows these values and also the compressibility of the powders in relation to the poured density. The powders are listed and ranked as lessening compressibility.

The ranking of the powder correlates with the flow function powder ranking. The increment of the compressibility between 0.1 and 2.5 MPa was similar for *Relenza*, *Lactohale200* and the *bimodal blend*, in between 6 and 7 %, and for *Lactohale300* was greater, 11%.

The compaction curve model showed good data fitting with the measurements obtained from the QTS. It compared the densities at the same conditions of the previous table to see the variability of the CC prediction. Table 5.6 shows the comparison and the coefficient of variation between the CC and the CC Model. The CC model showed good curve fitting data for the conditions analysed in table 5.5. *Relenza* presented greater variation than the other

three powders. The compaction curve model also showed a satisfactory prediction at double

of the stresses presented in figure 5.17; these results are shown in the appendix 6.

Comparison Between The Compaction Curve and The Compaction Curve Model								
Powder	CC density [kg/m³]			CC Model density [kg/m³]			CV %		
	Poured	$\cong$0.1 MPa	@ max. test stress	Poured	$\cong$0.1 MPa	@ max. test stress	Poured	$\cong$0.1 MPa	@ max. test stress
Lactohale300	241.44	665.75	928.63	240	673.45	939.47	0.4	0.8	0.5
Bimodal blend	392.34	928.26	1093.90	390	910.20	1101.35	0.4	1.4	0.8
Relenza	362.17	815.69	984.15	360	770.30	934.64	0.4	4.0	3.6
Lactohale200	543.24	907.43	1011.01	540	906.09	1004.47	0.4	0.1	0.6

Table 5.6. Coefficient of variation (CV) between compaction curve (CC) obtained in the QTS and the compaction curve model. It was compared the density at different conditions such as: poured, maximum stress in the QTS test and $\cong$0.1 MPa. For full explanation refer to the text.

5.4.5. Stress ratio K and lateral stress retained properties measurement

The stress ratio K was included in the model proposed in this project in chapter 8, to quantify

the horizontal stresses acting inside the dosator. It was integrated in the Janssen effect

application to calculate the effect of wall friction of the powder entering in the dose chamber.

The Janssen effect application was described in chapter 2.

5.4.5.1. Equipment and instrumentation

The equipment used was the k-meter engineered at The Wolfson Centre. The tester is

composed of a split ring system containing the sample (see figure 5.19a) mounted in the

Brookfield QTS texture analyser (see figure 5.19b) to apply vertical loads to the sample. The

split ring was mounted in a frame with counterweight hangers/beams aside to maintain the

balance of the system (see figure 5.19c). It was compressed using the QTS fitted with a

plunger of smaller diameter than the split ring.

The split ring system is shown in detail in figure 5.20. The powder sample (a) is contained in

the split ring (b). The ring is divided in two halves, one of which is welded to a bracket (d)

and to the other is connected a pair of load cells (c). The internal diameter and height

dimensions of the ring are 52 and 104 mm respectively.
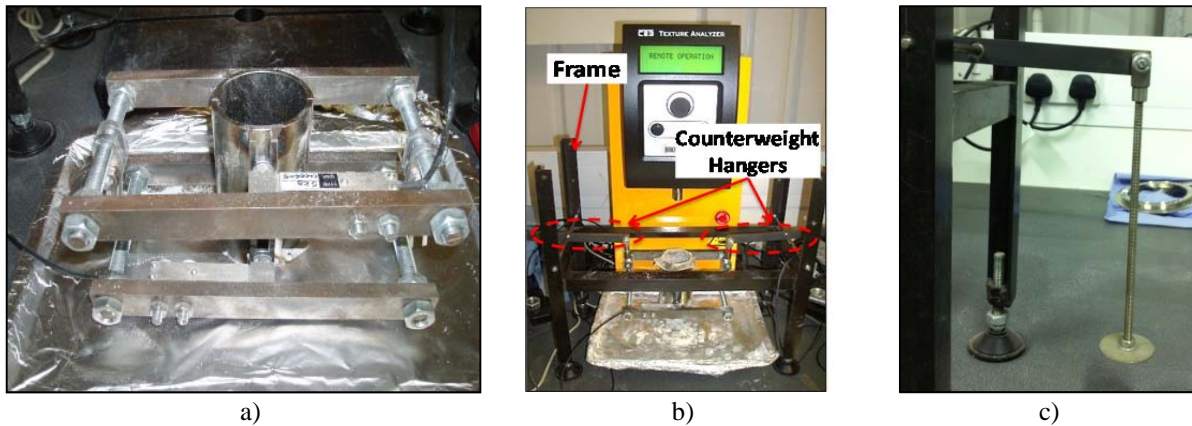
Figure 5.19. K-Meter engineered at The Wolfson Centre: a) split ring system containing the powder sample; b) split ring mounted in the Brookfield QTS texture analyser; c) counterweight beam hanger. For more information refer to the text.

The forces were measured using two BF2 stainless steel 5 kg range cantilever beam load cells; it used two load cells for stability and resolution issues. To reduce the wall friction effect, the ring inner-wall was covered with latex and a silicon lubricant release agent to assist the compression of the powder. The system was hung to avoid friction issues at the bottom of the split ring; a disc on the underneath of the cell restrained the powder sample.
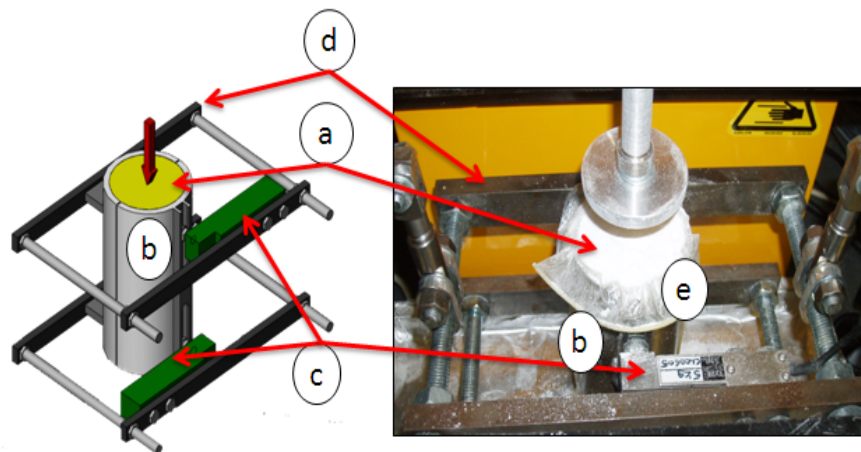
Figure 5.20. K-Meter split ring detail: a) powder sample; b) split ring; c) load cells; d) bracket; e) latex film. For more explanation refer to the text.

5.4.5.2.   Methodology

The ring halves walls were firstly covered by the latex and silicone lubricant and then joined together assuring there was no tension in the load cells. The system was counterweighted lifting the ring about 2 cm from the surface. The ring was filled with powder and increasing vertical loads (0.1, 0.2, 0.4, 0.8, 1.6 & 3.2 kg) applied via a lid in order to measure the

horizontal force response from the powder. Different lubricants were trialled and the silicone
lubricant showed the best response to diminish the friction in the system. Figure 5.21 shows
the latex film wrinkled after the powder compression.

Figure 5.21. Latex used to reduce wall friction effect in the K-meter. For full explanation refer to the text.

The load cells signals were connected to an analogue strain gauge amplifier[15] and sent to an
Advantech USB 4716 module connected to a laptop with Labview interface collecting the
data.

When the load compresses the sample, the system tends to be lowered and the volume of the
sample is reduced at the top and bottom. After the load is retrieved the system recovers the
distance shifted and the changes in the height, as the specimen is compacted, are manually
recorded with a measuring ruler.

5.4.5.3.   Results and discussions

Figure 5.22 shows a typical example of the raw data from a K-Meter test. The peaks
represent the horizontal force response to the vertical compression forces (labelled in red) that
were applied by the QTS.

K-Meter results obtained from the four test materials are presented in figure 5.23a. The
horizontal stresses are plotted as function of the normal stresses and the slope of the straight
line fitted to the data, corresponds to the stress ratio K value.

---

[15] Mantracourt manufacturer
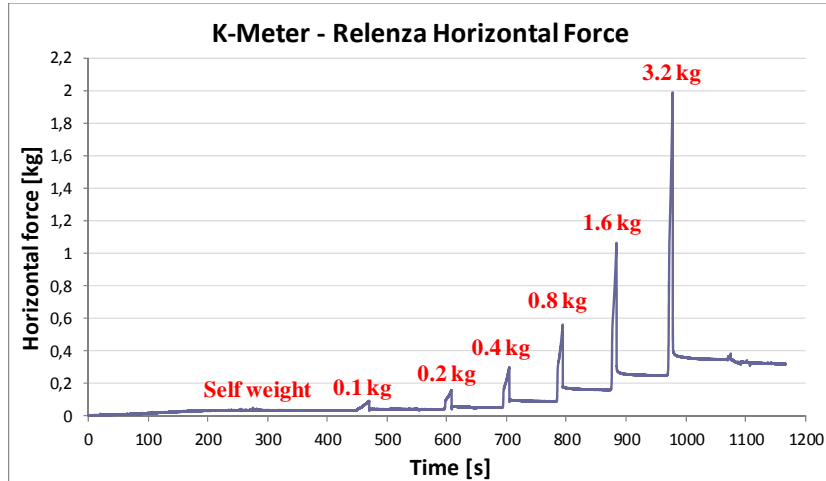
Figure 5.22. Raw data plotted from the K-Meter. For full explanation refer to
the text.

Lactohale300 showed the highest stress ratio K and the *bimodal blend* the lowest,
Lactohale200 and *Relenza* displayed intermediate values.   The powders where ranked
differently to the flow function.
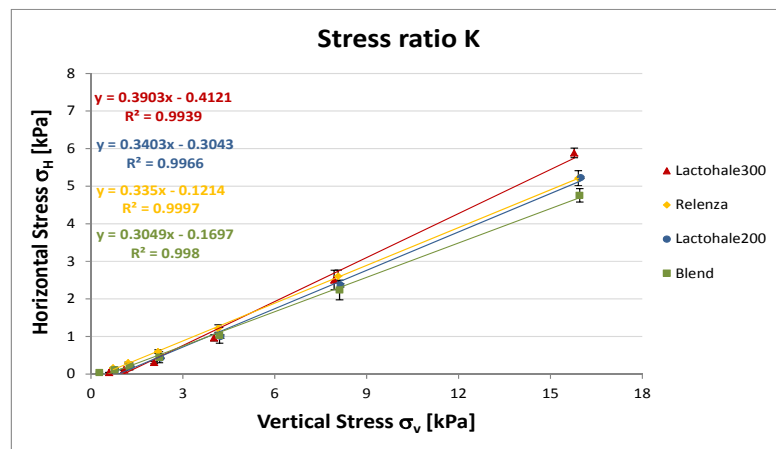
a)
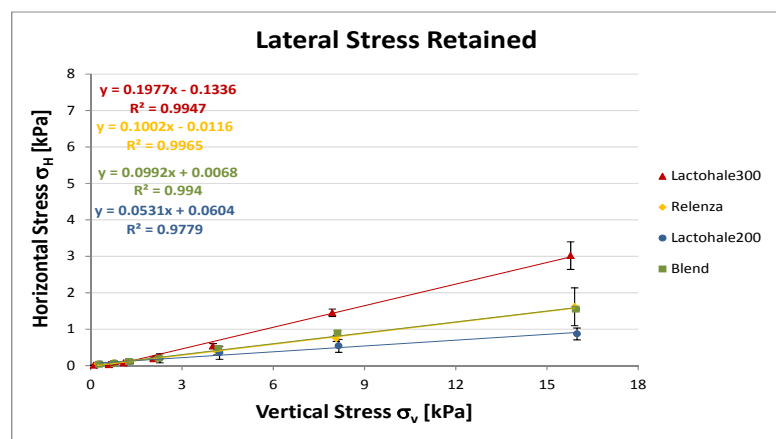
b)

Figure 5.23. Results from the K-Meter: a) Stress ratio K; b) Lateral stress retained. For full explanation refer to
the text.

The coefficient of variation of the test was satisfactory, around 7%. However, there are some settings in the test that need to be improved that could affect the measurements. These include:

- Setting the clearance gap between the two cell halves without inducing tensile forces in the load cells,

- Centering the disc restraining the base of the sample to prevent contact with the wall and frictional forces being transferred and affecting the measurements.

- The need to record the change in sample volume using a ruler.

- Minimising wall friction effects, using latex film and the silicone lubricant. Initial trials were carried out using *Relenza* and the K values increased from 0.28 to 0.33 employing more effective lubricants.

It was noticed that some lateral stress was retained by the powder after retrieving the increasing loads; this behaviour can be seen in figure 5.22. The lateral stress retained results are showed in figure 5.23b as function of the normal stress.

This ability of the powder to retain lateral stresses was associated in this thesis with the dose retention behaviour. This behaviour can be explained using the cam clay model (Roscoe cited in Nagaraj & Miura 2001) described in figure 5.24. This model describes the stress state of a soil sample subject to isotropic tri-axial compression. Figure 5.24 shows the voids ratio "ε" as function of the consolidation stresses; it can be seen the compression/voids reduction of the soil with the increment of the pressure. There is a point in figure (after the irrecoverable strain "p" zone in figure 5.24) where the compaction stress is retrieved and the powder tries to expand recovering the strain ("e" in figure 5.24). The sample is stressed again and because it retained the stresses from the previous compaction, the sample continues the compaction and reduction of voids ratio trend.

Even though the cam clay model is tri-axially compressed and the powder in dosator systems is uniaxially stressed, this stress retention can explains the dose retention in dosator with the vertical compression of the powder inside the dosator during the filling stage.
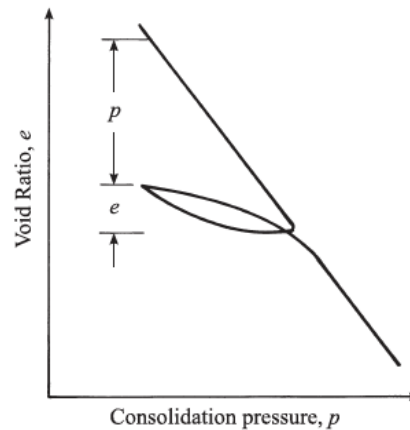
Figure 5.24. Cam clay model. Re-printed from Nagaraj & Miura (2001, p. 35). For full explanation refer to the text.

It can be seen from figure 5.23b that this behaviour is characteristic of each powder and it is different to the K values powder ranking. *Lactohale300* showed greater stress retention than the other powders, especially to the *Lactohale200*, and this was confirmed with the dose retention behaviour observed in the dosator test-rig. The two blends showed similar retaining behaviour as in the dosator test-rig behaviour observations.

Jolliffe & Newton (1978, 1980, 1982, 1983a, b, c) (see section 3.3, chapter3), published a series of work where the retention of the dose was associated to the formation of an arch in silo's theory and wall friction against the dosator walls. Based on the dosator process understanding developed through the research reflected in this thesis, it is the author's opinion that cohesive arching is not responsible for the dose retention in current machines, because the dose cavity is a cylinder and there are no converging walls for the material to arch across. It is accepted that at low stresses the wall friction is important to prevent the dose slipping and for the wall adhesion to exceed the self-weight of the dose (as mentioned in section 5.4.3). However this is not the main factor which ensures that the dose is locked in the dosator. The key to dose retention is the high stresses generated in the powder ahead of the dose at the bottom of the stroke, when the dosator body approaches the base of the trough. Under this high vertical stress, the stress ratio property of powder K generates a large lateral stress within the powder in the dosator, which locks the material in place in an elastic state of stress. This retained elastic stress property is material dependent as discussed in this section.

Another factor founded in this research work (discussed in section 7.4, chapter 7) preventing the formation of an arch at the dosator outlet, is the layer of compacted powder formed between the dosator tip and the trough at the end of the stroke. The gap at the end of the

stroke is small in current machines and the powder trapped generates high pressures causing different events that affect the dose weight (depending on the powder flow properties) and could prevent the formation of and arch. This topic is discussed in detail in section 7.4, chapter 7.

5.4.6. Voids fraction "ε" property measurement

The powder flow properties can be affected by the powder packing properties, the void fraction ε, at a given stress (Podczeck & Jones 2004, p. 104, 109 and Farnish, Berry & Hernandez 2012), which is a function of both particle size and shape.

The void fraction can be calculated using equation [5.2]:

$$\varepsilon = 1 - \left(\frac{\rho_b}{\rho_p}\right) \qquad [5.2]$$

where "ε" is the voids fraction, "ρ_b" the bulk density and "ρ_p" particle density.

By combining the compaction curve bulk density measurements with the particle density measurements, a voids fraction function can be calculated from the equation [5.2] to predict the powder packing behaviour. Table 5.7 shows the voids fraction at three stress conditions (same conditions as selected for the compressibility in table 5.5) and the reduction of the voids fraction related to the poured particle packing structure. The void fraction functions are presented in figure 5.25.

Voids Fraction					
Powder	Voids fraction (ε)			ε reduction %	
	Poured	0.1 MPa	2.5 MPa	0.1 MPa	2.5 MPa
Lactohale200	0.62	0.37	0.34	41	46
Relenza	0.74	0.41	0.37	45	51
Bimodal blend	0.74	0.33	0.28	56	62
Lactohale300	0.87	0.32	0.28	47	54

Table 5.7. Voids fraction at different stress conditions of the powders used in this research. For full explanation refer to the text.

For the poured condition, the freer flowing *Lactohale200* has the lowest void fraction and the cohesive *Lactohale 300* has the highest void fraction. The two blends presented intermediate poured void fractions and have not seemed to impact on the adhesive forces/attachment

between the fine and coarse particles. Nevertheless, as the powders are compacted and the void fractions reduce, there is a switch in the ranking. At the highest compaction stress (2.5MPa) void fractions are ranked as followed from lowest to highest: *bimodal blend*, *Lactohale300*, *Relenza* and *Lactohale200*. The *bimodal blend* showed tighter particle packing with compression than the rest of the powders. The powders packing ranking did not match with flow function ranking presented before.
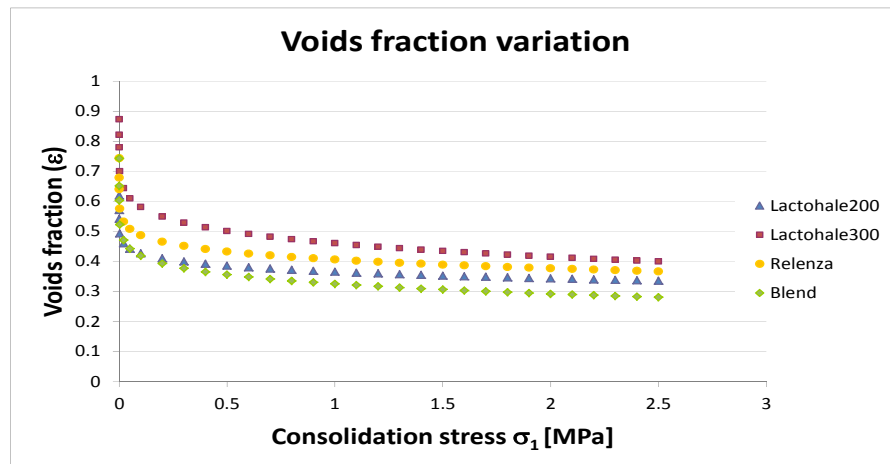
Figure 5.25. Voids fraction (ε) variation with the compression stresses, for the powders used in this research. For full explanation refer to the text.

The reduction of the voids fraction can be linked to the strength behaviour of the doses; for example in the coffee industry, some of the coffee presentations are vacuum packed and it can be very strong and hard because the voids fractions had been reduced. In the same way, lower voids fraction in powders indicates better packing of the particles, therefore could reflect the strength of the dose.

The voids fraction and gas velocity influences the powder permeability characteristic. In this research the impact of powder permeability on the dosator operation was not studied; but some considerations about powder packing are presented in this section and chapter 7, that deliver an idea about how the permeability could affect the dosators operation.

5.5. Summary

This section provided a complete list of flow properties that need to be take into the account for the manufacture of doses using dosator filling machines. The characterisation of the

powder does not take a lot of time and can potentially be used to minimise production down time to assist in the set-up of the filling machines to match the powder flow behaviour.

This research work found the main flow properties involved in the dosator process and some of these properties have not been published in the literature.

The characterisation of the relevant flow properties to dosator operation is summarised in table 5.8, for the powders used in this thesis. The powders were categorised between 1 and 4, 1 being the powder with the most critical ranking and 4 the least critical.

Flow Properties Powder Ranking					
Property\Powder	Lactohale300	Bimodal blend	Relenza	Lactohale200	Parameter
Flow function	1	2	3	4	1 cohesive 4 free flowing
PSD, D(50)	1	3	2	4	1 smallest 4 biggest
Wall Friction					
Stainless Steel	1	3	2	4	
Fablon Film	1	2-3	2-3	4	
Long Wall Friction	1	4	2	3	
Cohesion	1	2	3	4	1 highest
Wall cohesion					4 lowest
Stainless Steel	2-3	4	2-3	1	
Fablon Film	1	3	2	4	
Powder Build Up					
Stainless Steel	1	4	2	3	
Fablon Film	1	3	2	4	
Compressibility	1	2	3	4	1 most compressible 4 incompressible
Stress ratio K	1	4	2-3	2-3	1 highest
Stress Retained	1	2-3	2-3	4	4 lowest
Particle Density	4	3	2	1	1 denser 4 lighter
ε poured	4	2-3	2-3	1	1 tight 4 loose
ε reduction with stress	2	1	3	4	1 biggest 4 lowest

Table 5.8. Summary of the flow properties of the powders used in this research relevant to dosator operation. For full explanation refer to the text.

It can be seen from the overall results that *Lactohale300* is the most critical powder for dosator operation. Therefore it is likely to have the greatest variations in the dose fill weight. *Lactohale 300* is the most cohesive and compressible powder; it showed the highest wall friction in the different situations measured and tended to adhere to the walls. It also presented the most irregular particle packing that could not only affect the homogeneously of the dose, but also the powder bed conditions. One of its advantages is it potential to retain

lateral stresses, minimising the chance of doses dropping from the dose chamber prior to ejection.

Lactohale200 is the other extreme case; it has low adhesion and build up to the wall surfaces and low wall friction in the situations measured. However there are low ranking properties that make it unsuitable for dosator operation such as easy flowing behaviour, incompressibility and low retention of horizontal stresses. The latter makes it difficult to retain the dose in the dosator, during the retraction stroke.

The lactose *bimodal blend* and *Relenza* have better properties to fill the dosator and probably to retain the dose. Nonetheless, *Relenza* is less cohesive, with a lower wall friction and lower tendency to build up on surfaces; this makes it the most appropriate powder, within the powders used in this research, to obtain doses with lower variability in terms of powder flow properties.

The key challenge for characterisation was achieving a stress level relevant to that occurring during dosator operation; standard powder characterisation equipment is not designed to operate at such as pressures. While bulk density tests were measured over the actual stress, range all other flow properties required extrapolation. While it is anticipated that these properties will not change significantly over this increase in stress, there remains a level of uncertainty.

This chapter showed the measurement of particle and flow properties relevant to dosator operation for the powders used in this research. There were powders with different and extreme characteristics to encompass different behaviours in the dose manufacturing.

The measurement of the stress ratio K and lateral stress retained is a novel aspect in dosator operation founded in this research work; as well as the association of the lateral stress retained concept with the dose retention issue in dosator operation. This thesis proposes a different dose retention explanation in a different point of view than expressed by Jolliffe & Newton (1978, 1980, 1982, 1983a, b, c).

Chapters 6 presents the development of the single shot dosator test rig, whilst chapter 7 present the experiments undertaken with this machine using the four test powders, for different machine conditions to help understand the dosator operation and develop the model presented in chapter 8.

Chapter 6

Development of a Dosator Single Shot Test-Rig

6.1.   Introduction

At the project outset, the plan was to use the 3PI dosator single shot test-rig (detailed in chapter 9) owned by GSK, to validate the model. However, this tester was found unsuitable because it only measured the ejection forces on the pin and the dose weight, whereas the model validation required measurements of the forces on the dosator body as well. The cost of upgrading the test-rig to meet The Wolfson Centres' requirements was quoted at £5000, but there remained concerns over the consistency of the positioning of the dosator components (pin and body) relative to each other and the base of the powder bowl. Thus, it was decided that it would be more cost effective to engineer a new single shot dosator test-rig (at a cost of approximately £3500) that would guarantee the structural rigidity required to obtain accurate measurements of the displacements and forces required to understand the process.

The objectives of the machine, the forces measured and overview of dosing sequence are presented in sections 6.2, 6.3 and 6.4 respectively. An overview of the machine and the main components are presented in section 6.5, while the software interface is described in section 6.6 and a summary is given in section 6.7.

6.2.   Objective and principle of operation of the single shot dosator test-rig

The objective was to develop a machine that enabled the measurement of the forces acting on the dosator body and pin during dose procurement and ejection for the purpose of validating the dosator model proposed by this thesis. It was not an attempted to simulate the production machines or any other principle used commercially.

The test-rig did not operate under the same principle as a common dosator filling machine. Unlike the production machines, the dosator is static and the trough, containing the bed of

powder, moves upwards filling the dosator cavity. By securing the dosator, it is possible to measure the forces acting against the dosator, isolating effects of the speed.
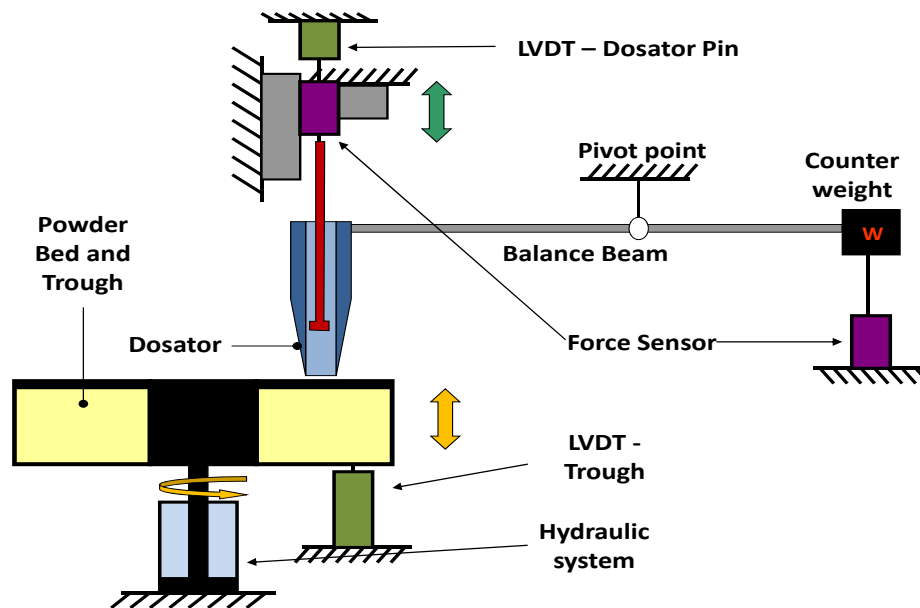
Figure 6.1. Sketch of the dosator test-rig principle. For full explanation refer to the text.

Figure 6.1 shows a schematic sketch of the test-rig operation that follows the dosator principle described in chapter 2. As it can be seen, the dosator is attached to a balance beam that contains a counterweight at the opposite end. At this end of the beam, a vertical force sensor measures the forces from the powder bed against the dosator body in each stroke.

The dosator pin is suspended, concentric as possible with the dosator body from a force sensor mounted on a combined vertical-horizontal slide and an assembly system, described in section 6.5.3. The slide is motorised and features a displacement gauge to drive and measure the dosator pin displacement, that allows the set up and control of the dose length and ejection.

A displacement gauge is connected to the trough to control the gap between the dosator and the bottom of the trough and record the stroke of the operation. The trough is attached to a hydraulic system and motor that allows the vertical and rotational movement of the powder bed. The test-rig is semiautomatic controlled by a computer through a Labview interface and the data is collected, displayed and save into excel format in a user friendly interface designed by the author.

The system is arranged for the dosator to procure a dose from the centre of the annular powder bed; however the test-rig can be manually set to stroke close to the trough's walls. This feature was not used in this research.

6.3. Forces measured in the test-rig

The dosator pin and body forces measured in the test-rig are shown in figure 6.2. The pin load sensor measures the forces from the powder inside the dosator (force in blue colour) during the filling stage and the force applied to the dose during ejection stage (force in yellow colour).
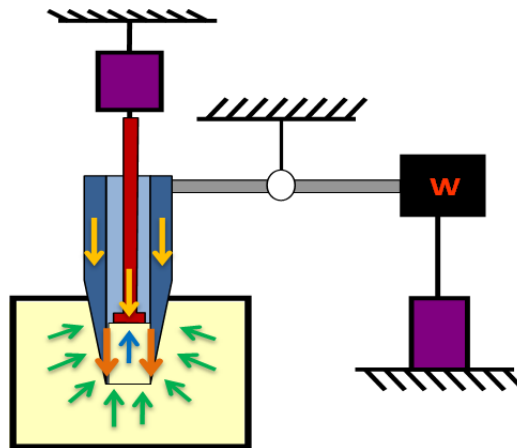
Figure 6.2. Forces measured in The Wolfson Centre dosator single shot test-rig. For full explanation refer to the text.

The body load sensor measures the forces from the powder inside and outside the dosator (forces in green and orange colour) during the filling stage and the forces inside the dosator (force in orange colour with inverted direction) during the ejection stage. As the powder bed is in a loose state (described in chapter 7 section 7.2.3) and the angle formed between the vertical axis and the decreasing external diameter is small[16], these external forces can be neglected (forces in green colour). This was confirmed when measuring dosator pin/body forces in experimental trial measuring the compaction ahead of the dosator with zero dose length set it (discussed later in section 7.6 in chapter 7). Therefore it is assumed that what is measured by the dosator body load sensor is mainly the vertical shear stress on the internal dose cavity wall due to the wall friction effect (forces in orange colours) at the filling and

---

[16] Angle approximately 4.65^0 degrees, according to information provided by GSK showed in the appendix 1

ejection stages. This was confirmed through tests to measure the pre-compaction ahead of the dosator and to obtain the infinite dose length that are presented later in chapter 7 (sections 7.6 and 7.7 respectively).

The force experienced by the dosator during the incoming stage is calculated by adding the measured dosator pin and body forces.

6.4.   Dosator operation sequence

Presented in figure 6.3 is a schematic of the dosator operation sequence from the forces and displacements measured in the test-rig; also illustrated are the equivalent stages of the dosator principle shown in figure 2.11 in chapter 2. The graph has two vertical axes as a function of the time in seconds. The primary vertical axis measures the forces on the pin (red series) and body (blue series) whereas the secondary axis presents the displacement of the pin (green series) and trough (yellow series).
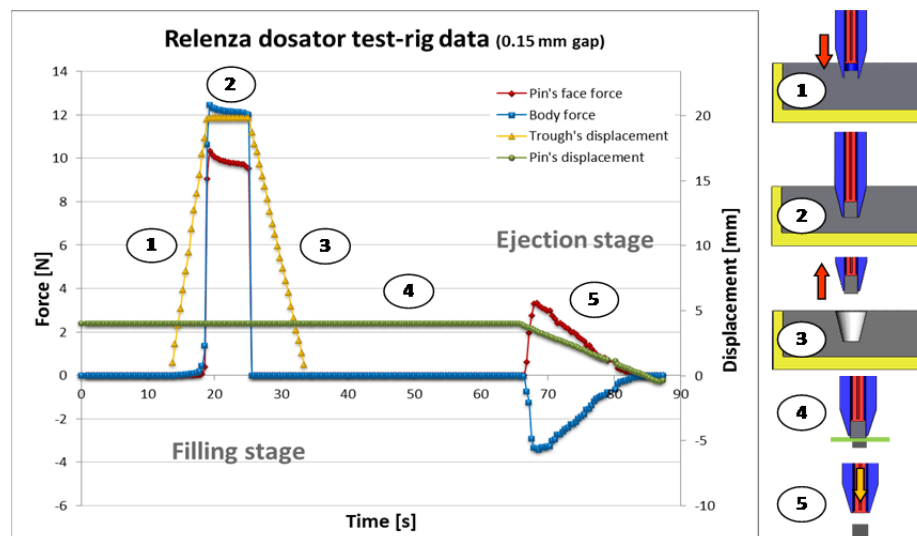
Figure 6.3. Dosator sequence example from The Wolfson Centre dosator single shot test-rig and equivalence to the dosator principle: 1) filling of the dosator; 2) end of the stroke; 3) dosator retraction; 4) powder doctored; 5) dose ejection. For full explanation refer to the text.

As the dosator is inserted into the powder bed (1) (by the movement of the trough), there is a considerable distance travelled before the sensors on the pin and body detect a force; the trough's insertion speed is approximately 7 mm/s. It can be seen that there is a rapid increase of the forces as the dosator approaches the end of the stroke. In this example, the forces on the dosator body start increasing before the pin force, because initially the cavity was not

filled. Once the full stroke is reached (2) the forces diminish; this might due to a relaxation of the stresses in the system or rearrangement of the particles packing. The trough is then retracted (3) and the forces go back to zero. Afterwards, the powder protruding the dosator is doctored (4) with the doctoring tool showed in figure 2.23, chapter 3. Later, the ejection stage (5) begins when the pin moves down generating a force, which peaks as the dose starts to move and diminishes slowly as it is pushed out of the cavity. During the ejection the force generated on the pin face is mirrored by the force measured on the body; this action also confirms the statement done about the force measured by the body load sensor in the previous section. The ejection speed is approximately 0.25 mm/s. The dose in manually collected and weighed using a Gec Avery scale.   The trough rotates ready for the next stroke.

6.5.   Description of the main parts of the test-rig

This section describes briefly the main characteristics of the dosator single shot test-rig after several modifications and improvements. Figure 6.4 shows design and the main parts of the dosator single shot test-rig, which are described in detail through this section.
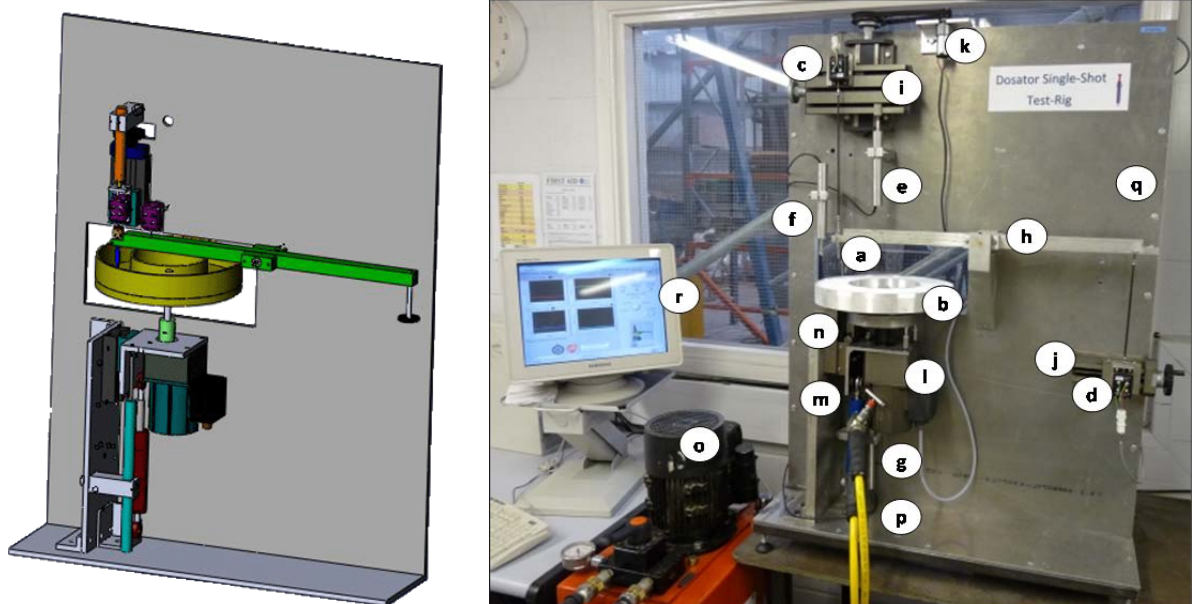
Figure 6.4. The Wolfson Centre dosator single shot test-rig design and main parts: a) dosator; b) trough; c) dosator pin force sensor; d) dosator body force sensor; e) dosator pin LVDT; f) gap "h" LVDT; g) trough's LVDT; h) beam balance; i) dual slide; j) slide; k) motor; l) geared motor; m) hydraulic cylinder; n) trough's support system; o) hydraulic system; p) gap "h" mechanical adjuster; q) test-rig chassis; r) Labview interface. For full explanation refer to the text.

The test-rig is framed and vertically supported by aluminium chassis of 20 mm thickness (see figure 6.4q). This chassis reduces deflection effects, makes robust the test-rig and reduces the effect of vibration from external sources.

6.5.1. Dosator and trough dimensions

The dosator used in this research is shown in figures 2.8a (in chapter 2), 6.4a and also described in the appendix 1. Only one dosator design was used, this was representative of that used by the industrial sponsor for Relenza and had a dose cavity diameter of 3.4mm and pin face diameter of 3.375 mm. The pin initially had three lobes along the shaft, but these were found to contribute frictional drag on the single shot dosator test rig and were removed. The dosator pin and body set used were supplied by the industrial sponsor was part of R&D trials testing new designs looking at the reduction of powder storage behind the pin's face (this design is showed in the appendix 1). The dosator, pin and body, were manufactured from stainless steel and polished to a mirror finish.

Figure 6.5. Dosator single shot test-rig annular trough.

The annular trough used in this research to contain the powder bed is shown in figures 6.4b and 6.5. The height, internal and external diameter dimensions of the trough bed are; 20, 142 and 263 mm respectively. When filled level to the top of the trough, the powder storage capacity is 770 cc.

The trough was manufactured from stainless steel with all internal wall polished to a mirror finish. It was machined in one single operation to ensure the top and bottom surfaces of the powder bed chamber were parallel; the reasons are explained later in section 6.5.5. The

tolerance of the distance between the surfaces planes was ± 0.02 mm and the flatness of the bottom of the trough was ± 0.01 mm.

6.5.2. Force and displacement measurement

The test-rig has two UF1 strain gauge transducers (see figures 6.4c, d and 6.6) to measure the forces in the system. Tests were initiated with ± 25 g range cell but as the research progress this was replaced with higher ranges up to ± 1500 g. This was the manufacturer's maximum rating for this range of sensors, but was still found to over range for some trials and powders as mention later in chapter 7, section 7.3.

According to manufacturer's technical sheet, the accuracy of the transducers was ± 0.07% of FRO. The calibration of the force sensors is showed in the appendix 7. The signals are amplified with a SGA signal conditioner. There is a rod at the bottom of the transducers measuring the applied tensile or compressive forces. Due to manufacturing variations this rod was not always perpendicular to the sensor casing, which hindered their direct connection to the pin and balance beam on the test-rig (as can be appreciated by inspection of figure 6.6).

Figure 6.6. UF1 load strain gauge transducer.
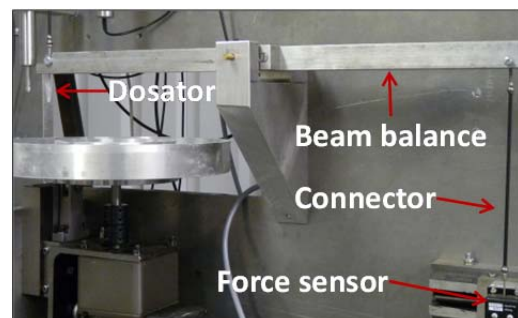
Figure 6.7. Balance beam connecting the dosator body and the UF1 force sensor.

One of the load transducers measures the dosator body forces (see figure 6.4d). It is connected to an aluminium balance beam (see figures 6.4h & 6.7), which in turn is connected to the dosator body. The beam balance has a counterweight, in the opposite extreme of the dosator, to ensure the mass balance in the system. This arrangement was considered to be the easiest way to deal with the complex geometry of the dosator and force sensor.

The other load transducer measures the dosator pin force (see figure 6.4c). The sensor is placed above the dosator, attached to a dual slide (see figure 6.4i) allowing movements in the vertical and horizontal axis; the dosator body sensor is also placed in a horizontal slide (see figure 6.4j). The slides were used for flexibility when centring the pin in the dosator body to correct misalignments and prevent contact that would lead to additional friction in the test-rig.

The test-rig has three LVDT's to measure the position of dosator pin, the trough and control the gap "h"; they are AML/EU ±12.5, ± 50 and ± 5 mm type respectively from Applied Measurements Limited manufacturer. The displacement transducer connected to the pin controls the dose lengths and ejection (see figures 6.4e & 6.8) and it is attached to the dual slide showed in figure 6.8. To control the trough's position/dosator stroke the second LVDT is attached top the trough (see figure 6.4g).
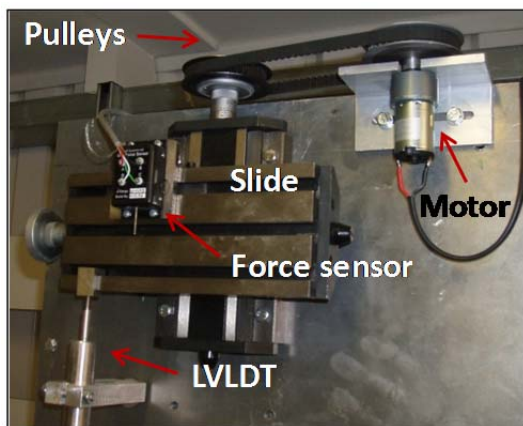
Figure 6.8. Dosator pin control arrangement. For full explanation refer to the text.
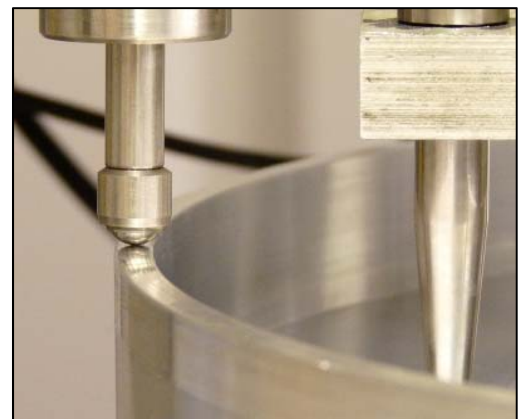
Figure 6.9. LVDT controlling the gap "h".

The third displacement gauge (see figures 6.4f and 6.9) ensures that the gap "h", previously manually set, is achieved; the LVDT acts on the top surface of external wall of the trough.

The manufacturer provided the calibration of the LVDT's and the transducer itself amplifies the signal; according to the technical sheets the accuracy is ± 0.25%.

6.5.3. Force sensor assembly

The force sensors are not directly connected to the dosator pin and body because of the dosator and test-rig complex geometry and misalignments issues. They are connected using the system showed in figure 6.10.

a)   b)   c)
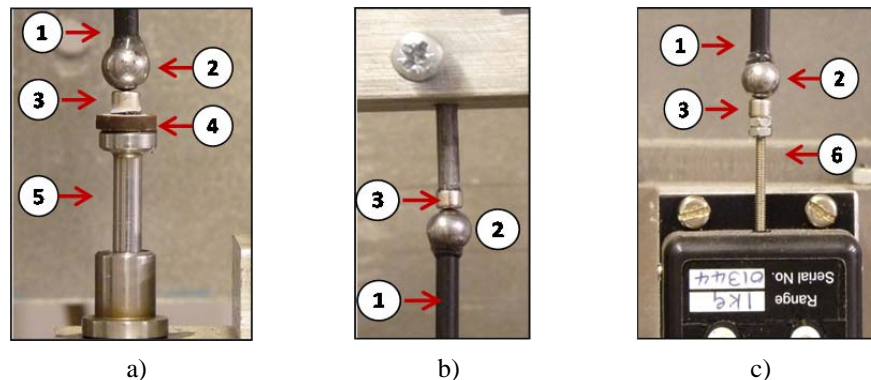
Figure 6.10. Force sensors connector: a) at dosator pin; b) at the beam balance; c) at the force sensors. 1) fibber glass rod; 2) steel sphere; 3) magnet; 4) isolator disc; 5) dosator pin; 6) force sensor threaded rod. For full explanation refer to the text

After several modifications and trials, fibreglass rods that had a steel sphere glued at each end were used in conjunction with small cylindrical magnets as connectors. The attachment of these connectors to the top of the dosator pin, to the balance beam and to the force sensors is shown in figures 6.10a, b & c respectively. The spherical ends of the connectors gives a degree of movement and help to correct horizontal misalignments in the system; thus maintaining the concentricity between the dosator pin and body as possible and minimize friction issues in the measurements. Meanwhile the fibreglass rod is rigid under the application of vertical forces measured by the transducers. Note that the attraction force of the magnets is strong enough to overcome the tensile force on the dosator body sensor during the dose ejection stage. To prevent magnetisation of the dosator and avoid dragging forces, the dosator pin was demagnetised[17] first and isolated by gluing a disc between the magnet and the pin (see figure 6.10a).

This assembly does not ensure concentricity of the dosator parts, however preliminary trials in the test-rig did not present friction issues. Another matter with either concentricity/eccentricity is the migration or binding of particles within the tolerance (25 μm) between the dosator pin and body that can develop situations such as pin jam, powder build up on the dosator body walls and some others described in section 7.4, chapter 7. The D50 of

---

[17] Using a Eclipse table top de-magnetiser type DA955

the materials used in this research was greater than 50 μm excepting for Lactohale300, which it was around 4 μm (refer to table 5.1, section 5.3.2, chapter 5); nonetheless it was not observed pin jams or other problems related to powder build up affecting the data, probably because the dosator only stroked 30 times in comparison to the thousands in production machines.

6.5.4. Trough and dosator pin's driving system

To procure the dose, a double action hydraulic system (see figure 6.4o) is used to operate a vertical cylinder[18] (see figure 6.4m), which raises and lowers the powder trough. The trough's stroke speed can be modified by the two flow valves connected to the cylinder. The dose ejection is driven by motor[19] (see figures 6.4k & 6.8), which is connected to the dual slide via a belt and pulleys (see figure 6.8) configuration. The speed of the dosator pin is controlled by a linear servo control amplifier[20]. After the dose has been procured the powder trough, which is connected to a geared motor[21] (see figure 6.4l), is rotated through approximately 30^0 positioning the powder bed for the next stroke.

6.5.5. Gap "h" setting and control

As the gap "h" (see figure 6.11) is considered critical in this research (as observed in preliminary trials in the test-rig), much care was taken to control and measure it accurately. It was therefore important that trough end stop position at the top of the stroke was consistent, over many strokes and as the trough rotated to present a fresh region of powder bed.

To achieve stability and consistency of the trough and drive assembly, the trough which was accurately machined to ensure parallel horizontal surfaces was mounted on 3 rotating bearing supports (see figures 6.4p and 6.12), one of which was under the dosator stroking point to prevent tipping. The trough support was mounted directly to the hydraulic piston, note that initially the trough was mounted to the motor shaft but this gave significant movement of the trough and was unacceptable.

---

[18] Rexroth CDL1
[19] 50:1 gear DC motor, 75 rpm, 12V
[20] Maxon 4-Q-DC LSC 30/2
[21] Panasonic M91A40GK4GE

Figure 6.11. Gap "h", clearance between the dosator tip and the bottom of the
trough. Picture taken from The Wolfson Centre dosator single shot test-rig

To achieve consistency of stroke, the end stop of the hydraulic cylinder was reset (by
adjusting the locking screw see figures 6.4n & 6.13) at the beginning of each test to the
required gap "h". With the stroke fully extended, this was achieved by raising the trough
using the locking nut until the base just contacts the dosator tip and a force is about to be
sensed. The LVDT on the trough is then zeroed and the trough lowered using the locking nut
until the LVDT senses the required gap "h". This is then rechecked using a feeler (depth)
gauge.
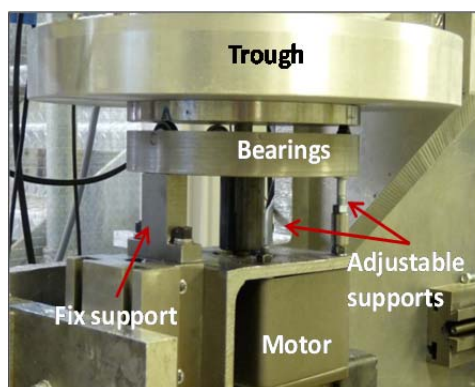
Figure 6.12. Trough's supporting system. For
full explanation refer to the text.

Figure 6.13. Gap "h" adjustable system. For
full explanation refer to the text.

6.6   Software interface

The test-rig is semi-automatic, controlled by a computer through a Labview interface (see
figure 6.4r) and the data is collected, displayed and save into an Excel format in a user
friendly interface. Labview communicates to the test-rig through a USB data acquisition

module[22]; that has analogue/digital outputs and inputs that array the signals from the force and position transducers and drive the motors in the test-rig.

The data arrayed by the data acquisition module is displayed in the PC through Labview software. The author programmed and designed the interface and figure 6.14 shows the main display panels of the interface.

a)

b)

c)

d)
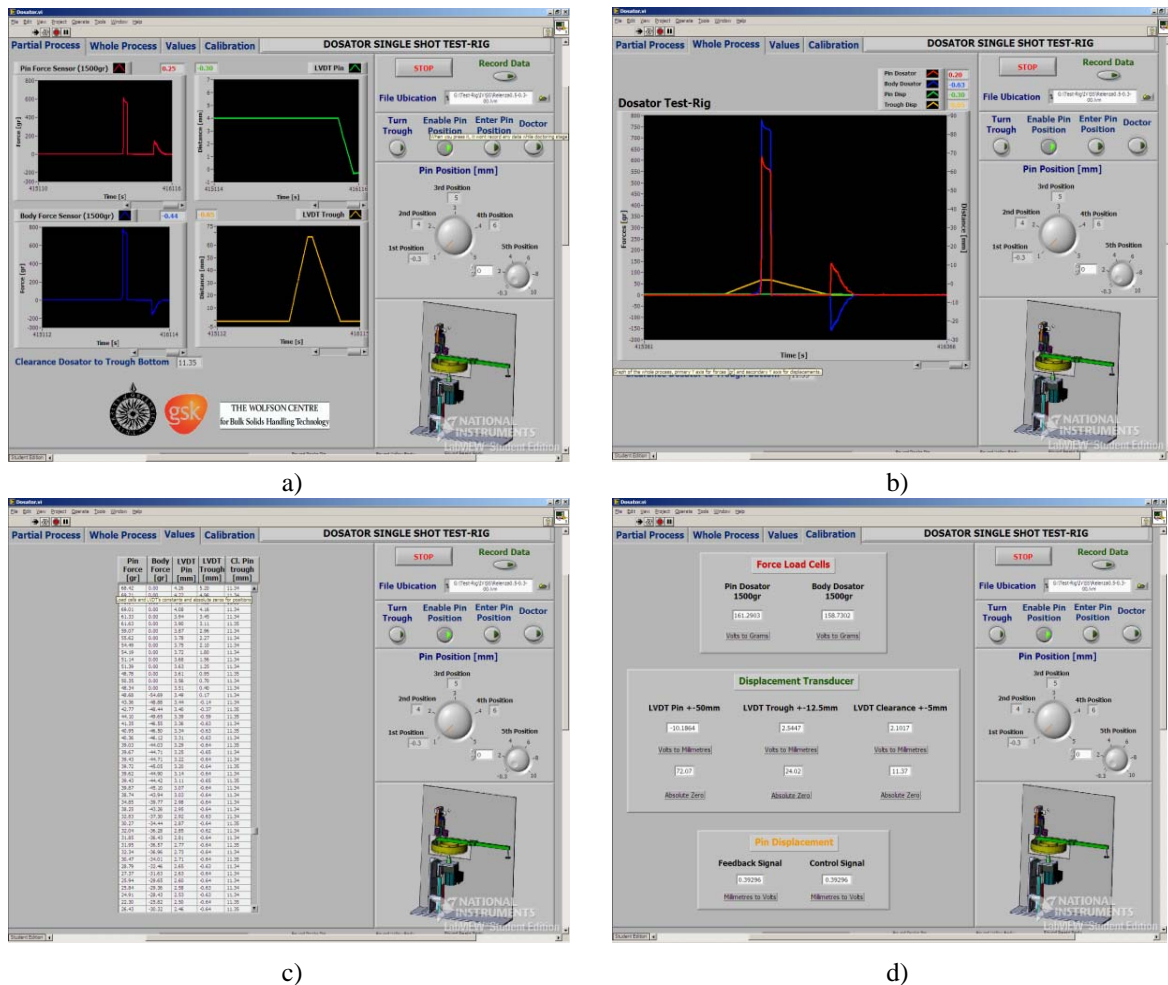
Figure 6.14. Dosator test-rig display in Labview: a) individual signals; b) combined signals; c) table of the results; d) instrumentation calibration. For full explanation refer to the text.

The software provides the user with tabs for four different options for visualization of the test. The main tab displays numerically and graphically the individual force and LVDT sensor signals (see figure 6.14a). In the second tab the four signals outputs are combined in one graph, showed in figure 6.14b. The third tab displays a table with the values that has been recorded in the test (see figure 6.14c) and the fourth tab shows the calibration values of the

---

[22] Advantech USB 4716 Module

transducers (see figure 6.14d). On all tabs there is a panel shown on the right hand side of each screen that operates the test-rig. Figure 6.15 shows the panel and its parts.
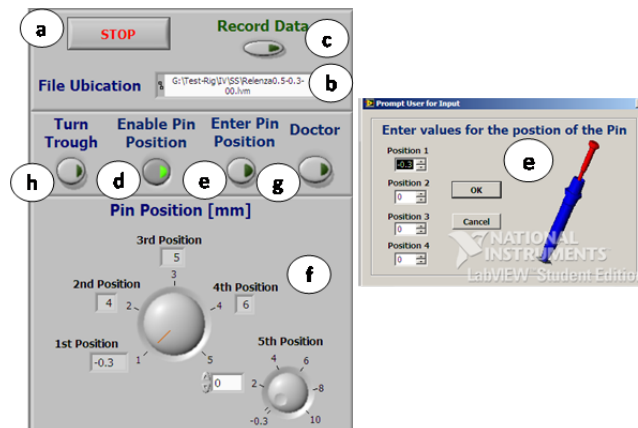
Figure 6.15. Dosator test-rig control panel. For full explanation refer to the text.

The dosator project is run like any other Labview project. In figure 6.15, there is a button (a) that finishes the loops and data iteration of the system. There is also an option to name the Excel file where the data will be saved. The recording of the data starts as soon as the button "Record data" (c) is enabled. For programing and signal issues, there is a button enabling the displacement of the pin that allows the pin to move to any position in the knob "Pin positioning" (f); if this function is disabled, the pin will not move. The button "Enter values for the position of the pin" (e) stores four dose lengths to be used during the tests; a pop up window appears to enter the four positions. These positions are set it as default in the "Pin Position" (f) knob that manages the displacement in the dosator pin; there is an option for a fifth position to be added manually. The control integrates a feature designated "Doctor" (g) that converts the signal in the dosator body as zero during the doctoring to eliminate the noise in the signal. After the dose is collected the button "Turn trough" (h) rotates the trough for the next stroke.

The dosator Labview project can be improved and more features can be added that were not covered in this research. Details about the dosator Labview project are shown in the appendix 7.

6.7   Summary

The results of the single shot dosator trials are presented in the following chapter 7. Developing and refining the operation of the test-rig increased the understanding of the dosator process, identifying factors involved in the variation of the dose weight.   This experience directed the test programme as presented in chapter 7, section 7.2.

Chapter 7

Dosator Single Shot Test-Rig Results

7.1. Introduction

This chapter presents the results obtained from experiments in The Wolfson Centre single shot dosator test-rig.

Early trials with the dosator test-rig (described in the appendix 7) led to incremental improvements in the test method (presented in section 7.2) and identified the three main factors affecting the dose fill weight were namely the:

- dose length,

- powder bowl/ dosator tip clearance gap "h" at the end of the stroke (see figure 6.11, chapter 6),

- and the powder bed conditions in terms of compaction and the presence of voids.

Hence the main focus of the single shot dosator test rig experiments were to investigate the above factors over a range values commensurate with those used by the industrial sponsor during dose manufacture.   The results of the tests to investigate the above three factors are presented and discussed in sections 7.3 for the four main test powders. Physical observation of the behaviour of the four main test powders, based on the condition of doses ejected and the cavities left in the trough bed are presented and discussed in section 7.4.

Other secondary machine operating factors that were briefly studied are presented in section 7.5, for a limited number of the test powders. These were the effects of the:

- powder bowl wall friction,

- "double shuffle" backward then forward rotation of the trough at the bottom of the dosator stroke.

In addition the factors that were important to understand were the:

- pre-compaction ahead of the dose.

- ultimate dose length,

To investigate the pre-compaction ahead of the dose, a series of tests with the pin face set level with the tip of the dosator body (i.e. a dose length of 0mm) were undertaken to measure this force for the four main test powders as a function of the dosator stroke as presented in section 7.6.

To investigate the ultimate dose length, a set of tests were undertaken where the dosator body (without the pin) was lowered into the powder bed to measure the filling force and the dose length. The results of these tests are shown in section 7.7.

Section 7.8 compares the density and void fractions of the doses obtained from the different test conditions with those measured in the characterisation tests presented earlier in chapter 5, sections 5.4.4 and 5.4.6 respectively.

Finally, a summary of the single shot dosator test rig results is presented in section 7.9.

7.2. Development of the single shot dosator test method

The following section present the machine settings and powder bed preparation method used in sections 7.2.1, 7.2.2 and 7.2.3.

7.2.1. Range of dosator machine settings

Summary of the tests conditions selected from the early trials in the test-rig are as follow:

- Dose lengths of 4, 5 and 6 mm were used for all tests. The extremes of length were found to provide well compacted and loose doses respectively.

- Powder bowl/dosator tip clearance gap "h" of 0.15, 0.3 and 0.6 mm. These distances covered the 0 and 0.3 mm range of industrial dosator filling machines. Lower than 0.15 mm resulted in overloading the force sensors, signal noise issues and inaccurate measurements.

- The bed was prepared by sieving the powder into the trough aiming to obtain homogeneous conditions. The influence of the bed conditions in the variation of the dose weight was simulated by applying distributed loads of 0.5 and 1 kg for a time period of 30s over the area of the powder bed. These gave normal stresses of 176 and 352 Pa respectively.

The smallest gap values were chosen because they are approximately equivalent to one and a half diameter, 3.4 and 1.75 mm respectively, and they were thought to be important distances for the dosator model (described in chapter 8).

Above of 6 mm dose lengths and 0.6 mm gap "h", the tests presented low filling and ejection forces and large dose weight variations.

The state of stress in the powder bowl is known to be poorly controlled in the production machines, since it was suspected that this could significantly affect the dose weight it was necessary to control this during the experiments. The pre-compacted conditions selected for the powder bed are not directly relevant to the production operation but cover the likely range stresses applied by the production machine scraper.

The standard dosator test run on a single powder comprised one gap "h", one powder bed stress condition and three dose lengths, giving 30 strokes per test. To achieve these strokes, it was necessary to prepare two fresh powder beds, each bed providing the powder for 15 dosator strokes at 2.5cm intervals. Initially it was anticipated that 12 strokes/doses would be taken around the annular powder bed, leaving approximately 5 cm separations between the strokes, because the radius of the stroke influence in the powder bed was unknown. However observations of the powder bed after preliminary tests indicated a maximum radius of perturbed bed at the end of the stroke up to 0.75 cm (shown in section 7.4.9).

The stroking sequence was 4, 5 and 6 mm for the dose lengths so that drifts in the bed conditions would lead to scatter in the data rather than a false upward or downward trend.

7.2.2 Test preparation and operation procedure in the test-rig

The procedure sequence for one test was as follows:

- manual preparation of the powder bed (described in section 7.2.3 and appendix 7),

- adjustment of the gap "h" (described in section 6.5.5),

- data input (file name and dose lengths) and recording in Labview software,

- stroke up and down of the trough by manual operation of the hydraulic system,

- doctoring and weighing of the powder protruded in the test, using the doctoring tool showed in figure 2.23, chapter 2;

- dose ejection by lowering the dosator pin controlled from Labview software,

- manual dose collection and weighing.

7.2.3 Powder bed preparation

The powder was sieved into the trough[23] to break the agglomerates and provide consistent packing conditions in the bed prior to measuring the forces in the dosator. In order to obtain homogeneous bed conditions the bed was manually prepared and the test-rig was not equipped with a powder bed reconditioning system. In order to pre-compact the powder bed to the required stress level and the fixed 20 mm bed height it was necessary to use mould rings to overfill the trough to account for the powders compressibility. If required, a uniform load was then applied to the powder using a flat concentric ring of the desired weight. The weight and mould rings were then removed and the powder bed levelled to the top of the trough using a rotating scrapper tool. Full details of the powder bed preparation are described in the appendix 7.

7.3 Results and discussion of the effect of the gap "h" and powder bed conditions in the fill dose weight and dosator forces

In this section it is shown the effect of the dose length, the gap "h" at the end of the stroke and the stress state in the powder bed, on the (doctored) dose weight, maximum filling/ejection

---

[23] Using a sieve with 355 μm mesh (larger than double of the maximum particle size of the powders used in this research).

forces and ejection force behaviour in sections 7.3.1, 7.3.2 and 7.3.3 respectively. The quantity of material removed by doctoring is presented in 7.3.4 for the different test conditions.

The test results showed in this section have been conducted for all four test powders: the red, green, yellow and blue series of the data presented below correspond to Lactohale300, the bimodal blend, Relenza and Lactohale200 respectively in the column type graphs. There are three colour shades for each powder relating the powder bed conditions in the columns type graphs; dark shade for normal bed state (no pre-compaction) and lighter shades for the different pre-compaction conditions applied to the bed (0.5 and 1 kg)

It was anticipated that there would be substantial scatter in the measurement of the dosator forces, due to the signal processing, noise in the signal and the sudden increase of the forces at the end of the stroke (occurred in fraction of seconds). The last mentioned made difficult to peak the maximum forces due to the speed of the tests and signal processing issues with the PC, data logger and Labview software settings.

The tests set at 0.5 & 1 pre-compacted bed and 0.15 & 0.3 mm gap "h" generated high stresses (presented in sections 7.3.2 and 7.3.3) and different situations (presented in section 7.4) were observed, depending on the powder flow properties, that could affect the data.

7.3.1   Mean dose weight results.

Figure 7.1 and table 7.1 show the mean dose weight as function of the gap "h" for all the powders used in this research varying the conditions in the powder bed. The results suggested that the gap "h" and the level of pre-compaction of the powder bed affected the variation of dose weight; each factor influenced more or less the variation depending on the flowability of the powders.

Can be seen a general increment of the dose weight as the gap "h" was reduced in all the dose lengths. Lactohale300 and the bimodal blend (according to chapter 5, cohesive and compressible powders) showed large dose variations with this factor than the incompressible and freer flowing Lactohale200 and Relenza.

a)

b)

c)

Legend

Lactohale300	0 kg PC Bed	0.5 kg PC Bed	1 kg PC Bed
Blend	0 kg PC Be	0.5 kg PC Bed	1 kg PC Bed
Relenza	0 kg PC Bed	0.5 kg PC Bed	1 kg PC Bed
Lactohale200	0 kg PC Bed	0.5 kg PC Bed	1 kg PC Bed

Figure 7.1. Mean dose weight varying the gap "h" and powder bed conditions for the dose lengths: a) 6 mm; b) 5 mm; c) 4 mm. Results obtained from The Wolfson Centre dosator single shot test-rig. For full explanation refer to the text.

Mean Dose Weight Results [mg]								
Lactohale300								
	4 mm dose length			5 mm dose length			6 mm dose length		
	Bed conditions [kg]			Bed conditions [kg]			Bed conditions [kg]		
Gap h	0	0.5	1	0	0.5	1	0	0.5	1
0.15	14.09	18.49	19.91	15.14	19.49	22.74	14.42	21.68	24.44
0.3	10.78	17.47	19.27	14.03	19.46	22.45	14.23	20.02	24.6
0.6	12.61	16.92	17.92	12.55	18.41	20.97	11.63	19.17	22.47
Bimodal Blend								
	4 mm dose length			5 mm dose length			6 mm dose length		
	Bed conditions [kg]			Bed conditions [kg]			Bed conditions [kg]		
Gap h	0	0.5	1	0	0.5	1	0	0.5	1
0.15	33.21	34.39	34.24	38.17	41.78	42.03	41.56	47.26	48.94
0.3	32.34	34.12	34.27	38.23	40.81	41.68	42.66	46.97	49.12
0.6	31.23	32.48	33.11	36.46	39.03	40.59	39.44	44.31	47.87
Relenza								
	4 mm dose length			5 mm dose length			6 mm dose length		
	Bed conditions [kg]			Bed conditions [kg]			Bed conditions [kg]		
Gap h	0	0.5	1	0	0.5	1	0	0.5	1
0.15	28.35	28.79	28.73	34.56	35.12	35.45	40.64	41.37	41.77
0.3	28.16	28.67	28.17	34.35	35.24	35.07	39.7	41.32	41.4
0.6	27.59	27.34	27.67	33.79	33.76	34.17	38.71	39.94	40.45
Lactohale200								
	4 mm dose length			5 mm dose length			6 mm dose length		
	Bed conditions [kg]			Bed conditions [kg]			Bed conditions [kg]		
Gap h	0	0.5	1	0	0.5	1	0	0.5	1
0.15	31.63	31.66	31.71	39.25	38.91	39.41	46.82	46.91	47.46
0.3	30.8	31.41	31.48	38.9	39.07	39.11	46.2	46.91	46.86
0.6	30.67	30.39	30.67	38.2	38.22	38.37	45.07	45.91	45.62

Table 7.1. Mean dose weight variation with the gap "h" and the conditions of the powder bed of the powders used in this research; for 4, 5 and 6 mm. dose lengths. Tests undertaken in The Wolfson Centre dosator single shot test-rig.

The dose weight also increased with the increase of the pre-compaction level of the powder bed; the variation was also greater for Lactohale300 and bimodal blend than for Lactohale200 and Relenza. The variation in the bimodal blend dose weight was diminished with the reduction of the dose length.

The variation of the fill dose weight of Lactohale200 and Relenza was greater with the gap "h" than the powder bed conditions; opposite was case for the Lactohale300 and bimodal blend.

The maximum dose weight variation as a function of changes in either the gap "h" or the level of bed pre-compaction for the powders tested in this thesis was up to 10 mg. This level of variation could significantly affect a patient's health.

The data suggests that the Lactohale300 and the bimodal blend doses could be compressed more inside the dosator under the different situations tested, while the incompressibility characteristics of Lactohale200 and Relenza did not affect the doses in such manner. However, Lactohale200 and Relenza dose weight variations were up to 5 %[24] (approximately 2 mg) that can be significant in dry inhaled powders applications.

Powder flow properties and dose lengths affected the reproducibility of the tests. Small length doses presented higher repeatability than the larger doses for all the powders. Lactohale300 and bimodal blend had larger dose weight variation than the Lactohale200 and Relenza.

The dose weight is dependant of the bulk density and not on the powder flowability. Nevertheless, the two Lactose grades presented doses according to their PSD and flowability; Lactohale300 light doses and Lactohale200 heavier doses. The two blends behaved differently; having similar PSD, the bimodal blend presented heavier doses than Relenza.

7.3.2   Maximum dosator filling and ejection force results

Figures 7.2 & 7.3 and tables 7.2 & 7.3 show the mean maximum dosator filling and ejection forces respectively as function of the gap "h" for all the powders used in this research, varying the conditions in the powder bed.

The variations of the gap "h" and the powder bed conditions, in the filling/ejection forces, had the same trend as the dose results presented in section 7.3.1. The filling/ejection forces increased with the reduction of the gap "h" and increment of the pre-compaction of the powder bed.

---

[24] Taking 0 Kg pre-compacted bed and 0.6 mm gap "h" as a reference.
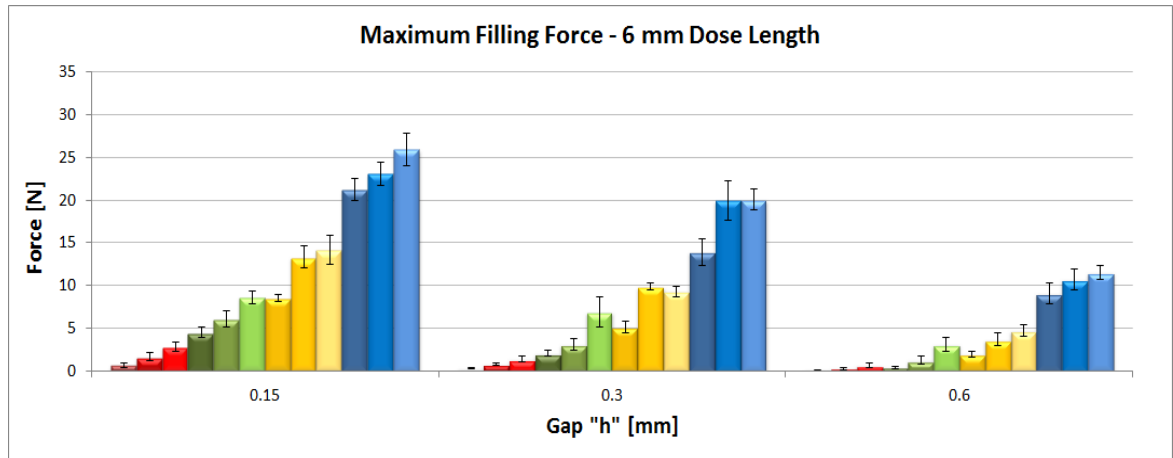
a)
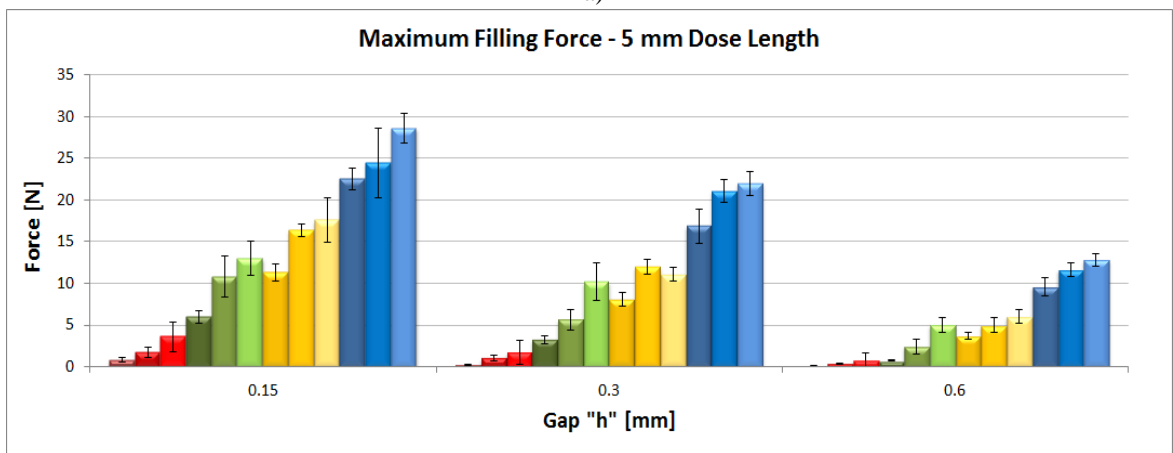
b)
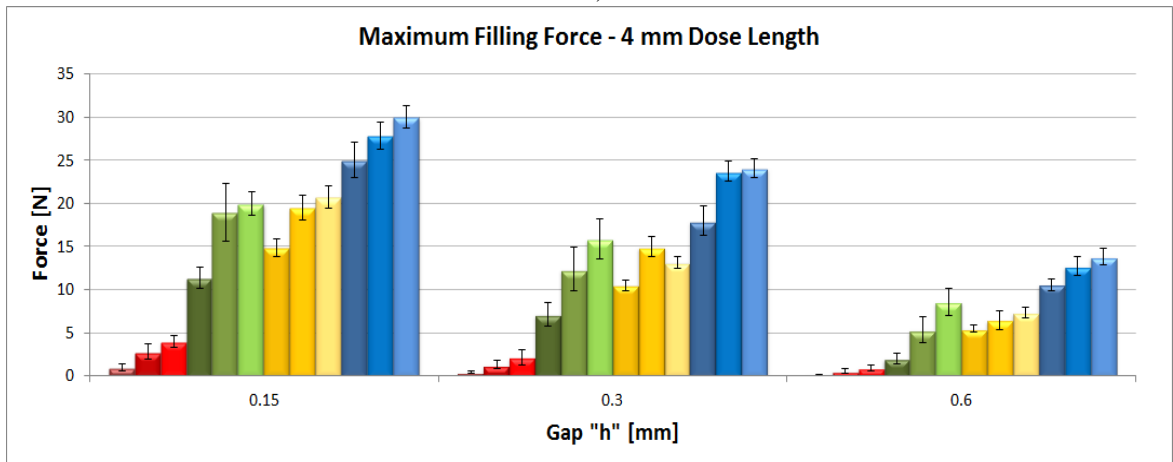
c)

Legend

■ Lactohale300	■ 0 kg PC Bed	■ 0.5 kg PC Bed	■ 1 kg PC Bed
■ Blend	■ 0 kg PC Be	■ 0.5 kg PC Bed	■ 1 kg PC Bed
■ Relenza	■ 0 kg PC Bed	■ 0.5 kg PC Bed	■ 1 kg PC Bed
■ Lactohale200	■ 0 kg PC Bed	■ 0.5 kg PC Bed	■ 1 kg PC Bed

Figure 7.2. Maximum mean dosator filling force varying the gap "h" and powder bed conditions for the dose lengths: a) 6 mm; b) 5 mm; c) 4 mm. Results obtained from The Wolfson Centre dosator single shot test-rig. For full explanation refer to the text.

147

Maximum Mean Dosator Filling Force Results [N]								
Lactohale300								
	4 mm dose length			5 mm dose length			6 mm dose length		
	Bed conditions [kg]			Bed conditions [kg]			Bed conditions [kg]		
Gap h	0	0.5	1	0	0.5	1	0	0.5	1
0.15	0.94	2.77	3.98	0.82	1.75	3.61	0.67	1.60	2.76
0.30	0.38	1.25	2.13	0.26	1.02	1.78	0.23	0.75	1.32
0.60	0.16	0.58	0.92	0.11	0.36	0.81	0.09	0.27	0.60
Bimodal Blend								
	4 mm dose length			5 mm dose length			6 mm dose length		
	Bed conditions [kg]			Bed conditions [kg]			Bed conditions [kg]		
Gap h	0	0.5	1	0	0.5	1	0	0.5	1
0.15	11.34	18.93	20.00	5.96	10.83	13.02	4.46	6.06	8.60
0.30	7.09	12.35	15.85	3.20	5.67	10.20	2.01	3.06	6.87
0.60	2.02	5.33	8.57	0.73	2.45	5.03	0.38	1.18	3.07
Relenza								
	4 mm dose length			5 mm dose length			6 mm dose length		
	Bed conditions [kg]			Bed conditions [kg]			Bed conditions [kg]		
Gap h	0	0.5	1	0	0.5	1	0	0.5	1
0.15	14.84	19.52	20.75	11.35	16.37	17.58	8.47	13.30	14.16
0.30	10.50	14.96	13.18	8.08	11.97	11.07	5.10	9.83	9.26
0.60	5.45	6.48	7.33	3.70	4.95	6.04	1.90	3.62	4.72
Lactohale200								
	4 mm dose length			5 mm dose length			6 mm dose length		
	Bed conditions [kg]			Bed conditions [kg]			Bed conditions [kg]		
Gap h	0	0.5	1	0	0.5	1	0	0.5	1
0.15	25.07	27.90	30.06	22.51	24.46	28.64	21.23	23.11	25.96
0.30	17.96	23.71	24.12	16.90	21.10	22.03	13.91	19.97	20.06
0.60	10.60	12.74	13.85	9.62	11.64	12.81	9.05	10.71	11.52

Table 7.2. Maximum mean filling force variation with powder bed conditions and gap "h" for the powders used in this research; for 4, 5 and 6 mm dose lengths. Tests undertaken in The Wolfson Centre dosator single shot test-rig.

a)

b)

c)
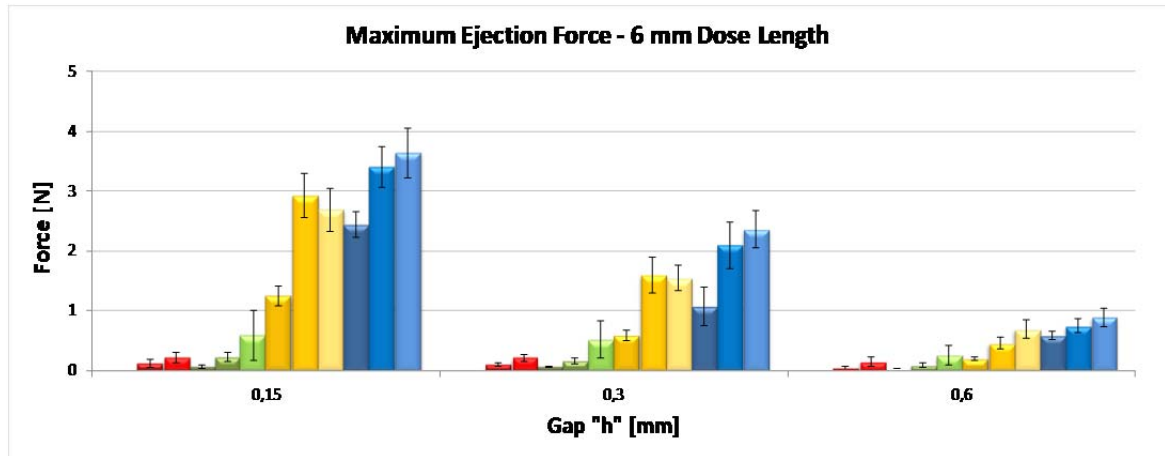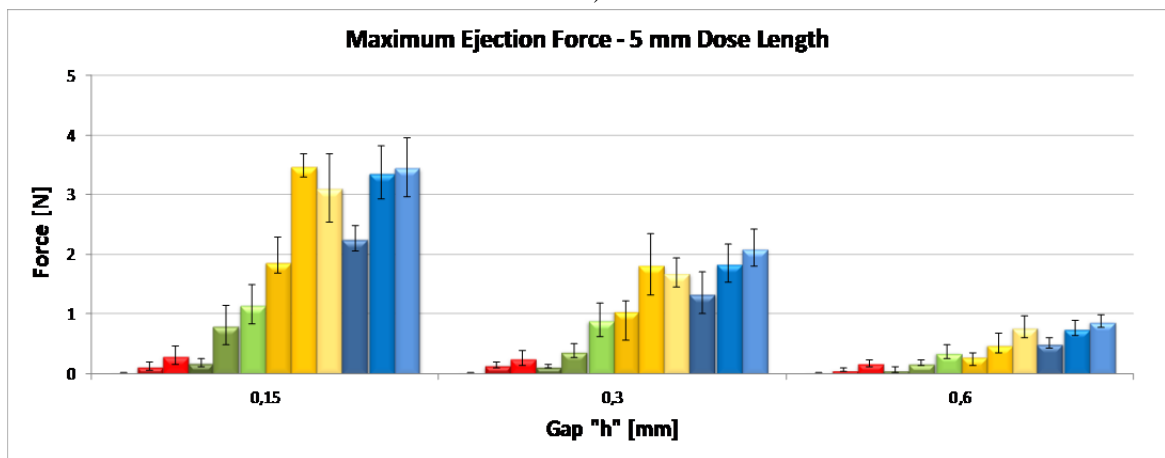
Legend

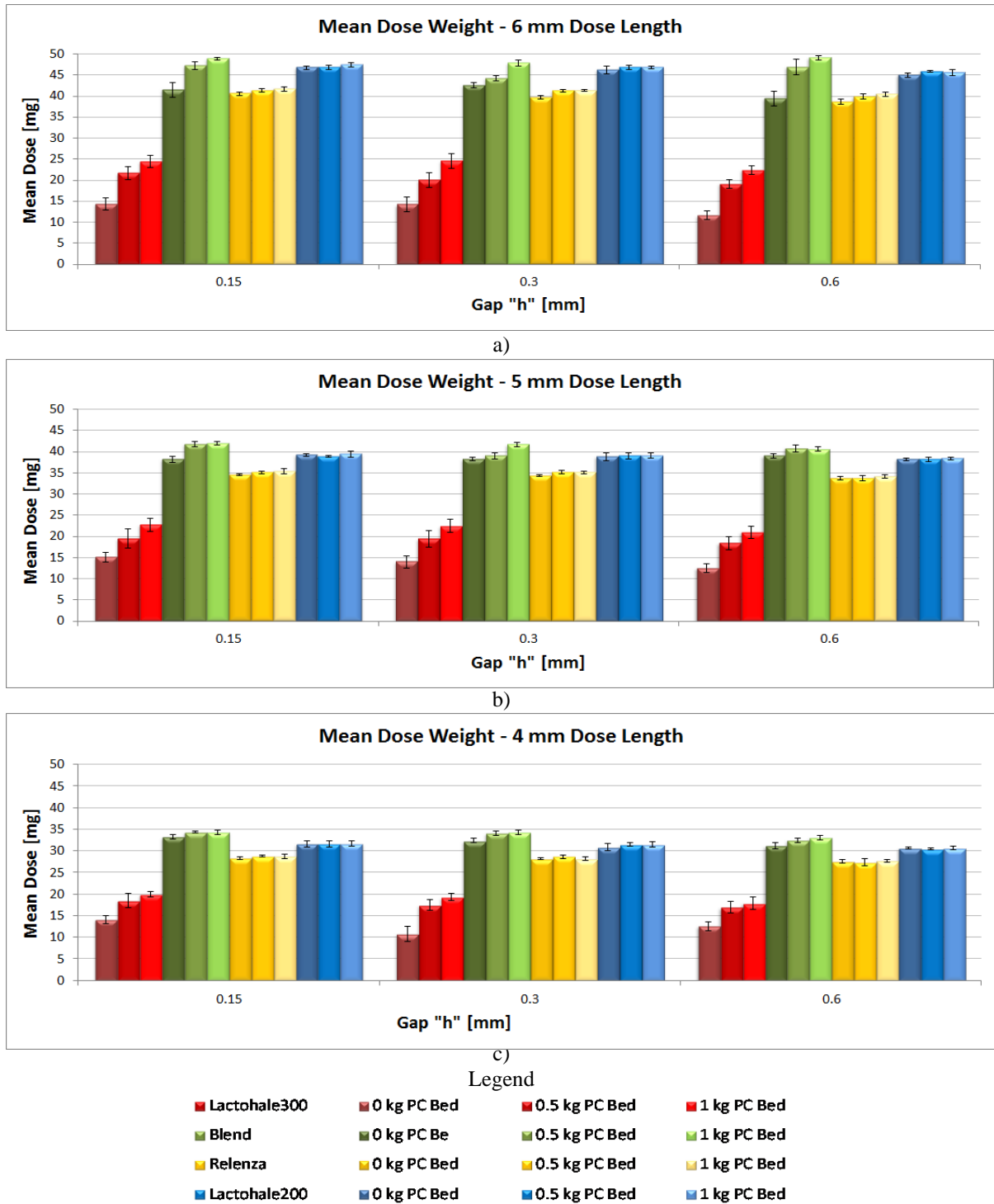Figure 7.3. Maximum mean dosator ejection force varying the gap "h" and powder bed conditions for the dose lengths: a) 6 mm; b) 5 mm; c) 4 mm. Results obtained from The Wolfson Centre dosator single shot test-rig. For full explanation refer to the text.

Maximum Mean Dosator Ejection Force Results [N]									
Lactohale300									
	4 mm dose length			5 mm dose length			6 mm dose length		
	Bed conditions [kg]			Bed conditions [kg]			Bed conditions [kg]		
Gap h	0	0.5	1	0	0.5	1	0	0.5	1
0.15	0.02	0.21	0.31	0.01	0.12	0.31	0.00	0.12	0.22
0.30	0.13	0.13	0.23	0.01	0.14	0.26	0.01	0.09	0.21
0.60	0.01	0.08	0.14	0.01	0.06	0.17	0.01	0.04	0.15
Bimodal Blend									
	4 mm dose length			5 mm dose length			6 mm dose length		
	Bed conditions [kg]			Bed conditions [kg]			Bed conditions [kg]		
Gap h	0	0.5	1	0	0.5	1	0	0.5	1
0.15	0.64	1.47	1.76	0.18	0.81	1.15	0.06	0.22	0.59
0.30	0.37	0.75	1.28	0.12	0.38	0.90	0.06	0.15	0.52
0.60	0.11	0.29	0.59	0.06	0.18	0.36	0.02	0.09	0.25
Relenza									
	4 mm dose length			5 mm dose length			6 mm dose length		
	Bed conditions [kg]			Bed conditions [kg]			Bed conditions [kg]		
Gap h	0	0.5	1	0	0.5	1	0	0.5	1
0.15	2.32	3.58	3.33	1.87	3.49	3.12	1.25	2.93	2.69
0.30	1.17	2.21	1.69	1.06	1.83	1.69	0.59	1.59	0.59
0.60	0.37	0.55	0.74	0.29	0.50	0.78	0.20	0.46	0.69
Lactohale200									
	4 mm dose length			5 mm dose length			6 mm dose length		
	Bed conditions [kg]			Bed conditions [kg]			Bed conditions [kg]		
Gap h	0	0.5	1	0	0.5	1	0	0.5	1
0.15	1.98	2.96	2.66	2.26	3.37	3.46	2.44	3.40	3.63
0.30	1.02	1.61	1.73	1.34	1.85	2.11	1.07	2.10	2.36
0.60	0.41	0.60	0.77	0.51	0.76	0.88	0.58	0.75	0.89

Table 7.3. Maximum mean ejection force variation with powder bed conditions and gap "h" for the powders used in this research; for 4, 5 and 6 mm dose lengths. Tests undertaken in The Wolfson Centre dosator single shot test-rig.

Lactohale200 and Relenza filling/ejection forces had the same trend as the dose weight results; the variation was higher with the gap "h" than with the conditions of the bed. Lactohale300 and the bimodal blend filling/ejection forces also had the same trend as the dose results, but the variation was larger with the bed pre-compaction conditions than the gap "h".

The results suggest a clear correlation between the filling/ejection forces with the flowability of the powders; Lactohale300 (the most cohesive powder) presented low filling/ejection forces while Lactohale200 (a less cohesive powder) presented higher forces. Nonetheless, the

variation of these forces with the gap "h" and the conditions of the powder bed were not proportional to the variation of the dose weight (shown in figure 7.1). This suggests that the pre-compaction ahead of the dosator in the powder bed, the variation of the gap "h" and the flowability of the powder are factors involved in the variation of the dose weight.

It can be seen also that the filling/ejection forces were affected by the dose lengths; shorter doses produced higher *filling* forces than longer doses. The *ejection* forces presented contradictory behaviour they increased with increasing dose length.

In figure 7.3, Relenza showed higher ejection force than Lactohale200. Apart from the similarity of the flowability, the cohesive strength of these two powders, Relenza had higher wall friction (measured in section 5.4.3 in chapter 5) and this could be the reason of the discrepancy of the ejection force behaviour in comparison to the filling forces. .
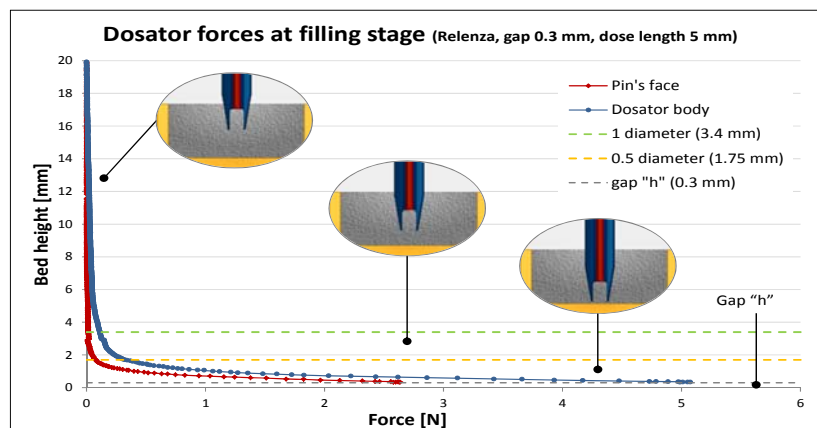
Figure 7.4. Relation between the experimental dosator filling forces and the dosator principle stages. For full explanation refer to the text.

Close analysis to the raw data can be seen in figure 7.4 and table 7.4. Figure 7.4 shows an example of the pin/body forces measured in Relenza 5 mm dose lengths and table 7.4 shows the approximately bed depth when measuring 1 g in both dosator body and pin force sensors; it is also illustrated the different dosator positions in the filling of dosators

The dosator test-rig results in table 7.4 indicates that the dosator body force sensors starts gauging 1 g in approximately 5 - 15 % of the dosator stroke; this is equivalent to 1 – 2 mm of the 20 mm bed depth. This distance varied with the condition in the powder bed. The friction forces in the dose chamber became big enough to be sensed at this point suggesting the filling of the dosator. The forces in the dosator body slowly increase as the dosator descends (in the case of the test rig stroke, as the trough moved upwards) and it is assumed that the dose

chamber is filled but probably the dose allows further compression because the pin force sensor does not gauge significant forces in the equivalent bed depth.

When the gap "h" is around 4 - 3 mm (80 – 85 % of the bed depth, see figure 7.4) the increments in the body force sensor are greater and the pin force sensor start gauging 1 g; this indicates a further dose compression of the dose with the proximity to the trough.

Approximately Bed Depth % Gauging 1 g in The Force Sensors of The Dosator Test-Rig												
Bed state [kg]	Relenza				Bimodal blend				Lactohale200			
	Body sensor	Pin sensor Dose length [mm]			Body sensor	Pin sensor Dose length [mm]			Body sensor	Pin sensor Dose length [mm]		
		4	5	6		4	5	6		4	5	6
0	10	83	86	89	10	84	88	93	8	54	67	80
0.5	8	61	78	86	10	82	85	90	5	42	60	60
1	5	59	75	84	5	69	83	84	5	25	47	50

Table 7.4. Bed depth percentage travelled sensing 1 g in The Wolfson Centre dosator single shot test-rig body and pin sensors for three of the powders used in this research; the bed depth in the test-rig was 20 mm. For full explanation refer to the text.

When the dosator is approaching the trough at the end of the stroke, there is a greater and sudden increment of the forces when the gap "h" is approximately 2 – 1.5 mm gap (90 – 92.5 % of the bed depth, see figure 7.4). Notice that these intervals correspond to one and half dosator diameters respectively. This was a general behaviour in the forces measured in the dosator test-rig.

Incompressible powders applied pressures to pin's face earlier than the cohesive powders. As the dose length increase the distance was larger and as the powder bed conditions increase the distance was shorter. Table 7.4 shows the data for three powders except for Lactohale300 which most of the forces were very low making difficult to distinguish it from the signal noise.

7.3.3   Ejection force behaviour

In this section are presented examples of the ejection force behaviour measured in the dosator test-rig. Figure 7.5 shows one randomly selected ejection force measurement for each condition measured in the test rig.
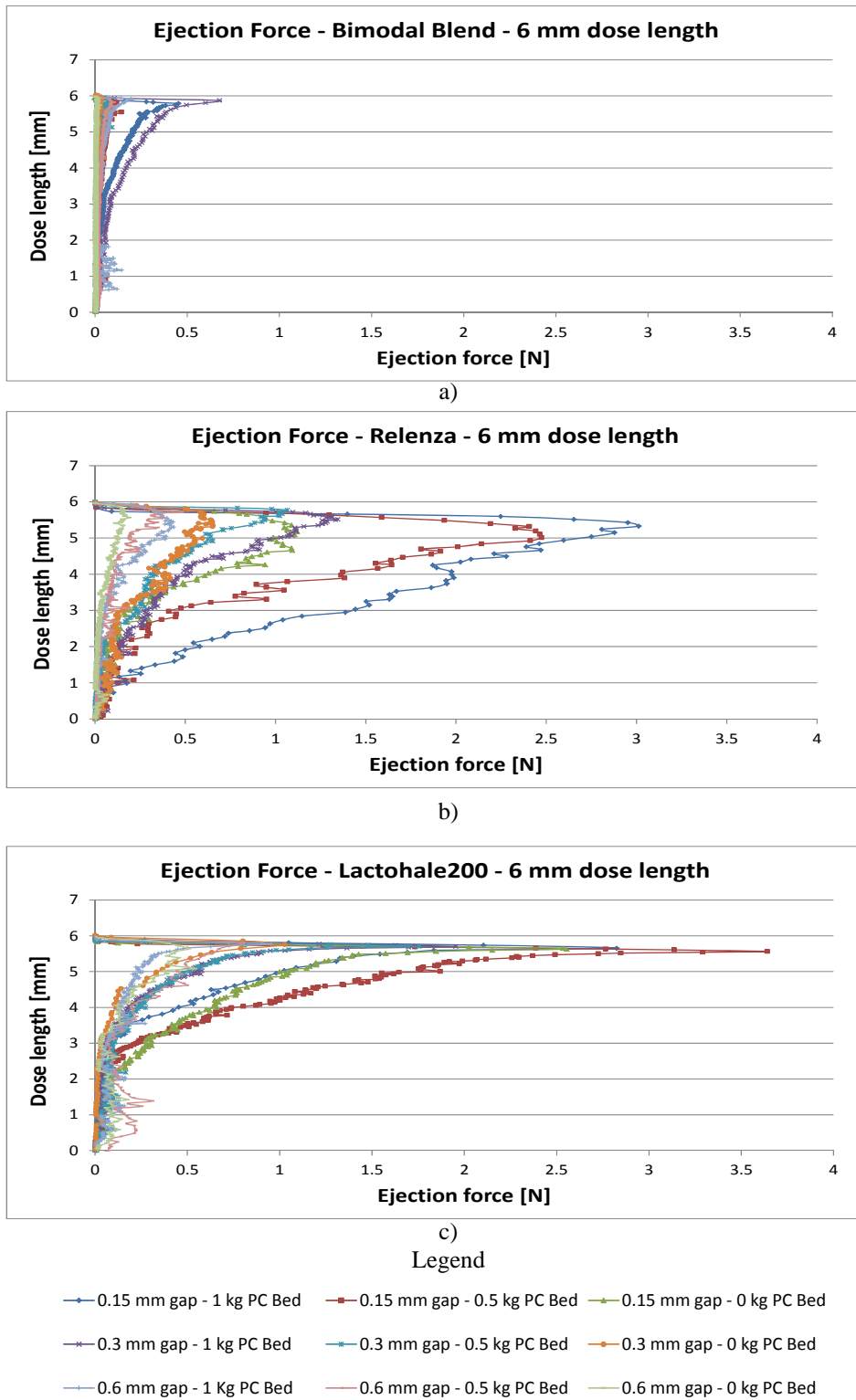
Figure 7.5. Ejection force behaviour of: a) bimodal blend; b) Relenza; c) Lactohale300. Forces measured in The Wolfson Centre dosator single shot test-rig. For full explanation refer to the text.

The profiles for the of 6 mm dose length have been chosen because they showed greater force magnitudes.   As the ejection forces in Lactohale300 tests were almost zero, they were undistinguished from noise in the signal; its profiles are not presented. Shown are the profiles for the bimodal blend, Relenza and Lactohale200. Profiles for the other dose lengths (4 and 5 mm) are shown in the appendix 7.

The "Y" axis in figure 7.5 represents the dose length in the dosator cavity and the "X" axis the force applied by the dosator pin to eject the dose.

It can be seen different behaviours of the three materials. For the bimodal blend (see figure 7.5a), the ejection force presented a small peak and then small drop followed by gradual reduction with the length. The profile obtained from Relenza ejection force tests (see figure 7.5b) was different, presenting a peak gradually reduced with the length in the cavity. Besides, Lactohale200 ejection force (see figure 7.5c) presented a peak and faster reduction of the magnitude to almost half of the dose length.

The data suggests that gradual decrease of the force is due to the wall friction of the powder with the dosator walls; Relenza presented the highest wall friction in between the three powders compared in this section. The steeper reduction of the force seen it in Lactohale200 also is related to the low wall friction characteristic of this powder.

It can be seen also the small displacement of the pin to reach the maximum force; this suggests the compression of the dose before to be ejected. This was steeper in large doses (see appendix 7).

7.3.4   Powder doctored results

As explained in section 7.2.2, the protruded adhered powder, after the dosator stroke, was doctored with the doctoring tool showed in figure 2.23, in chapter 2. This amount of powder removed was weighed and figure 7.6 and table 7.5 show the mean weight of the powder doctored in the tests undertaken in the dosator test-rig. It was expected to display significant variation in the tests because the amount of this powder is subject to different variables explained in section 7.4.

a)

b)

c)

Legend

■ Lactohale300	■ 0 kg PC Bed	■ 0.5 kg PC Bed	■ 1 kg PC Bed
■ Blend	■ 0 kg PC Be	■ 0.5 kg PC Bed	■ 1 kg PC Bed
■ Relenza	■ 0 kg PC Bed	■ 0.5 kg PC Bed	■ 1 kg PC Bed
■ Lactohale200	■ 0 kg PC Bed	■ 0.5 kg PC Bed	■ 1 kg PC Bed
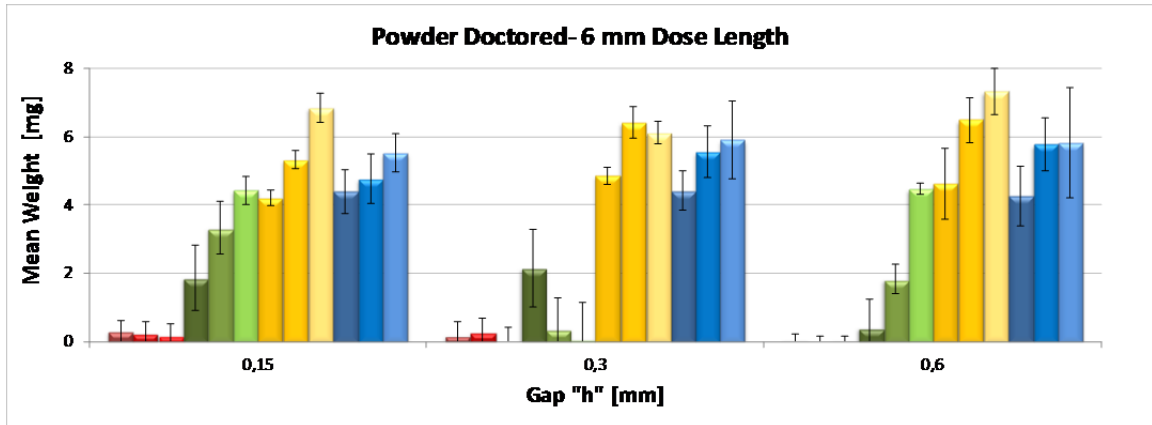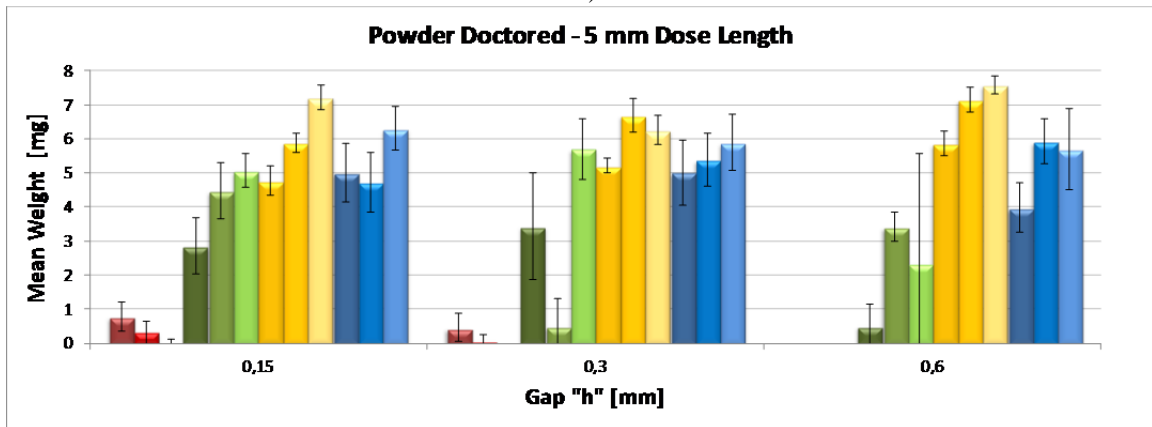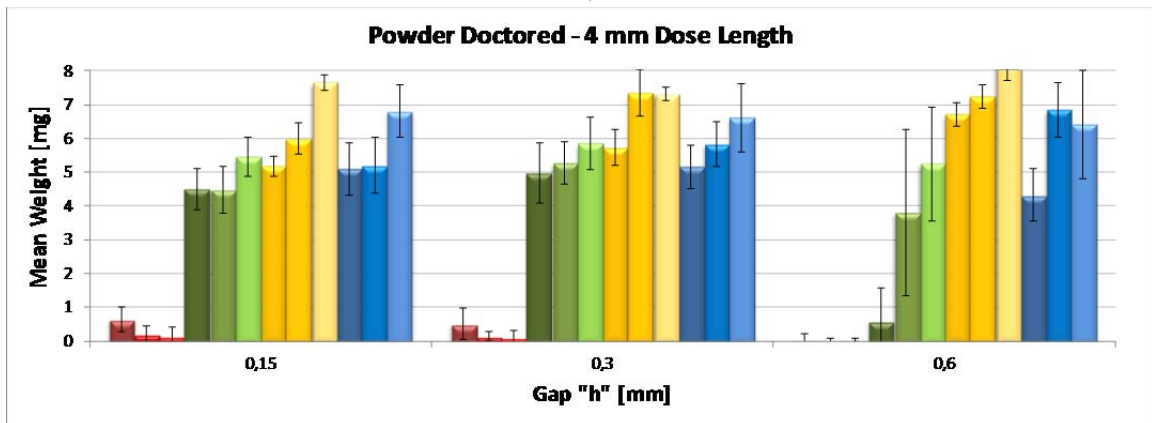
Figure 7.6. Mean dose weight of the powder doctored varying the gap "h" and powder bed conditions for the dose lengths: a) 6 mm; b) 5 mm; c) 4 mm. Results obtained from The Wolfson Centre dosator single shot test-rig. For full explanation refer to the text.

Powder Doctored Mean Weight [mg]								
Lactohale300								
	4 mm dose length			5 mm dose length			6 mm dose length		
	Bed conditions [kg]			Bed conditions [kg]			Bed conditions [kg]		
Gap h	0	0.5	1	0	0.5	1	0	0.5	1
0.15	0.65	0.20	0.14	0.79	0.33	0.03	0.30	0.24	0.18
0.3	0.51	0.15	0.10	0.46	0.09	0.00	0.18	0.27	0.00
0.6	0.05	0.20	0.65	0.00	0.00	0.00	0.05	0.00	0.01
Bimodal Blend								
	4 mm dose length			5 mm dose length			6 mm dose length		
	Bed conditions [kg]			Bed conditions [kg]			Bed conditions [kg]		
Gap h	0	0.5	1	0	0.5	1	0	0.5	1
0.15	4.50	4.48	4.50	2.86	4.48	5.07	1.88	3.33	4.44
0.3	4.98	4.48	5.45	3.43	3.42	5.71	2.15	1.83	4.48
0.6	0.61	3.80	5.25	0.30	0.52	2.35	0.41	0.37	0.08
Relenza								
	4 mm dose length			5 mm dose length			6 mm dose length		
	Bed conditions [kg]			Bed conditions [kg]			Bed conditions [kg]		
Gap h	0	0.5	1	0	0.5	1	0	0.5	1
0.15	5.18	6.00	7.65	4.78	5.89	7.22	4.22	5.34	6.86
0.3	5.73	7.35	7.31	5.21	6.69	6.23	4.87	6.43	6.12
0.6	6.70	7.23	8.19	5.86	7.14	7.58	4.63	6.50	7.34
Lactohale200								
	4 mm dose length			5 mm dose length			6 mm dose length		
	Bed conditions [kg]			Bed conditions [kg]			Bed conditions [kg]		
Gap h	0	0.5	1	0	0.5	1	0	0.5	1
0.15	5.09	5.21	6.79	5.01	4.72	6.30	4.41	4.77	5.53
0.3	5.16	5.82	6.61	5.02	5.38	5.89	4.42	5.56	5.91
0.6	4.32	6.83	6.42	3.98	5.93	5.69	4.27	5.78	5.83

Table 7.5. Powder doctored mean weight variation with bed conditions and gap "h" of the powders used in this research; for 4, 5 and 6 mm dose lengths. Tests undertaken in The Wolfson Centre dosator single shot test-rig.

The weight of powder doctored decreased with the cohesiveness of the powders and increased with the level of powder bed pre-compaction, but seemed to be constant with the variation of the gap "h". The excess of bimodal blend, and allegedly Lactohale300, tended to decrease with the increment of the dose length. Lactohale200 and Relenza powder doctored seemed to be constant with the dose length and also increases with the increment of the gap "h".

This behaviour suggests that the compressibility of the cohesive powders allow the extra filling of the dosator at the end of the stroke, whereas incompressible powders compact the powder bed to higher stresses, being higher the cohesion forces than the tensile strengths in the interface dose/powder bed.

The doctoring stage was included in the tests to obtain the net dose weight avoiding external variables to the ones controlled in the test procedure; otherwise the fill dose weight could probably be affected up to 8 g in some cases, as showed in figure 7.6 for the bimodal blend, Relenza and Lactohale200. This stage also provided valuable information because showed major powder doctored from the less compressible powders (Lactohale200 and Relenza) and contrary case for the compressible powders. This could make to think that the high pressure generated at the end of the stroke in the powder bed (within the gap "h") can push powder into the dosator with compressible powders or protrude doses in incompressible ones (because the dose chamber is already filled).

7.4   Physical observation of the powder behaviour

This section shows some of the behaviours observed in the experimental tests of the dosator test-rig; these behaviours were also seen in dosator production machines, as expressed by the industrial sponsor and the machine manufacturers (MG2, Harro Höfliger and IMA). The observations contributed to the understanding of the process and the identification of situations, triggered by machine settings that also affected the variation of the dose weight.

7.4.1   Compacted powder marks at the bottom of the trough

Figure 7.7 shows compacted powder marks at the bottom of the trough caused by the high pressures generated at the end of the stroke. The adhesion of the compacted powder marks was in agreement to the measurement of this property in chapter 5, section 5.4.3.4 using the "wall flow function" technique; Lactohale300 presented thicker marks than the bimodal blend.

According to table 2.3 in chapter 2, current dosator filling machines can produce up to 250,000 capsules per hour which it means the powder bed is re-filled several times and the dosator might stroke in the same place, or nearby, several times incrementing the thickness of these marks. According to the powder and machine manufacturers this behaviour is often seen with the formation of a layer of compacted powder.
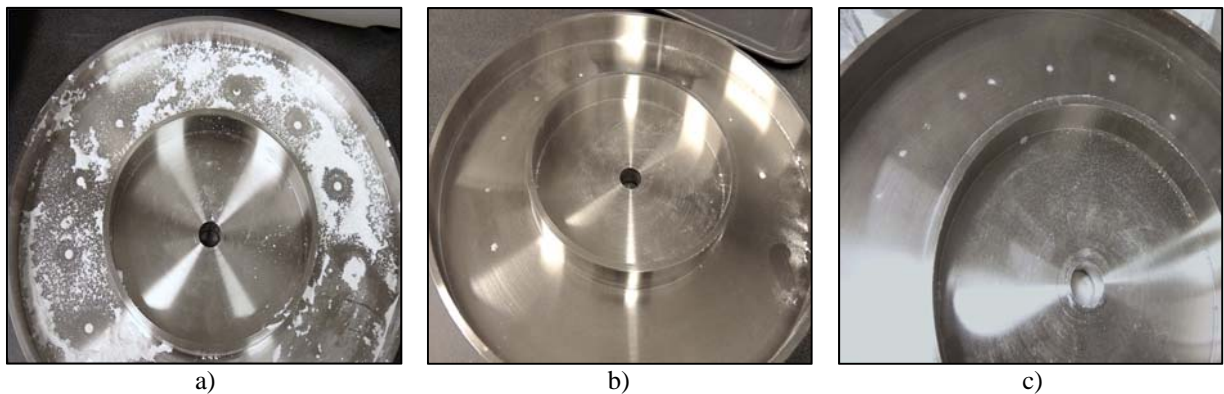
Figure 7.7. Compacted powder marks at the bottom of the trough: a) Lactohale300; b) Lactohale200; c) bimodal blend. Behaviour observed in The Wolfson Centre dosator test-rig. For full explanation refer to the text.

This behaviour is attributed to the adhesion characteristic of the powder and the pressures exerted in the gap "h". The build up of this layer of compacted powder in production lines might result in degradation of the particles after several strokes in the same position and the locally high stress applied; this was not confirmed in this research.

7.4.2   Doses partially filled

Figure 7.8 shows examples of doses that partially filled the chamber due to the presence of cavities on the underside, as a result of powder adhering to the base of the trough during the retraction stroke.
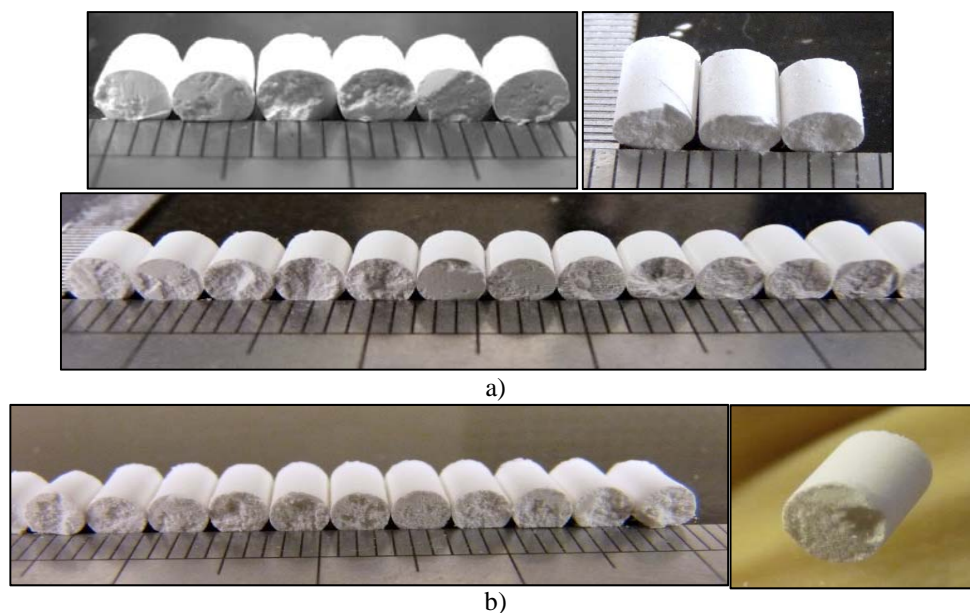
Figure 7.8. Doses partially filled: a) *Lactohale300*; b) Bimodal blend. Doses obtained at The Wolfson Centre dosator single shot test-rig. For full explanation refer to the text.

This behaviour was observed in Lactohale300 and bimodal blend, the cohesive powders used in this research. Consequently, figure 7.9 shows part of the doses left in the powder bed. This behaviour corresponds to the cavities shown in figure 7.8.

This behaviour is attributed to the cohesiveness of the powder and the compression of the powder bed within the gap "h". The powder in the bed is highly compacted making difficult for cohesive powders to overcome tensile stresses in the interface powder bed/dose at the retraction of the dosator. This behaviour could be potentially responsible for the variations in the fill dose weight of cohesive powders in dosators.

a)

b)
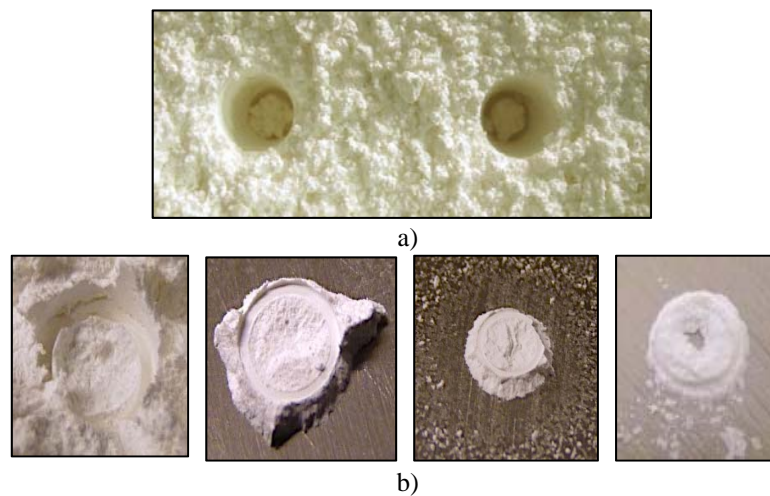
Figure 7.9. Part of the dose added to the bottom of the trough after dosator retraction: a) Relenza; b) Lactohale300. Pictures taken from tests carried out in The Wolfson Centre dosator single shot test-rig. For full explanation refer to the text.

There are some other situations causing doses that are partially filled, as the detachment of a lump from the dose during the doctoring stage; this behaviour is shown in figure 7.10a. The cavities in the dose underside (see figure 7.10b) was one of the common problems observed in cohesive powder in the dosator test-rig.

a)   b)

Figure 7.10. Doses partially filled caused by the doctoring stage: a) lump of powder doctored; b) dose underside cavities inside the dosator. Pictures taken from The Wolfson Centre test-rig. For full explanation refer to the text.

7.4.3   Protruding doses

The opposite behaviour to that described in the previous section (section 7.4.2), it was the occurrence of protruded doses (see figure 7.11). It was observed mainly in easy flowing/incompressible powders.

a)

b)
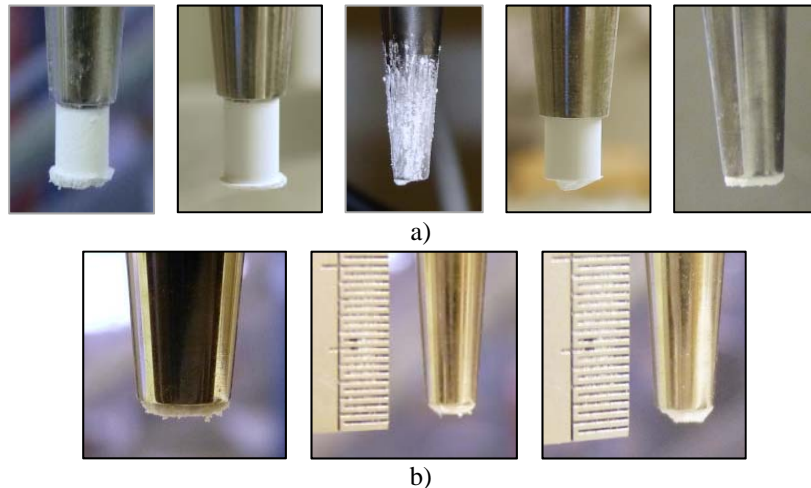
Figure 7.11. Protruded doses: a) Relenza; b) Lactohale200. Pictures taken during test in The Wolfson Centre dosator single shot –test-rig. For full explanation refer to the text.

It is also reflected in the powder bed and figure 7.12 illustrates it in the powder beds of Relenza and Lactohale200.

a)

b)
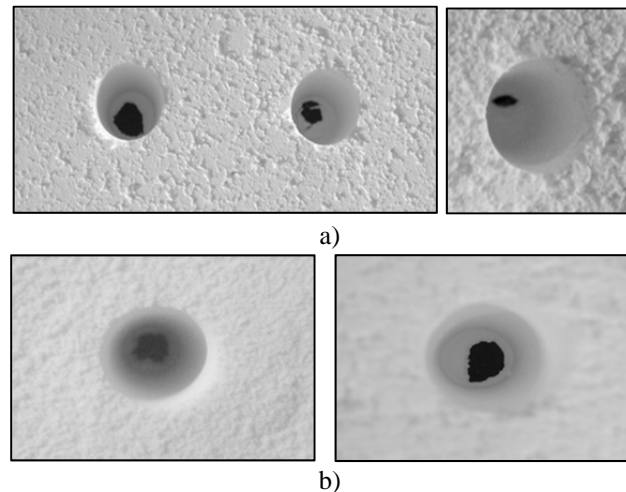
Figure 7.12. Powder removed from the powder bed layer between the trough and the end of the dosator stroke: a) Relenza; b) Lactohale200. For full explanation refer to the text. Pictures taken from The Wolfson Centre dosator single shot test-rig trough.

This behaviour was attributed to the powder incompressibility, low adhesion characteristic of the powder to surfaces and the high stresses generated at the end of the stroke (within the gap "h"). The observations suggest that the dosator chamber at the end the stroke, with

incompressible powders, is fully filled and due to the later causes mentioned the powder tend to adhere to the dosator tip.

7.4.4   Part of the doses adhered to the pin' face

Another situation observed to significantly affect the fill dose weight variation was the powder adhesion to the pin's face after the dose ejection (see figure 7.13). It was a situation controlled in the experimental work of this thesis because dose collection was done manually and the dose was forced to eject; but this is difficult to overcome in production machines. However, as mentioned in section 2.3.4.3 in chapter 2, IMA's dosator capsule filling machines to avoid this problem use a forced extraction feature by slightly sliding the capsule body close to the pin's face[25].
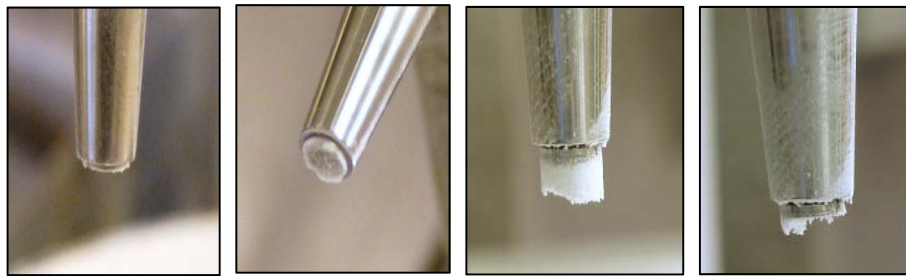
Figure 7.13. Part of the dose adhered to the pin's face after the ejection stage. For full explanation refer to the text. Pictures taken in The Wolfson Centre test-rig.

The amount of the powder added to the pin's face could range from a thin layer of powder to a significant portion of the dose; this behaviour mainly depends on the powders adhesion to surfaces. Podczeck (1999) proposed some metal coatings in tamping pins to reduce powder adhesion and observed the coating of chromium nitride provided significant reduction of the powder adhesion.

7.4.5   Partial or complete dose dropping before the conclusion of the ejection stage

Partial and complete doses were seen dropping before the conclusion of the ejection stage in The Wolfson Centre dosator test-rig (see figure 7.14). This was mainly observed in large

---

[25] According to Pietro Pirera (IMA's Product Manager for Encapsulation).

Lactohale200 and Relenza doses. This behaviour probably occurs in production machines due to deficient ability of the powder to retain lateral stresses, the wall friction, the adhesion characteristic of the powders and the machine jolts.
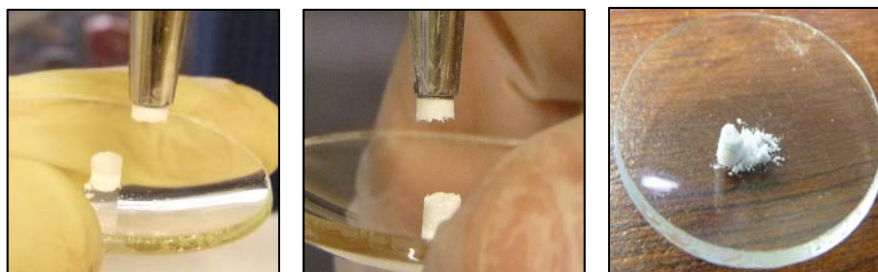
Figure 7.14. Partial doses dropped before the ejection stage in The Wolfson Centre dosator single shot test-rig. For full explanation refer to the text.

In the experimental work in the dosator test-rig probably the later was not the reason of this behaviour; due to the low ejection speed of the dosator pin and the lateral stress retention characteristic, the self-weight might overcome the tensile stresses in the dose. It is likely that the uneven compression across the dose, due to the wall friction, affects the weight balance in the system and contributes to the partial or full dropping of the dose.

7.4.6   Powder build up

As anticipated by the experience of The Wolfson Centre and from the literature reviewed in chapter 3, powder build up behaviour was observed in the tests undertaken in the dosator test-rig.

 Powder build up areas were behind the pin's face (see figure 7.15a) and coating the dosator inner-walls (see figure 7.15b). This behaviour was minimal in The Wolfson Centre test-rig because it performed only 30 dosator strokes per test compared to the order of 1000 strokes in a production machine.

This behaviour was attributed to the adhesion characteristic, "stickiness" of the powders, which causes gradual build up a layer of powder on the inner surfaces. It is difficult to prevent it because pharmaceutical blends are composed by powder with small particles and API's with high surface energies.
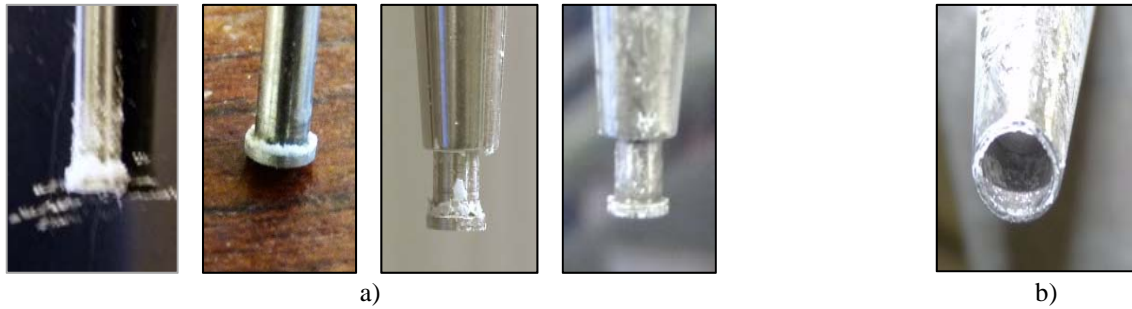
Figure 7.15. Powder build up behaviours: a) powder stored behind the pin's face; b) dosator inner-wall coating. For full explanation refer to the text.

These behaviours in production filling machines can be critical as the powder build up, in either of the situations mentioned, could reduce the size the dosator pin/body clearance eventually causing the dosator pin to jam, thus stopping production until the dosator system is cleaned and re-calibrated. Pin jamming was not observed in the experimental work of this thesis (due to limit number of strokes), but according to the powder/machines manufacturers and the literature reviewed (Jolliffe & Newton 1980), it is one of the common manufacturing problems, especially with powder with cohesive characteristics.

7.4.7   Powder bed state

As mentioned in chapter 4 and the literature reviewed in chapters 3 (Irwin et al. 1970, Woodhead et al. 1982 and Demetry et al 1998), the powder bed stress state is one of the main factors affecting the fill dose weight. Figures 7.16 and 7.17 show some of the powder bed conditions observed in the dosator test-rig.

Figure 7.16 shows voids in the powder bed that might compromise the dose weight. This was observed mainly on Lactohale300, Relenza and bimodal blend beds.

Figure 7.17 shows different powder bed state of the powders used in this thesis. It can be seen that the better the flowability of the powder, the more homogeneous the condition of the powder bed (see figures 7.17b & c). Cohesive powders (see figure 7.17c) showed heterogeneous state of the powder bed. This heterogeneous bed state is more significant in current dosator filling machines due to the deficient powder re-conditioning systems used.
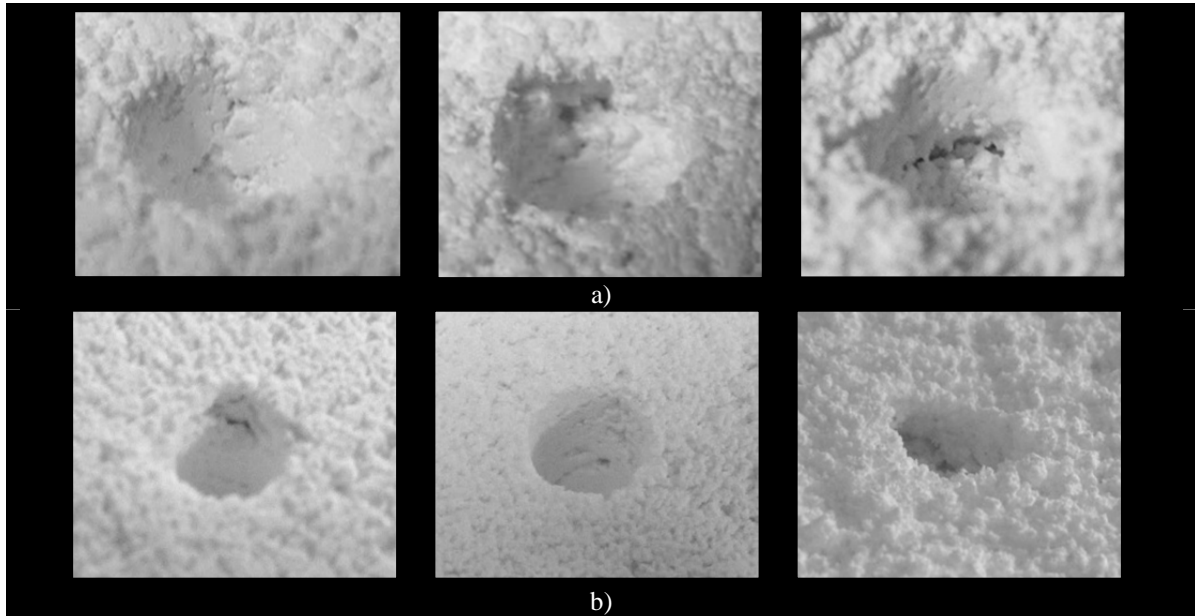
Figure 7.16. Voids in The Wolfson Centre dosator test-rig powder bed in the holes left by the dosator stroke: a) Relenza; b) Lactohale300. For full explanation refer to the text.
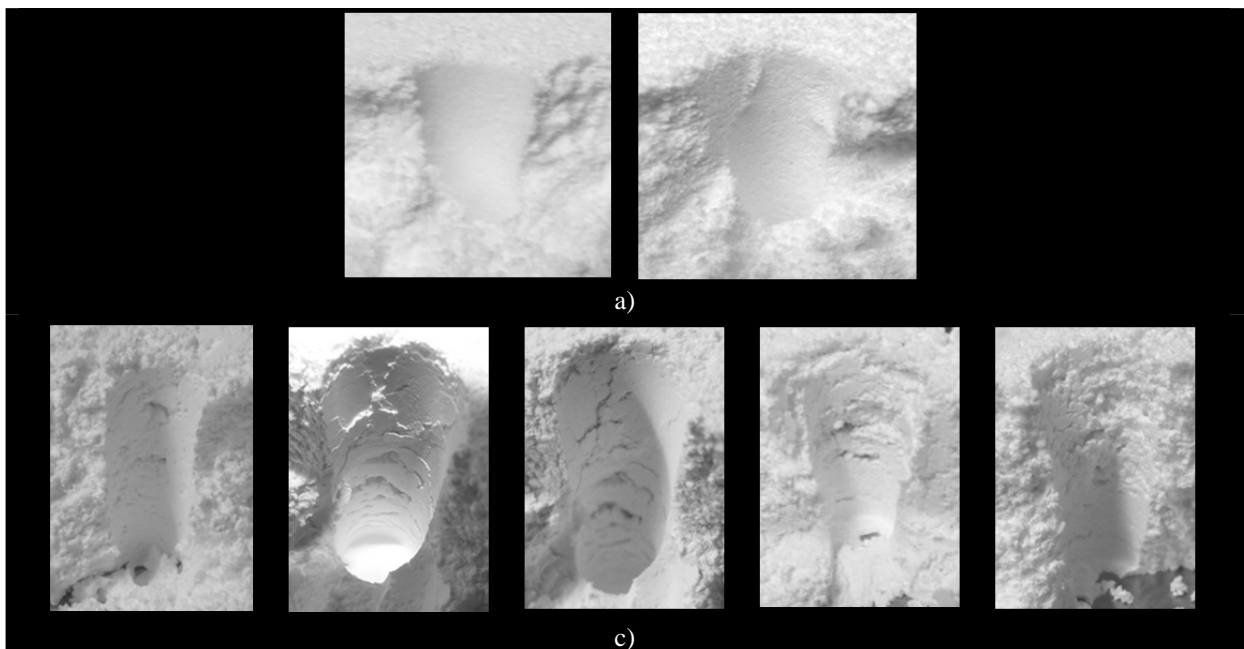
Figure 7.17. Powder bed state after dosator stroke, cross section cut: a) Lactohale200; b) Lactohale300. Tests undertaken in The Wolfson Centres dosator test-rig. For full explanation refer to the text.

7.4.8   Uneven dose density distribution

Figure 7.18 shows the distribution of the dose density observed for Lactohale300 obtained in the dosator test-rig. It can be seen that for the larger dose length this cohesive powder tended

to produce doses that are denser at the bottom, where higher stresses occur. Short doses are visually more homogeneous and compacted than the larger doses. Wall friction and ratio between the dose diameter and length could be the causes of this behaviour.
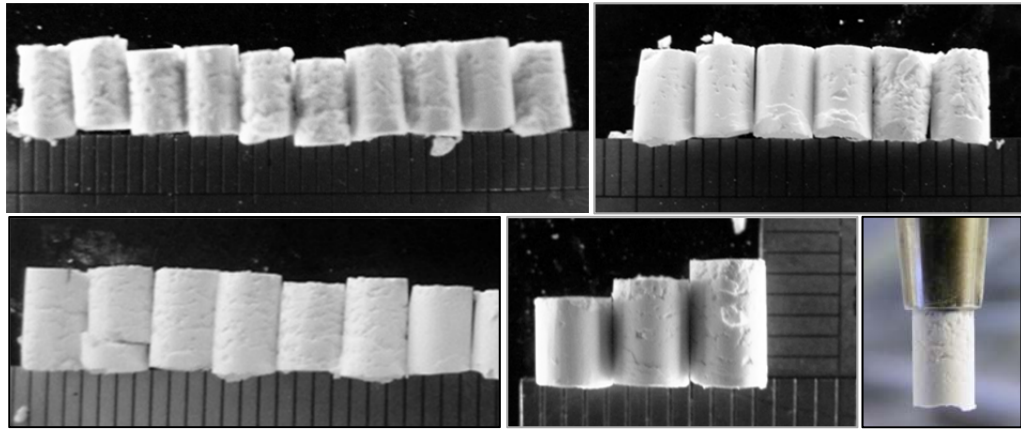
Figure 7.18. Lactohale300 dose density distribution. For full explanation refer to the text.

7.4.9   Perturbed zone in the powder bed

Something that is still unknown about dosator operation is the radius of the perturbed zone around the dosator during its insertion stage; it is a topic that was not found in the literature reviewed in chapter 3. There is currently no design guide for the distance between two dosators in production machines to avoid any problems during the dose procurement due to their proximity. Even though it was not an objective of this research, its existence was noted and it could help further investigations of the powder bed state and its re-conditioning system in current machines.

This thesis considers the greatest disturbance of the bed to occur at the end of the stroke when pressures peak. In the experimental work the powder bed was upturned at the end of the test and figure 7.19 shows the perturbed areas observed at the bottom of the powder bed.

Circular zones of compacted powder were observed around the dosator strokes, evidencing the radius of this altered zone at the end of the stroke. It was visible for the two cohesive powders used in this thesis (Lactohale300 and the bimodal blend). The diameter of this zone of influence was measured and they varied from 8 to 15 mm; the major external diameter of the dosator body used in the tests was 8 mm. It was not observed any pattern of this behaviour correlating the flowability of the powder. Probably the studies of Meyerhof (1951)

and further studies in this application of ultimate bearing capacity can serve as starting point to the study of this zone of influence.

a)

b)
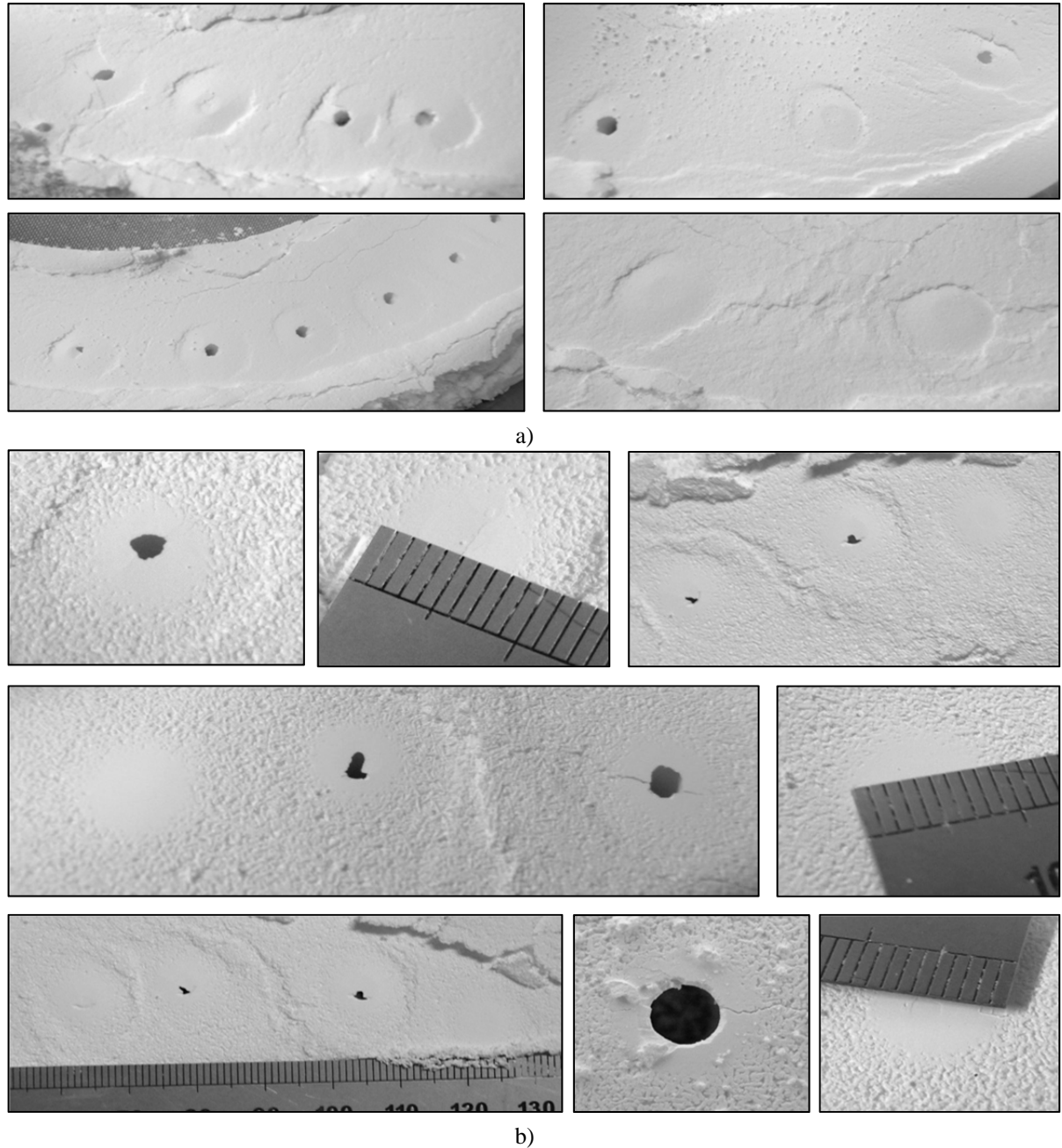
Figure 7.19. Perturbed zone in the powder bed at the end of the dosator stroke in tests carried out in The Wolfson Centre dosator single shot test-rig: a) Lactose bimodal blend; b) *Lactohale300*. For full explanation refer to the text.

7.4.10   Dose compression during the ejection stage

Depending on the cohesiveness of the powder, wall friction effect and the relation between dose diameter and length, the dose can experience extra compaction during the ejection.

Figure 7.20 shows examples of doses obtained in the dosator test-rig. It was evident from the doses made with the two cohesive materials in the 6 mm long cavity, that the actual dose length was less than 6 mm after ejection. Indicating compaction of the dose by the pin during the ejection stage.

a)

b)
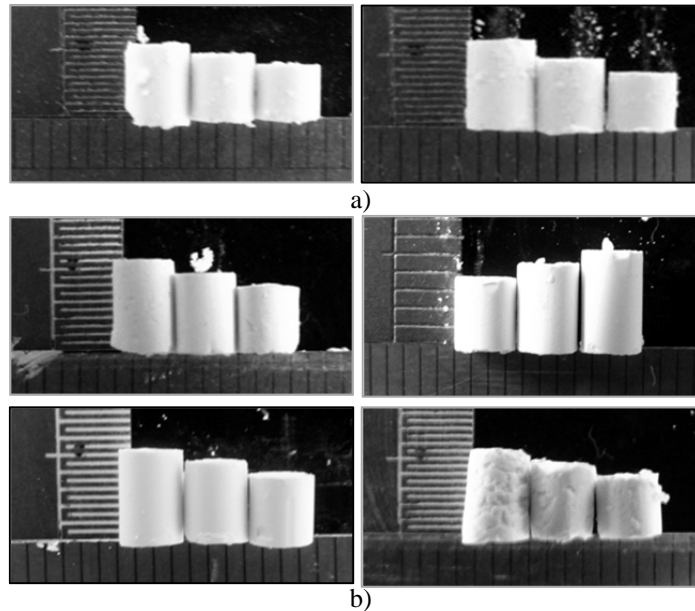
Figure 7.20. Dose length reduction attributed to ejection force: a) Lactose *bimodal blend*; b) *Lactohale300*. Doses with diameter Φ 3.4 mm and 6, 5 and 4 mm dose length obtained in The Wolfson Centre dosator single shot test-rig. For full explanation refer to the text.

7.5   Results and discussion of the effect of the powder bowl lining material in the fill dose weight and dosator maximum filling forces in the operation

In order to study the wall friction effect on the lateral spreading of the powder adjacent to the trough base at the end of the stroke, the lining material of the trough was changed by covering it with fablon plastic film. This is a common material used to cover and protect workbenches.

The test-rig was set at no pre-compaction of the powder bed and critical gap "h" of 0.15 mm to analyse the variation of the doses and the filling/ejection forces. The test was done for all the powders.

Table 7.6 shows the comparison and the percentage variations of the dose results obtained with stainless steel and fablon film trough surfaces for all the powders used in this research. It can be seen that the doses were not affected by changing of the lining material of the trough. If there was a change it was about 2 % that can be attributed to errors in the test.

Mean Dose Weight Results [mg] (0.15 mm gap, 0 PC Bed)									
	4 mm dose length			5 mm dose length			6 mm dose length		
	Trough's surface			Trough's surface			Trough's surface		
Powder	SS	Film	% Var.	SS	Film	% Var.	SS	Film	% Var.
Lactohale200	31.63	31.35	-1	39.25	39.21	-0.1	46.82	46.88	0.1
Relenza	28.35	29.03	2	34.56	34.93	1	40.64	40.73	0.2
Bimodal blend	33.21	33.26	0.2	38.17	38.74	2	41.56	42.07	1
Lactohale300	14.09	14.32	2	15.14	14.32	-5	14.42	14.55	1

Table 7.6. Mean dose weight and variation percentage changing the lining material of the trough; Stainless Steel (SS) and Fablon Film (Film) surfaces were used. The test conditions were 0.15 mm gap "h" and no pre-compaction of the bed (0 PC Bed). For full explanation refer to the text.

Nevertheless, the maximum filling forces increased and it was larger the variation for incompressible powders than for cohesive. Table 7.7 shows the maximum filling force of table 7.6. Only the Lactohale200 showed a variation in comparison with different lining materials.

Maximum Mean Filling Force Results [N] (0.15 mm gap, 0 PC Bed)									
	4 mm dose length			5 mm dose length			6 mm dose length		
	Trough's surface			Trough's surface			Trough's surface		
Powder	SS	Film	% Var.	SS	Film	% Var.	SS	Film	% Var.
Lactohale200	25.07	29.97	20	22.51	27.71	23	21.23	25.22	19
Relenza	14.84	14.98	1	11.35	11.39	0.3	8.47	8.16	-4
Blend	11.34	12.83	13	5.96	6.89	16	4.46	4.77	7
Lactohale300	0.94	1.03	10	0.82	1.03	25	0.67	0.93	39

Table 7.7. Mean maximum dosator filling force and variation percentage changing the lining material of the trough; it was used stainless steel (SS) and Fablon film (Film) surfaces. The test conditions were 0.15 mm gap "h" and no pre-compaction of the bed (0 PC Bed). For full explanation refer to the text.

Table 7.8 shows the corresponding ejection force to table 7.6. There was not significant variation of the ejection force for these tests; only Lactohale200 presented the major variation.

Mean Maximum Ejection Force Results [N] (0.15 mm gap, 0 PC Bed)									
	4 mm dose length			5 mm dose length			6 mm dose length		
	Trough's surface			Trough's surface			Trough's surface		
Powder	SS	Film	% Var.	SS	Film	% Var.	SS	Film	% Var.
Lactohale200	1.98	3.06	55	2.26	3.33	47	2.44	3.39	39
Relenza	2.32	1.64	-29	1.87	1.29	-31	1.25	0.80	-36
Blend	0.64	1.07	67	0.18	0.33	80	0.06	0.08	33
Lactohale300	0.02	0.03	0	0.01	0.01	0	0.00	0.01	0

Table 7.8. Mean maximum dosator ejection force and variation percentage changing the lining material of the trough; it was used stainless steel (SS) and Fablon film (Film) surfaces. The test conditions were 0.15 mm gap "h" and no pre-compaction of the bed (0 PC Bed). For full explanation refer to the text.

In general the changing of the trough's lining material did not have significant effect in the doses and dosator forces. However, it was observed that the adhesion behaviour to the trough was higher in some powders; according to the measurement of the wall friction in chapter 5, section 5.4.3.2, this property increased for all the powders. Figure 7.21 shows the behaviour observed of Lactohale300. There were bigger lumps of compacted powder added to the fablon film.
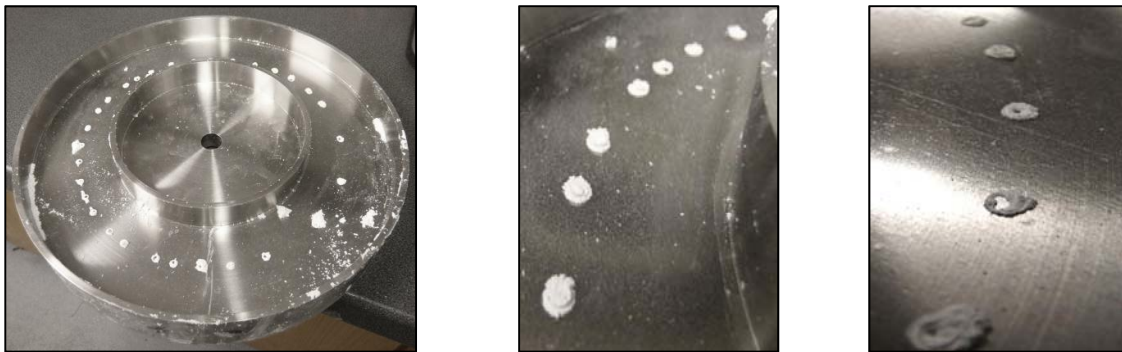
Figure 7.21. Lactohale300 adhesion behaviour to the dosator test-rig trough covered with fablon film. For full explanation refer to the text.

Figure 7.22 shows the Lactohale300 bottom of the dose of the tests covering the trough with fablon film. The appearance of the dose underside in Lactohale300 slightly improved (in comparison to figure 7.8) and there were lesser cavities in the different dose lengths.

Another test performed included a "double shuffle" (explained in section 2.3.4.3, figure 2.24, chapter 2) at the end of the stroke to see the variation in the dose weight. It was only undertaken for the powder that had the greatest dose variation in previous tests, which was Lactohale300. It used the same test procedure as before with the addition of a "double shuffle" at the end of the stroke. Table 7.9 shows the results of the Lactohale300 mean dose weight and variation percentage of the tests with different trough's lining material (fablon film) and "double shuffle".

a)

b)

c)
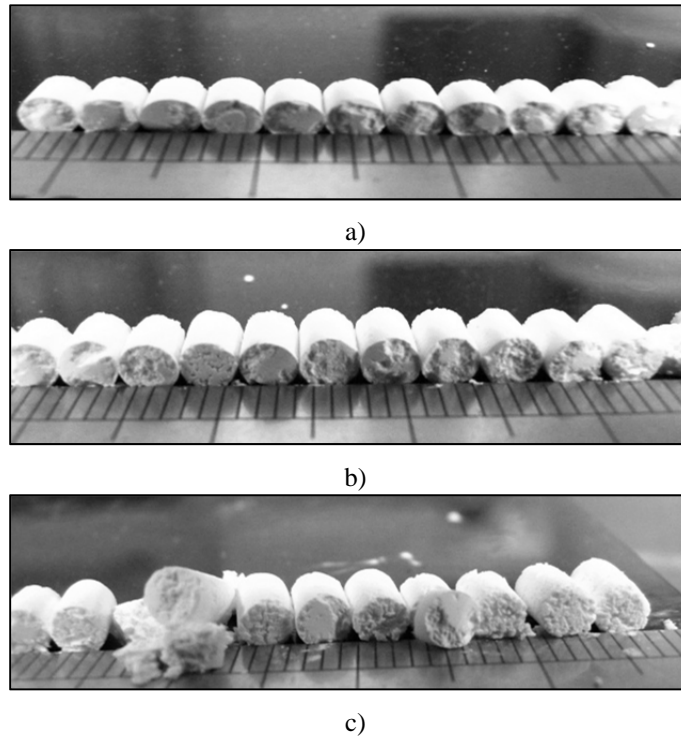
Figure 7.22. Lactohale300 dose underside in the test undertaken covering the trough surface with fablon film: a) 4 mm dose length; b) 5 mm dose length; c) 6 mm dose length. For full explanation refer to the text.

Can be seen significant incr ease of the mean dose weight with the addition of the "double shuffle" (see table 7.9). The 4 mm dose length had approximately 10 % increase whereas the 6 mm dose length had around 15 %.   The 5 mm dose length had a small decrease of approximately 8 %. Some production machines, like Harro Höfliger dosator filling machines, have this feature of "double shuffle" at the end of the stroke that showed in this test increase of the fill dose weight.

Lactohale300 results (0.15 mm gap, 0 PC Bed)														
	4 mm dose length					5 mm dose length					6 mm dose length			
Dose weight	Trough's surface			Double Shuffle	%	Trough's surface			Double shuffle	%	Trough's surface			Double shuffle	%
	SS	Film	%			SS	Film	%			SS	Film	%		
[mg]	14.09	14.32	2	15.62	11	15.14	14.32	-5	16.3	8	14.42	14.55	1	16.66	16

Table 7.9. Lactohale300 mean dose and variation percentage changing the lining material of the trough and doing the double shuffle at the end of the stroke; the test settings were 0.15 mm gap "h" and no pre-compaction of the bed (0 PC Bed). For full explanation refer to the text.

The cavities at the bottom of the dose observed in the previous tests were reduced by performing the "double shuffle" using Lactohale300 (see figures 7.8, 7.22 and 7.23), this

suggested that increases in the fill weight are the result of an improved filling efficiency. Figure 7.23 shows this behaviour for all the dose lengths.
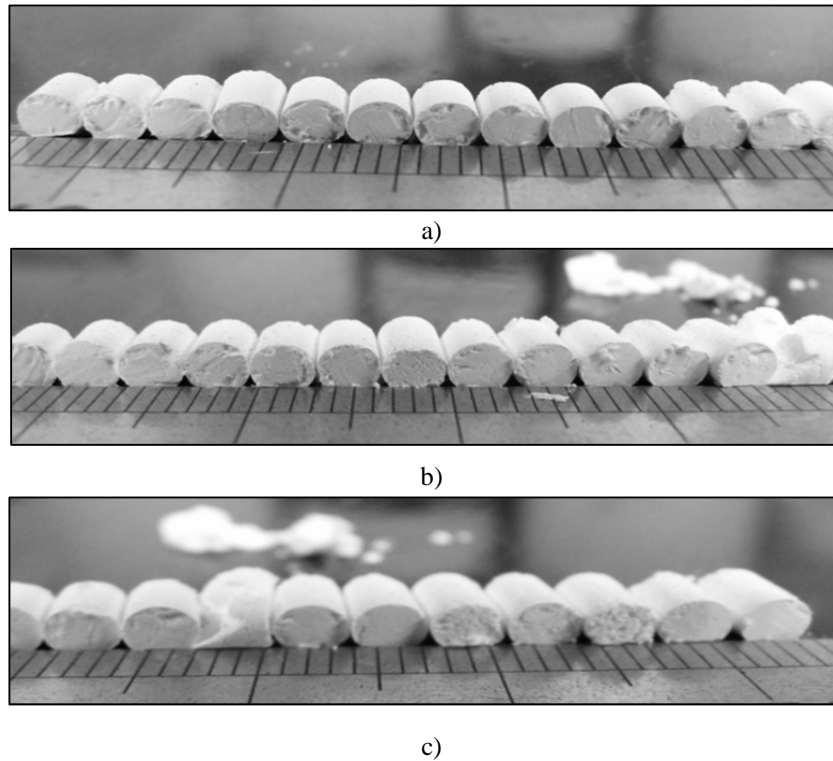
Figure 7.23. Lactohale300 dose underside behaviour during the double shuffle test: a) 4 mm dose length; b) 5 mm dose length; c) 6 mm dose length. For full explanation refer to the text.

7.6   Measurement of the pre-compaction ahead of the dosator

These trials were undertaken to measure the compaction of the powder ahead of the dosator underside and to observe the stress compression behaviour in the powder bed, for purposes explained in chapter 8. To do this the dosator was stroked down into the powder bed (20 mm bed height) with the dosator pin's face and dosator body underside levelled as illustrated in figure 7.24a & b. The plan was to run the test until the pin/body touch the bottom of the trough, but had to be stopped before this point because the force sensors were overloading (15N range). In figure 7.24a is also illustrated the possible forces acting in the system.

Results of these tests for the four powders used in this research are shown in table 7.10 and later in chapter 8, section 8.5.2. Table presents the maximum forces measured by both pin and body sensors and their percentage of the total dosator force. It can be seen that the body forces are significantly lower than the total forces reached in the trials. This suggests that the

powder bed does not exert significant forces onto the dosator body and therefore it can be assumed that forces measured by the body force sensor are the friction effect; as described in chapter 6, section 6.3.
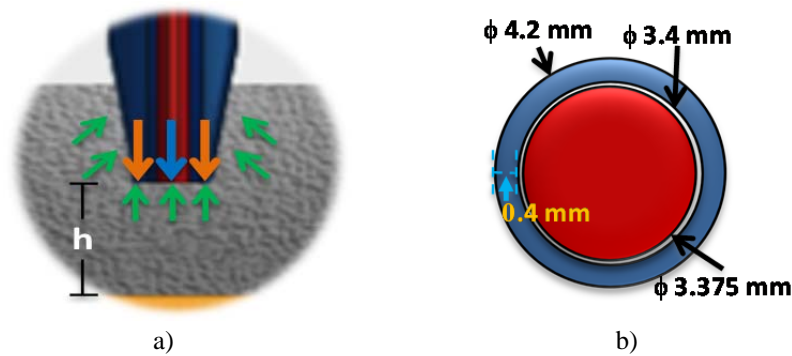
Figure 7.24. Representation of the trials undertaken in the dosator test-rig measuring the compaction ahead of the dosator: a) forces in the system; b) dosator body underside and pin's face dimensions. For full explanation refer to the text.

In addition, it is shown the equivalent gap "h" when *the dosator body force sensor* measured 1 N. It was not possible to figure out what triggered the increase in the body force sensor at approximately 0.25 mm gap "h", remaining in the powder bed when the tests were stopped. It could be either forces against the dosator underside area from the trapped powder in the gap "h" (showed in figure 7.24b) or small friction effect, as the dosator pin assembly was not rigid (explained in chapter 6, section 6.5.3) and there was a small dose (approximately 1 mm) in some cases.

Results Of The Compaction Ahead Of The Dosator (0 mm Dose Length Trials)							
Powder	Maximum Force [N]			Force %		Gap "h" [mm]	
	Pin	Body	Total	Pin	Body	When body force reached 1 N	Min
Lactohale300	15.82 +	3.37 =	19.19	82	18	0.6	0.24
Bimodal blend	14.38 +	1.46 =	15.84	91	9	0.65	0.5
Relenza	15.77 +	3.02 =	18.80	84	16	0.8	0.49
Lactohale200	15.81 +	2.15 =	17.96	88	12	0.77	0.49

Table 7.10. Maximum forces in trials undertaken in the dosator test-rig measuring the compaction ahead of the dosator. For full explanation refer to the text.

Table 7.11 shows the calculated dosator pin and body stresses of the forces presented in table 7.10 in MPa. The dosator pin stresses were calculated with the dosator pin's face area showed in figure 7.24b (red colour). The dosator body stresses were calculated using two areas, the body underside area (blue area in figure 7.24b) and the projected lateral area (see figure 7.24a). These calculations also confirms the assumption made it in section 6.3, chapter

6, that the forces acting against the dosator lateral side can be neglected and what is measured is mainly the wall friction effect in the dose chamber.

Maximum Dosator Stress [MPa]			
Powder	Dosator pin	Dosator body	
	Dosator pin area	Dosator body underside area	Projected dosator body lateral area
Lactohale300	1.77	0.71	0.09
Bimodal blend	1.61	0.31	0.04
Relenza	1.76	0.63	0.08
Lactohale200	1.77	0.45	0.06

Table 7.11. Equivalent stresses of the forces showed in table 7.9. Pin force applied to the dosator pin underside area and for the body force was used the body underside area and body lateral projected area. For full explanation refer to the text.

7.7   Infinite dose test results

To investigate the infinite dose length, a series of tests were undertaken where the dosator body was stroked down into the powder bed, without a pin. This tests where aimed to see the effect of the wall friction in the doses and the conditions of the powder bed. This test does not represent the Janssen effect described in section 2.7.1 in chapter 2, because the amount of powder entering in the dosator is always equivalent to the bed depth and what it was seen was the effect of the wall friction and dose density with the powder bed conditions.
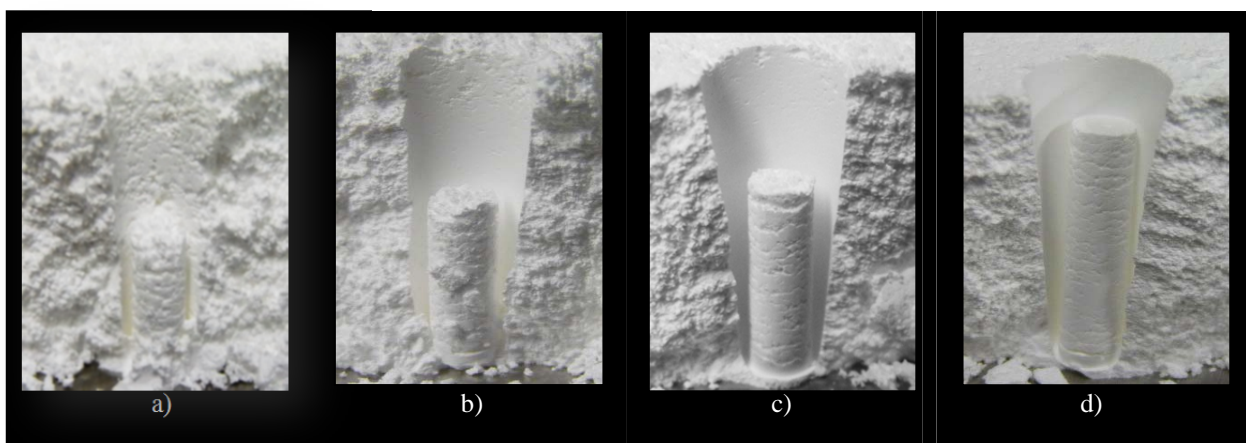
Figure 7.25. Influence of the powder bed conditions of *Lactohale300* in the infinite dose tests. Powder bed cross-section cut of the hole left by the dosator body and powder bed with different pre-compaction conditions: a) no pre-compaction, 0 kg; b) 0.5 kg; c) 1 kg; d) 2 kg load. For full explanation refer to the text.

Figure 7.25 shows an example of the preliminary infinite dose tests behaviour in the dosator test-rig. It can be seen that the dose length increased with the increment of the powder bed conditions and consequently the wall friction was higher. This is another demonstration of the powder bed stated effect in the variations of the fill dose weight.

Table 7.12 shows the maximum filling force measured in infinite dose tests. These results correspond to the tests conditions described in section 7.2.1. The magnitude of the forces were small and it can be seen the augmentation of the forces with the condition in the powder bed and the force decreasing with the increment of the gap "h". The variation of the force was larger in Relenza and the bimodal blend. This can be attributed to the high wall friction of these powders.

Maximum Filling Force [N] Of The Infinite Dose Length Test											
	Lactohale200			Relenza			Bimodal blend			Lactohale300		
	Bed conditions [kg]			Bed conditions [kg]			Bed conditions [kg]			Bed conditions [kg]		
Gap "h"	0	0.5	1	0	0.5	1	0	0.5	1	0	0.5	1
0.15	0.8	1	1.2	1.6	2.6	2.1	1.5	1.6	1.9	0.5	0.6	0.8
0.3	0.1	0.3	0.5	0.6	0.61	0.5	0.4	0.4	0.5	0.1	0.4	0.4
0.6	0.1	0.2	0.3	0.2	0.25	0.3	0.2	0.4	0.4	0.1	0.2	0.3

Table 7.12. Maximum filling force of the infinite dose length tests. For full explanation refer to the text.

These tests demonstrated the low effect of the area of the dosator body underside and outer surface confirming that the wall friction on the (internal) dose cavity wall dominates the body force measurement in the system. Table 7.13 shows the height of the doses in these tests.

Dose Length [mm] Of The Infinite Dose Length Test											
	Lactohale200			Relenza			Bimodal blend			Lactohale300		
	Bed conditions [kg]			Bed conditions [kg]			Bed conditions [kg]			Bed conditions [kg]		
Gap "h"	0	0.5	1	0	0.5	1	0	0.5	1	0	0.5	1
0.15	12	14	14	12	13	15	15	17	17	9	9	12
0.3	11	13	16	12	13	14	15	16	17	8	8	11
0.6	10	12	13	12	12	14	15	16	16	8	11	11

Table 7.13. Dose length of the infinite dose tests. For full explanation refer to the text.

The results show the increase of the dose length with the powder bed conditions and also visually the density and strength of the dose.

Measuring the dose length was inaccurate because the powder bed had be dug and removed carefully to isolate the dose and measure the length. However, it showed a trend of the variation of the fill dose weight. These tests showed the increment of the wall friction, the density and the compaction of the dose in dosator operation due to the powder bed conditions and the dose length limitation.

7.8   Density and voidage properties of the doses

It was compared the density of the doses obtained from the dosator test-rig with the compaction curve model proposed in chapter 5 (refer to the equations in figure 5.18). Figure 7.26 shows the bulk density as function of the maximum filling stresses of the tests in the dosator test-rig and the compaction curve model proposed in chapter 5, section 5.4.4.2 for all the powders used in this research.

Lactohale200 and Relenza showed good consistent dose density from the tests in the dosator test-rig and the tests followed the increment trend. The bimodal blend showed scatter in the density being lower the density of the doses at normal powder bed conditions; as the bed stated changed the density was constant following the same trend. Lactohale300 presented more variability and as the powder bed conditions increased, the density was constant following the same increment trend.

Figure 7.26 also shows the CC model from the Brookfield QTS texture analyser. The CC was in disagreement with the density changes of the doses in the dosator test-rig. This could be attributed to differences in the compaction mechanism in dosator operation and measuring the compaction curve. The mechanism measuring the compaction curve is compressing the powder in a confined space whereas the compaction in dosators is confining powder in a constraining space that is compacted as it is pushed upwards. The disagreement between the density of the doses in the tests and the predicted with CC model is similar for three of the powders used (Relenza, Lactohale200 and bimodal blend). The factor of the difference for these powders is approximately a factor of 0.8; for the most cohesive powder (Lactohale300) the factor varies between 0.5 and 0.7 depending on the condition of the powder bed.

a)

b)

c)

d)
Legend
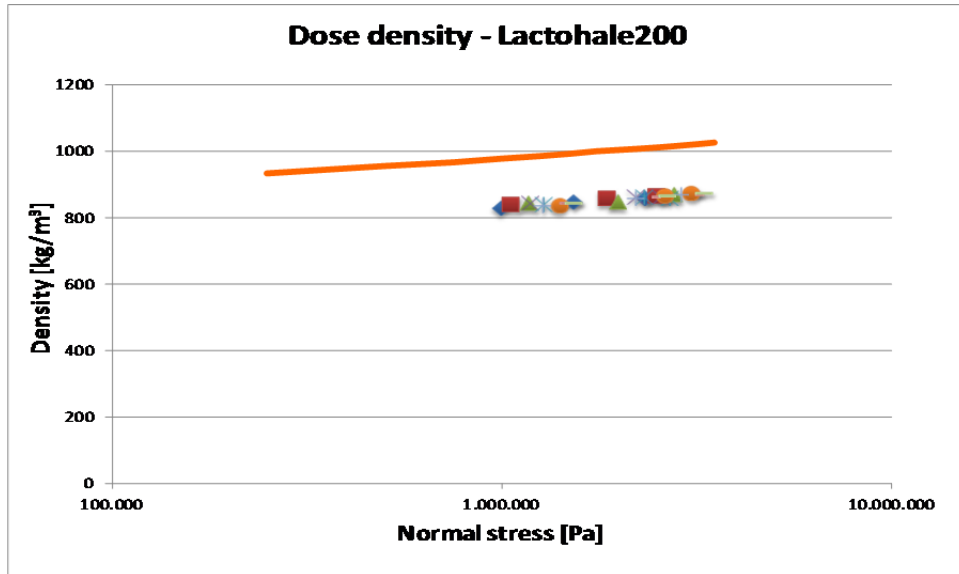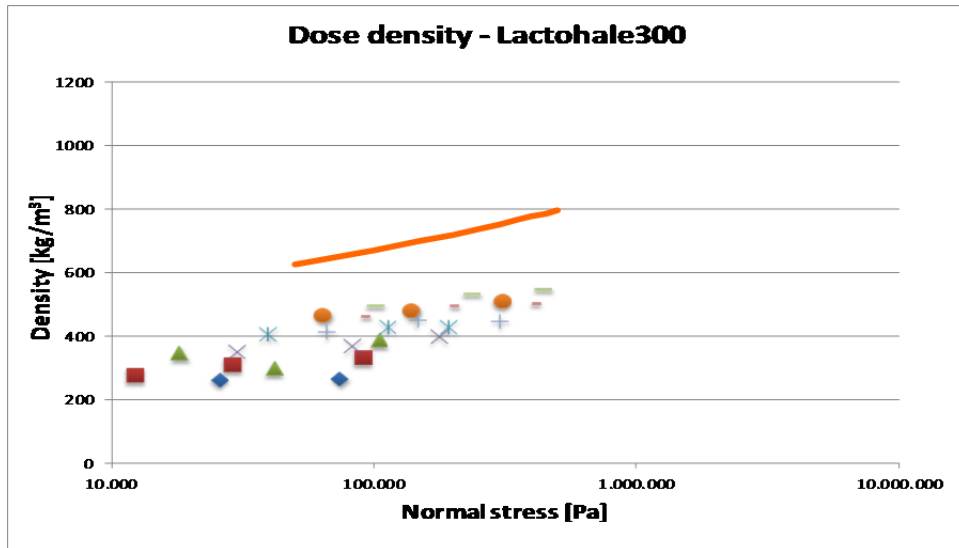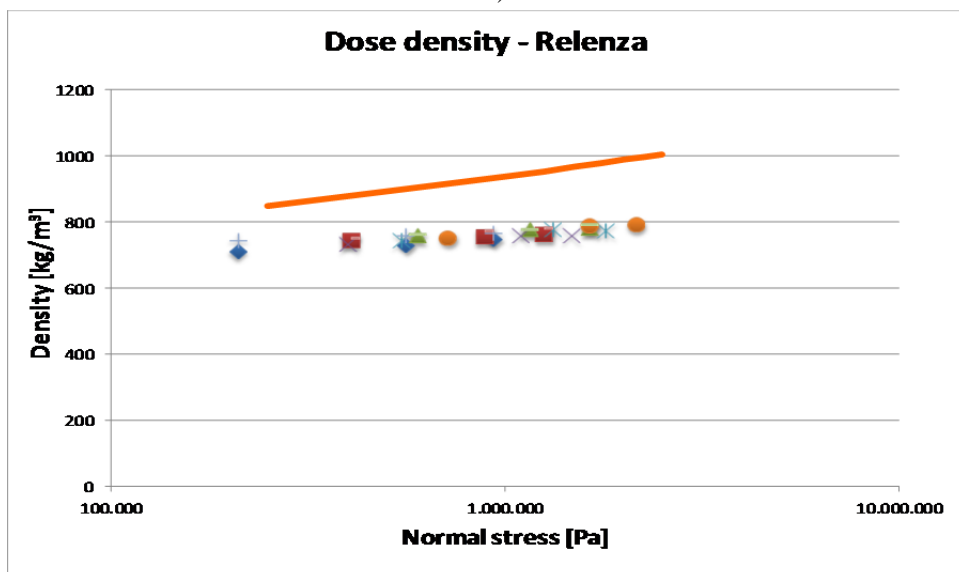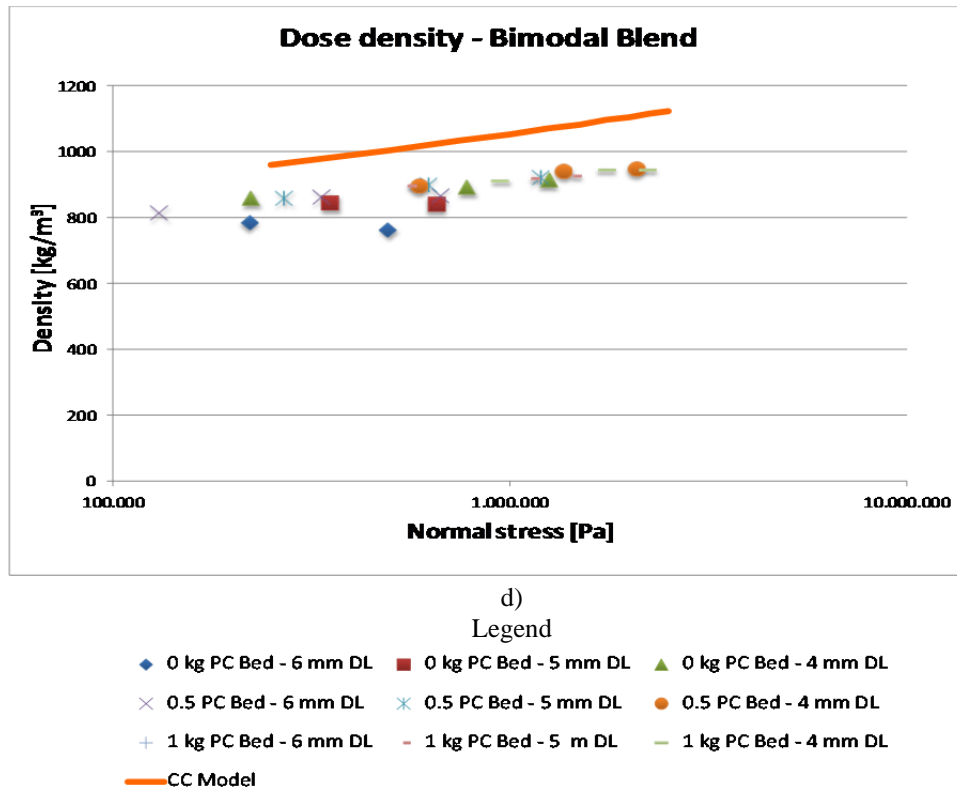
Figure 7.26. Comparison of the compaction curve model and dose density behaviour in The Wolfson Centre dosator single shot test-rig: a) Lactohale200; b) Lactohale300; c) Relenza; d) Bimodal blend. For full explanation refer to the text.

With the particle density values calculated in chapter 5, the void fraction (ε) can be calculated of the doses obtained from the dosator test-rig for all the powders used in this thesis. The void fraction can provide an overview of the particle packing in the doses and therefore know about the permeation presented in the tests. It does not show the impact of the powder permeability in the variation of the dose weight; it shows how it was the permeation in the test and what it was the final particle packing to figure out the voids in the doses.

Figure 7.27 shows the void factions (ε) of all the powders used in this research, as a function of the dose lengths in the different bed states measured in the dosator test-rig. The different colours (blue, green and red series) in figure 7.27 represent the level of pre-compaction of the powder bed (1, 0.5 and 0 respectively). Each colour has different shades that correspond to the variations of the gap "h".   It is also shown the initial voids fraction in the powder bed before the dose was obtained.

177
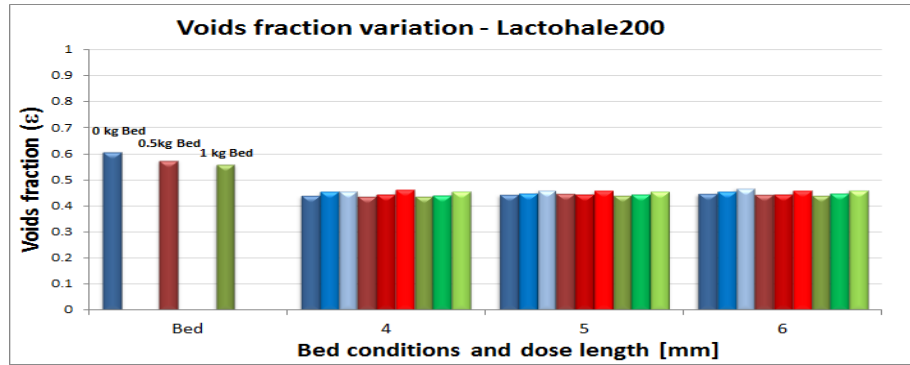
a)

b)

c)

d)

Legend

- 0 kg PC Bed - 0.15 mm gap   0 kg PC Bed - 0.3 mm gap   0 kg PC Bed - 0.6 mm gap
- 0.5 kg PC Bed - 0.15 mm gap   0.5 kg PC Bed - 0.3 mm gap   0.5 kg PC Bed - 0.6 mm gap
- 1 kg PC Bed - 0.15 mm gap   1 kg PC Bed - 0.3 mm gap   1 kg PC Bed - 0.6 mm gap

Figure 7.27. Voids fraction (ε) comparison between the powder bed conditions and the doses obtained from The Wolfson Centre dosator single shot test-rig: a) Lactohale200; b) Lactohale300; c) Relenza; d) Bimodal blend. For full explanation refer to the text.

The Lactohale300 bed showed higher void fractions than the rest of the powders, the opposite case was for Lactohale200 bed having the smallest void fractions and the two blend beds were in the middle with similar void fraction values.

Analysing the void fractions in the doses, the powders were ranked in order of lessening void fraction, from loose to tight packing, as namely: Lactohale300, Relenza, Lactohale200 and the bimodal blend. This ranking was not expected and the powders showed different behaviour to the values predicted from the compaction curve in table 5.7 and figure 5.24 in chapter 5. The difference is due to the discrepancy between the compaction curve and dose densities as shown in figure 7.26.

There were small differences between the packing of the Lactohale200, Relenza and the bimodal blend doses which indicated that the particles were very close to each other and there were small voids where the gas can permeate. In contrast, Lactoahele300 doses have significant voids between the particles that would ease the passage of the air. This could be consequence of the heterogeneity of the density observed in the Lactohale300 doses.

Figure 7.28 shows the reduction percentage of the doses voids fraction with respect to the powder bed conditions. The largest reduction was seen in the bimodal blend doses and the smallest variation in the Lactohale300; Relenza and Lactohale200 had similar variation. The doses obtained from normal powder bed conditions presented large reductions in all the powders except for the Lactohale300. As the powder bed pre-conditioning conditions increased the reduction of voids fraction was of lesser in the dose lengths.

It can be seen a general trend of reduction of the voids fraction with the increment of the powder bed conditions and also with the decreasing of the gap "h". Lactohale300 and the bimodal blend had greater voids fraction variation with the increase of the pre-compaction in the bed; the other two powders showed small variation with the powder bed conditioning.

The data suggested that the incompressible powders had low variations of the void fraction with the pre-conditioning of the powder bed and bimodal blend; powders with cohesive behaviour had greater reductions in the void fraction. Lactohale300 showed an expected behaviour; it showed lesser reduction of the voids fraction and small voids fraction in the doses. May be the cohesiveness of the powder and the small particle size, agglomerates the particles leaving voids in the doses.

a)

b)

c)

d)

Legend

Figure 7.28. Voids fraction (ε) variation percentage between the powder bed conditions and the doses obtained from The Wolfson Centre dosator single shot test-rig: a) Lactohale200; b) Lactohale300; c) Relenza; d) Bimodal blend. For full explanation refer to the text.

The voids fraction of the pre-conditioned beds can simulate particle packing in the doses and powder bed states in current dosator process. The packing behaviour not only can be important to the permeation characteristic of the powder, it can also affect the flow properties and consequently compromise the filling dose weight.

7.9 Summary

The results of the tests undertaken in the dosator single shot test-rig presented valuable information of the dosator process and the factors affecting the variability of the dose length.

The novel design of The Wolfson Centre dosator single shot test-rig allowed the measuring of the body and pin forces in dosator filling systems and provided valuable information to the understanding of the dosator operation.

Cohesive powders showed low repeatability of the dose results. This was attributed to the cohesiveness and compressibility of the powders, and the issues in the interface dose underside/powder bed at the end of the stroke (described in section 7.4).

Doctoring stage in the dosator test-rig results provided valuable information to see the adhesion trend of the powders to the bottom of the trough and the importance of the doctoring stage in dosator filling machines in production lines, especially for incompressible powders.

It was seen that small changes of the gap "h" have a great impact in the dose weights, powder doctored, filling/ejection forces and triggers other situations that affect the variation of the fill dose weight (due to the compression in this distance and the powder flow behaviour).

The data obtained in the dosator single shot test-rig suggested that incompressible powders presented lower variation of the doses in the different conditions tested; therefore it is ideally to dosage them to avoid variations caused by the flow properties and machines settings. However, there is more powder to be doctored that can affect the variability of the dose weight and also the powder flow properties can compromise the dose retention when transferring the dose to the ejection stage.

The behaviour observed in the experimental data of the dosator test-rig can be correlated to the powder flow characterisation. Table 7.14 shows the ranking of the powders according to

the different test settings in the dosator test-rig; it is also included the powder ranking for some flow properties presented in table 5.8 in chapter 5. The powders were ranked between 1 to 4, being 1 the highest value of critical property and 4 the lowest powder with this parameter or property; it is indicated in front of the property/variation.

Ranking Comparison Of Powder Flow Characterisation And The Results From The Dosator Test-Rig					
Powder\ Property-Variations	Lactohale300	Bimodal blend	Relenza	Lactohale200	Parameter
Flow function	1	2	3	4	1 cohesive 4 free flowing
Wall friction	1	2-3	2-3	4	1 highest 4 lowest
Compressibility	1	2	3	4	1 most compressible 4 incompressible
Cohesion	1	2	3	4	1 highest 4 lowest
Adhesion to surfaces	1	3	2	4	1 highest 4 lowest
Dose variation with gap "h"	1	2	3-4	3-4	
Dose variation with bed conditions	1	2	3-4	3-4	
Powder doctored	4	3	1-2	1-2	
Maximum filling force	4	3	2	1	1 highest 4 lowest
Filling force variation with gap "h"	4	3	2	1	
Filling force variation with bed conditions	4	2	3	1	
Maximum ejection force	4	3	1-2	1–2	

Table 7.14. Ranking comparison between the powders flow properties and the results from The Wolfson Centre dosator single shot test-rig. For full explanation refer to the text

It can be seen form table 7.14 that the filling behaviour in dosator operation can be correlated with the powder flow properties. The measurement of these properties can explain the dose weight and filling/ejection forces variations. The characterisation of the flow properties in conjunction with the test-rig tests provided a complete panorama of the dose obtaining and valuable information to understand the filling, compression and ejection of the doses in dosator filling systems.

There are other factors affecting the fill dose weight not studied in this thesis and they are discussed in the appendix 7.

The factors affecting the data obtained in The Wolfson Centre dosator test-rig are described in the appendix 7.

This chapter shows critical machine factors that compromise the fill dose weight such as the clearance of the dosator to the trough at the end of the stroke and the powder bed conditions. It was also identified in section 7.4 other situations triggered by the variation of the gap "h" that also affect the fill dose weight.

The experience with the dosator test-rig enriched the project and provided a better understanding of the dosator operation.

With all the knowledge gained in the experimental work of this research was possible to propose a phenomenological explanation of the process and also model the stress and predict dose weights in dosator operation; this is explained in chapter 8.

Chapter 8

Dosator Model

8.1. Introduction

This chapter presents a dosator model for the filling and discharge of powders based on a phenomenological approach to explain the dosator operation. It also presents the key tools and the background surrounding the development of the model.

The approach and model were supported by the identified factors affecting the process and the tests, observations and data analysis from The Wolfson Centre single shot dosator test-rig (described in chapters 4, 5 and 7) and dosator demonstrator (described in section 8.2).

This chapter is structured as follows. Tests undertaken with a transparent model to visualise the powder flow in the dosator are presented in section 8.2. A phenomenological overview of the different stages of the model is presented in section 8.3 to introduce the model presented in section 8.4. After a comparison of the model predictions with the actual dosator behaviour measured in the single shot test rig are presented in section 8.5 and a summary of chapter is presented in section 8.6.

8.2.   Dosator demonstrator

One of the tools used in this research to understand the dosator process was the dosator demonstrator (see figure 8.1a). A transparent acrylic box and half dosator model were manufactured in plastic using a rapid prototype machine. The dosator body was manufactured in yellow plastic and the dosator pin in a contrasting green plastic. The powder bed had layers of Relenza and black dyed Relenza powder to differentiate the situations in the demonstrator. Relenza was chosen because after the dying and drying process applied to the powder, it did not show at visual inspection any agglomeration behaviour, as observed with other powders.

Figure 8.1 shows the behaviour observed in the demonstrator captured using a burst shooting setting on the digital Panasonic FZ-28 camera.

After carefully preparing the layered powder bed (see figure 8.1a), the dosator was pushed down manually to fill the pre-fixed dose chamber in the dosator guided by two acrylic blocks. Within approximately a quarter of the dosator stroke, the dosator cavity was filled (see figure 8.1b). It can be seen that the stroke of the dosator is affecting a small radial area around the dosator in the powder bed and also pre-compacting a couple of powder layers ahead of the dosator tip. As the dosator continued descending (see figure 8.1c) more powder entered the dose chamber and the pre-compaction in the powder bed remains limited to a couple layers approximately 1 diameters depth below the dosator.
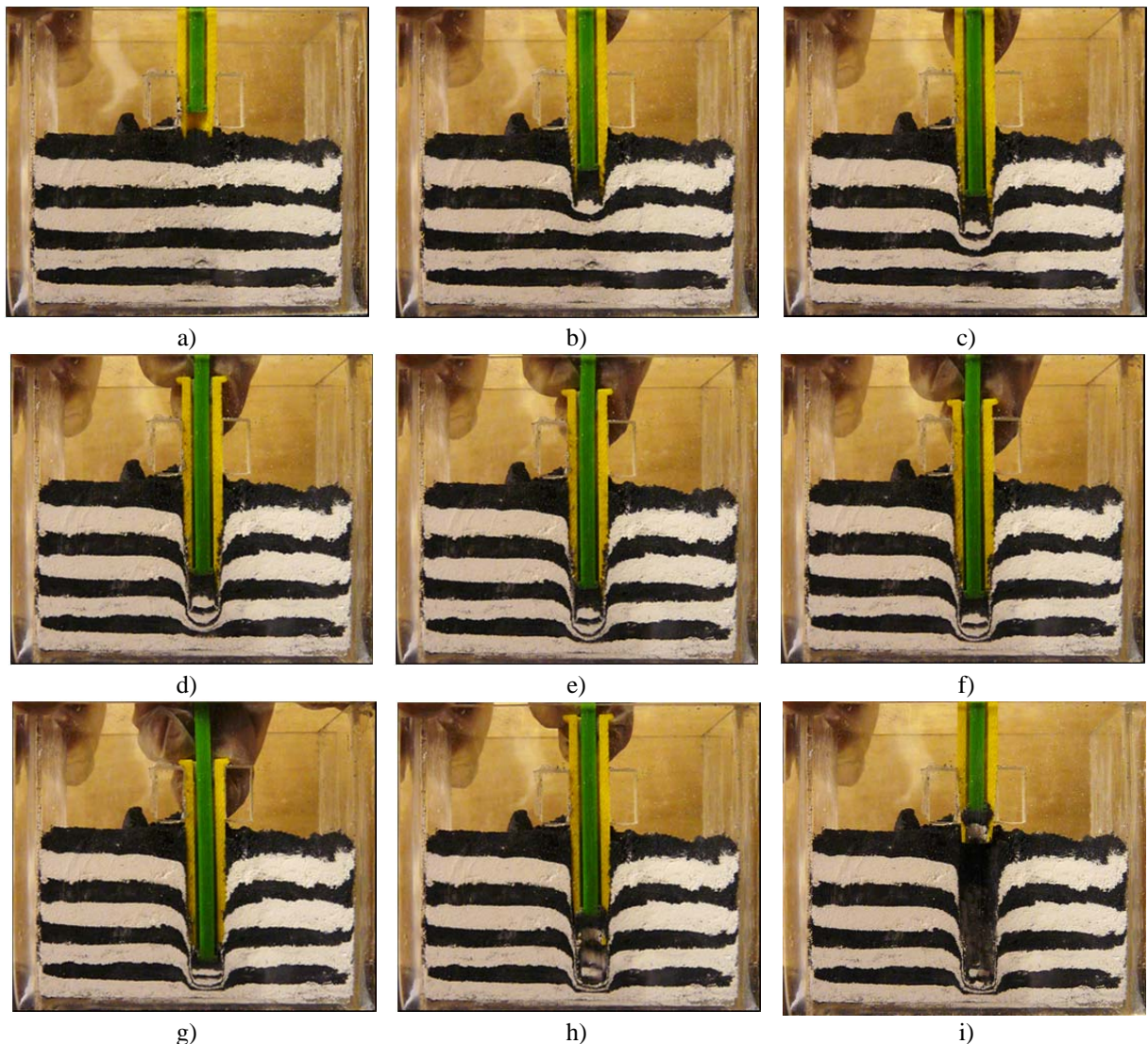
Figure 8.1. Different stages of the dosator demonstrator. For full explanation refer to the text.

The dosator stroke continued in figure 8.1d and the dose appears to reach a stable state and there is no more powder is entering the dose chamber. Inspection of the first layer (black) that entered the chamber appears to have retained its initial height. Also the compaction ahead of the dosator appears to have a more defined cone than in figure 8.1c. As the dosator descended further approaching the bottom of the trough (figure 8.1e) the dose seemed to remain the same and the compaction in the powder bed increased. As the gap "h" was reduced further to rupture the cone ahead of the dosator see figure 8.1f), powder was forced to enter into the dosator cavity and the first layer to enter the dosator (black) was significantly compacted. Figure 8.1g shows the end of the stroke where more powder was pushed into the dose cavity compressing the dose. The perturbed zone in the powder bed seemed to remain constant during the stroke; with no significant radial migration of powder but the powder ahead of the dosator was highly compacted. Figure 8.1h shows the ejection stage where tensile strength of the dose was lower than the wall adhesion to the base of the trough as a part of the dose was left in the bed. The heterogeneous state of the powder bed after the dosator retraction can be seen in figure 8.1e; this state is supposed to be removed in current machines by the bed reconditioning system, but this does not reach down to the base of the trough. The consequence of this is that there is layer of compacted powder at the bottom of the trough that gains strength over time from repeated strikes of the dosator.

It could be seen in the dosator demonstrator that the spreading of the powder in the powder bed in the dosator operation is similar to the spreading stress distribution proposed by Meyerhof (1951) (showed in figure 2.39 in chapter 2).

The process illustration in the demonstrator was affected by the:

- friction effects from the artificial presence of the transparent section wall, which would increase the compaction forces,
- manually operation of the dosator which reduces consistency and
- deflection of the dosator tip from section wall at the end of the stroke, which reduced compaction (presences of powder between dosator section wall and transparent end wall can be seen in figs 8.1d, e, f & g.

However, the dosator demonstrator provided a better understanding of where the compaction/flow was occurring through the different stages of the process which

complemented the experimental results of the single shot dosator test-rig and was used to improve the model proposed in this thesis.

8.3.   Phenomenological approach of the dosator operation

This section explains the phenomenological approach proposed in this thesis to explain the compression mechanism, the stress distribution and dose weights obtained during dosator operation. I.e. understanding was guided by investigations with an experimental dosator to determine the interactions between the bulk flow properties and the machine settings as presented previously in chapter 7 and flow observation from the dosator demonstrator tool presented in previously in section 8.2. It was important to unify the knowledge and concepts learned in this research about dosator operation in order to propose a suitable model for predicting the dose weight obtained in this filling system.

For modelling purposes the dosator operation is divided into key five stages described below, namely the:

- Filling of the dose chamber (to point of spreading),

- Formation of compacted cone ahead of dosator and bed spreading,

- Compaction of the powder ahead of the dose,

- Rupture of the cone as trough base is approached,

- Dose ejection.

8.3.1. Filling of the dose chamber stage

In this stage the dosator is inserted into the powder bed and the dosator descends at constant speed. Even though the bed is in active state (as described in chapter 4, section 4.3.1) the powder is loose and it is assumed that there is no pre-compaction of the bed ahead of the dosator at this stage. The powder bed is divided in slices of constant height "T" (see figure

8.2a) that will be compacted as they enter into the dosator. Initially the thickness of the slice as it enters the dosator is equal to the stroke.
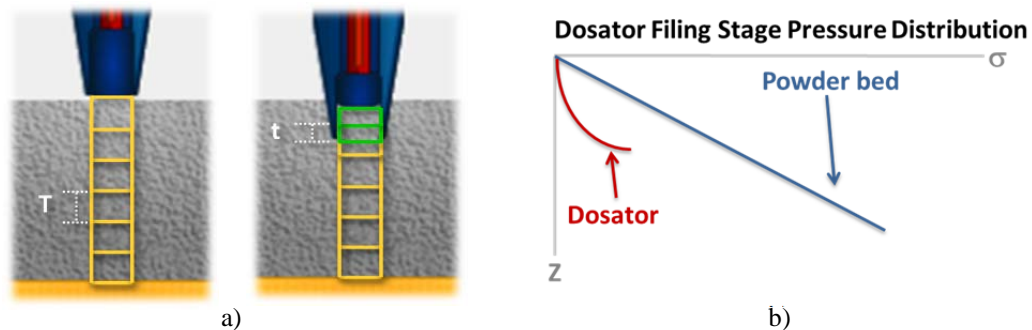
Figure 8.2. Filling of the dose chamber stage: schematic filling; b) stress distribution in this stage. For full explanation refer to the text.

Due to the presence of friction between the powder slices and the dosator wall the slices are compressed. To account for this the thickness of the slice changes to a value "t" (see figure 8.2a), the reduction of the slice thickness can be determined from the Janssen effect by calculating the stress distribution of each slice (treating the slice as incompressible) and then correcting the thickness by reference to the measured compaction curve (presented in chapter 5 section 5.4.4). Thus all the slices inside the dosator will have different height (thinnest at the tip) as the shear stress varies with the length.

The stress distribution of the system (figure 8.2b) shows the exponential increase in the stress in the dosator due to the effect of the wall friction, which will eventually exceed the hydrostatic increase in stress in the powder bed. The point where this occurs limits the filling of the dose cavity, as the stress in the dosator is equal to the stress in the bed. Therefore for further displacement will cause powder spread ahead of the dosator rather than compact into the dose cavity.

It is uncertain the proportion of powder ahead of the dosator tip that enters to the dose chamber and the proportion that spreads laterally (radially) in the cavity filling stage. In this thesis it is assumed that all the powder in the bed enters the dose chamber until it is filled, or the ultimate dose length is reached. Note that there is a possible condition of the infinite dose length (as measured in chapter 7, section 7.7) where the force required to push material into the cavity becomes infinite due to exponential increase. However this is not a real problem because the length to diameter ratio at which this occurs (assuming typical, wall friction and

stress ratio values) was of the order of 2 to 5, significantly greater than the ratios (1 to 1.5) typically used in industrial dosators.

8.3.2. Cavity filled and formation of the compacted powder cone stage

In this stage the dosator with a filled cavity continues stroking down and the powder is compressed exerting forces against the dosator pin. The lateral normal stresses in the dosator increase with the uniaxial compression and the presence of wall friction results in an increase in the wall shear stress that compacts the dose in the cavity. The dosator cavity is filled to a certain dose densification state.

At this stage, the lateral stresses in the dosator are equal or higher than the stresses in the powder bed (see figure 8.3a & b). These stress conditions in the system prevent the powder in the bed from entering the dosator cavity (only greater vertical stresses in the powder bed would force powder entering into the dosator). As the dosator continues stroking down the material spreads laterally around the dosator and only a small proportion is compressed into the cavity.
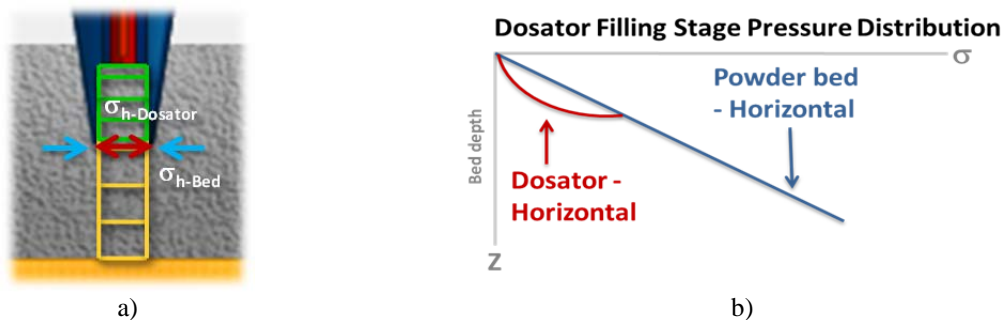
Figure 8.3. Cavity filled stage: a) cavity filled; b) stress distribution in the stage. For full explanation refer to the text.

During this spreading process a formation of a cone of compacted powder ahead of the dosator underside is assumed (see figure 8.4a). This assumption was made according to the observations in the dosator demonstrator, observation in the experimental work of this research, powder mechanics theory (Schulze 2008) and the application of ultimate bearing capacity described in chapter 2, section 2.7.2 (Prandtl 1923, Terzaghi 1943, Meyerhof 1951, 1974, Meyerhof & Chaplin 1952, Marshal 1966, Mandel & Salecon 1972, Pfeifle & Das 1979 and Das 2009).
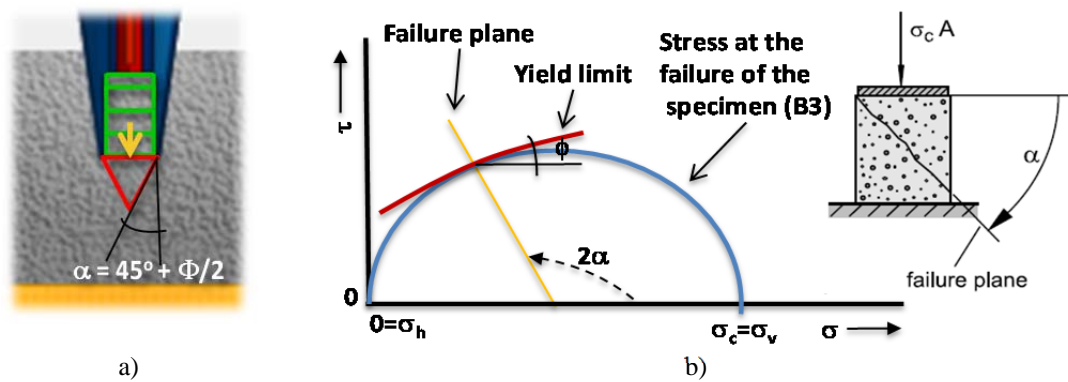
Figure 8.4. Formation of compacted powder cone: a) cone dimensions; b) Powder failure plane in the Mohr's circle and the uniaxial compression test, re-printed from Schulze (2008, p. 41).

The cone is assumed to form an angle "α" to the plane of the major principal consolidation stress (see figure 8.4b) ahead of the tip. The angle $\alpha = 45^o + \phi/2$ is the direction of the failure plane as defined in the theory of powder (Schulze 2008, p. 41) and soil mechanics (Terzaghi 1943, p. 20, 21 and Das 2009, p. 12), where the angle "ϕ" gives the gradient of the failure locus measured in the flow function test. Figure 8.4b also shows the stress failure circle "B3" illustrated previously in figure 2.33 in chapter 2; it is also shown the angle "α" in the failure plane analogy in the uniaxial compression test.

Compacted Powder Cone's Height Ahead of the Dosator Underside				
Powder	Max. angle of failure plane ϕ [°]	Half max. angle of failure plane ϕ [°]	Cone's angle α [°]	Cone's height [mm]
Relenza	32	16.0	61	1.9
Lactohale200	33	16.5	61.5	1.8
Lactohale300	29	14.5	59.5	2.0
Bimodal blend	31	15.5	60.5	1.9
Average	31.3	15.6	60.6	1.9

Table 8.1. Height of the compacted powder cone, from the angle "α=45+ϕ/2" and angle of the failure locus "ϕ" measured in the flow function test in the Brookfield PFT. For full explanation refer to the text.

Table 8.1 shows the maximum failure locus angle "ϕ", the angle of slip plane from the major principal plane "α" and the calculated cone's height for all the powders used in this research. The maximum failure plane angle was obtained from the flow function measurement in the PFT (described in chapter 5, section 5.4.1).

The calculated angle "α" in table 8.1 showed an average of 60° for all the powders used in this research. The measured maximum angle of the failure locus was approximately 30° in all

the powders.   Therefore the cone's height was approximately 2 mm for the dosator dimensions[26] used in this thesis.

Figure 8.5 shows some examples of ejected doses that exhibited a conical tip, which might be the remains of the tip formed ahead of the dose during the pre-compaction stage (see fig 8.1c, d & e).   Alternatively this could just be a tensile failure surface resulting when sample is retracted from the bed. These behaviours where mainly observed in doses at 0.6 mm gap "h" where there are lower stresses in the powder bed at the end of the stroke, where cone suffers less deformation (as trough base is approached) and is therefore better preserved.

Figure 8.5. Possible cone formation behaviour observed in The Wolfson Centre dosator single shot test-rig. For full explanation refer to the text.

8.3.3.   Compaction ahead of the dosator underside stage

The next stage in the operation is the remainder of the dosator stroke travelling with the dose chamber filled and the cone of compacted powder ahead (see figure 8.6a).   The cone is assumed to push the powder in the bed aside.   However as the stress level increases with depth, it is assumed that this slight increase will compress further material into the dose.
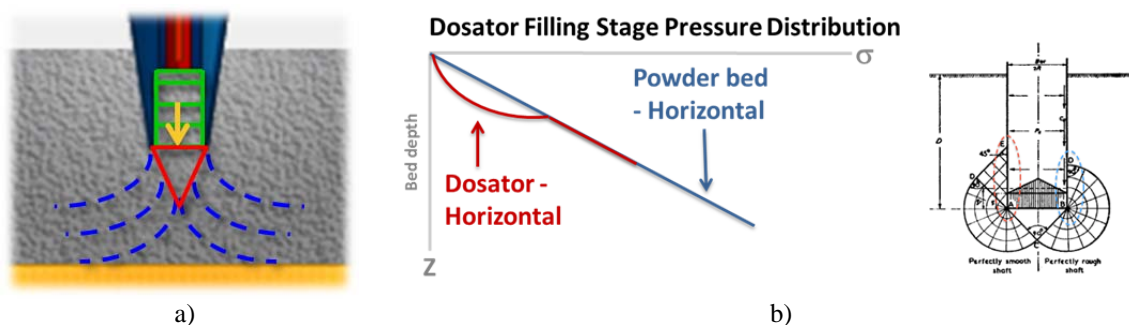
Figure 8.6. Compaction and spreading ahead of the dosator underside stage: a) schematic sketch of the stage; b) stress distribution in the stage and possible spreading behaviour (figure re-printed from Meyerhof 1951, p. 312). For full explanation refer to the text.

---

[26]Dosator diameter used in 3.4 mm

The powder spreading in the bed might present the stress distribution behaviour proposed by Meyerhof (1951) in this stage of the dosator operation. Similar patterns were observed in the dosator demonstrator (see figure 8.1).

Figure 8.6b shows the stress distribution of the bed and dosator in this stage. It is assumed the linear increment of the dosator stresses with the bed depth as the lateral stresses are balanced indicating the spreading of the powder aside. The spreading of the powder is unknown and it was not investigated by this thesis.

8.3.4. Cone rupture and end of the stroke stage

This stage starts when the tip of the compacted powder cone ahead of the dosator contacts the base of the trough, i.e. gap "h" is approximately 1.9 mm (see table 8.1); it is assumed that the stresses in the system starts increasing rapidly.

Figure 8.7a shows the instance where the cone touches the bottom of the trough. The conditions in the system change because the cone cannot push powder aside and the spreading in the bed becomes difficult as the powder in the bed could be sheared against the trough's surface at high stresses and the stresses ahead of the dosator reflected back. Therefore the vertical stresses in the dosator start increasing rapidly. The mechanism for the compaction, as illustrated by Meyerhof and Chaplin (1952) (see figure 8.7c bottom), is as follows: for a large clearance gap a radial feeder zone emanating from the cone which causes lifting of the powder. The conditions in the filling stage of the dosator become critical when the gap "h" at the end of the stroke is much smaller than the cone's height; this situation provokes the rupture of the cone increasing the stresses in the system (see figure 8.7b). As the clearance gap narrows, further horizontal feeder zones are set up between the dose tip and the trough base. The stress field is dictated by the magnitude of the friction at the boundaries, weak wall "slip at wall" or rough wall were powder adheres to the surface. This forces the lateral migration of powder (against the wall friction at the base of the trough), pushes powder from the bed/cone inside the dose chamber, highly compresses the bed ahead of the dosator and forces the entrance of powder into the dosator.

Figure 8.7c shows the stress distribution of this stage and also the stress distribution proposed by Meyerhof and Chaplin (1952) that suit the compaction ahead of the dosator for case of the rupture of the cone.
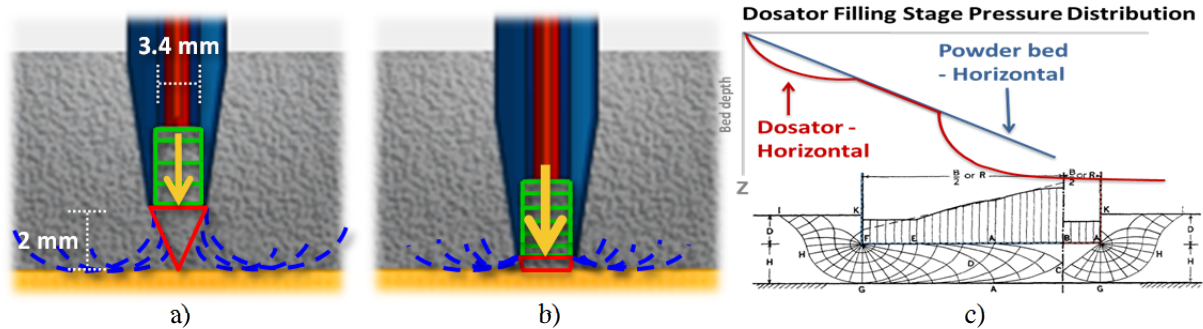
Figure 8.7. Cone rupture and end of stroke stage: a) cone before the rupture; b) end of the dosator stroke and cone rupture; c) stress distribution in this stage (figure in the bottom right hand side re-printed from Meyerhof & Chaplin 1952, p. 24). For full explanation refer to the text.

To illustrate the above effects, figure 8.8 shows the gradient of the pin force increase as function of the height of the dosator (Δdosator filling force/Δpenetration of the dosator) tip above the trough base measured in the dosator test-rig. The above tests were undertaken at four dose lengths of: 0 (no dose length, pin's face and body underside levelled), 4, 5 and 6 mm for all the powders used in this research. The tests at 0 mm dose length were mentioned in chapter 7, section 7.6. The red line illustrates the estimated height at which the cone ahead of the dosator contacts the base of the trough to initiate a ramp up in the vertical force. Lactohale200, Relenza and bimodal blend showed increases in the force gradient at a gap "h" of approximately 2 mm. Lactohale300 at 0 mm dose length showed the same behaviour as the other powders, but the other length conditions showed variations in the gradient at a gap "by the h" of approximately 1 mm.

The majority of the experimental tests were in good agreement with the assumption that the rapid increase of the stresses in the dosator occurred at a bed depth equivalent to the height of the cone, except for the doses of the cohesive powder, *Lactohale 300*.

At this final stage of the dose obtaining, the dose weight depends mainly on the gap "h" at the end of the stroke.
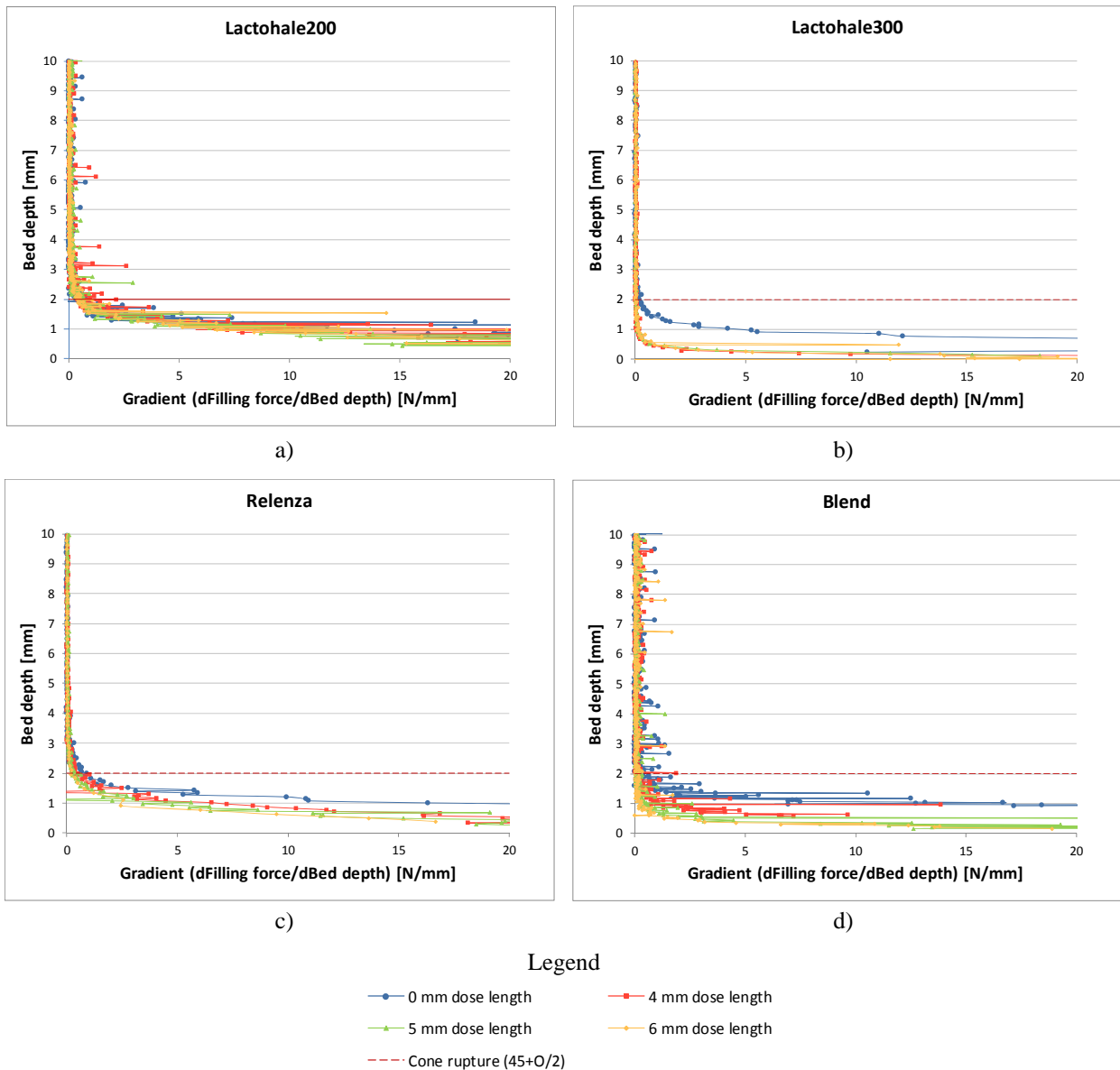
Figure 8.8. Dosator force gradient variation with the bed depth at different dose lengths: a) Lactohale200; b) Lactohale300; c) Relenza; d) Bimodal blend. For full explanation refer to the text.

8.3.5. Dose ejection stage

The dosator is retrieved from the powder bed and the dose is ejected (see figure 8.10) into the receptacle packing presentation overcoming the wall friction influenced by the retention of the lateral stresses of the powder. For long dose lengths where there is poor uniformity of the dose density, the ejection can cause compaction at the top of the resulting in final doses that are below the target length.

Figure 8.9 shows the typical stress distribution observed in the dosator single shot test-rig at the ejection stage. The shape varies with the flowability of the powder but the trend is the same.
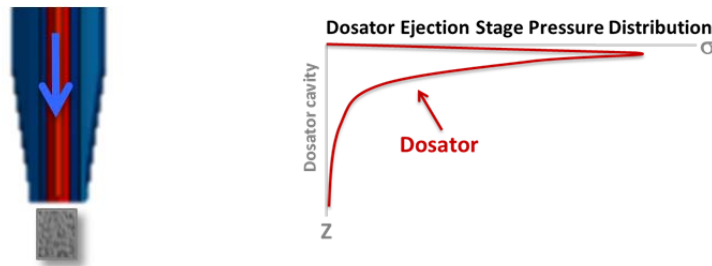
Figure 8.9. Ejection stage of the phenomenological approach of this thesis. For full explanation refer to the text.

8.4.   Dosator model

This section presents the dosator model proposed as a result of the understanding of the dosator operation gained through this research. It is an analytical Excel based model that models that predicts the pressures in the dosator during the stroke, taking into the account the powder flow properties. Figure 8.10 shows the general inputs and outputs of the proposed model.
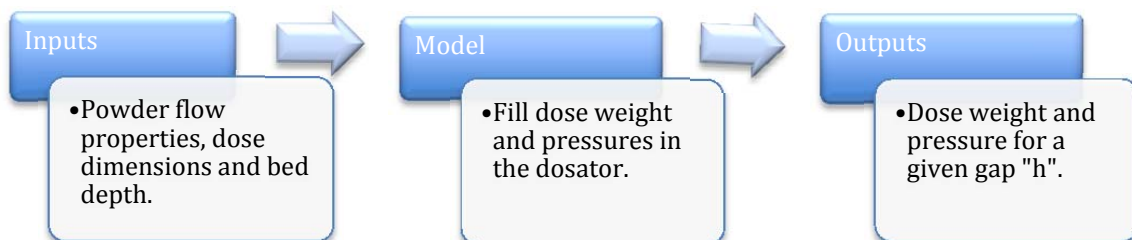
Figure 8.10. Inputs and outputs of the dosator model

The dose dimensions and machine settings inputs of the model are namely: dose length and diameter, the gap "h" and bed depth in [m]. The flow properties included are a compaction curve function, poured bulk density and compaction curve constants, the stress ratio K, the wall friction angle ϕ_w, the gradient of the failure locus ϕ, the retained stress and a function for pre-compaction ahead of the dosator at the end of the stroke for zero dose length.

8.4.1. Concept model

At the beginning of the project, the following factors were identified as affecting dosator operation: the compression of the material during the process, flowability of the powder, wall friction, stress ratio and geometry of the dosator. With these parameters the initial excel based, mathematical and numerical models were developed, for the dosator filling and discharge stages with the method of differential slices by Janssen (Arnold, McLean & Roberts 1982, p. 1.7 and Schulze 2008, p. 259) illustrated in chapter 2, section 2.7.1 and chapter 4, section 4.3.   Subsequent identification of the significance of the gap "h", powder bed conditions and lateral retained stress on the dose fill weight enriched the understanding of the system but significantly complicated the modelling of stresses.

Combining particle/powder flow properties and machine settings factors made it difficult to solve mathematically or numerically the problem using the first versions of the model. For this reason it was decided to develop an analytical solution to take into the account the influence of the gap "h" empirically, by measuring the pre-compaction ahead of the dosator in the test rig (for zero dose length) and fitting the force distribution curves in MatLab, as presented in section 8.4.2.   However before arriving at this solution a range of options measuring/ predicting the pre-compaction ahead of the dosator were trialled as discussed in section 8.4.2.1.
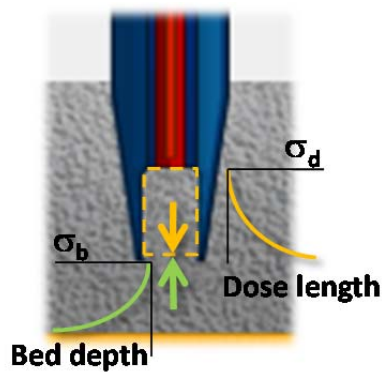
Figure 8.11. Dosator model principle. For full explanation refer to the text
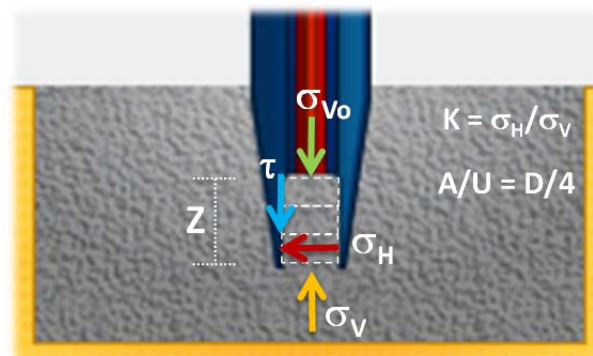
Figure 8.12. Janssen effect application applied to dosator systems. For full explanation refer to the text.

The general concept is to model the stresses inside the dosator based on the measured pre-compaction behaviour in the powder bed (see figure 8.11) ahead of the dosator. Measurements of the pre-compaction of the bed ahead of the dosator (described in chapter 7, section 7.6 and results presented in section 8.4.2) showed that the stress distribution inside the

dosator is equivalent to the stress distribution of the pre-compaction ahead of the dosator shifted by the compressibility of the dose.

The Janssen model (see figure 8.12) was then applied to model the stresses inside the dosator. It is assumed that σ_v in the dosator stress distribution is dictated by σ_v of the pre-compaction profile ahead of the dosator tip. The stress is then calculated decreasing with the length in dose cavity.

The different stages of the model are presented below.

8.4.2. Calibration and stress distribution of the powder bed compression stage

This is the first stage of the model where the compaction ahead of the dosator is measured to calibrate the model and calculate the stress distribution inside the dosator.
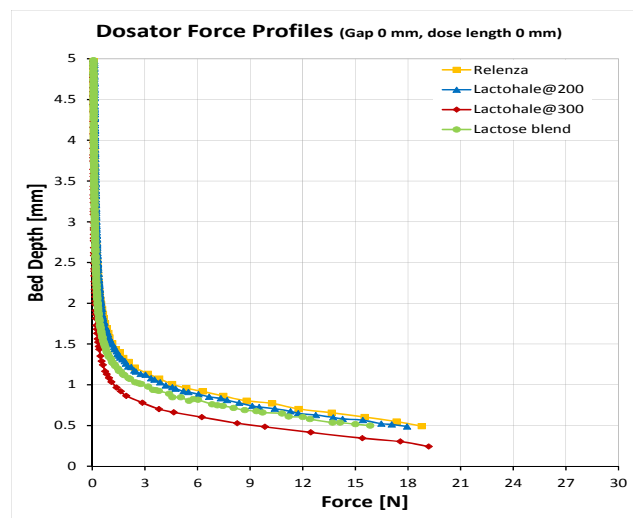
Figure 8.13. Dosator force (pin + body force) profiles at 0 mm gap "h" and dose length for all the powders used in this thesis. For full explanation refer to the text.

The pre-compaction behaviour ahead of the dosator was measured in the dosator test-rig (see figure 8.13) for all the powders used in this research. Low speed stroke trials, approximately 0.2 mm/s with no dose length[27] and gap "h" (described in chapter 7, section 7.6), showed the compaction behaviour of the powder head of the dosator underside. The stroke in these tests finished either when touching the bottom of the trough, no gap "h", or reaching the maximum range of either the dosator pin or body force load cells (16 N).

---

[27] Dosator pin's face and dosator body underside levelled.

The low speed tests allowed the measurement of a greater range of forces at the end of the stroke. Figure 8.13 shows the results of these tests with the four main powders used in this research; in all the cases the tests were stopped just prior to over ranging of the force sensors. The curves had similar shapes and the profiles were lower with the cohesiveness of the powder.
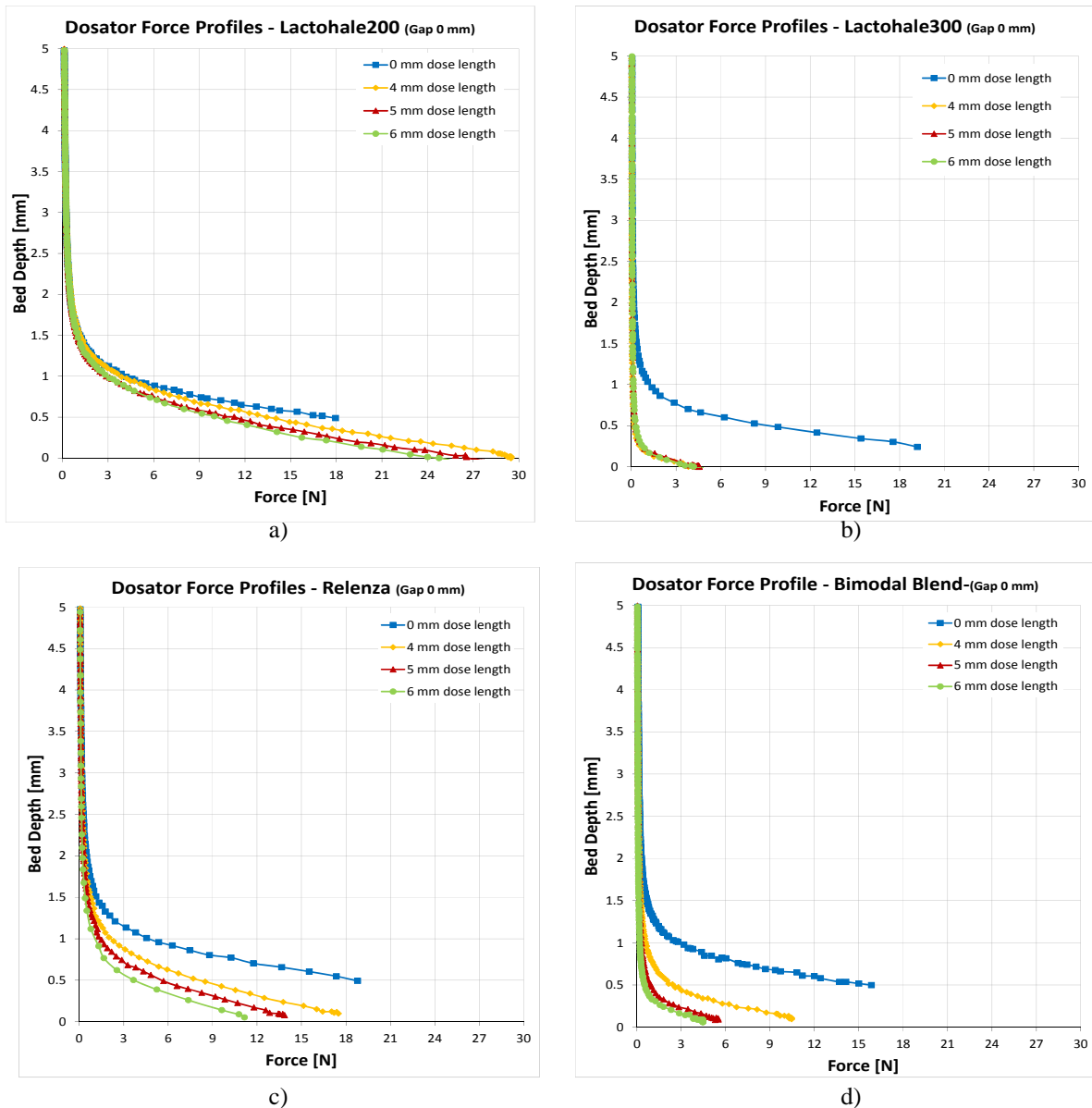
Figure 8.14. Dosator force (pin + body force) profiles at different dose lengths: a) Lactohale200; b) Lactohale300; c) Relenza; d) lactose bimodal blend. For full explanation refer to the text.

The force calculated in these tests, is transmitted to the dose and the dose stress distribution vary with the dose lengths. As mentioned in chapter 7, there could be a small error in the measurements because the fibre-glass rod attached to the dosator pin was deformed elastically

and small doses, up to 1 mm length, were obtained in some tests due to the high pressures at the end of the stroke.

Figure 8.14 shows the force profiles for all the powders used in this research over the range of dose lengths tested (0, 4, 5 and 6 mm). The Lactohale300 and the bimodal blend, the most compressible and cohesive powders, showed similar force distributions in long dose lengths. Lactohale200 force profiles showed small variations with the dose lengths due to its incompressibility and Relenza showed constant variation in the profiles with the increment of the dose length.

These profiles were measured at 0 mm gap "h" because the only difference of the profiles at different gap "h" was the magnitude of the stress where the test stopped.

In general for a given powder, the pre-compaction ahead of the dosator curve (0 mm dose length) was shifted down as the dose length increased in most of the cases (according to figure 8.14). This suggests that the stress distribution in the dosator could be calculated by shifting the pre-compaction ahead of the dosator with the compressibility of the powder.

8.4.2.1. Alternate approaches for measuring/predicting the pre-compaction ahead of the dosator

Although the powder pre-compaction ahead of the dosator in the model can be experimentally measured for each material using the single shot dosator test rig, this is not a very satisfactory long term solution. Therefore a range of alternative options for measuring/predicting this were:

- To model analytically using the soil bearing capacity equations of Meyerhof & Chaplin (1952) based on measured flow properties that were found in the literature.

- To modify the Meyerhof & Chaplin (1952) analytic equations to better fit the experimental data.

- To identify a simpler more universally accessible characterisation test that captures the pre-compaction characteristics of different

Meyerhof & Chaplin (1952) proposed the equations [2.9] and [2.10] in chapter 2 (showed again below) to calculate the vertical bearing capacity of foundations in cohesive soils within a shallow rocky base.

$$\sigma_z = \frac{2mc(R-r)}{H} + A \qquad\qquad [2.9]$$

$$A = \left[\frac{sin^{-1}m}{m} + \sqrt{(1-m^2)}\right] c \qquad\qquad [2.10]$$

As described in chapter 2 and showed in figure 2.40 (in section 2.7.2, chapter 2), σ_z is vertical stress in the system, $m = \tan(\varphi)$, "φ" is the angle of internal friction of the material, "c" is the cohesion of the material, "R" is the radius/width of the footing, "H" the gap between the footing base and the rough base, "r" a radial position within the radius/width and "φ" is the measurement of the angle of the internal friction (probably because it was assumed rough surface at the base and flow is caused by the internal friction of the powder). These equations, in the context of the dosator operation, are function of the bed depth/gap "h" ("H" in equation [2.9]), powder cohesion and angle of wall friction (as the surface of the powder bowl in dosator operation is smooth).

Figure 8.15a shows the comparison of the Relenza experimental pre-compaction of the bed force distribution (red series) from the dosator test rig and the Meyerhof & Chaplin (1952) equation [2.9] (blue series). Both stress distribution were in disagreement, probably because the failure criterion in both equations or the cohesion in soils mechanics is measured in the MPa stress range where this value does not change significantly, whereas in powder mechanics the stress range normally varies from zero to 100 kPa where cohesion is strongly dependent on the stress.

The term "H" in the equation [2.9], which is the most critical parameter in dosator operation, was raised to a power of a factor "n" (see equation 8.1) modifying the Meyerhof & Chaplin (1952) approach. The bearing capacity force distribution shifted up, being in better agreement with the experimental force distribution form the dosator test-rig (see figure 8.15b) at high forces. For the case of Relenza this factor "n" was 1.85.

$$\sigma_z = \frac{2mc(R-r)}{H^n} + A \qquad\qquad [8.1]$$
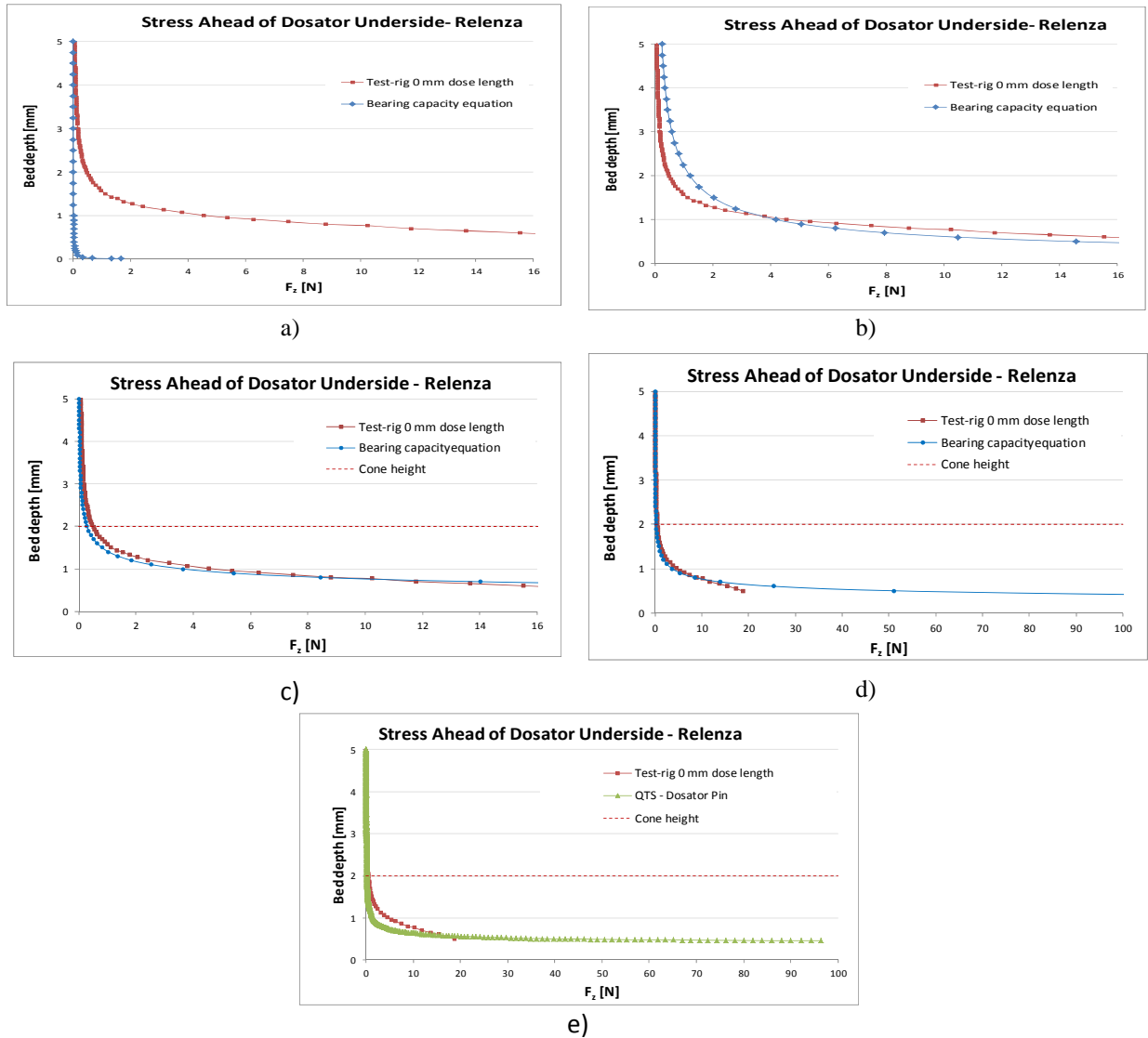
Figure 8.15. Relenza bed force distribution ahead of the dosator underside, comparing the experimental data from The Wolfson Centre dosator single shot test-rig at 0 mm dose length with: a) Meyerhof & Chaplin (1952) equation; b) modification of the Meyerhof & Chaplin (1952) equation; c) iteration of the modified Meyerhof & Chaplin (1952) equation with cohesion as function of the consolidation stress; d) large range of the modification of the Meyerhof & Chaplin (1952) equation; e) experimental bearing capacity of the dosator pin. For full explanation refer to the text.

However, the shape of the curve at low forces was not satisfactory. As discussed before, in soil mechanics the cohesion is not dependent of the consolidation forces. In powder mechanics, is possible to extract information of the cohesion of the materials as function of the consolidation stresses from the flow function measurement (described in chapter 5). Therefore, equation [8.1] was iterated adjusting the cohesion value from the cohesion expressions as function of the consolidated stress (shown in figure 8.16), until stresses values in both expressions were similar. The shape of the curve at low forces was smoothed and the force distribution from the bearing capacity equation was in better agreement with the

experimental forces obtained from the test-rig (see figure 8.15c). With the iteration, the factor "n" for Relenza also reduced to 1.43. As mentioned before, this factor was different for all the powders; 1.65 for Lactohale200, 1.3 for the bimodal blend and 1 for Lactohale300.

a)

b)

c)

d)
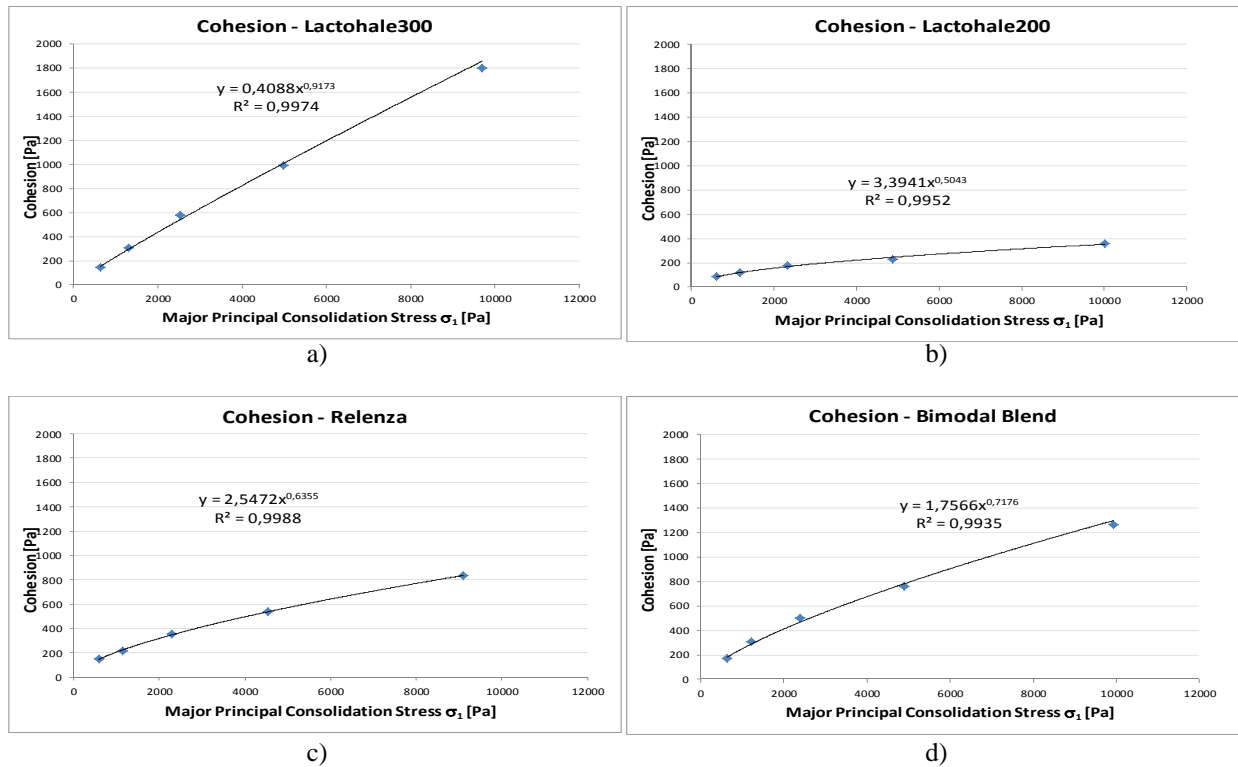
Figure 8.16. Cohesion property as function of the major consolidation stress: a) Lactohale300; b) Lactohale200; c) Relenza; d) Bimodal blend. Test undertaken from the Brookfield PFT.

One of the limitations is that the PFT works at low range of stresses making it difficult to determine the course of the powder cohesion into the high stress range.

The "x" axis scale of figure 8.15 c is shown up to 16 N, which is the maximum range of the force sensors. If the range is extended, as it is shown in figure 8.15d, the trend changes and it seemed to be asymptotic at large stresses. Unfortunately the experimental data did not reach these levels and it is not reliable to use this modified equation.

In the search for a potential characterisation test to simulate the pre-compaction properties of the powders ahead of the dosator, experiments were undertaken using the Brookfield QTS to compact a dosator pin into an unconstrained bed of powder. The results are shown in figure 8.15e. This experimental procedure corresponded to the measuring of the dosator bearing capacity, but at larger bed depths the stresses were larger than the theoretically calculated in the modified equation of Meyerhof & Chaplin (1952).

None of the methods mentioned above gave a satisfactory fit to the experimental measurements, so it was decided to use the curve fitting tool in MatLab software, using an exponential method[28], to express the pre-compaction force distribution in the powder bed using the data from figure 8.13. The expressions obtained are shown below in the equations [8.2], [8.3], [8.4] & [8.5]. With these expressions the model was calibrated and the dose compression was calculated using the Janssen effect to shift the points in the pre-compaction ahead of the dosator for a given powder and dose length.

$$F_z = 76.97 * e^{(z*(-2.743))} + 0.1519 * e^{(z*(-0.1483))} \qquad \text{for Relenza} \qquad [8.2]$$

$$F_z = 77.44 * e^{(z*(-2.951))} + 0.3447 * e^{(z*(-0.1896))} \qquad \text{for Lactohale200} \qquad [8.3]$$

$$F_z = 46.76 * e^{(z*(-3.365))} \qquad \text{for Bimodal blend} \qquad [8.4]$$

$$F_z = 89.16 * e^{(z*(-3.438))} + 0.2122 * e^{(z*(-0.219))} \qquad \text{for Lactohale300} \qquad [8.5]$$

Where "z" is the bed depth in millimetres.

8.4.3. Filling of the dosator cavity stage

The second stage of the model is the filling of the dose chamber. The powder bed is divided by slices/intervals, representing the dosator speed or the constant dosator displacement. It was used fix intervals of "T" = 0.05 mm (see figure 8.12); the smaller the number is the better the resolution of the model is. In the model the units of distance used are "meters", therefore this interval is 0.00005 m. Lower than this mentioned value, Excel starts presenting problems with the decimals altering the calculations and the recognising values in the cells based in formulas. There are 400 slices in the powder bed with fixed thickness "T" for the given 20 mm bed depth used in this research.

As mentioned in the beginning of this section, to run the model the user must first input the different dose and powder flow characteristics in order to calculate the stresses in the system. The entrance of each slice or increment into the dosator is confirmed by two conditions: incompressible and compressible dose state.

---

[28] It showed to be the best method for all the powders force distribution

For each slice entering into the dosator, it is calculated the stress distribution using the Janssen effect application equation [2.6] (described in chapter 2 and appendix 2). According to figures 8.12 and 2.36 in chapter 2, at this stage the only stress acting in the vertical direction is the pre-compaction of the powder bed and the wall friction around the circumference. The stress σ_{vo} in the slice facing the dosator pin is zero because the cavity is not filled yet.

		Incompressible dose				
		Initial calculations				
Bed depth [mm]	**Dose length [m]**	**Thickness S_{Slice} [m]**	**σ_V [Pa]**	**σ_{VO} [Pa]**	**σ_H [Pa]**	
1 19.85	0	0	0	0	0	**5**
Bed depth [m]	0.00004525	0.00004525	859.829	0	300.9402	**6**
2 0.01985	0.00009048	0.00004523	869.894	859.8291	304.4629	**7**
σ_v [Pa]	0.00014048	0.00005	881.157	869.894	308.4051	**8**
3 881.1574265						
σ_{vo} [Pa]						
4 0						
Weight dose [kg]						
5 7.48873E-07						
Dose length [m]						
6 0.0001357						
Length in cavity [m]						
7 0.0038643						
Dose compression [m]						
8 0						
ρ_{avg} in dosator[kg/m³]						
9 607.8278663						
Weight dose [mg]						
10 0.748872995						

Figure 8.17. Incompressible dose state of the filling stage in the dosator model. For full explanation refer to the text.

Figure 8.17 shows the incompressible powder state of the dosator model; for the particular example, the dosator has stroked down three slices or increments (figure 8.17 columns 2-6 and rows 5-8). In the left hand side can be seen a panel (figure 8.17 column 1) with general characteristics and calculations of the actual dose inside the dosator. The first two values in this panel are the current bed depth in [m] and [mm]. The third value is the vertical stress at the dosator tip equivalent to the pre-compaction of the powder bed at the stated bed depth. The fourth value is the stress against to the pin's face in the current step; it is zero because the dose chamber has not been filled. The following three values are the current weight in the dosator, the current dose chamber length filled and remaining length to be filled. The next value is the actual dose compression in the dosator, it does not apply so has a value zero in this stage and it is explained in the next stage. The last two values are the average density in the dosator and the dose weight in [mg].

In this incompressible dose state, it is assumed that each slice in the powder bed ideally enters into the dosator with an assumed thickness of T = 0.05 mm, like the last slice in figure 8.17 (seed figure 8.17 column 3, row 8). With the equivalent vertical stress from the powder bed

at the corresponding bed depth, in the left hand side panel the third value, the stress distribution of each slice is calculated using the Janssen effect equation [2.36] (see figure 8.17 column 4, row 8). In this stage, the forces due to the self-weight of the slices are eliminated as it has minimal effect on the stress. The idea is to get a stress distribution in the system in order to correct the thickness of the slices for the compressible stress state of the model. The calculations in the incompressible state start from the first slice (at the dosator outlet) by knowing the vertical stress, σ_v, from the pre-compaction of the bed and calculating the surcharges at the top of the slice, σ_{vo}, with the Janssen effect [2.36] in chapter 2. This stress at the top of the slice, σ_{vo}, is in turn the vertical stress, σ_v, of the next slice and so on (compare columns 4 and 5 in figure 8.17). The last slice (close to the pin's face) has $\sigma_{vo}=0$ because the dose chamber has not been filled (column 5, row 6 in figure 8.17).

For a given stress the determination of the compressible state of the dose starts by calculating the equivalent bulk density (see figure 8.18 column 1), calculated from the compaction curve in chapter 5, based on the stress distribution for an incompressible state (see figure 8.17 column 4). The calculated density is compared with the poured density entered into the model and the thickness of the slice is corrected (see figure 8.18 column 2); i.e. reduced from the initial assumed value of the poured density value (see figures 8.18 column 2, row 8 and figure 8.17 column 3, row 8). Afterwards, the dose length already filled and the remaining cavity length are re-calculated (see figure 8.18 columns 3 & 4) to track when the dosator is filled. Next, there is a correction of the compression stage (see figure 8.18 columns 5-8), which it does not apply to this stage. The next columns (see figure 8.18 columns 9–11) calculate the stress distribution using the Janssen effect, in the same way as in the incompressible state, but taking into the account the corrected density (see figure 8.18 column 1) and thickness of the slice (see figure 8.18 column 2). In the last columns (see figure 8.18 columns 12 & 13) the weight of each slice is calculated and the accumulative weight of the dose at this penetration depth of the dosator into the bed.

It is assumed that the slices are displaced upwards as the new slice enters, each maintaining their corrected thickness (t_1, t_2, etc.) during the remaining filling length in the dose chamber, as it is shown in the diagram of figure 8.18 and for the two first slices in the model sample showed in figures 8.17 (column 3) and 8.18 (column 2). Therefore, in each penetration of the dosator, the thickness of the slice entered is corrected and the existent slices displaced

upwards keeping the corresponding corrected thickness in the previous steps. The variation of the stress as the slice is pushed upwards is assumed not to be significant.

Considering the displacement of the dosator in the bed, this would be the corrected dose length (see figure 8.18 column 3 and 7) plus the fixed increment T = 0.05 mm and so on.

	ρ_{slice} [kg/m^3]	Thickness$_{Slice}$ [m]	Dose length [m]	Length cavity [m]	Thickness$_{LastSlice}$ Correction [m]	$\rho_{LastSlice}$ [kg/m^3]	Correction Dose length Correction [m]	Length in cavity [m]	σ_V [Pa]	σ_{VO} [Pa]	σ_H [Pa]	Weight$_{Slice}$ [kg]	Weight$_{Dose}$ [kg]
5	0	0	0.0001357	0.0038643	0	0	0.0001357	0.0038643	0	0	0	0	0
6	607.4698	0.00004525	0.00004525	0.00395475	0.00004525	607.4697643	0.00004525	0.00395475	860.354029	0	301.1239	2.5E-07	2.4957E-07
7	607.8156	0.00004523	0.00009048	0.00390952	0.00004523	607.8156014	0.00009048	0.00390952	870.696275	860.354	304.7437	2.5E-07	4.9917E-07
8	608.1985	0.00004522	0.0001357	0.0038643	0.00004522	608.1984734	0.0001357	0.0038643	881.157426	870.6963	308.4051	2.5E-07	7.4887E-07

Figure 8.18. Compressible dose state of the filling stage in the dosator model. For full explanation refer to the text.

8.4.4. Compression stage

The dosator continues the downward stroke until the powder completely fills the dose chamber and the calculations stop when the corrected dose length reaches the required dose length input in the model. This is assessed by the difference between the calculated and required dose length. The correction filling stage columns 5-8 in figure 8.18 are used to adjust the thickness, density, dose and remaining dose length of the last slice entering into the dosator to fill exactly the dosator with the required dose length. The last slices of the columns 7 and 8 should be equal to the dose length required and 0 respectively.

The compression stage follows for the remaining displacements of the stroke. To account for the compressibility when the dose is stressed further, the weight of the slices is increased based on the stress, bulk density function.

Figure 8.19 illustrates the dose compression stage where the position 1 is a distance T_1 from the bottom of the trough with stress σ_1 at the dosator tip, dose weight W_1 and density ρ_1

characteristics. The dosator descends $\Delta T = T = 0.05$ mm distance in the next displacement of the stroke, where the conditions changed to σ_2, W_2 and $\rho_2 > \sigma_1$, W_1 and ρ_1.
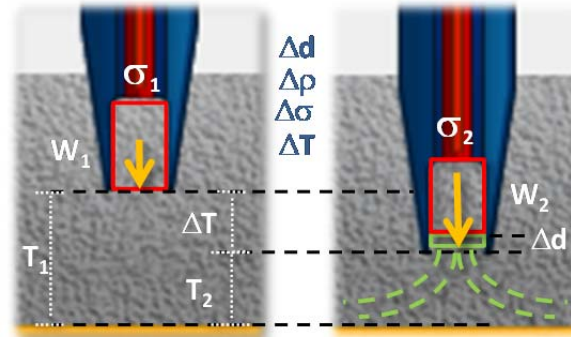
Figure 8.19.   Dosator displacement and dose compaction in the compression stage of the dosator model. For full explanation refer to the text.

Not all the powder ahead of the dosator would enter into the dose chamber, some could spread aside and a slice with Δd thickness would be pushed inside the dosator depending on the stresses in the system. As mentioned before, the thickness of the slice entered into the dosator is integrated into the model as an increment of the mass weight in order to calculate the compression of the dose. It is assumed that the slice about to enter from the bed has the same density as the first slice inside the dosator outlet; the vertical stress and friction conditions are considered equal in both slices. Therefore the thickness of the slice entered into the dosator is calculated with the variation of the weight, ΔW, between the two positions and the calculated density from the compaction curve as function of the stress distribution of the dose. The thickness Δd of the slice entered into the dose is shown in the "Dose compression" cell (value 8) at the left hand side panel in figure 8.17.

As the dose is compressed, the displacement of the dosator T_2 is no longer $T_1 + \Delta T$; and would be $T_2 = T_1 + \Delta T + \Delta d$, because the stress variation $\Delta \sigma = \sigma_2 - \sigma_1$ causes two movements ΔT and Δd. The change of the dosator displacement is a function of the stress $\Delta T (\Delta \sigma)$, see figure 8.19, but there is also a density and weight variation as function of the stress variation, $\Delta \rho (\Delta \sigma)$ and $\Delta W (\Delta \sigma)$, see compaction curve in chapter 5.

Consequently, the next dosator displacement would be $T_2 = T_1 + \Delta T + \Delta d$ until the end of the stroke and the calibration stress distribution in the powder bed shifts the bed depth axis and the stress distribution for the required dose length should be obtained.

8.4.5.   Dosator model results and discussion

Figures 8.20 and 8.21 show the validation of the dosator model with the experimental results from The Wolfson Centre single shot dosator test-rig. Presented is the variation of the dose weight and filling forces as function of different gap "h" conditions. A positive difference means an overestimation and negative underestimated. As it can be seen in figures 8.20, the model over-predicted the doses in most of the cases, especially for the small dose length. The difference was smaller for long doses. The very cohesive Lactohale300 showed greatest discrepancy in the results.

The dose weight difference between the model predictions and the experimental doses of Lactohale200, Relenza and the bimodal blend between approximately 10 – 20% for the different dose lengths; the difference in the Lactohale300 was between 30 – 50 %.

One of the reasons of the discrepancy of the dose weight is the incongruity of the compaction curve calculated in chapter 5. As it can be seen in figure 7.26 in chapter 7, the density of the doses obtained differs with the compaction curve measured in chapter 5. This suggests that the method used to assess the compressibility of the powder (compaction curve) does not replicate the compression mechanism in dosator operation. As mentioned in chapter 7, in the compaction curve measurement powder is uniaxially compacted into a confined space, i.e. an active stress field where major stress is vertical, whereas in the dosator, an unconstrained bed of powder is being compacted into a constrained space, i.e. a passive stress field where the major pressure is horizontal. It is suspected that the latter condition gives a lower bulk density, which is why the model over predicts the dose weights. The difference factor between the predicted doses from the model and the doses obtained in the test-rig is equivalent to the factor of the discrepancy between the compaction curve model and the density of the doses obtained in the test-rig (mentioned in section 7.8, chapter 7). Applying this factor provides a better dose weight prediction in the model, which confirms that the measurement of the compaction of the powder in dosator operation needs to be revised.

a)

b)

c)
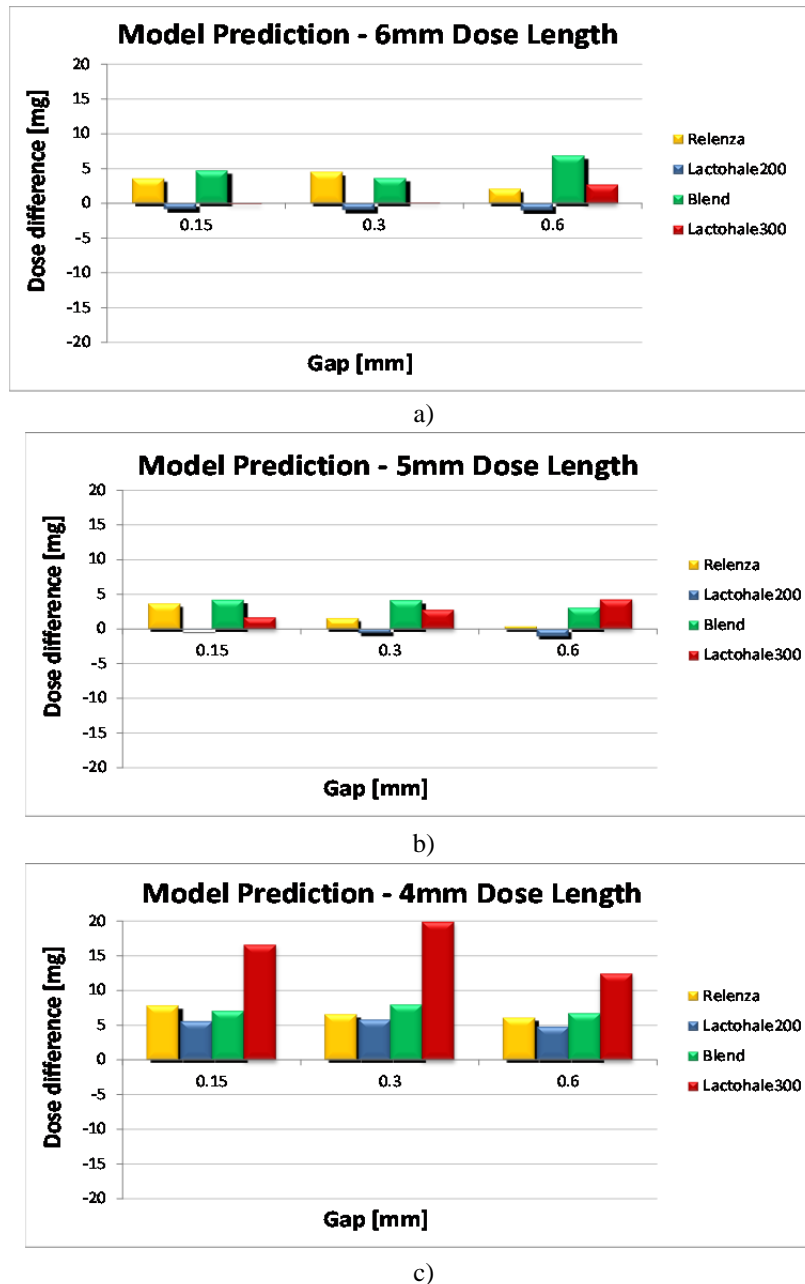
Figure 8.20. Dosator model validation at different gaps "h" conditions; dose weight variation: a) 6 mm dose length; b) 5 mm dose length; c) 4 mm dose length. For full explanation refer to the text.

The model did not present significant changes in the dose weight with the variation of the other powder flow properties (stress ratio K, poured bulk density and wall friction). However, the accumulation of errors measuring these properties, could contribute to the discrepancy of the results.

The predicted filling forces in figure 8.21 also show a discrepancy with the experimental data. It shows an overestimation of the filling forces, but in fact this is not correct at all. Figure 8.22 shows an example of the filling force from experimental data and predicted in the model.
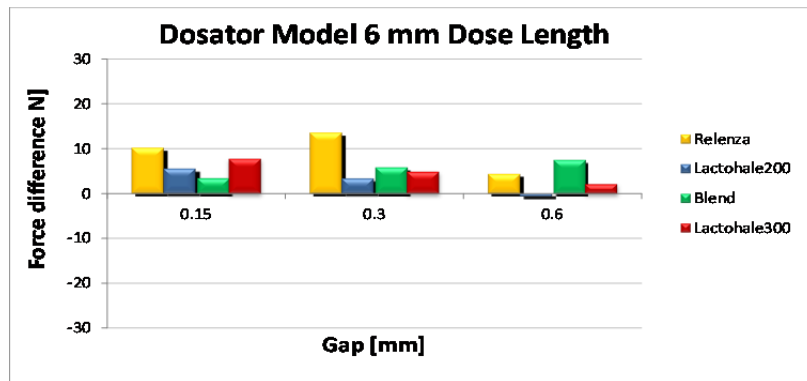
a)
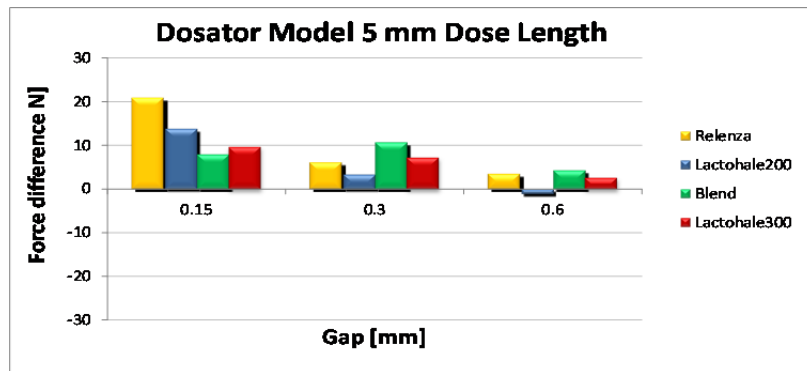
b)
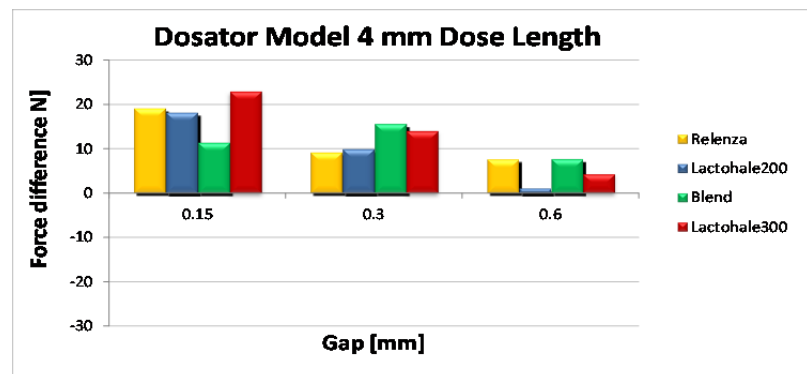
c)

Figure 8.21. Dosator model validation at different gaps "h" conditions; filling force variation: a) 6 mm dose length; b) 5 mm dose length; c) 4 mm dose length. For full explanation refer to the text.

The series in blue and bright red colour corresponds to the pre-compaction ahead of the dosator and the prediction of the model for 4 mm dose lengths. The predicted forces in the model should match the experimental force plotted in the green series. The values presented in figure 8.19b where at a negative dose length. These results suggest that the increments of the compression in the model are greater than the compression in the dosator process. The assumptions of the amount of powder entering in the dosator need to be revised.
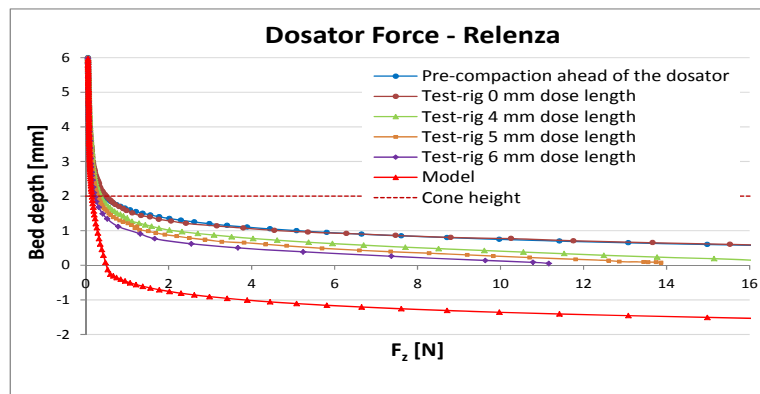
Figure 8.22. Relenza force distribution example in the dosator model. For full explanation refer to the text.

Nevertheless, the shape of the curve predicted met the anticipated shape, which indicates that the compression in the dosator model should be revised.

8.4.6.   Summary

This chapter presented the dosator model proposed in this thesis as result of influences from the literature reviewed, experimental work with the dosator test-rig, physical observations of the process and understanding of the dosator operation.

The accuracy of the fill dose weight predicted by the model was poor and it is suggested that the experimentally measured compaction data is the problem. The results were not good as were hoped for, but the work has contributed significantly to the knowledge and understanding of dosator operation.

The work has also demonstrated how controlled experiments for simplified operating conditions can be used to establish the filling force, dose weight and mechanical strength of the dose, that are sought by machine manufacturers.

The following chapter 9 presents the last machine factor studied in this thesis, the effect of the dosator speed, which was evaluated using the 3PI test-rig, which operates at speed much closer to that of the production machines.

Chapter 9

3PI Dosator Single Shot Test-Rig

9.1.   Introduction

The development of the research project lead to the development of single shot dosator test-rig engineered at the Wolfson Centre to validate the model. However from the project outset the 3PI test-rig property of GSK was originally proposed for this purpose, but did not meet the requirements to validate the model.

Both test-rigs were designed with different objectives, nevertheless both measure the dose weight and ejection force.   The test-rigs differ in the dosator operation, bed preparation/perturbation, forces/dose measurements and dosator speed.

The 3PI test-rig measures the dose weight and the pin force/velocity at the ejection stage of the dosator process.   This test-rig operates following the normal production machines principle by inserting the dosator into the static bed of powder to obtain the dose. The dosator speed insertion (approximately 30mm/s) and the pin ejection speed (approximately 300 mm/s) are higher to The Wolfson Centre trough's stroke and pin ejection speed[29]; but are still significantly lower than the dosator speed insertion in production machine (approximately 130 mm/s).

This chapter presents some tests that were undertaken by the author using the 3PI test-rig at GSK Harlow to analyse whether the difference in speed has a significant effect on the dosator operation. Some of the behaviours during these trials were shown earlier in chapter 7.

9.2.   Objective of the tests undertaken

The objective of these experiments was to analyse the dosator speed effect on dose weight and ejection force by comparing results from the 3PI test rig in GSK Harlow with those obtained in The Wolfson Centre test-rig.

---

[29] Approximately trough's stroke 7 mm/s and the pin ejection 0.25 mm/s

9.3.   Apparatus and operation

The 3PI dosator single shot test-rig (see figure 9.1) was designed by 3PInnovations to replicate the commercial dosator process and obtain real time data on pin ejection forces and weight of every dose.

a)   b)   c)
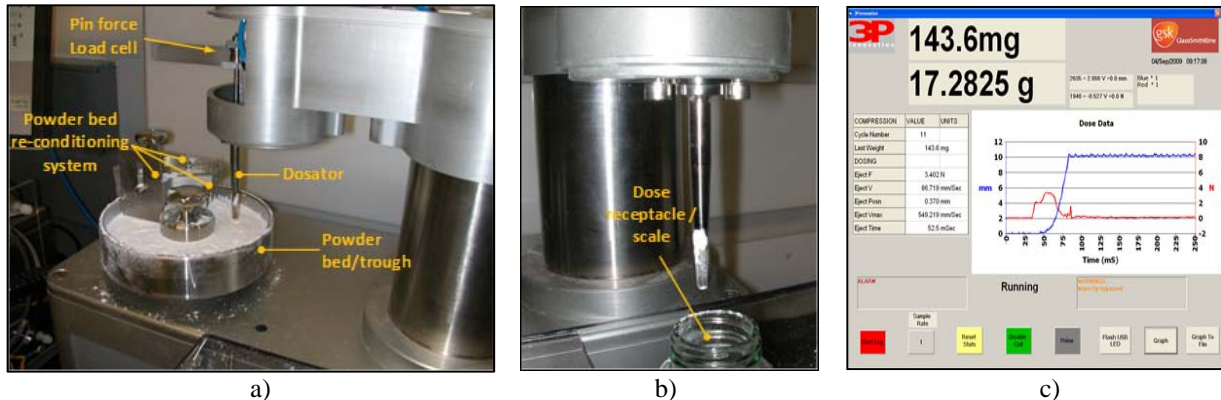
Figure 9.1.   3PI dosator single shot test-rig: a) filling stage; b) ejection stage; c) test-rig display.   For full explanation refer to the text

As it is shown in figure 9.1a, the dosator is attached to a rotational arm; the dosator body is connected to the chassis and the dosator pin to a linear pneumatic actuator to eject the dose. The dosator pin is connected to an Omega LCMKD-10N load cell and Leuze optical laser distance sensor ODSL8 to measure the pin ejection force and displacement.

The dosator descends into the powder bed and fills the dose cavity; then strokes up and rotates 90° to eject the dose (see figure 9.1b) into a receptacle placed on a scale to weight each dose.

The trough is fitted with a re-conditioning system in order to perturb, refill and level the powder bed as the trough rotates through a defined angle after each stroke. Three perturbing pins, a feeder hopper and scrapper compose the re-conditioning system, as described earlier in chapter 2 section 2.3.6.

The test-rig does a "double shuffle" (i.e. is rotated backward then forward), at the end of the stroke as some production dosator machines do. The dosators pin and body set can be interchanged for sets of different sizes, representative of those used in production.

The information about the test is displayed on an interface shown in figure 9.1c; it contains a graph on the right hand side with two "Y" axes for the pin ejection force and displacement and "X" axis for the time. On the left hand side it has a panel with the stroke number and some force/velocity information for the ejection stage of the dosator operation. At the bottom

of the interface there are control buttons to run/stop the program, calibrate the load cell and other functions to manage the measurements variables.

The dosator set used was the same as that used with The Wolfson Centre test-rig having a diameter of 3.4 mm (as used in MG2 machines). The trough was manufactured from stainless steel like the production machines and the external diameter was 98 mm and the internal diameter 47 mm. The level of the bottom of the trough had a variation of $\pm$ 0.1 mm and for each revolution, in which it was possible to get around 15 strokes/ doses.

The doses were weighted on a balance at the end of the operation that reads the total weight before the ejection and subtracts it from the total weight after the ejection.

9.4.   Test Materials

A Lactose Supertab powder was used for preliminary tests to understand the operation of the 3PI dosator. The main powder used for the trials was Relenza with an additional trial for the lactose bimodal blend; to establish correlations with the Wolfson Centre single shot dosator test rig.

9.5.   Methodology

Different tests and procedures were undertaken with the 3PI test-rig at GSK Harlow. Normally the bed of powder was prepared by sieving the powder for the first revolution of the trough (without the three pins), for consistency with the normal bed preparation used for The Wolfson Centre dosator test-rig. Then the pins were replaced and the powder fed manually to run the 3PI test-rig in the normal manner. These test conditions are referred to in the results as "Sieve" and "Long run" tests to denote the first run and the normal operation of the test-rig respectively.

The dose length was set it for 4, 5, 6 mm and the gap "h" between the dosator undersize and the bottom of the trough was 0.3 mm and for one case was adjusted to 0.6 mm. One test was done by applying 1 Kg pre-compaction to the powder and another covered the stainless steel

base of the trough with the fablon film. The dosator was thoroughly cleaned with isopropanol before the setup of each test.

9.6.   Results and discussions

The preliminary setup tests undertaken with the Lactose Supertab had 4.8 mm diameter (same as used for Harro Höfliger), 5.5 mm dose length and the dose gap "h" set to 0.3 mm. Two tests with two and three pins in the powder bed pre-conditioning system were undertaken to observe typical variations in the dose weight and ejection force over time. 211 cycles were measured in the two pins test and 782 cycles in the three pins test, figure 9.2 shows the corresponding results, with no clean down in between.

a)   b)
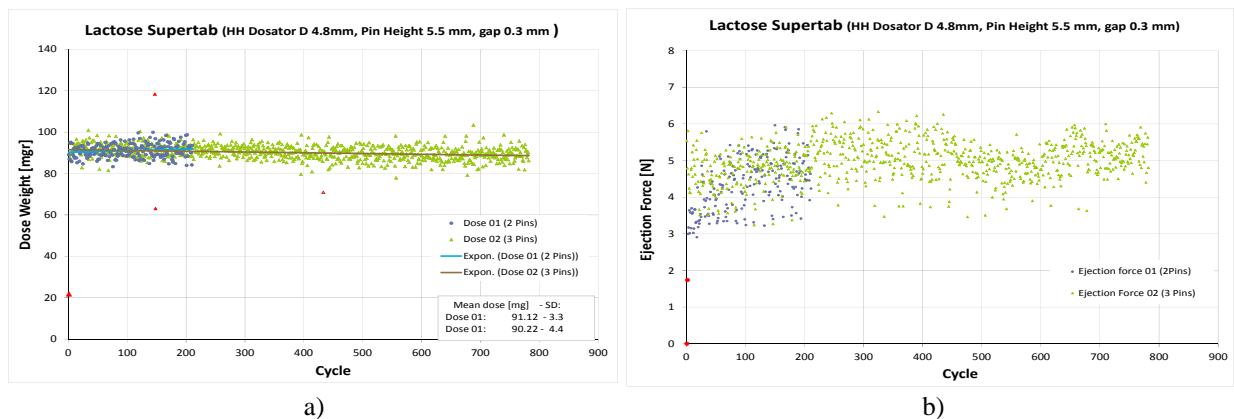
Figure 9.2. Lactose Supertab test using 2 and 3 perturbing pins in the re-conditioning powder bed system: a) dose weight; b) ejection force. For full explanation refer to the text.

Figure 9.2 shows the results of Lactose Supertab tests and demonstrate scatter of ±10 mg in the dose weight and ±1.5 N in the magnitude of the ejection force with no significant difference being attributable to the number pins (two or three) in the powder bed pre-conditioning system. Note that the ejection force at the beginning of the first tests is lower (see figure 9.2b, blue data series), this could be due to the wall friction effect with particle build-up on the walls. There were a few points (market in red) that were far from the general trend, potential explanations for this are presented below.

The scattered behaviour of the dose weight and ejection force was seen for the majority of the trials undertaken in the 3PI test rig. Figure 9.3 shows the dose weight and ejection forces for Relenza, as function of the cycles or number of strokes at a 0.3 mm gap "h".   It can be seen in (figure 9.3a highlighted) numerous low doses that are followed by over doses. This is

attributed to the adhesion of the powder to the pin's face; the low doses are due to partial ejection leaving material stuck to the pin's face. On the following stroke the powder adhered to the pin effectively reduces dose length increasing compaction resulting in an over-dose. The ejection force of the highlighted doses is shown in figure 9.3b; for most of the cases there was an increase of the ejection force as a function of the increase in the dose weight. The ejection force tended to increase significantly with the number of strokes/ dosing cycles, suggesting the evolution of the wall friction.

a)   b)
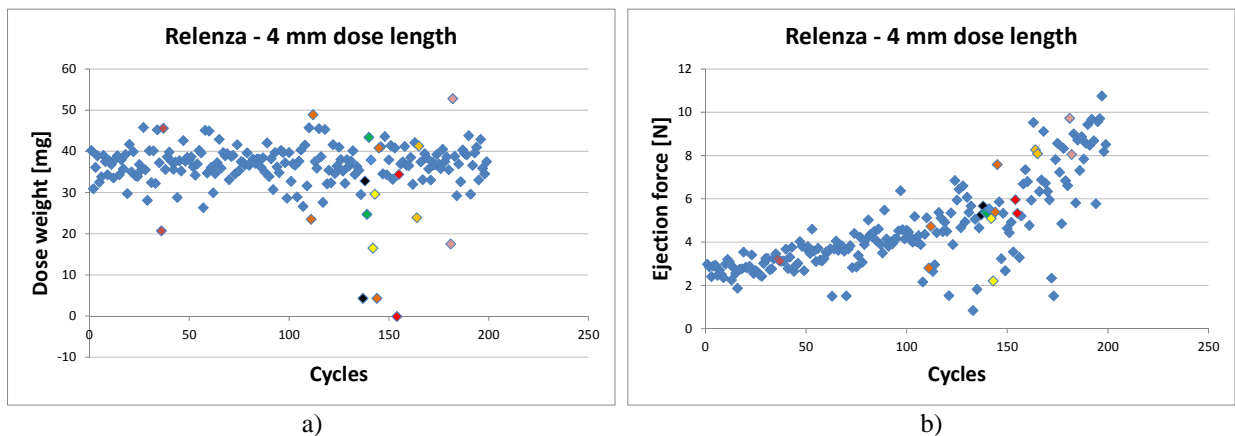
Figure 9.3. Relenza 4 mm dose length results at 0.3 mm gap "h": a) dose weight; b) ejection force. For full explanation refer to the text.

Other factors observed affecting the data were attributed to signal processing errors and either portions/entire doses dropping out before ejection due to acceleration forces resulting from the mechanical movement of the dosator, or lack of retained strength of the powder.

The dose weight results shown below are presented using bar charts to compare the different tests, whereas the ejection force results are presented using scatter charts to see the trend with the number of cycles. In the case of figure 9.3b, the ejection force is not only scattered, as average ejection force also increased over time.

Figure 9.4 shows all the Relenza 4 mm dose length results for different conditions on the 3PI test rig. These are the first run (with the sieved powder bed condition), the long run (normal operation of the test-rig) and the results undertaken on the Wolfson Centre single shot dosator. The machine settings used were as follows; the gap "h" was set at 0.3 mm except for one test at 0.6 mm. One of the tests was carried out pre-compacting the powder bed with 1 kg distributed load and another test by lining the trough base with fablon film in place of stainless steel. For the 0.3 mm gap tests, the bed was sieved twice before following the normal operation; the first run was clean and the second sieved test was with the dosator dirty.
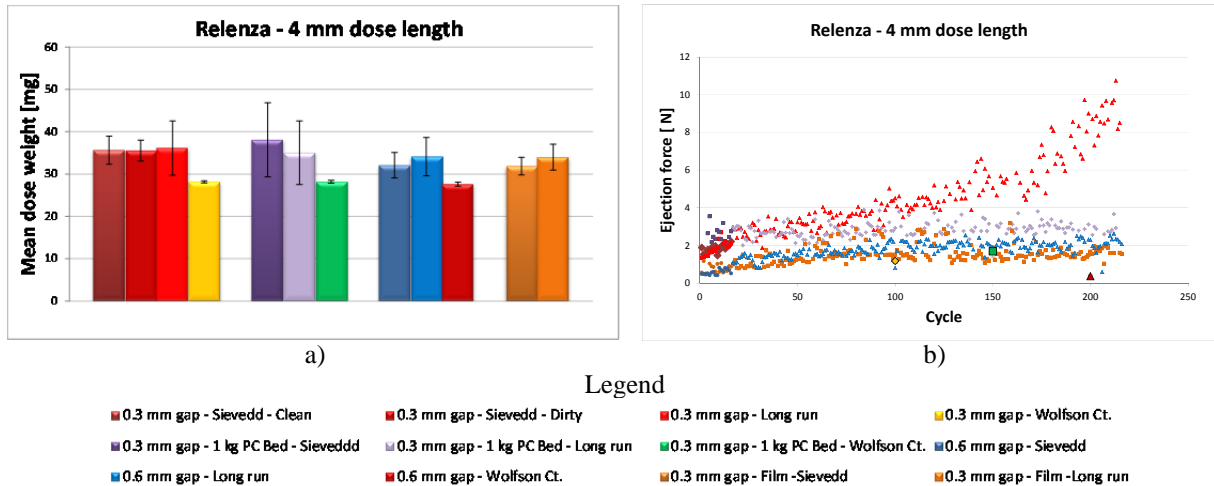
Figure 9.4. Relenza 4 mm dose length tests at different conditions: a) mean dose weight; b) ejection force. For full explanation refer to the text.

It can be seen from figure 9.4a that there was a large variation between the 3PI and The Wolfson Centre test rig dose weights for all the test conditions. The variation was approximately 4-6 mg. The conditions in the powder bed did not seem to affect the dose weight for this powder in the first run; this was also seen in the tests undertaken in The Wolfson Centre dosator test-rig. The increase of the gap "h" and the changing of the trough's lining material caused a decrease in the dose weight compared to the normal operation.

The ejection force (see figure 9.4b) increased in the long run tests by comparison with the initial sieved bed conditions in all the tests. The ejection force following the 1 kg pre-compaction of the powder bed was expected to be higher, as seen in The Wolfson Centre test-rig, but decreased in the 3PI test-rig. The long run at normal conditions and 0.3 mm gap the ejection force tended to increase with the time, especially after 100 strokes, for the other test conditions there was a small increase. The Wolfson Centre mean dose ejection results are presented at the 100, 150 and 200 cycles of figure 9.4b; the magnitude of the ejection force in the 3PI test-rig was larger than the forces obtained from The Wolfson Centre test-rig. There was a large scatter in the ejection force results. The first run, sieving conditions, presented lower ejection forces than the normal operation; this could be attributed either to the condition in the bed of powder or to the powder build up at the dosator inner-wall.
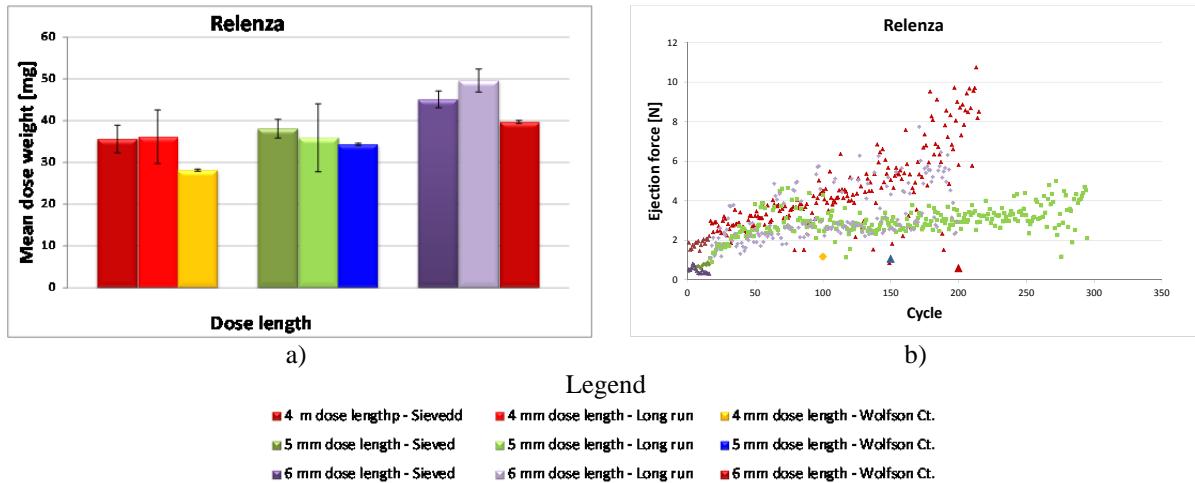
Figure 9.5. Relenza tests at different dose lengths: a) mean dose weight; b) ejection force. For full explanation refer to the text.

Figure 9.5 shows Relenza results for the different dose lengths. The doses in the 3PI test-rig are heavier than the doses produced in The Wolfson Centre test-rig (see figure 9.5a); there is a difference of between 4 to 8 mg. It can be seen that the first run of the results with the sieved powder bed had less variation of the results than the long run tests using the bed re-conditioning unit. The 5 mm dose length, long run test had significant scatter affecting the average and standard deviation of the data. The ejection forces of the 6 mm dose length long run test had significant scatter whereas the dose weights presented small variations. In contrast the weights of the 5 mm length doses had a bigger variation than the ejection forces. The ejection forces decreased with the increase of the dose length in the Wolfson Centre test-rig (cycles 100150 and 200 in figure 9.5b), this was not possible to evaluate in the 3PI test rig due to the scatter in the data.
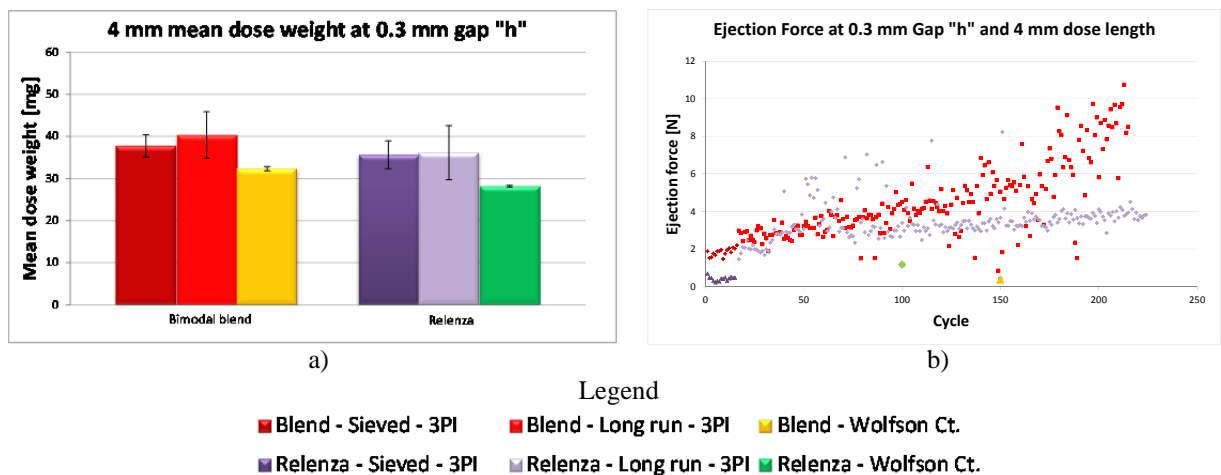
Figure 9.6. Relenza and bimodal blend tests results at 0.3 mm gap "h" and 4 mm dose length: a) mean dose weight; b) ejection force. For full explanation refer to the text.

218

Figure 9.6 shows the results of Relenza and the bimodal blend tests at 0.3 mm gap "h" and the 4 mm dose length. The 3PI test rig measured dose weights between 4 and 6 mg higher than The Wolfson Centre test-rig (see figure 9.6a). The Relenza ejection force was lower than the bimodal blend in both test rigs. Ejection forces in the 3PI test rig are higher than The Wolfson ejection force results.

The ejection force profiles from the results were not consistent and showed different shapes and tendencies (see figure 9.7). These shapes could be attributed to misalignments in the test rig, noise in the signal, the ejection speed and signal processing issues. In some cases the forces were gradually increasing instead of rapidly increasing to overcome the wall friction. This ejection force profiles in the 3PI test r-rig were in disagreement with the ejection force profiles obtained in The Wolfson Centre test-rig (see figure 7.5 in chapter 7, section 7.3).
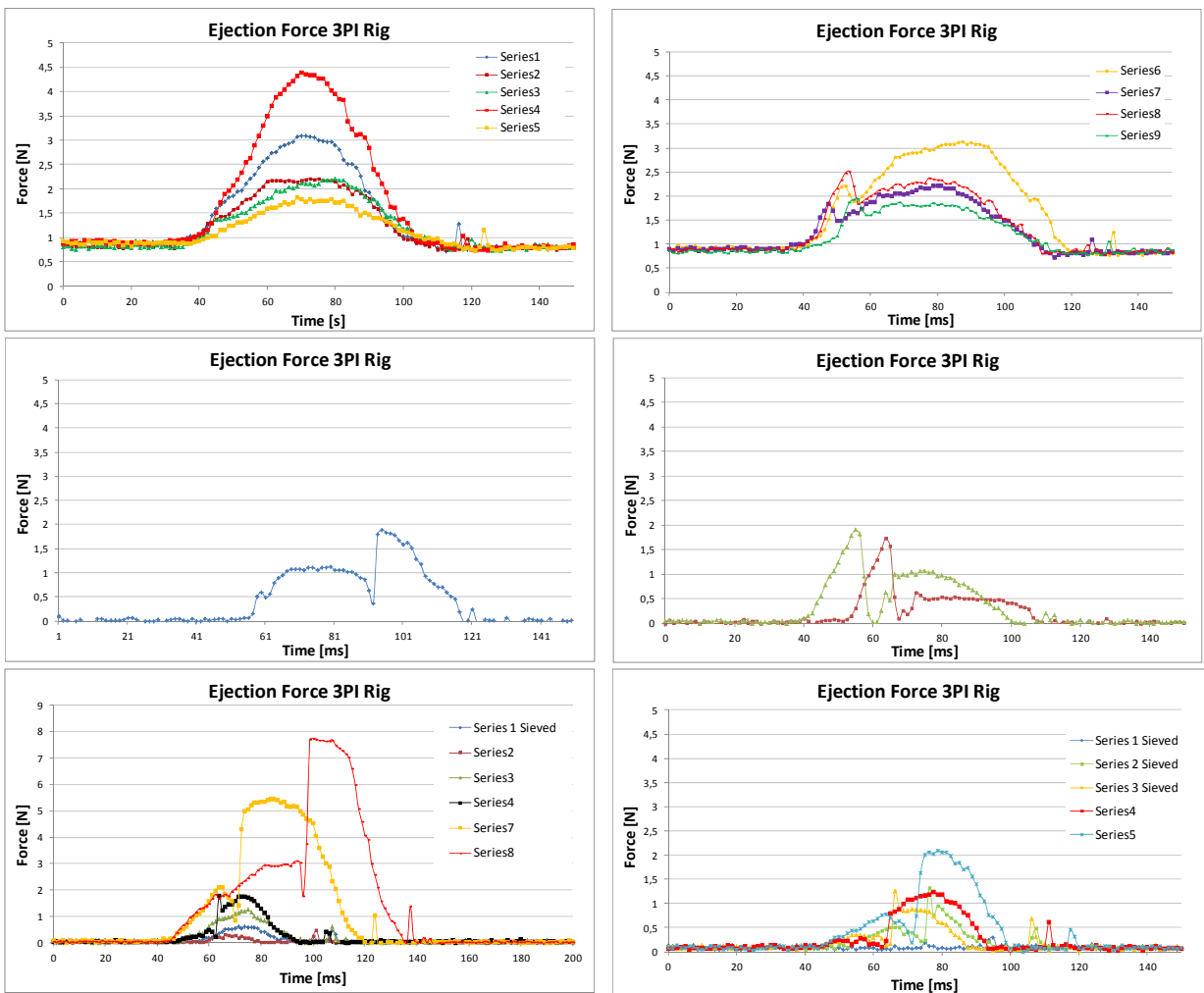
Figure 9.7. Ejection force profiles from the 3PI dosator single shot test-rig results. For full explanation refer to the text.

The variations in the dose weight results could be caused by the ± 0.1 mm level of the trough, the powder bed state and re-conditioning system, the signal processing issues, misalignments in the test-rig, assembly of the dosator body and pin in the test-rig.

The load cell weighing the doses seems to be affected by the signal processing as sometimes gave negative values.

The assembly of the dosator pin to the test-rig is shown in figure 9.8. The dosator body was mounted to the test-rig by two screws (see figure 9.8a) that hold the dosator body base and with the time the screws work loose due to vibrations, from the motion of the machine. This causes misalignments in the dosator assembly, resulting in mis-reading of the ejection force and build-up of material (in dosator body inner wall and on the ledge on the back face of the dosator pin). This could also reduce the gap "h" and alter the conditions in the trials.

| a) | b) | c) |
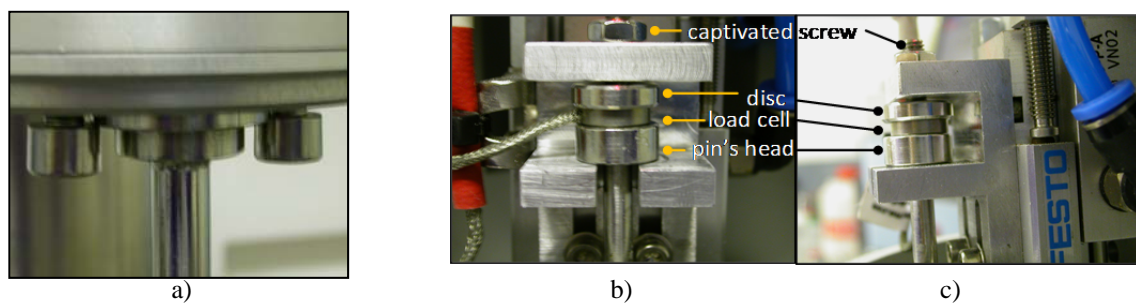
Figure 9.8. Dosator assembly in the 3PI dosator single shot test-rig: a) dosator body assembly; b) dosator pin assembly front view; c) dosator pin assembly right view. For full explanation refer to the text.

The major factor causing the dose weight difference between the 3PI and Wolfson Centre dosator test-rigs could be attributed to the assembly of the force sensor and the dosator pin. Figures 9.8b and c show the dosator pin assembly. The pin's head lies on the lower part of a bracket which is F shaped; the bracket is connected to a pneumatic cylinder assembly. The disc shaped load cell is located on top of the pin's head and a disc is fitted in between the upper part of the bracket and the load cell. There is a small gap between the disc and the bracket that is taken up by a captivated screw; the disc then protects the load cell from the high local pressure that would be transmitted if it were retained directly by the captive screw. The screw cannot be tightened because the load cell would be under compression and therefore the measurements affected. As a consequence the system is set-up loose so the pin can move up thus causing an increase in the dose length and therefore increasing the dose weight. Taking into the account this tolerance and the horizontal gap between the pin's shaft and the bracket (see figure 9.8b), where the pin's head rests, the dosator pin is free move

slightly in the horizontal and vertical axis. Thus the dosator pin is not centred during the operation which could lead to build up of powder (behind the pin's face and shaft and in the dosator body inner wall), changing the volume of the dosator cavity, increasing wall friction and affecting the ejection force measurements.

The procedure used to set up the dose length could also affect the results as it was inaccurate. It was determined by inserting a thin rod to the bottom of the dosator cavity and marking the height, this then measuring using a steel rule. There were two variables involved setting up the dose length; the first one was the mentioned tolerance between the disc and captivated screw and the second one was the adjustment of the pneumatic cylinder length to displace the dosator pin. In figure 9.8c can be observed the FESTO cylinder and on the top there is a screw with a black rubber at the end that adjust the position of the pin; the rubber and the screw also could influence the accuracy of the dose length set up.

9.7.   Behaviour observed

Figure 9.9 shows a layer of powder adhered to the bottom of the trough - varying the surface finish of the trough.

a)   b)
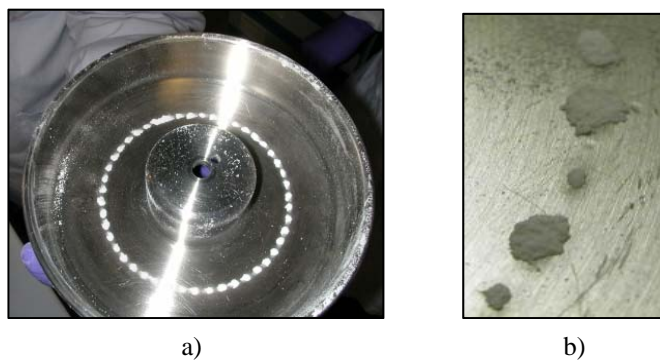
Figure 9.9. Layer of compacted powder at the bottom of the trough for two trough surfaces: a) stainless steel; b) fablon film. For full explanation refer to the text.

This behaviour was observed in The Wolfson Centre at small scale (see figures 7.7 & 7.21 in chapter 7) and also in production machines (as mentioned by the industrial sponsor and dosator machine manufacturers).

Figure 9.10 shows part of the dose ejected (blue dotted circle) and part of the dose adhered to the face of the pin (red dotted circle) during the ejection stage; it also shows the dosator re-

positioned in preparation for the next stroke with the powder still adhered in position. The dose ejected would be light and the following dose would be heavier and over compacted. This situation was frequently observed in this test-rig and it is likely to occur in production machines. The data from the experimental tests undertaken using this test-rig was significantly affected by this behaviour. This situation was also seen in The Wolfson Centre test-rig (see figure 7.3 in chapter 7).
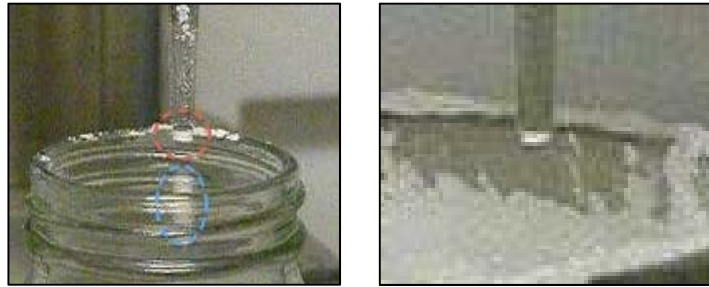
Figure 9.10. Part of the dose added to the pin's face after ejection stage. For full explanation refer to the text.

Dose dropping was another behaviour observed in this test-rig. This is mostly provoked by machine jolts during the dosator operation. Figure 9.11 shows this situation with two cases; the first one (see figure 9.11a) where doses dropped outside the test-rig during the operation and second one (see figures 9.11b and c) where a puff of powder detached and dose slip were seen due to a machine jolt at the end of the dosator retraction.

a)   b)   c)
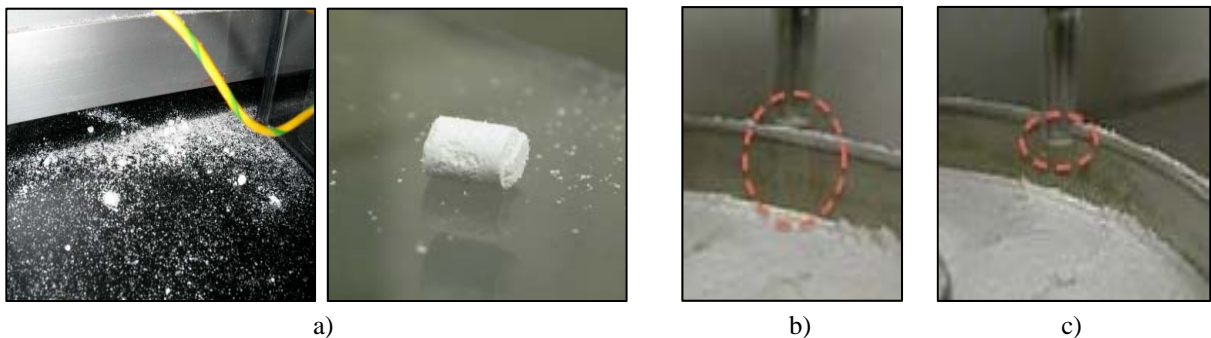
Figure 9.11. Full/partial doses dropped before the ejection: a) doses dropped during the dose transfer to the ejection stage; b) puff of powder detached as result of machine jolts; d) dose slip as result of machine jolt. For full explanation refer to the text.

Powder build up behaviour of the dosator pin was also seen in these experiments (see figure 9.12). The same behaviour was observed in The Wolfson Centre test-rig (see figure 7.15 in chapter 7)

Figure 9.12. Examples of powder stored behind the pin's face. For full explanation refer to the text.

9.8.   Summary

The 3PI test-rig gave a good approximation of what happens in production machines and showed several different problems that could be present during large scale manufacturing operations nevertheless the dosator speed was higher than Wolfson Centre test-rig but still significantly slower than production machines.

The acceleration forces detected in the rotational and vertical displacements of the arm carrying the dosator could potentially contribute to problems of dose or partial dose release prior to the ejection stage thus affecting the dose weight.

The objective of assessing the impact of the stroke and ejection velocity on dose weight variation and ejection force was not achieved due to the variability in the 3PI data (due to, signal processing, operational and assembly problems). However the fact that the 3PI machine measures forces of a similar magnitude to those detected with The Wolfson Centre dosator test rig suggested that there is not a significant velocity effect on the results.

There was no consistency in dose weight and ejection force values measured between the 3PI test-rig and The Wolfson Centre test-rig.

The re-conditioning system of the powder bed used by 3PI test-rig and production machines is poor and inefficient because it does not remove the stress history from the powder bed, caused by the previous dosator strokes. This was evidenced by the fact that when the central pin used to perturb the powder bed was removed, this had no obvious effect on the long run tests

undertaken with the Lactose Supertab. Significant ejection force and dose weight variations were observed in all long runs in the 3PI test-rig trials.

The behaviours observed in The Wolfson Centre test-rig, i.e. powder adherence to the trough base at the dosator strike points, build up in the dosator tube and behind the pin face, were also seen in the 3PI test-rig, which suggest that the Wolfson Centre test-rig experiences problems often found in production machines.

Regardless, both the Wolfson and 3PI test-rigs were constructed with different objectives in mind.

- The Wolfson Centre single shot dosator test-rig was developed to accurately measure the forces generated and the dose weight obtained in a dosator for scientific analysis. To achieve this required a design that gave close control of the dosator geometry, position and powder bed conditions. Thus the developed equipment gave very repeatable dose weights and forces, but bears little resemblance to the production machine.

- The 3PI test rig was constructed to replicate a production machine. As such the 3PI test-rig presented poor control over the dose volume which leads to variation in vertical stress, the pre-compaction of the powder bed and hence the dose weight. These variations could replicate the problems in the manufacturing environment due to the relatively large tolerances in the equipment design. However its mechanical design bears little resemblance to the machines used in manufacturing and is less likely to represent all the problems in the production machines. The experimental work in this test-rig complemented the understanding of the variations of the dose weight in dosator operation.

Chapter 10

Concluding Remarks and Recommendations for Further Work

10.1.   Concluding remarks

The conclusions drawn from the work presented in this thesis are presented below in terms of the initial and revised objectives of the project outlined in chapter 1, section 1.2.

10.1.1. Dosator operation

The outputs in this research demonstrated that the dose weight obtained is strongly affected by powder flow properties and machine settings. Thus, machines parameters such as dosator speed, clearance at the end of the stroke and additional manufacturer features should be adjusted according to the flow properties of the powder to be dosed. Dosator production machines are often designed inadequately because product manufacturers provide placebos for the machine design that are unrepresentative in terms of the flow behaviour of final pharmaceutical powdered blends.

There is a limited comprehension of the dosator operation by the powder and equipment manufacturers and this is due to the absence of a scientific understanding of the dosator operation. This lack of process understanding has led to:

- limited research in solid dosage manufacturing correlating powder flow characteristics, machine settings and product requirements,

- poor control of the dose volume and dosator position during manufacturing, due to tolerances in the design/assembly of the production machines and poorly understood machine settings that compromise the final product dose weight,

- development of various dosator operation principles, by different dosator equipment manufacturers, that have been standardised by trials and error. If a successful dosating

principle were found, all the different dosator equipment manufacturers would copy this.

- uncontrolled dose manufacturing can affect the strength, dissolution, delivery device performance and potency of dosator doses.

Manufacturing engineers and formulators in the pharmaceutical industry do not work together in the development of new products. Therefore, the dose manufacturing problems that arise at the launch of the new product could be avoided or anticipated if powder flow properties of the powder were measured at the formulation stage.

This thesis studied in depth the dosator operation through the literature reviewed, observations in the production process, information gathered from powder and machine manufacturers, dosator demonstrator and The Wolfson Centre and 3PI single shot test-rigs. The mentioned sources provided this research project with an advanced understanding of the dose manufacturing and the factors affecting the dose weight in the dosator operation.

The phenomenological approach proposed by this thesis, gives an explanation of the dosator process from the manufacturing point of view integrating powder flow properties and machine settings factors. The approach could provide a unification of dosator operating principles in the market or the standardisation of a new procedure.

The outputs in dose compaction and metering in this research can be applicable to other volumetric filling systems used in the industry such as tableting and tamping filling machines.

10.1.2. Literature reviewed

The literature reviewed provided a good foundation for the understanding of the problems affecting dosator operation. Due to the finality of the pharmaceutical products, to improve the patients' health, the majority of research in this area focus on the chemical properties, blend formulation, dissolution behaviour and potency issues, rather than ensuring that dose manufacturing will provide the requirements for good device delivery performance and efficient potency.

There were limited investigations in the literature reviewed correlating factors of the powder flow properties and machines settings affecting the fill dose weight in dosator operation.

The dosator filling models published in the literature were too simplistic and do not take into the account of the compressibility of the powders, the wall friction issues and the lateral stresses in the dose.

10.1.3. Factors affecting the variation of the fill dose weight

This research work identified the factors affecting the variation of the dose weight in dosator operation and they are categorised into powder flow properties and machine settings.

This thesis provided a complete characterisation of the key flow properties affecting the dose manufacturing. The key powder properties are the:

- compressibility as function of vertical stresses,

- wall friction angle and how this evolves with increasing shear displacement ,

- wall adhesion (wall flow function),

- stress ratio K,

- lateral stress retained,

The compaction curve fitting model proposed by this thesis presented an accurate expression for the bulk density changes as function of normal compression stresses. However, the compaction curve does not replicate the compression mechanism that occurred in the dosator process and overestimated the density of the powders for the dosator operation. The difference is the stress state, in a conventional powder compaction test (as with the QTS texture analyser), the powder is compressed into a confined space and the stress is in active state where the major principal stress is vertical. However in the dosators, the powder in an unconfined bed is being vertically compressed into a confined space where the stress is in passive state and the major principal stress is horizontal.

Lateral stresses, calculated using the stress ratio K, affect the dosator process in the sense that it increases the wall friction as result of the uniaxial compression during the dosator operation. It was proposed the K-meter equipment to measure this property, which it showed satisfactory results.

The manufacturing in the pharmaceutical industry is normally a batch system and the powder flow properties can be affected from batch to batch therefore the flowability characterisation need to be undertaken on each batch, which may necessitate changes in the dosator settings to achieve the required dose weights.

A significant limitation to the measurement of the flow properties was the high stresses occurring in the dosator. These were significantly higher than the upper range of conventional testers. Hence higher stress range tests were developed for the critical compaction curve measurements.

The machine factors encountered in this research affecting the dosator operation are:

- powder bed conditions

- clearance between the dosator tip and the trough at the end of the stroke (gap "h")

Powder bed state was demonstrated to affect the dose weight in the experimental work of this thesis. It is inadequately controlled in the dosator filling machines due to the inefficient re-conditioning system used.

It was also demonstrated that the clearance between the dosator tip and the trough at the end of the stroke is a *critical* factor affecting the dose weight variation and strongly compromises the dose compaction and the dosator forces. This gap is not controlled in current filling machines and its importance in the process is clear.

10.1.4. Dose retention

The dose retention in this research was attributed to the ability of the material to retain stresses, this behaviour is well explained by the cam clay model in soil mechanics theory. This characteristic can be measured in the k-meter equipment proposed in this thesis. This finding is in disagreement with the formation of an arch theory reviewed in the literature.

10.1.5. Powder and soil mechanics theories

The stress distribution in ultimate bearing capacity application of compression of cohesive soils above rock base in shallow foundations, showed potential agreement with the stress distribution of the pre-compaction of the powder bed when the dosator approaches the trough at the end of the stroke. This behaviour in the soil mechanics application illustrates the spreading of the powder and the stresses reflect back from the trough base as the gap "h" approaches zero. Application of an adapted soil mechanics model did not give a large enough increase in the stress by comparison with the experiments.

10.1.6. Concluding remarks regarding to test equipment

This research project used three non-established pieces of test equipment. These were the 3PI and Wolfson Centre single shot dosator test-rigs and the K-meter tester. The latter two test rigs were designed and developed by the author.

The K-meter presented a good approach for calculating the stress ratio K and also led to the identification of the ability of the powders to retain lateral stresses, which was selected as important characteristic in dosator filling processes.

The Wolfson Centre dosator single shot test-rig engineered in this thesis was designed to validate and calibrate the model, to complement the understanding of dosator process and to analyse the affect of machine settings and powder flowability in the variation of the dose weight. The test-rig showed good repeatability of the measured dose weights and dosator filling and ejection forces. It controls the variation of the gap "h" in the process. The test-rig was robust and isolated the speed issues measuring forces against the dosator in the filling of powders. The careful manual preparation of the powder bed in the tests contributed to the accurate measurements of the forces in the system. The tests undertaken in this test-rig demonstrated the effect of the gap "h" and the powder bed state in the variability of the dose weight; also correlated it with the powder flow characteristics of the powders tested.

The Wolfson Centre dosator test-rig was also useful to measure the compaction ahead of the dosator. This is an important factor in current dosator machines where the gap "h" at the end of the stroke is minimal and the spreading behaviour of the powder bed at this proximity is unknown.

The 3PI dosator test-rig, owned by GSK, was used to investigate the speed issues in the dose procurement. The aim was not achieved due to machines instrumentation, assembly and signal processing issues. However it demonstrated that the speed effect was not significant because the measured forces were of a similar magnitude in the two different dosators test rigs. However, these tests also provided valuable information of the problems encountered in production machines and variations in the dose chamber volume due to misalignment and assemblies of the machines.

10.1.7. Dosator model filling and discharge

The analytical model proposed by this thesis, integrated machine settings and powder flow properties in the prediction of the dose weight and dosator forces. It was not possible to validate it, mainly because of discrepancies in the calculation of the compressibility of the powder. Probably the measured compaction curve does not represent the compaction mechanism in dosators; therefore the calculations are affected.

The approach presented in the dosator model could predict dose weights based on the powder flow properties or possibly the powder flow properties require for a given dose requirements or dose requirements for specific product.

10.2. Contribution to existing knowledge

The research work presented in this thesis contributed substantially to the understanding of the dosator process. It has identified the different stages during the filling and ejection of the dosators.

- As the dosator is inserted in the powder bed, the powder entering into the dose chamber is compacted by the wall friction in the operation. Once the dosator is filled up to certain densification state of the dose, the lateral stresses in the system are equal, to the stresses in the powder bed preventing the entrance of any more powder into the dosator.

- As the dosator continues the stroke there is the formation of compacted powder ahead of the tip that spread the powder aside. The cone dimensions showed to form 60^0 with the vertical axis for the powders used in this research.

- When the cone tip contacts the bottom of the trough the forces in the system rise significantly. This cone effect was correlated with the experimental work of this research. The problems arise with the rupture of the cone and the stresses in the system increase considerably affecting the dose weight and forces in the system. The gap "h" at the end of the stroke dictates the level of stresses in the system and the dose compaction. With the dosator retraction, there are some situations overcoming the tensile stresses in the interface dose/powder bed that depend on the flowability of the powders. The dose is then ejected overcoming the wall friction, influenced by the retained lateral stresses of the powder.

A significant contribution of this work was identifying the factors affecting the dose weight variation related to powder flow properties and machine factors were recognised and linked in the powder behaviour during the dosator operation. It was found that the machine setting gap "h" is critical in current dosator operation and triggers other situations that depending on the powder flowability of the powder compromises the dose weight.

The dose retention attributed to the lateral stress retention characteristic of the powders was another finding in this research.

Pre-compaction and spreading ahead of the dosator are important in dosator process and their study can lead to the understanding of powder spreading and stresses applied to the dose. Pre-compaction of the powder ahead of the dosator underside was measured in The Wolfson Centre test-rig and it was observed to change with the compressibility of the dose.

10.3.　Recommendations for further work

It is apparent from the findings of this work that there are number of areas in which further work could usefully be carried out, with a view to advancing the understanding of dosator operation. These are:

- The compaction mechanism in dosators in order to measure the density changes with the vertical compression. In this way it could predict accurately the dose weight in this filling process.

- The pin jamming and the powder build up in dosators can be predicted and measured by combining long wall friction tests with pin jamming test in the 3PI dosator test-rig. These tests might avoid and prevent manufacturing problems such as pin jamming and therefore reactive maintenance to clean the dosator and re-set the system to continue the production.

- The bed conditioning system used in manufacturing is ineffective and does not remove the stress history. The careful preparation used in this study could not be replicated in an industrial process. Therefore a useful programme of investigation would be to investigate alternative automated techniques for loosening the bed to remove the stress history and then reconsolidating to a consistent bulk density.

- The pre-compaction of the powder bed can be investigated by inserting a blade (instrumented with a load cell) into a square/rectangular box containing a bed of powder. The blade is then gradually inserted towards the walls and measures the reflection stresses in the blade with the proximity of constraining wall. This test can provided valuable information about the powder bed spreading at the end of the stroke.

- Additional experimental work in the dosator test-rig using different dose dimensions and bed depths can be undertaken to investigate the dose strength and variability, and also the effect of the pre-compaction of the powder bed with the length of the bed.

- Study the effect of the speed by instrumenting and adjusting the test-rig for this purpose. However, speeds as high as the production machines cannot be achieved in this test-rig because the deceleration at the top of the stroke would disturb the stress state of the powder bed.

10.3.1.   Liaison with equipment manufacturers

During the development of the project, the author visited the machine manufacturers MG2 (Italy) and Harro Höfliger (Germany) to observe the operation and manufacturing of the machines, as well as to exchange knowledge about this process. The Wolfson Centre has been in contact with IMA (Italy) and they are keen on further collaboration for dosator research.

It was noted that they are aware of many of the problems affecting the operation but lack the scientific and academic support to solve them, and rely on development comes from experience and trial and error. The University of Greenwich through this project has taken our understanding of dosator operation far beyond that of the Dosator manufacturers and industrial sponsor.

The manufacturers are keen to improve their knowledge in powder flow behaviour and filling system understanding, but client's demands, a lack of time and academic/scientific support lead them to use provisional solutions.

Other limitation that manufacturers have is the reduced accessibility for the testing of pharmaceutical products before designing the machines. Pharmaceutical companies normally give them a placebo/i.e. cheap powder like Lactose to design their machines, but as we have seen in chapter 5 the flow properties of individual fillers are completely different to the finished product, and hence behaviour in a dosator machine is also completely different. It is therefore no surprise that a dosator optimised for the product filler does not work well in the finished product.

Machine makers are keen to collaborate with academia in the investigation of this process. This initiative can be taken as sponsorship of further investigation to complement this research work.

REFERENCES

A guidebook to particle size analysis, Copyright 2010, Horiba instruments, inc.

Arnold PC, McLean AG, & Roberts AW 1982, 'Storage and flow of bulk solids' paper presented at the seminar Applications in the storage, flow and handling of bulk solids seminar, Tundra bulk solids handling research associates, The University of New Castle, 4-5 April.

ASTM International 2000, *Standard Test Method for Shear Testing of Bulk Solids Using the Jenike Shear Cell* (D6128-00), West Conshohocken, USA.

Augsburger, L 2002, 'In Modern Pharmaceutics' in *Hard and soft shell capsules,* eds, G. Banker and C.T. Rhodes, New York, pp. 335-380

Bolton, MD & Lau, CK 1993, 'Vertical bearing capacity factors for circular and strip footings on Mohr-Coulomb soil', *Canadian Geotechnical Journal,* vol. 30, pp. 1024-1033.

Bradley, MSA & Berry, RJ 2009, 'Evolution of wall friction with realistic displacements wall "Conditioning" and the need to measure wall friction over a long distance of travel', 6TH *International conference for conveying and handling of particulate solids with 10th ICBMH + BULKEX;* Australia, Brisbane, pp.1-6.

Bradley, MSA, Berry, RJ, Sohel, MS, & Reed, AR 2009, 'Wall flow function measurements to assess wall cohesion and adhesion', 6TH *International conference for conveying and handling of particulate solids with 10th ICBMH + BULKEX;* Australia, Brisbane, pp.1-6.

Breitenbach, J 2002, 'Melt extrusion: from process to drug delivery technology', *European Journal of Pharmaceutics and Biopharmaceutics*, vol. 54, pp. 107-117.

British Stainless Steel Association 2012, *British Stainless Steel Association*, viewed 5 June 2012, <http://www.bssa.org.uk/topics.php?article=47>.

Britten, JR, Barnett, MI & Armstrong, NA 1995, 'Construction of an intermittent-motion capsule,' *Pharmaceutical Research*, vol. 12, no. 2, pp. 196-200.

Britten, JR, Barnett, MI & Armstrong, NA 1996, 'Studies on powder plug formation using a simulated capsule filling machine,' *Journal of Pharmacy and Pharmacology*, vol. 48, pp. 249–254.

Brookfield Engineering Laboratories 2012, *Brookfield Engineering Laboratories,* viewed 30 May 2012, http://www.brookfieldengineering.com/education/applications/powder-grated-cheese.asp.

Cerato, AB & Lutenegger, AJ 2006, 'Bearing capacity of square and circular footings on a finite layer of granular soil underlain by a rigid base' *Journal of Geotechnical and Geoenvironmental Engineering,* vol. 132, no.11, pp. 1-6.

Chowhan, ZT & Chow, YP 1980, 'Powder flow studies I. Powder consolidation ratio and its relationship to capsule filling-weight variation,' *International Journal of Pharmaceutics,* vol. 59, pp. 547–550.

Coatsworth, T & Castle, B 1990, *Powder filling machine,* United States patent 4,949,766.

Cole, G 1990, Pharmaceutical production facilities, design and applications, 2nd ed, *Ellis Horwood*, New York; London.

Cole, GC & May, G 1975, 'The Instrumentation of a Zanasi LZ/64 capsule filling machine,' *Journal of Pharmacy and Pharmacology,* vol. 27 no. 5, pp. 353-358.

Copley Scientific, Quality Solutions for the testing of Pharmaceuticals, 2009, Copley Scientific Limited catalogue and guide is Copyright 2009.

Das, BR 2009, Shallow foundations, bearing capacity settlement, 2nd ed, *CRC Press*, London; New York.

DEF Pharma 2011, *DEF Pharma, viewed 18 November 2011,* <http://www.dfepharma.com/en/Excipients/Lactose.aspx>.

Denny, PJ 2002, 'Compaction equations: A comparison of the Heckel and Kawakita equations', *Powder Technology*, vol. 127, pp. 162 – 172.

Duffield, HP 2005, *Method and Apparatus for Transferring a Defined Quantity of Powder*, United States Patent 6886612 B2.

Edwards, D 2010, 'Application of capsule dosing techniques for use in dry powder inhalers,' *Therapeutic Delivery*, vol. 1, no 1, pp. 195-201.

Farnish, RJ, Berry, RJ & Hernandez, E 2012, 'The effect of segregation on handling characteristics' paper to be published at *The BulkSolids Europe*, Germany, Berlin, pp. 1-5.

Gamberini, EN 1985, *Method for filling containers with metered quantities of powdered materials,* United States Patent 4542835.

Gold, G, Duvall, RN, Palermo, BT & Hurtle, RL 1971, 'Granule strength as a formulation factor I; Instrumentation,' *Journal of Pharmaceutical Science,* vol. 60, no. 6, pp. 922-925.

Gold, G, Duvall, RN, Palermo, BT & Slater JG 1966, 'Powder flow studies II, Effect of glidants on flow rate and angle of repose,' *Journal of Pharmaceutical Science,* vol. 55, no. 11, pp. 1291-5.

Gold, G, Duvall, RN, Palermo, BT & Staler, JG 1968a, 'Powder flow studies II. Effect on glidants on flow rate and angle of repose,' *Journal of Pharmaceutical Science,* vol. 55, no. 11, pp. 1291-1295.

Gold, G, Duvall, RN, Palermo, BT & Staler, JG 1968b, 'Powder flow studies III. Factors affecting the flow of lactose granules,' *Journal of Pharmaceutical Science*, vol. 57, no. 4, pp. 667-671.

Guo, M, Muller, F & Augsburger, L 2002, 'Evaluation of the plug formation process of silicified microcrystalline cellulose,' *International Journal of Pharmaceutics*, vol. 233, pp. 99-109.

Harro Höfliger *Laboratory filler Omnidose.* Harro Höfliger.

Heda, PK, Muteba, K & Augsburger, LL 2002, 'Comparison of the formulation requirements of dosator and dosing disc automatic capsule filling machines', *AAPS PharmaSci,* vol. 4, no. 3, pp. 1-16

Hillery, AM, Lloyd, AW, Swarbrick, J 2002, Drug Delivery and Targeting for Pharmacists and Pharmaceutical Scientists, viewed 31 October 2008, <http://www.mylibrary.com/browse/open.asp?ID=2178&loc=cover >.

Howard, PD 2005, *Method and apparatus for transferring a defined quantity of powder,* United States patent 6,886,612 B2.

IMA *Low-medium speed capsule filling machines,* Zanasi *2008* Bologna: IMA active division.

Irwin, GM, Dodson, GJ, & Ravin, LJ 1970, 'Encapsulation of clomacran phosphate {2-chloro-9-[3-(dimethylamino) propyl] acridan phosphate}. I. Effect of flowability of powders blends, lot-to-lot variability, and concentration of active ingredient on weight variation of capsules filled on an automatic filling machine,' *Journal of Pharmaceutical Sciences*, vol. 59, pp. 547–550.

Jenike, AW 1961, 'Gravity Flow of Bulk Solids' *Utah Engineering Experimental Station*, University of Utah, Bulletin 108, 1961.

Jenike, AW 1964, 'Storage and flow of solids' *Utah Engineering Experimental Station*, University of Utah, Bulletin 123, 1964.

Jolliffe, IG & Newton, JM 1978, 'Powder retention within a capsule dosator nozzle,' *Acta Pharmaceutical Technology*, vol. 30, pp. 41

Jolliffe, IG & Newton, JM 1980, 'The effect of powder coating on capsule filling with a dosator nozzle.' *Acta Pharmaceutical Technology*, vol. 26, pp. 324-326

Jolliffe, IG & Newton, JM 1982, 'Practical implications of the theoretical consideration of capsule filling by the dosator nozzle system,' *Journal of Pharmacy and Pharmacology*, vol. 34, pp. 293–298.

Jolliffe, IG & Newton, JM 1983a, 'Extension of theoretical considerations of the filling of pharmaceutical hard gelatin capsules to the design of dosator nozzles,' *Powder Technology,* vol. 35, pp. 151–157.

Jolliffe, IG & Newton, JM 1983b, 'Capsule filling studies using an mG2 production machine,' *Journal of Pharmacy and Pharmacology*, vol. 35, pp. 74–78.

Jolliffe, IG & Newton, JM 1983c, 'The effect of dosator nozzle wall texture on capsule filling with the mG2 simulator,' *Journal of Pharmacy and Pharmacology*, vol. 35, pp. 7–11.

Jones, BE 2001, 'The filling of powders into two-piece hard capsules,' *International journey of Pharmaceutics, no.* 227, pp. 5-26.

Jones, EB 2006, 'Tablets & Capsules: Evolution of the Technology for Filling Two-Piece Hard Capsules With Powders,' CSC Publishing, *advertiser 2006*.

Khawam, A & Schultz L 2011, 'Modelling powder encapsulation in dosator-based machines: II. Experimental evaluation,' *International Journal of Pharmaceutics,* vol. 421, pp. 210-219.

Khawam, A 2011, 'Modelling powder encapsulation in dosator-based machines: I. Theory,' *International Journal of Pharmaceutics,* vol. 421, pp. 230-209.

Mandel, J & Salençon, J 1972, 'Force portante d'un sol sur une assise rigide (étude théorique),' *Géotechnique,* vol. 22, no. 1, pp. 79-93.

Marshall, EA 1967, 'The compression of a slab of ideal soil between rough plates,' *Acta Mechanica,* vol. 3, no. 2, pp. 82-92.

Mehta, AM & Augsburger, LL 1980, 'Simultaneous measurement of force and Displacement in an automatic capsule filling machine,' *International Journal of Pharmaceutics*, vol. 4, pp. 347-351.

Mehta, AM & Augsburger, LL 1981, 'A preliminary study of the effect of slug hardness on drug dissolution from hard gelatin capsules filled on an automatic capsule-filling machine,' *International Journal of Pharmaceutics,* vol.7, pp. 327-334.

Meyerhof GG & Chaplin TK 1952, 'The compression and bearing capacity of cohesive layers', *British journal of applied physics,* vol. 4, no. 1, pp. 20-26.

Meyerhof, GG 1951, 'The ultimate bearing capacity of foundations,' *Géotechnique,* vol. 2, no. 4, pp. 301-332.

Meyerhof, GG 1974, 'Ultimate bearing capacity of footings on sand layer overlying clay,' *Canadian Geotechnical Journal,* vol. 11, no. 2, pp. 223-229.

MG2 *Powder dosing unit, MG2* 2004, Italy.

Nagaraj, TS & Miura, N 2001, Soft clay behaviour, analysis and assessment, *A.A. Balkema,* Totterdam; Brookfield.

Nedderman, RM 1992, Statics and kinematics of granular materials, *Cambridge University Press,* Great Britain.

Newton, JM & Bader, F 1981, 'The prediction on the bulk densities of powder mixtures and its relationship to the filling of hard gelatin capsules,' *Journal of Pharmacy and Pharmacology,* vol. 33, pp. 621-626.

Patel, AS 2011, 'A mathematical model to predict the deblending of pharmaceutical powder when discharged from an intermediate bulk container into an unvented chute,' PhD. Thesis, University or Greenwich.

Pfeifle, TW & Dass, BM 1979, 'Bearing capacity of surface footings on sand layer resting on a rigid rough base,' *Japanese Geotechnical Society,* vol. 19, no. 1, pp 1-11.

Podczeck, F & Jones, BE 2004, Pharmaceutical Capsules, 2nd edn, *Pharmaceutical Press,* London SE1 7JN.

Podczeck, F & Miah J 1996, 'The influence of particle size and shape on the angle of internal friction and the flow factor of unlubricated and lubricated powders,' *International Journal of Pharmaceutics,* vol. 144, pp. 187-194.

Podczeck, F 1999, 'Investigations into the reduction of powder adhesion to stainless steel surfaces by surface modification to aid capsule filling,' *International Journal of Pharmaceutics,* vol. 178, pp. 93-100.

Podczeck, F, Blackwell, S, Gold, M & Newton, M 1999, 'The filling of granules into hard gelatine capsules,' *International Journal of Pharmaceutics,* vol. 188, pp. 59-69.

Prandtl, L 1923, 'Anwendungsbeispiele zu einem Henckyschen satz über dasplastische gleichgewicht,' *Zamm,* vol. 3, no. 6, pp.401-406.

Prescott, JK & Barnum, R 2000, *On Powder Flowability*, viewed 23 March 2008 <http://www.jenike.com/Articulos/on-powder-flowability.pdf>.

Reier, G, Cohn, S, Rock, S & Wagenblast, J 1968, 'Evaluation of factors affecting the encapsulation of powders in hard gelatin capsules I,' *Journal of Pharmaceutical Sciences,* vol. 57, pp. 660–666.

Ridgway, K 1987, *Hard capsules, development & technology*, The Pharmaceutical Press, London.

Ridgway, WA & Armstrong, A 2008, Tablet and Capsule Machine Instrumentation, *The pharmaceutical press*, London.

Rowley, DJ, Hendry, R, Ward, MD & Timmins, P 1983, 'The instrumentation of an automatic capsule filling machine for formulation design studies', *in Proceedings of the 3rd international conference on pharmaceutical technology*, Merseyside, pp. 287-291.

Schulze, D 2008, *Powders and Bulk Solids,* Springer, Berlin.

Small, LE & Augsburger, LL 1997, 'Instrumentation of an automatic capsule-filling machine,' *Journal of Pharmaceutical Science*, vol. 66, no. 4, pp. 504-509.

Standar Test Method 2006, *Shear testing of bulk solids using the jenike shear cell* (D 6128-06), ASTM, United States.

Stegemann, S 2002, *Hard Gelatine Capsules Today - and Tomorrow,* Capsugel, viewed 5 June 2011, <http://capsugel.com/media/library/hard-gelatin-capsules-today-and-tomorrow.pdf>.

Tan, SB & Newton, JM 1990a, 'Capsule filling performance of powders with dosator nozzles of different wall texture,' *International Journal of Pharmaceutics*, vol. 66, pp. 207–211.

Tan, SB & Newton, JM 1990b, 'Influence of compression setting ratio on capsule fill weight and weight variability,' *International Journal of Pharmaceutics,* vol. 66, pp. 273–282.

Tan, SB & Newton, JM 1990c, 'Minimum compression stress requirements for arching and powder retention within a dosator nozzle capsule filling machine,' *International Journal of Pharmaceutics*, vol. 63, pp. 275–280.

Tan, SB & Newton, JM 1990d, 'Observed and expected powder plug densities obtained by a capsule dosator nozzle system,' *International Journal of Pharmaceutics* Vol. 66, pp. 283–288.

Tan, SB & Newton, JM 1990e, 'Powder flowability as an indicator of capsule filling performance,' *International Journal of Pharmaceutics*, vol. 61, pp. 145–155.

Tan, SB &Newton, JM 1990f, 'Influence of capsule dosator wall texture and powder properties on the angle of wall friction and powder-wall adhesion,' *International Journal of Pharmaceutics*,' vol. 64, pp. 227-234.

Tarozzi, G, Rivalta, R, Roberto, T & Ragazzini P 2006, *Method for optoelectronically inspecting pharmaceutical articles,* United States patent 7,012,242 B2.

Terzaghi, K 1943, *Theoretical soil Mechanics*, John Wiley and Sons, Inc, New York – London.

Vesky, P & Marvola, M 1991, 'Design and use of equipment for simulation of plug formation in hard gelatin,' *Acta Pharmaceutica Fennica,* Nov, no.100, pp.19-25

Woodhead, PJ & Newton, JM 1981, 'The influence of nozzle / piston clearance on the efficiency of a capsule-filling dosator,' *Journal of Pharmacy and Pharmacology*, Suppl. 33, 21P.

Woodhead, PJ, Hardy, JG & Newton, JM 1982, 'Determination of the porosity variations in powder beds,' *Journal of Pharmacy and Pharmacology*, vol. 34, pp. 352–358.

Appendixes

Appendix 1

Dosator Design

The industrial sponsor provided the dosator used in this research. It has the main dimensions of a MG2 dosator. The dosator was part of GSK design improvements trials in collaboration with 3PI. The figure A1.1 shows the dosator designed used in this research; the pin's shaft had three lobes that were removed for assembly issues to The Wolfson Centre dosator single shot test rig. The internal diameter of the dosator body is 3.4 mm and the pin's diameter is 3.375 mm as it can be seen in the figure A1.1.

a)   b)
Figure A1.1. Dosator design: a) dosator body; b) dosator pin.
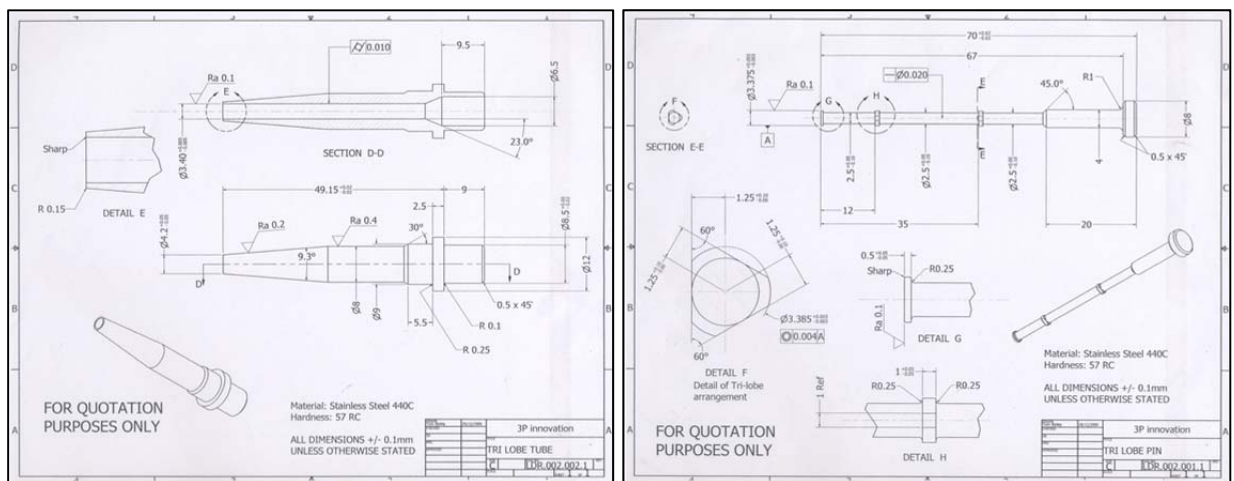
Appendix 2

Janssen Effect Application

As mentioned in the chapters 4 and 8, the Janssen effect is used to illustrate distribution of internal stresses in silos. For the bulk solid, in silos, the self weight is partially supported by the wall friction around the circumference of the slice and the pressure curve decays exponentially to an asymptotic value at a great depth (typically 4 diameters) in the silo. By comparison for the liquids where there is no wall friction the pressure increases linearly with the depth.

One of the specific applications of the Janssen effect is applied to force a column of bulk solid material to flow up a circular tube (Arnold, McLean & Roberts 1982, p. 1.7 and Schulze 2008, p. 263) as illustrated in the figure 2.35 in chapter 2.

From this situation is possible to find the minimum stress in the piston to force the column of bulk material upwards from the force balance (Arnold, McLean & Roberts 1982, p. 1.7 and Schulze 2008, p. 259-263).

With the assumptions of constant vertical stress σ_v, and bulk density ρ, the equilibrium of forces gives:

$$\sigma_z.A + g.\rho.A.d_z + \tau_w.U.d_z = (\sigma_z + d\sigma_z) \qquad \text{[A1.1]}$$

where U is perimeter and A cross section area. The friction stress is calculated as:

$$tan(\varphi) = \tau_w/\sigma_h \qquad \text{[2.5] [A1.2]}$$

due to uniaxial compression in a constrain space it is possible to define stress ratio K as:

$$K = \sigma_h/\sigma_v \qquad \text{[2.4] [A1.3]}$$

re-arranging [A1.1] a first order differential equation for the vertical stress is obtained,

$$\frac{d\sigma_v}{d_z} - \sigma_v.K.\frac{U}{A}.tan(\varphi) = g.\rho \qquad \text{[A1.4]}$$

Where A/U=D/4 for cylinders. The equation has the form y'+a(x)y=b(x) that can be solved using the integral factor $f(x) = e^{\int a(x)dx}$ and the solution is $y.f(x) = \int f(x).b(x).dx + c$. Therefore the integral factor:

$$f(z) = e \int \frac{-\tan(\varphi).k.u.dz}{A} \qquad\qquad [A1.5]$$

and the solution:

$$\sigma_v.e^{\int \frac{-\tan(\varphi).k.U.dz}{A}} = \int e^{\int \frac{-ta(\varphi).k.U.dz}{A}}.(g\rho.dz) + C \qquad [A1.6]$$

Assuming ρ, φ and k constant, the bordering condition of the surcharge stress, σ_{vo}, acting on the top of surface is $\sigma_v = \sigma_{v0}$ when z=0; therefore:

$$\sigma_{vo} + \frac{g.\rho.A}{k.\tan(\varphi).U} = C \qquad [A1.7]$$

The solution is:

$$\sigma_v = -\frac{g.\rho.A}{K.\tan(\varphi).U} + \left[\sigma_{vo} + \frac{g.\rho.A}{K.\tan(\varphi).U}\right].e^{\frac{K.\tan(\varphi).U.Z}{A}} \qquad\qquad [2.6]\ [A1.8]$$

Without surcharge stress (σ_{vo}) it follows:

$$\sigma_v = \frac{g.\rho.A}{K.\tan(\varphi).U}\left[e^{\frac{K.\tan(\varphi).U.Z}{A}} - 1\right] \qquad\qquad [2.7]\ [A1.9]$$

Appendix 3

Permeability Test

Permeability tests were undertaken to the powders used in this research and below it is described the test procedure and results.

Two of the major factors affecting the tests were the chamber geometry and the vacuum airflow rate. Due to the low density of the pharmaceutical powders, it was not possible to blow air into the system since the powders did not show adequate resistance and the whole powder sample end up being displaced upwards without any drop pressure. The system was vacuumed instead showing better response to the test. The test was noticed to be dependent of the flowability of the powder and the sample dimensions.

The figure A3.1a shows the permeability test sketch used in this thesis, where the air was vacuumed across the sample passing through a membrane; the airflow was controlled by a flow meter and a monometer recorded the drop pressure in the system. Two membrane diameters where used (see figure A3.1b and c), for a range of specimen heights. It was difficult to find an optimal standard relation between the airflow, diameter and height of the sample for all the materials used; in some cases, it was observed a rapidly crack formation before to be able to measure any drop pressure (see figure A3.1d).
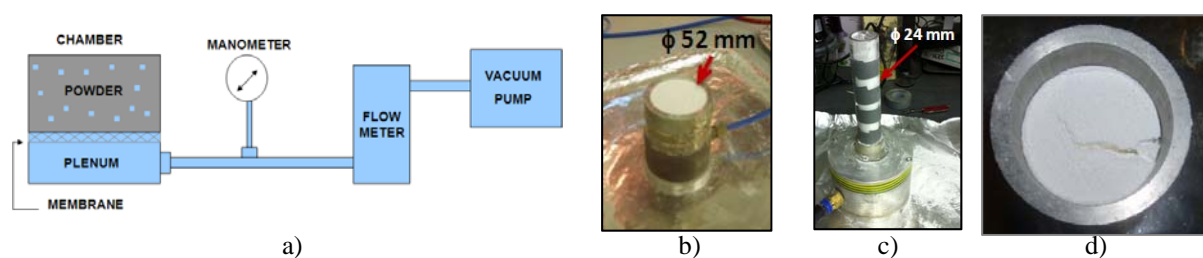

Figure A3.1. Permeability test used in this research: a) test sketch; b) test with Φ 52 mm sample; c) test Φ 24 mm; d) crack during test. For full explanation refer to the text.

The permeability was measured using a permeability factor equation [A3.1] described by Arnold, McLean & Roberts (1982) as it follows:

$$c = \frac{h}{\Delta p} \cdot \frac{Q}{A} \quad \left[\frac{m^4}{N\,min}\right] \qquad \text{[A3.1]}$$

Where "c" is the permeability factor, "h" height of the sample, "Δp" pressure drop across de sample, "Q" air volumetric flow rate and "A" cross sectional area of the test cylinder.
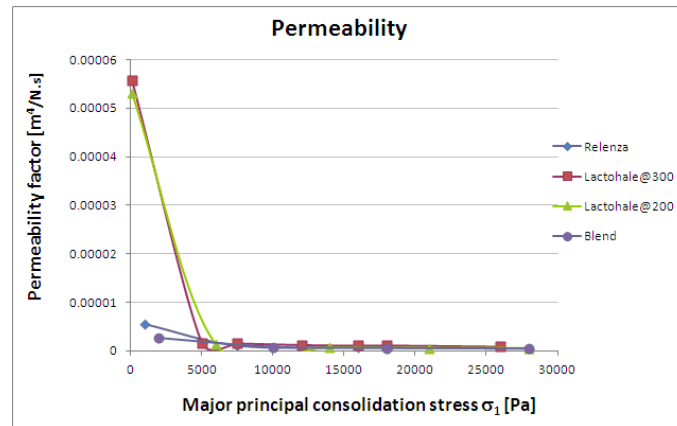

Figure A3.2. Permeability test results of the powders used in this research.

The geometry of the cylindrical sample used in the permeability test was a diameter of 24 mm and height of 154 mm for range of airflow sets and powders. The geometry was chosen empirically based on the best powder response during the tests. The figure A3.2 shows the permeability test results undertaken in this thesis; the results were not satisfactory and it is advisable a deep study of this dosator parameter.

Appendix 4

Particle Size Distribution (PSD)

There are several techniques to measure particle size but rarely two of them will be in agreement. These techniques generally use standard statistical calculations such as a mean or standard deviation, to process the results (Horiba instruments customer leaflet). Depending on the manufacturer, the results are expressed as volume or mass percentage as function of particles size distribution; that could be presented a sphere diameter of equivalent volume, surface area, weight, and so on.

The main techniques are:

- Image analysis; among which stand out optical microscopy (measures particles up to 150 µm) and scanning electron microscopy (SEM). The last one is useful for particles below 1 µm.

- Sieving; it is the most common method used, where the powder is passed through series of decreasing sizes of mesh. There are two methods; dry sieving if vibration is used to push the particles, or wet if a liquid is used instead of the vibration. The most common is the dry sieving, being limited by the particles size (up to 50 µm) and time consuming (it could take half an hour to complete a test).

- Spectrometry; it uses radiation of energy. It can be found two main methods, laser diffraction and near infrared (NIR) spectroscopy. The first one is the most common used in the industry and works on the principle of scatter light at an angle whose logarithm is inversely proportional to particle size; it measures the particle in random orientation, giving average of the diameter of equivalent volume sphere.

- Electrozone sensing; where particles flow through an orifice with two electrodes giving a voltage pulse.

From the mentioned techniques, the most frequently used are sieving and laser diffraction. Laser diffraction generally reports the media particle size below of the 10, 50 and 90 % (D10, D50 and D90) based on the volume distribution. D50 represents the media of the particles

diameter where half of the population lies below this value (Horiba instruments customer leaflet).

The figure A4.1 shows an example of particle size distribution data; in this case it was used laser diffraction technique with the Malvern Mastersizer S. The material used was a *bimodal blend* of Lactose monohydrate and it can be seen from the graph two solid heaps that represents the fine and coarse fractions of the Lactose blended; it can be seen also the quantity of these powders in the blend in the area occupied under the curve. This curve uses the primary "Y" axis that corresponds to the differential accumulative volume of the sample. The values of the D10, D50 and D90 of this test were respectively: 2.88, 69.07 and 140.44 μm that are represented in the curve using the volume percentage of the sample in the secondary "y" axis.
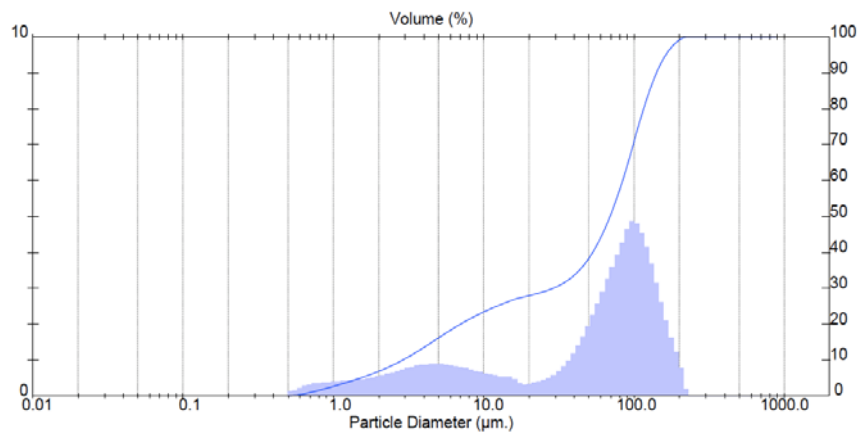

Figure A4.1. Example of particle size distribution of lactose *bimodal blend* in the Malvern Mastersizer S. Snapshot of the results presentation from the Mastersizer S software. For full explanation refer to the text.

Appendix 5

Moisture Content Test

Three of the four powders used in this research were pure/mix Lactose forms. Lactose was found to be not sensitive to high temperature and humidity levels. This was confirmed by moisture contain test and Lecturer of the School of Science at the University of Greenwich[1]. The weight increment in the tests for the powders used in this research was in between 0.15 and 0.35% at 80% RH. It was also stated in the Lactose powders technical sheets that the maximum water loss when drying is maximum 0.2 and 0.5 % correspondingly. One of the possible reasons is because lactose contains one internal molecule of water in its structure and only at extreme temperatures and relative humidity conditions this water molecule can be detached[2].

The figure A5.2 show the results of the moisture contents test undertaken at 30^0 C with increments of 30 to 80 of RH% at The Wolfson Centre environmental chamber. It was prepared three samples of each powder of 2 grams each and they were weighed when the conditions in the system were stable (approximately every 24 hr).
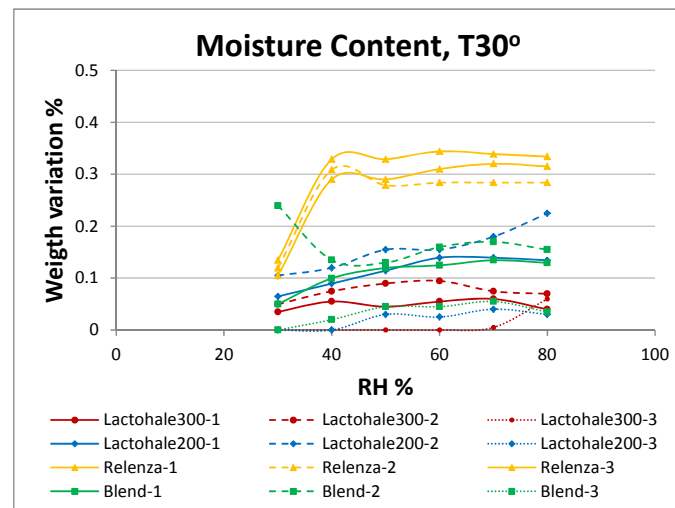

Figure A5.1. Moisture content test.

As it can be seen in the figure A5.1, the powders used in this research were not sensitive to moisture.

---

[1] Confirmed by Dr. Ali Nokhodchi, Lecturer at the School of Science at the University of Greenwich.
[2] DFE Pharma website www.dfepharma.com

Appendix 6

Bulk Density Property Measurement

1.   Introduction

In this thesis, it was used the compaction curve (CC) to study the changes of the density as function of the normal stress of all the powders tested in this work research. The CC is an easy and practical test that shows the compressibility of the powders in the possible range of the working loads in the industrial applications.

The principle of the CC test is similar to the uniaxial test mentioned in the chapter 2; the main difference is that the sample is always in the cylindrical mould and the walls neither are nor removed. The sample is vertically compressed until reaching the maximum normal load desired. The load and the changes in the sample volume are measured simultaneously; with this information the CC is plotted and it is expressed the density of the powder as function of the normal stress applied.

This appendix presents the equipment instrumentation and methodology details (sections 2 and 3) not mentioned in the chapter 5 related to the calculation of the compaction curve carried out in this thesis; in the same way some relevant results.

2.   Equipment and instrumentation

There could be several testers and methods to measure the CC; in this thesis it was used Brookfield QTS texture analyser (also called uniaxial tester) and a Civil Engineering uniaxial compression tester used to compress concrete samples (see figure 5.13 in chapter 5).

All the testers work under similar principle. The QTS operates by descending a beam to compress the sample allocated in a cylindrical cell; the software digitally displays the results of the force and displacement of the beams. Conversely, in the Civil Engineering tester the sample is pushed against the beam connected to a proving ring gauging the compression

force; the data is collected manually reading the dials connected to the beam gauging the beam's displacement and compression of the proving ring.

The QTS has force sensor with a range up to 10 kg and the Civil Engineering tester has a proving rings with a range from 2 to 28 kN. The flexibility of the sample dimensions was an advantage of these testers.

The dosator stresses measured in the experimental work of this thesis were approximately 2.5 MPa (see chapter 7, section 7.3.2), therefore it was sought a compaction curve test measuring the compression characteristic of the powders at the same stress range. The QTS with the sample dimensions like the Jenike shear cell (diameter of 95 mm and height of 16 mm) reached 10 kPa and it was far from the stress range required. Even reducing the cell sample to diameter and height to 22X4 mm respectively (to maintain the cells dimension relation and correlate the results) was obtained 800 kPa.

Due to the superior load range in between the testers, the Civil Engineering compression tester was considered to measure the CC in the stress interval were the QTS did not extent and the results are shown in the section 3. However, the experimental work with this with the Civil Engineering compression tester was fraught with difficulties, preparing and placing the samples, locating the starting point of the compression, reading simultaneously the force and displacement values from dials and the poor sensitivity at low stresses. The key problem was that the powder sample was pushed upwards against the compression plate, which had a larger diameter than the sample cell; therefore it was necessary to place a shallow cylindrical piston on top of the sample to apply the compression. The self-weight of the piston compacted the sample by an unmeasured value, which was estimated to be 0.1 mm. The sample used in this tester had diameter and height of 22X4 mm in order to achieve 70 MPa and maintain the proportion of the Jenike shear cell.

The Brookfield QTS Texture Analyser was the selected tester to quantify the CC because it showed better results and accuracy than the other testers considered in this thesis to measure this property in the range of dosator operation stresses.

3.   Methodology

The initial tools to measure the CC at high stresses in this research were the QTS and the cell used for the Jenike shear cell test. In order to be able to reach high stresses occurring during dosator operation, the sample rings dimensions were reduced. A range of cell rings were used with diameters and heights of 95x16, 54x14, 22x4, 22x15, 10x10 and 7.5x7.5 mm respectively (see figure A6.1). The first three cell dimensions where proportional reduced to keeping the same dimensions ratio of the Jenike shear cell. It was necessary to gradually reduce the dimensions of the cell to make sure that the compaction curve was accurate and followed the same trend. These cell areas generated compaction stresses of; 0.01, 0.04, 0.3, 0.3, 1.2 & 2.2 MPa when used in conjunction with the standard 10 kg load cell of the QTS.

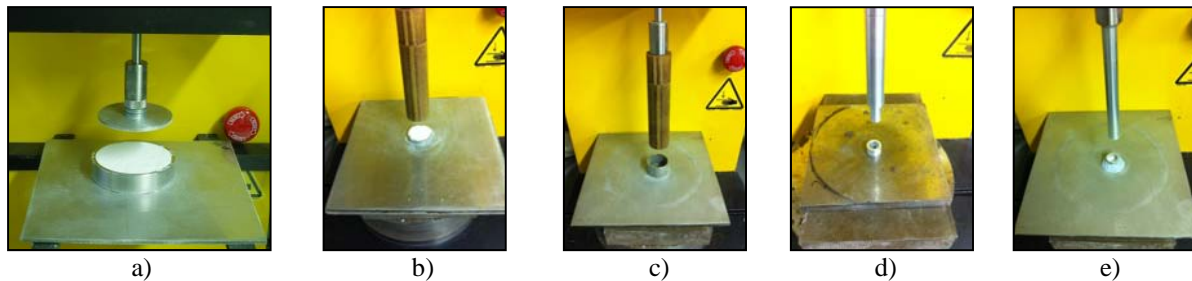| a) | b) | c) | d) | e) |

Figure A6.1. Cells used in the Brookfield QTS Texture Analyser to measure the compaction curve; dimensions of the cell diameter and height were: a) 54x14 mm; b) 22x4 mm; c) 22x15 mm; d) 10x10 mm; e) 7.5x7.5 mm. For full explanation refer to the text.

The sample was carefully prepared by breaking the lumps and trying to avert voids in the sample. Then, the maximum load of the tester was applied by the beam/plunger at speed of 0.5 mm/s. The speed of the plunger can be adjusted, but it was decided to set it low for better test resolution and increase the measured points at high stresses.

According to the manufacturer's technical sheet the accuracy of the load is $\pm$ 1 g and the displacement $\pm$ 0.1 mm. The variance of the load would not affect significantly the test measurements, may be at low stresses, but the displacement tolerance could affect the results depending on the cell size.

4.   Results, compaction curve model

It was chosen one of the powders used in this thesis to first present the CC results and explain the process followed to determine the suitable test for the dosator operation powder

characterisation. The normal stress units in the results presented in this section are expressed in Pascal's; as the model proposed by this thesis uses the CC in this format.

The figure A6.2 shows the *Relenza* CC results from all the testers mentioned above. The vertical axis scale was reduced for illustration purposes because all the tests had different stress range. It is presented three QTS set of tests corresponding to three diverse sample dimensions and two tests in the Civil Engineering compression tester using range of compression rings.

It can be appreciated the good agreement of the results in between the QTS tests and the two Civil Engineering tests. The last one showed good repeatability with the different ring and slightly concordance with the trend of the QTS tests; bearing in mind that the distance was altered to take account of the volume reduction of the block placed on the top of the sample. The tests with the 28 kN compression ring reflected the poor sensibility of the test at low stresses; with this ring was possible to achieve pressures up to 70 MPa.
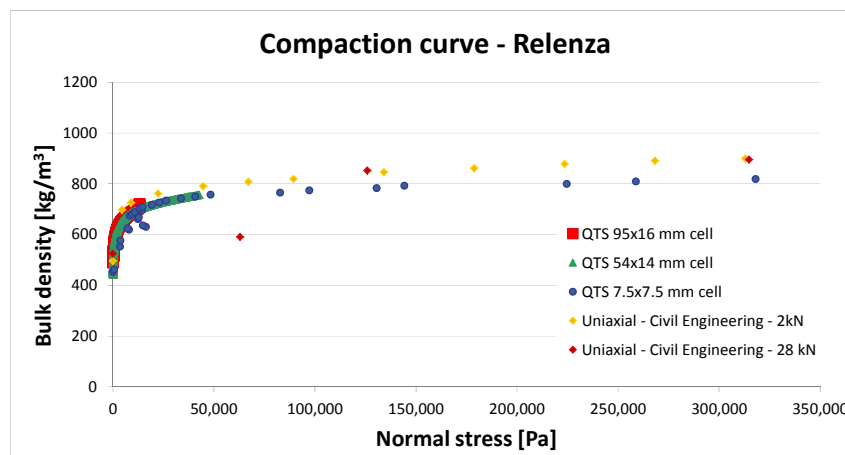

Figure A6.2. *Relenza* compaction curve results using different testers and sample dimensions. For full explanation refer to the text.

There was an issue selecting the tester that would provide the best trend for the powder compression; the cell size to achieve high stresses in these tests was small, doubting about the reliability of the tests. The diameter and height dimensions were 22x4 and 7.5x7.5 mm for the Civil Engineering and QTS testers respectively.

The figure A6.3 shows the tests undertaken in this research in the large range of stresses; three set of tests with the Civil Engineering compression tester using the two compression rings and one set in the QTS with the smallest sample cell. The tests with the civil

engineering tester showed good repeatability but the trend was higher than the QTS results tendency; this can be attributed to the reason exposed above about the procedure of this tests. This was another reason to discard the Civil Engineering uniaxial compression test and use the QTS tester to measure the CC.
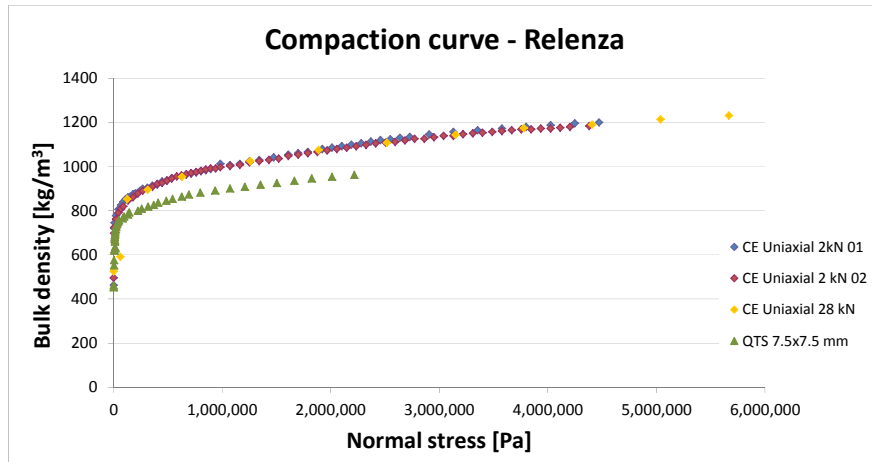

Figure A6.3. *Relenza* compaction curve results using the Civil Engineering uniaxial compression and QTS testers. For full explanation refer to the text.

The figure 5.14 in chapter 5 shows the CC's measured in the QTS using the range of cell sizes. It could be seen the good agreement between the curves maintaining the compaction trend. From the above data and the figure 5.14 in chapter 5, it can be appreciated that the QTS CC (using the cell with diameter and height of 7.5x7.5 mm respectively) showed the best approach to address the bulks density property. It was also seen how small increments in the CC trend yield to significant density values at high stresses and it is important for dosator operation to use the correct technique to characterise this property.
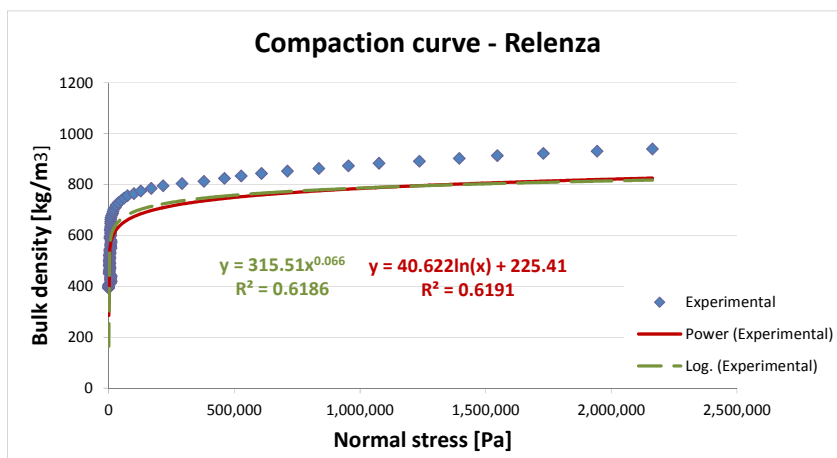

Figure A6.4. *Relenza* compaction curve trend lines using excel tool; test undertaken it in the Brookfield QTS texture analyser. For full explanation refer to the text.

The results from the QTS tests presented significant scatter, which is function of the wide range of data, test speed and signal noise, wherefore precluded the normalisation of data to quantify deviations. This scatter also leads to miscalculations using the trend fitting data tool in excel to obtain a relation of the density as function of the stresses. The figure A6.4 shows the Excel logarithmic and power trend lines for *Relenza* data set.

Consequently, it was considered to alter the data to remove the noise and reduce the amount of data at lower stresses and correct the trendlines, but this process was inaccurate and time consuming. For some powders this technique was satisfactory, but for some others did not meet the expectations. The figure A6.5 shows the CC logarithmic and powder trend lines for *Relenza* and *Lactohale300*. In general the logarithmic trend line showed the best curve fitting for all the powders used in this research.
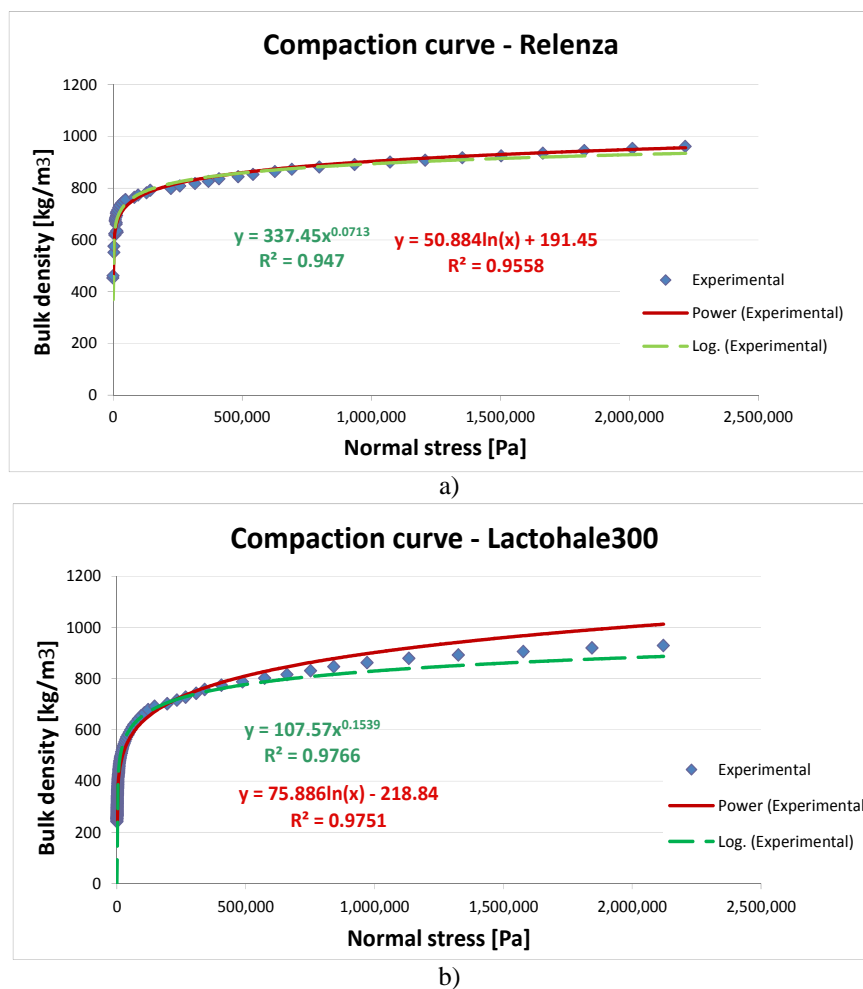

a)

b)

Figure A6.5. Compaction curve trendlines reducing the scatter in the signal; tests undertaken in the Brookfield QTS texture analyser: a) *Relenza*; b) *Lactohale300*. For full explanation refer to the text.

In the figure A6.5 can be seen the good data fitting for *Relenza* but the inaccurate for *Lactohale300*. These graphs suggest that this technique is not suitable for the data fitting of the CC. There is another fact in the Excel trend lines, the experimental data of the CC does not start from the origin, it starts from the poured density value and these trend lines methods fit the data from the origin.
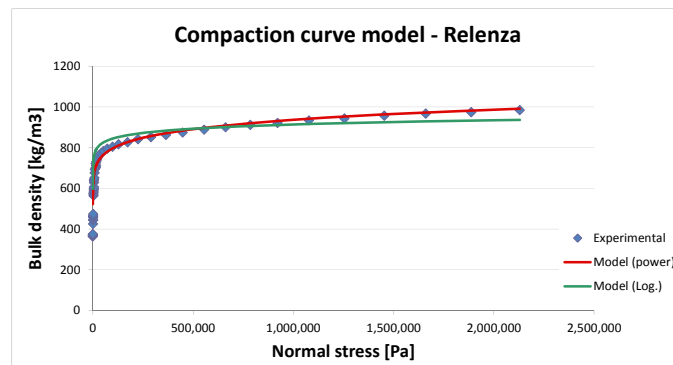

Figure A6.6. Logarithmic and powder curve fitting model. For full explanation refer to the text.

Taking into the account the need to curve fit the data and bearing in mind that it is one of the most important flow properties in dosator operation, this thesis proposes a straightforward model to fit the data of the CC. The model consists in the addition of the "Y" axis intercept using either the form $y=(a.ln(x)+b)+c$ or $y=(a.x^b)+c$ and it was explained in chapter 5, section 5.4.4. Although logarithmic trendline showed better fitting of the data, the power compaction curve fitting model presented better fitting of the data. The figure A6.6 shows both the logarithmic and exponential compaction curve model.

The density of the powders seemed to keep slowing increasing with the stresses (see figure 5.17 in chapter 5); therefore the CC curve fit model proposed in this research was extended to higher stress range and showed a good trend. The figure A6.7 shows this trend. *Lactohale300* and the *bimodal blend* exhibited larger increments at double of the stress range measured in the dosator operation. *Lactohale300* and *bimodal blend* curves are stepper and seemed to carry on compressing it. The *Lactohale200* curve is less steep with tendency to stabilise.
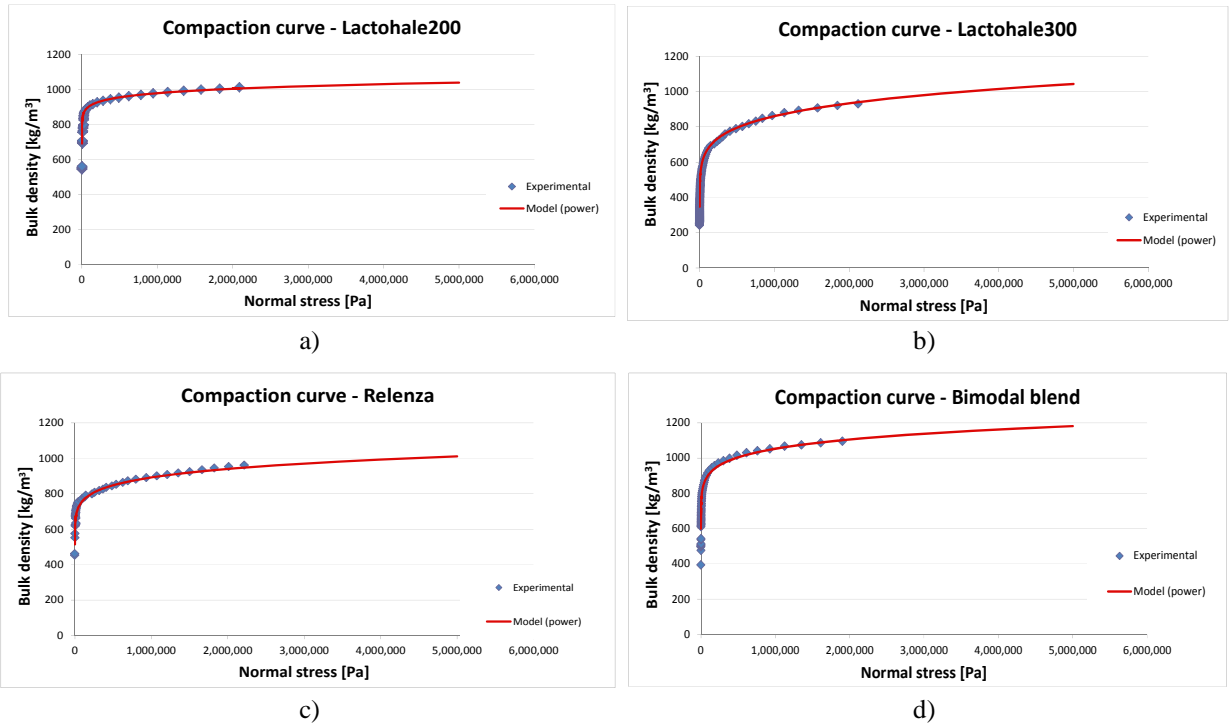
Figure A6.7.   Compression behaviour predicted from the compaction curve model: a) *Lactohale200*; b) *Lactohale300*; c) *Relenza*; d) *Bimodal blend*. For full explanation refer to the text.

Appendix 7

Dosator Single Shot Test-rig

1. Introduction

This appendix presents the development/procedures details and results not presented in the chapters 6 and 7 that are relevant to The Wolfson Centre dosator single shot test-rig engineered in this thesis for the experimental work in dosators.

The section 1 shows the calibration of the force sensors. In the section 2 is described the summary of the preliminary trials undertaken in the test-rig. The procedure to prepare manually the powder bed is presented in the section 4. Some behaviours observed in the ejection force profiles are illustrated in the section 5 and some factors affecting the measurements in the test-rig are presented in the last section (6).

2. Force sensors calibration

The figure A7.1 shows the calibration of the body and pin force sensors equipped in the dosator test-rig. The UF1 force sensors were vertically mounted in the dosator test-rig and calibrated weights were hanged at the extreme of the threaded rod of the transducer.
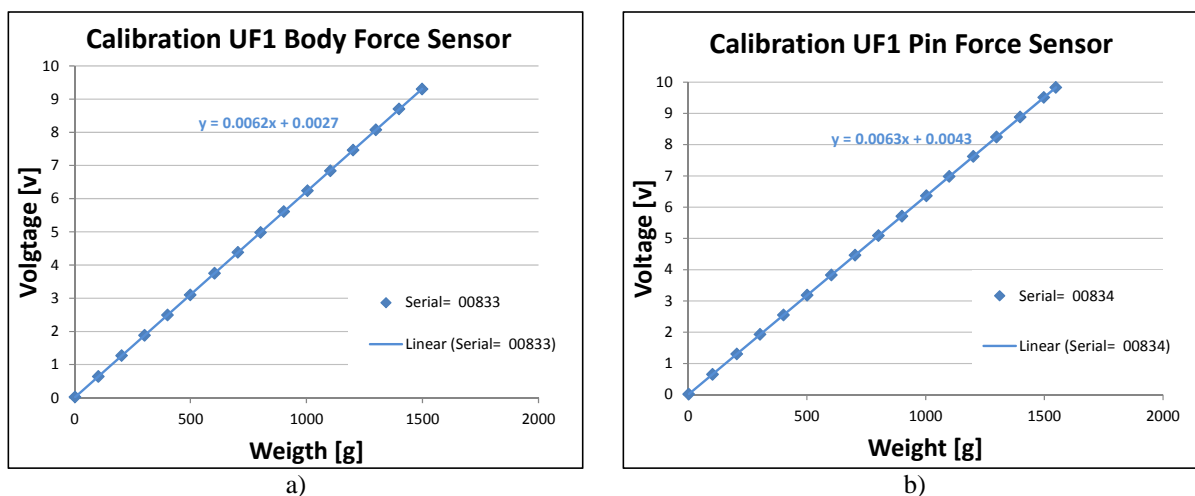

Figure A7.1. Calibration of the dosator force sensors equipped in the test-rig: a) body force; b) pin force.

3.   Summary of preliminary trials with the single shot dosator test-rig

The dose lengths were selected based on the diameter of the dosator and on previous trials undertaken in the early versions of the dosator test-rig. It was chosen one compacted and loose doses and another one in between these dimensions. The dose lengths chosen to test in this thesis were 4, 5 and 6 mm. It was found in the previous tests undertaken that as the dose length was increased the forces in the system decreased and 6 mm dose length dose showed small strength and forces in the system.

As mentioned in the chapter 2 and 4, the bowl/ dosator tip clearance gap "h" in the industrial dosator filling machines varied between approximately 0 to 0.3 mm. It was decided to choose 0.15, 0.3 and 0.6 mm gap "h" for the tests in the dosator test-rig to cover this range. Lower than 0.15 would be difficult to achieve in the dosator test-rig (due to force sensor over load, signal noise and assembly errors) and bigger than 0.6 mm the system could not be stressed enough to measure forces. The smallest gap values were also chosen because are approximately equivalent to one and a half diameter, 3.4 and 1.75 mm respectively, and they are important distances in the model proposed by this thesis.

The powder bed conditions were difficult to represent because the bed in current dosator machines is in heterogeneous state. To simulate this, it was decided to apply distributed weights to the powder bed for a period of 30 s, using rings of the same area of the bed to pre-compact it. The compaction conditions were uniformly distributed loads 0.5 and 1 kg that correspond to 176 and 352 Pa respectively of applied normal stress. Probably these values are not experimented in the normal conditions, or perhaps higher, but as it is unknown it could show the influence of the powder bed conditions.

4.   Powder bed preparation

The powder bed was tried to prepare as homogeneously and uniform as possible to measure and obtain consistent doses and forces. The procedure used to prepare the powder bed is showed in the figure A7.2.

The powder was filtered through a sieve (see figure A7.2a) of 355 μm (larger than 2 times the biggest particle size) in order to make a consistent bed. As some of the tests demanded pre-

compaction of the bed at fixed bed height, it was necessary to use mould rings to increase the height of the trough. This was the same principle used in the Jenike shear cell tests. Therefore, it was added a mould ring (see figure A7.2b) of 15 mm; the extended bed chamber was then filled (see figure A7.2c and the in the test required pre-compaction was applied with disc of the same annular area as the trough. The walls were taken off and the excess of powder removed using and scrapper (see figure A7.2d) to even the powder bed depth (see figure A7.2e). This arrangement allowed the application of rings of 0.5 and 1 kg weight to compress the powder bed and preserve the same bed height for all the tests.
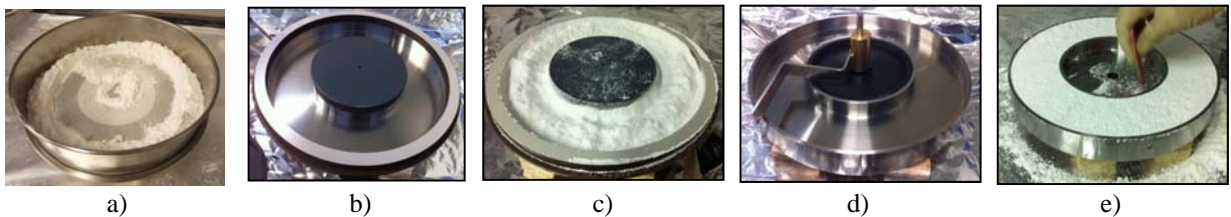

| a) | b) | c) | d) | e) |

Figure A7.2. Powder bed preparation: a) sieve; b) wall extension; c) powder bed in the extended walls; d) scrapper; e) powder bed. For full explanation.

5.   Ejection force behaviour

In the chapter 7, figure 7.5, was illustrated the ejection force behaviour for three powders used in this research; it was not illustrated for Lactohale300 (cohesive powder used in this work) because did not show large magnitudes of this force and it was no possible to undistinguished from the signal noise.

The figure in chapter 7 showed random profiles (one out of ten tests) of the 6 mm dose lengths; complementary, the figure A7.3 shows random profiles of the corresponding 5 and 4 mm dose lengths.

Comparing both figures (7.16 and A7.3), it can be appreciated the same shape of the curves for all the dose lengths. This force reduced with the dose length contrary to the behaviour observed in the filling forces in the figure 7.2 in chapter 7. In can be also seen the large initial displacement of the pin to peak force in long doses than in the short dose lengths.
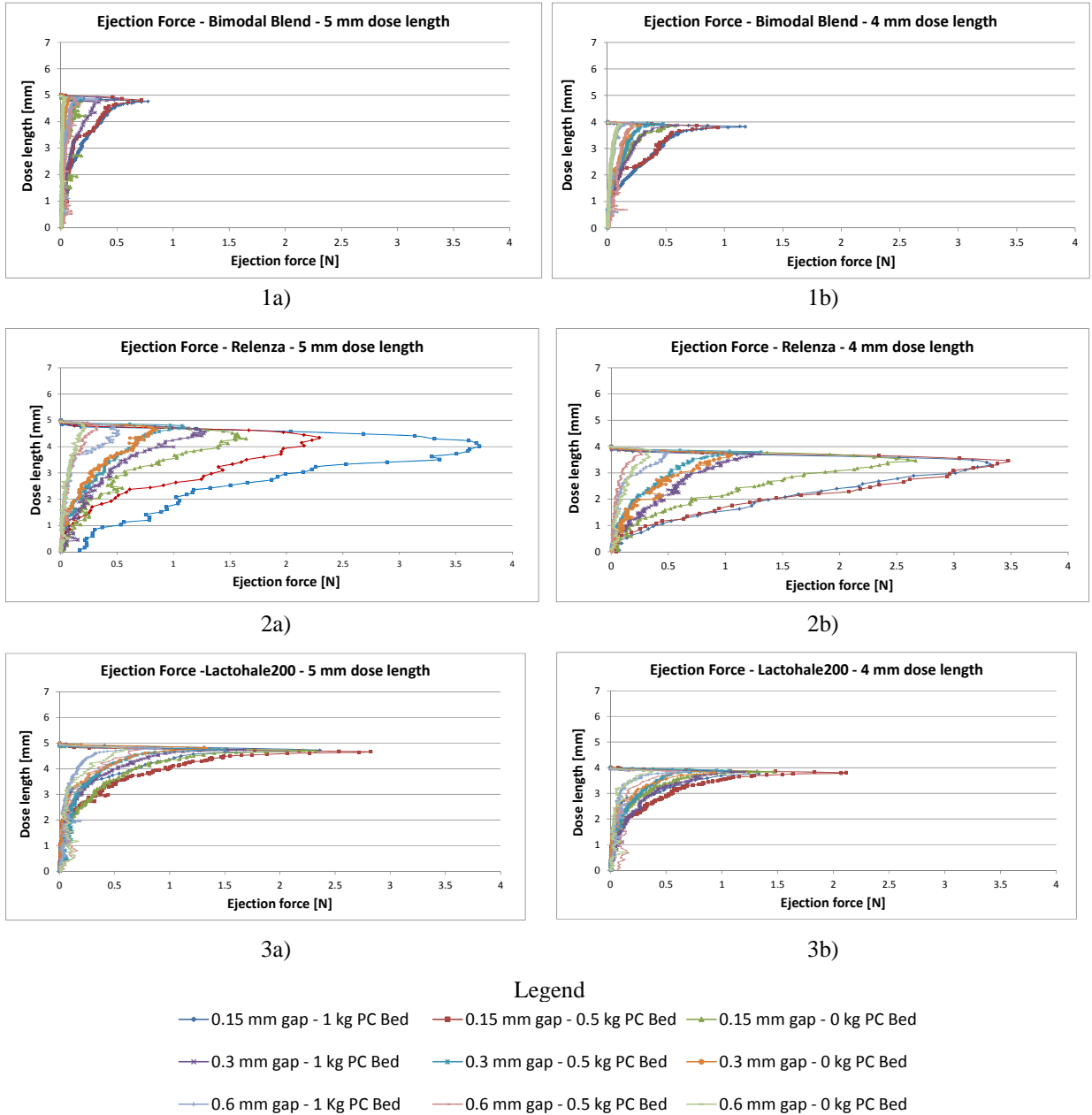
Figure A7.3. Ejection force behaviour observed in the experimental data of: 1) dimodal blend; 2) Relenza; 3) Lactohale200; for the dose lengths a) 5 mm; b) 4 mm.

6.   Factors affecting the data

There were various factors affecting the data in The Wolfson Centre dosator single shot test-rig and they are mentioned in this section.

The gap "h" had approximately 5 % variation that corresponds to 1.5 % mm of the level of the trough and 3.5 % of the LVDT accuracy and precision of the gap "h" adjusting system and

misalignments of the test-rig. The tests set at 0.15 mm gap "h" were affected by these variations as small changes in this gap could affect the forces.

The 5 signals of the force sensors and LVDT's were affected by external noise. There was installed filters in the wired up to reduce it. However, low forces and displacements were affected by the noise in the signal in approximately 4 %.

The test-rig misalignments could affect the reading in the signals and also the gap "h" affecting the force measurements.

The room temperature and moisture could affect the flowability of the powders, especially for cohesive powders in different weather season.

The history in the powder could affect its behaviour because it was used for the powder characterisation and testing in the dosator test-rig.

The hydraulic unit operation the trough strokes, had some vibrations that could affect the measurements and the powder bed state of the powder; the last one could be beneficial as the particle packing of the powder bed could be re-arranged. The operation of the hydraulic valve and the action of the cylinder could induce vibration that could affect the signals. The Test-rig was placed in a stainless steel bench that isolates the test-rig from external noise and vibration. The test-rig chassis and frame also helped to keep the test-rig isolated and robust.

The Hydraulic system helped the trough's stroke to be smooth and avoid jolts when reaching the maximum and lowest displacement.

The preparation of the powder bed was carried out in an environmental chamber to avoid dustiness of the powder when filtering it. The air extraction stream could affect the even filling of the powder bed; it was seen zones in the middle and close to the walls being filling first. This was another reason to use the trough's extension walls, because as the powder reached the interface powder bed/ sieve, the powder accumulated and it was compacted by the filtering of the sieve.

The dose weight could be also affected by the sensitivity of the scale. The scale measured the weight in "g" and the sample was enclosed. The scale measures up 4 decimal digits that made it sensitive even to external air stream.